

Hiroshima University Doctoral Thesis

**Development of a New Series of Chromophores
with Nitrobiphenylamines for Application to
Photoremovable Protecting Groups**

ニトロビフェニルアミン骨格をもつ
新しい光アンテナ部位の開発と
フォトケージへの応用

September 2024

Graduate School of Advanced Science and
Engineering
Hiroshima University

NGUYEN TRAN BAO LINH

Table of Contents

1. Main thesis

Development of a New Series of Chromophores with Nitrobiphenylamines for Application to Photoremovable Protecting Groups

(ニトロビフェニルアミン骨格をもつ新しい光アンテナ部位の開発と
フォトケージへの応用)

2. Main articles

(1) “Tris(4'-nitrobiphenyl)amine – an octupolar chromophore with high two-photon absorption cross-section and its application for uncaging of calcium ions in the near-infrared region”

Linh Tran Bao Nguyen, Cheng-Lin Wu, Tzu-Chau Lin*, and Manabu Abe*

J. Org. Chem. **2022**, *87*, 15888–15898

(2) “Study on factors affecting quantum yield for the design of improved ortho-nitrobenzyl photoremovable protecting groups”

Linh Tran Bao Nguyen and Manabu Abe*

Bull. Chem. Soc. Jpn. **2024**, uoae067

3. Supplementary articles

(1) “Development of photoremovable protecting groups responsive to near-infrared two-photon excitation and their application to drug delivery research”

Linh Tran Bao Nguyen and Manabu Abe*

Bull. Chem. Soc. Jpn. **2023**, *96*, 899–906

(2) “Structural Transformation of the 2-(*p*-Aminophenyl)-1-hydroxyinden-3-ylmethyl Chromophore as a Photoremovable Protecting Group”

Miyu Sasaki, Linh Tran Bao Nguyen, Sohshi Yabumoto, Tatsuo Nakagawa, and Manabu Abe*

ChemPhotoChem **2020**, *4*, 5392–5398

(3) “Photoexcitation of (diarylmethylene)amino benziodoxolones for alkylation of styrene derivatives with carboxylic acids”

Daichi Okumatsu, Kensuke Kiyokawa*, Linh Tran Bao Nguyen, Manabu Abe*, and Satoshi Minakata*

Chem. Sci. **2024**, *15*, 1068–1076

(4) “Bidirectional Neuronal Actuation by Uncaging with Violet and Green Light”

Lorenzo Sansalone, Jun Zhao, Linh T. B. Nguyen, Swati Gupta, Deanna L. Benson, Manabu Abe, and Graham C. R. Ellis-Davies*

Angew. Chem. Int. Ed. **2024**, *63*, e202315726

Main Thesis

Contents

Chapter 1. General introduction

1.1. Caged compound	7
1.2. One-photon (1P) excitation and two-photon (2P) excitation.....	9
1.3. Molecular designs of two-photon responsive chromophores	11
1.4. Caged calcium	13
1.5. Purpose of this study	15

Chapter 2. Design and synthesis of an octupolar chromophore tris(4'-nitrobiphenyl)amine with high two-photon response for releasing calcium ions in the near-infrared region

2.1. Introduction	17
2.2. Photophysical properties of 1a and 2a	18
2.3. 2P absorption properties of 2a	21
2.4. Photophysical properties of 1b-c and 2b-c	22
2.5. Ca ²⁺ binding affinities of 1c and 2c	24
2.6. 1P photoreactions of 1b-c and 2b-c	26
2.7. 2P photoreactions of 1b-c and 2b-c	28
2.8. Uncaging of Ca ²⁺ by 1P and 2P excitation.....	30
2.9. Summary.....	32
2.10. Experimental section	33

Chapter 3. Substituent effects on the uncaging quantum yield of amino-substituted nitrobiphenyl units

3.1. Introduction	59
3.2. Photophysical properties.....	61
3.3. Photoreactions	68
3.4. Quantum chemical calculations.....	74
3.5. Summary.....	81
3.6. Experimental section	81

Chapter 4. Conclusions and outlook

References

List of Publications

Acknowledgements

Chapter 1

General introduction

1.1. Caged compound

Biologically active compounds, such as Ca^{2+} , neurotransmitters, and amino acids, play critical roles in our lives as they contribute to various biological functions. These compounds are thus potential sources for new drugs. Spatiotemporal control of biologically active substances by protection (caging) and deprotection (uncaging) using photoremovable protecting groups (PPGs) has emerged as a robust tool to investigate the functional mechanisms of bioactive molecules in physiological studies¹⁻⁷. Since the release of biologically active molecules from temporally inactivated compounds, that is, caged compounds, can be done merely by light irradiation, this caging and uncaging method enables concentration jumps of bioactive substances under mild conditions with high spatiotemporal control to efficiently stimulate biological processes⁸. To be practically employed in physiological studies, PPGs need to satisfy several requirements, such as low toxicity to living tissues, high solubility and thermal stability in an aqueous environment, high molar extinction coefficient, and high uncaging quantum yield³. The evolution of novel PPGs meeting these criteria for caging a diverse range of biologically active molecules such as calcium⁹⁻¹² and neurotransmitters¹³⁻¹⁶ has always continued¹⁷.

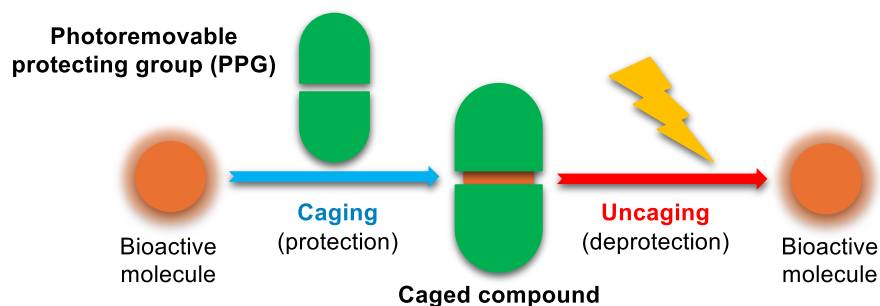


Figure 1. Caging and uncaging of bioactive molecules using PPGs.

Ortho-nitrobenzyl (oNB)^{18,19} is the first PPG utilized in biological experiments to cage adenosine cyclic 3',5'-phosphate (cAMP)²⁰ and adenosine 5-triphosphate (ATP)²¹ and simulate their bioactivities in cellular processes. As shown in Figure 2, the photochemical release of bioactive compounds (X) from oNB-type PPGs starts from the intramolecular hydrogen abstraction by the nitro group to generate an aci-nitro intermediate (A), which subsequently undergoes cyclization (B) and ring-opening to form a hemiacetal intermediate (C)¹⁹. Hydrolysis of the hemiacetal then releases the caged molecule and a nitroso photoproduct (D). The first step in this mechanism, the intramolecular hydrogen abstraction (oNB → A), is important in determining the uncaging quantum yield of oNB-type PPG. This process is triggered by the local $n \rightarrow \pi^*$ excitation within the nitro group.

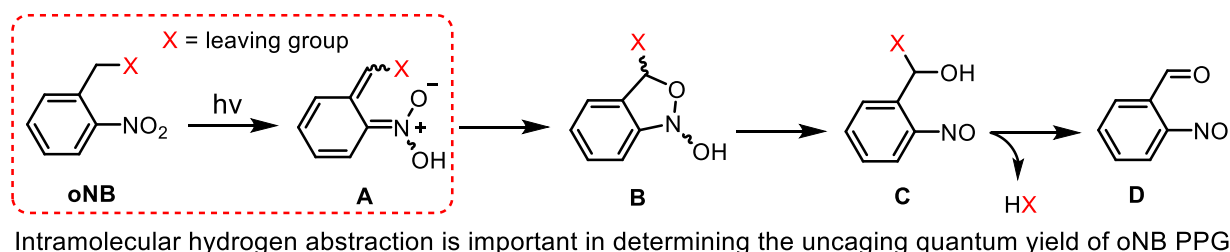


Figure 2. Uncaging mechanism of oNB-type PPGs.

On the other hand, photo-S_N1-type PPGs release the bioactive compounds (X) via direct bond cleavage (Figure 3). Numerous PPGs, such as coumarin (CH)²², *p*-hydroxyphenacyl (pHP)²³, quinoline (Qu)²⁴, BODIPY²⁵, and pAPHi²⁶, can be classified in this category.

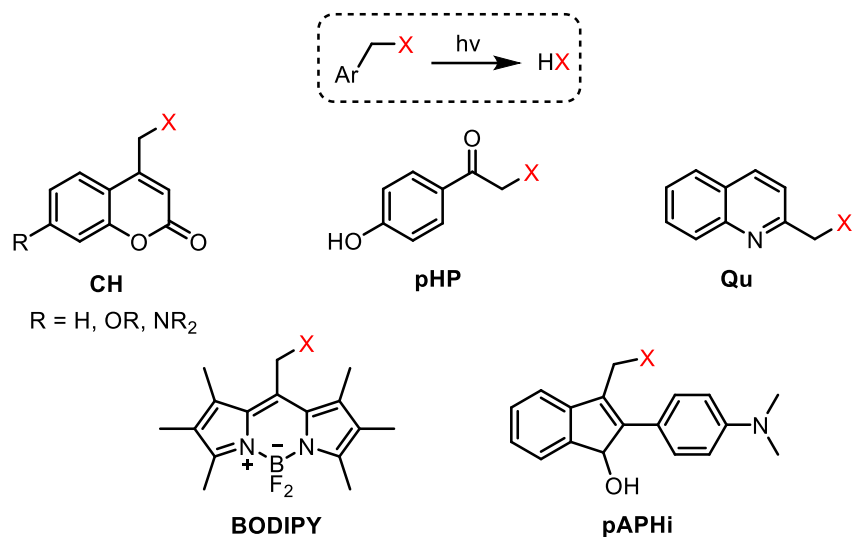


Figure 3. Examples of photo-S_N1-type PPGs.

1.2. One-photon (1P) excitation and two-photon (2P) excitation

Irradiation with high-energy ultraviolet (UV) light effectively breaks the relatively strong C-X bonds in caged compounds and liberates the bioactive molecules. However, UV light is not convenient for uncaging in living cells because it cannot penetrate deep areas of biological samples and may cause cytotoxicity due to high-energy photons. On the other hand, near-infrared (NIR) light (650 – 1050 nm, known as a biological window) has significantly better bio-permeability and less cytotoxicity. However, its low energy challenges the efficient release of biologically active substances. To solve this problem, two-photon (2P) excitation has been introduced.

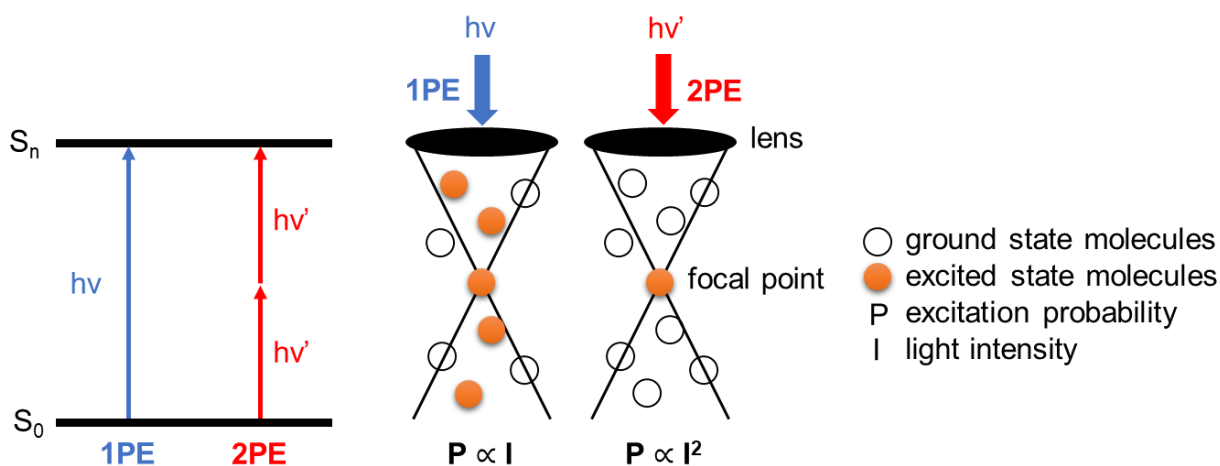


Figure 4. One-photon excitation (1PE) and two-photon excitation (2PE) process.

The theory of 2P excitation was proposed by Göppert-Mayer in 1931²⁷ and became practically accessible with the development of intense ultrashort pulsed lasers²⁸, such as Ti:Sapphire lasers. This process enables the excitation of molecules to the same electronic excited state as that given in 1P excitation by simultaneous absorption of two lower-energy photons. Thus, it reduced the photodamage and improved the penetration in deep areas within biological tissues. Furthermore, as 2P excitation is a nonlinear process in which the excitation probability (P) is proportional to the square of light intensity (I), it is possible to limit the excitation to molecules at the focal point of the laser and achieve the three-dimensional control of photoreactions. These benefits make 2P excitation a revolutionary tool for uncaging biologically active substances in physiological studies and also for a diverse range of applications, including 2P fluorescence microscopy^{29,30} and photodynamic therapy³¹.

1.3. Molecular designs of two-photon responsive chromophores

The growing popularity of 2P excitation has created a demand for developing organic molecules that demonstrate improved 2P absorption character, evaluated by the 2P absorption cross-section (σ_2 measured in GM, named after Göppert-Mayer, 1 GM = 10^{-50} cm⁴ s photon⁻² molecule⁻¹). The 2P uncaging efficiency (δ_u) of a caged compound is determined by the equation $\delta_u = \sigma_2 \times \Phi_u$, in which Φ_u is the quantum yield of the uncaging reaction. Although a caged compound with 2P uncaging efficiency of 0.5 GM was successfully employed in biological studies³², a minimum value of 3 GM has been suggested for optimal application³³. Enhancing the 2P absorption ability is typically accomplished by the elongation of π -conjugation system and functionalization with donor/acceptor groups (Figure 5).

Benzene, the simplest aromatic compound, has no 2P absorption, but naphthalene with lengthened π -conjugation exhibited a slightly increased 2P absorption cross-section (0.9 GM at 530 nm)³⁴. Introducing a double bond between two benzene rings, as in *trans*-stilbene, further enhanced the value (12 GM at 514 nm)³⁵. These results clearly demonstrated the importance of extending π -conjugation length in designing 2P-responsive molecules, although the water solubility of the chromophores may be decreased.

2P absorption cross-section can also be significantly enhanced if electron-donating (D) and electron-withdrawing (A) groups are inserted to increase the transition dipole moment of the chromophores. Substitution with donor-acceptor groups (dipolar systems, D- π -A), donor-donor groups or acceptor-acceptor groups (quadrupolar systems, D- π -D or A- π -A) at both ends of *trans*-stilbene considerably increased σ_2 values compared to the non-substituted molecule. For example, 100 GM at 830 nm and 110 GM at 620 nm were reported for the D-

π -A-type³⁶ and D- π -D-type³⁷ *trans*-stilbene, respectively. The 2P absorption process in dipolar systems can be interpreted using a two-state model, and their 2P absorption maxima are at twice the wavelength of the corresponding 1P absorption maxima. In contrast, a three-state model, which is associated with the transition from the ground state S_0 to the excited state S_2 , describes the 2P absorption process in quadrupolar systems. These molecules have the 2P absorption maxima at wavelengths shorter than twice the 1P absorption maxima.

Notably, octupolar systems with triangular or star-shaped structures $D(-\pi-A)_3$ or $A(-\pi-D)_3$ have been found to exhibit exceptional 2P absorption performance, e.g., approximately 1200 GM at 740 nm was recorded for an octupolar chromophore based on a triphenylamine core³⁶. Molecules of this type typically have degenerated S_1 and S_2 states, to which transitions from the ground state S_0 are allowed by 1P excitation. In contrast, the transition from S_0 to a higher-energy S_3 state is highly allowed by 2P excitation. As a result, the 2P absorption maxima of octupolar compounds are observed at wavelengths shorter than twice the corresponding 1P absorption maxima, which are similar to those in quadrupolar systems.

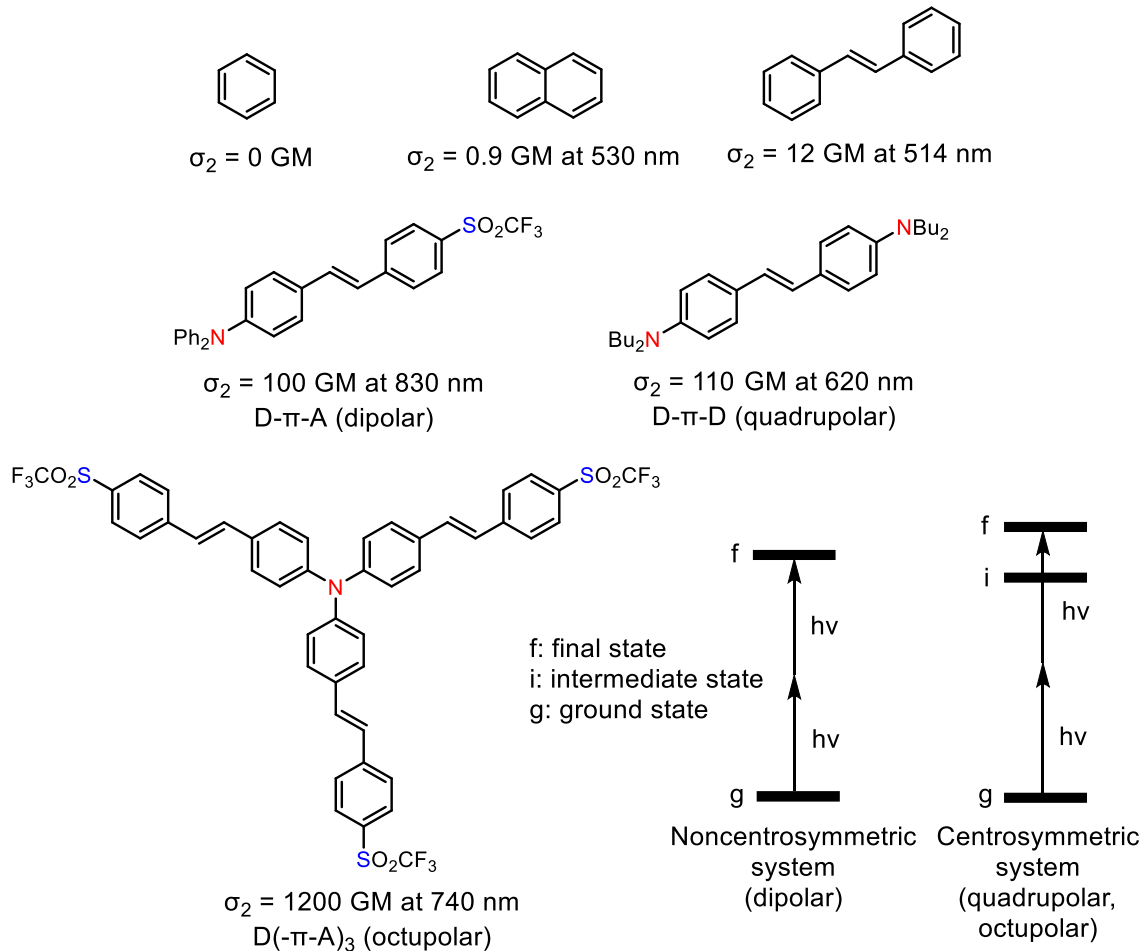


Figure 5. Molecular designs of 2P-responsive chromophores.

1.4. Caged calcium

Calcium ion (Ca^{2+}), as a second messenger, regulates a variety of biological processes within organisms and cells, such as the release of neurotransmitters in cell signaling pathways³⁸. Spatiotemporal control of the intracellular concentration of Ca^{2+} is essential for the study of functional mechanisms related to human memory and learning ability.

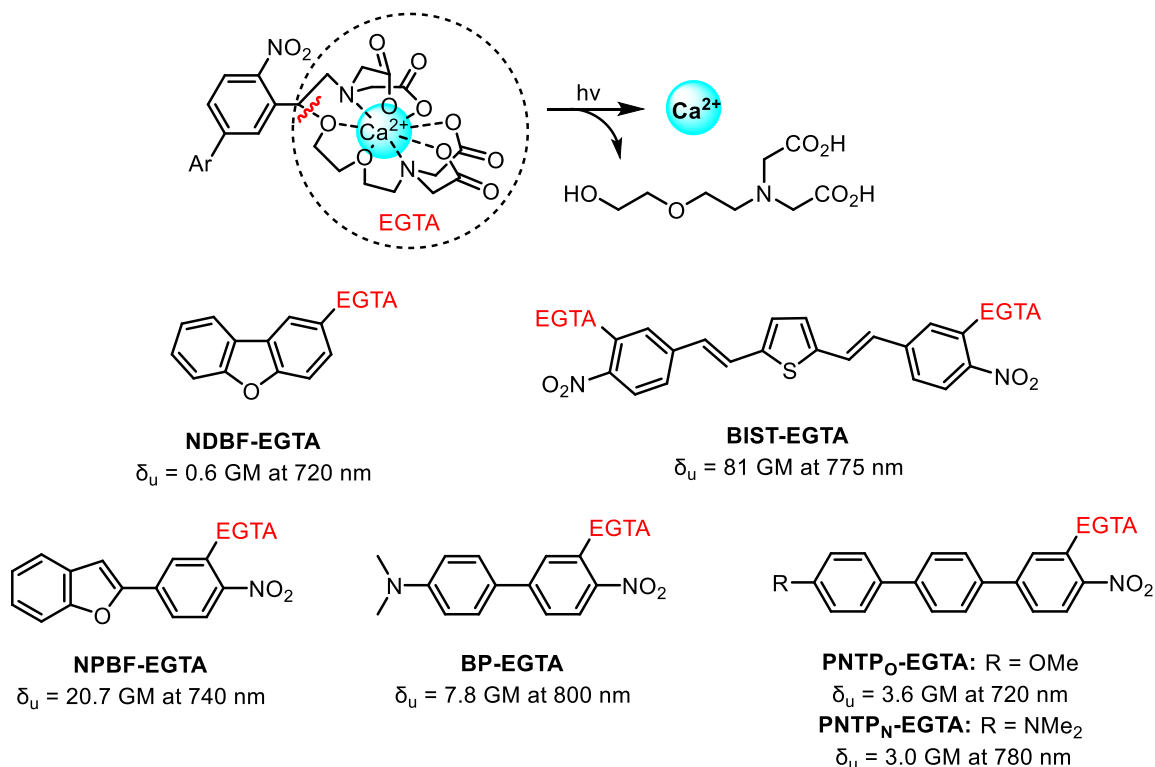


Figure 6. Structures and 2P uncaging efficiencies of EGTA-based Ca^{2+} chelators.

EGTA (ethylene glycol tetraacetic acid) has been known as an organic chelator with high binding affinity and selectivity towards Ca^{2+} , which can be released by the photodecomposition of the chelator⁹. Several photolabile derivatives of EGTA, with the chelator moiety attached at the reactive site of oNB PPG, have been developed for the uncaging of biologically active Ca^{2+} in physiological studies. The first Ca^{2+} chelator having 2P absorption ability, nitrodibenzofuran (NDBF)-substituted EGTA (NDBF-EGTA, $\delta_u = 0.6$ GM at 720 nm), was reported by Ellis-Davies et al. in 2006³⁹. Later, they introduced a bisstyrylthiophene (BIST)-substituted EGTA (BIST-EGTA) with an exceptional 2P response ($\delta_u = 81$ GM at 775 nm)¹¹. Our laboratory also succeeded in developing a number of Ca^{2+} chelators with relatively high 2P uncaging efficiency, such as nitrophenylbenzofuran

(NPBF)-substituted EGTA (NPBF-EGTA, $\delta_u = 20.7$ GM at 740 nm)⁴⁰, biphenyl-substituted EGTA (BP-EGTA, $\delta_u = 7.8$ GM at 800 nm)⁴⁰, and *p*-nitroterphenyl (PNTTP)-substituted EGTA (PNTTP_O-EGTA, $\delta_u = 3.6$ GM at 720 nm and PNTTP_N-EGTA, $\delta_u = 3.0$ GM at 780 nm)¹² (Figure 6).

1.5. Purpose of this study

As mentioned above, biphenyl scaffolds with amino substituents as electron donors are potential candidates for developing novel chromophores with high 2P responses. These platforms can also be utilized to generate octupolar systems, which, despite having sizable 2P absorption cross-section σ_2 values, have not been exploited in 2P uncaging reactions. Therefore, in Chapter 2, we designed and synthesized tris(4'-nitrobiphenyl)amine, an octupolar chromophore with a simpler structure than previous star-shaped compounds but still exhibits comparable 2P absorption capability. We performed the 2P-induced release of Ca²⁺ in NIR region using its EGTA-substituted derivatives.

Since the uncaging quantum yield Φ_u is also a crucial parameter in determining the 2P uncaging efficiency ($\delta_u = \sigma_2 \times \Phi_u$), in Chapter 3, we developed a series of nitrobiphenyl scaffolds by varying their amino substituents and examined the effect of these substituents on the uncaging quantum yield of oNB PPG. Photophysical characterization and quantum chemical calculation were carried out to explain the influence of the lowest excited states on uncaging reactivity.

Chapter 2

**Design and synthesis of an octupolar chromophore
tris(4'-nitrobiphenyl)amine with high two-photon
response for releasing calcium ions in the near-
infrared region**

2.1. Introduction

Octupolar systems containing an electron-rich triphenylamine center are highly advantageous for molecular engineering and increasing 2P responses. The functionalization of triphenylamine-based compounds that respond to 2P excitation has been performed using different acceptors such as typical electron-withdrawing groups (triflyl^{36,41}, cyano^{42,43}, formyl^{44,45}) or electron-poor heteroaromatics (pyridine^{43,46}, pyridinium^{47,48}). These groups are linked to the triphenylamine core through extended π -conjugated linkers such as phenylene-vinylene or phenylene-ethynylene (Figure 7a). Nevertheless, the large molecular sizes and strong aromaticity of these chromophores could hamper the compatibility with biological samples. Therefore, there is a high demand for designing compounds that can balance optical properties and biocompatibility.

Our study focuses on enhancing the 2P responses while maintaining reasonable molecular sizes of the chromophores. As a result, we introduced a novel and simple octupolar molecule, tris(4'-nitrobiphenyl)amine (TNBPA) **2a** (Figure 7b), which contains three nitro moieties connected to the central nitrogen atom via biphenylene bridges. These nitro groups can act as strong electron acceptors and, at the same time, participate in the uncaging reactions of oNB PPG. A dipolar analog **1a** (Figure 7b) was also synthesized to analyze the differences in photophysical (including 2P absorption) and photochemical properties of dipolar and octupolar systems. Subsequently, we prepared the EGTA-substituted derivatives with dipolar (**1b-c**) and octupolar (**2b-c**) nature, which serve as photolabile Ca²⁺ chelators. The investigation into 1P and 2P photochemical behaviors and the release of Ca²⁺ from these caged calcium compounds were conducted.

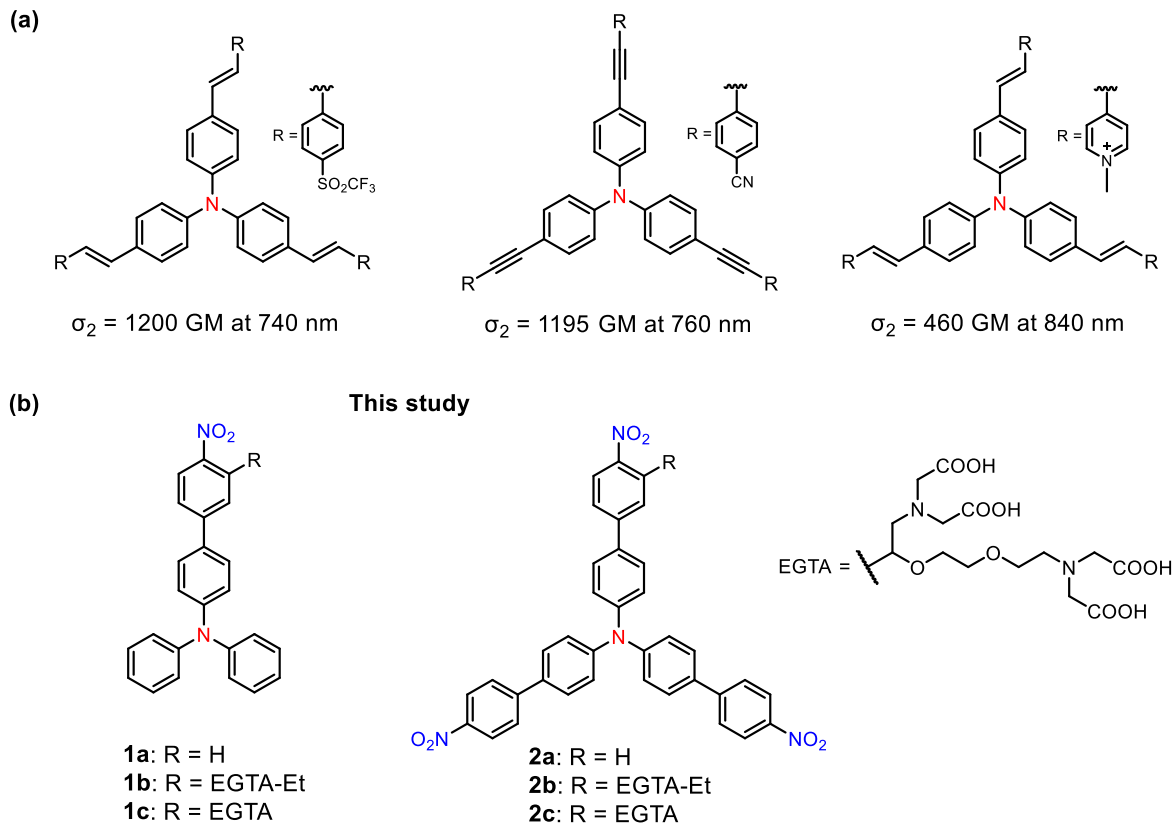


Figure 7. (a) Structures and 2P absorption cross-sections of some octupolar chromophores; (b) Molecular designs of this study.

2.2. Photophysical properties of **1a** and **2a**

The 1P absorption and fluorescence spectra of the dipolar molecule **1a** and octupolar molecule **2a** were measured in solvents of varying polarities: toluene ($E_T(30) = 33.9$), chloroform (CHCl_3 , $E_T(30) = 39.1$), dimethyl sulfoxide (DMSO, $E_T(30) = 45.1$), acetonitrile (MeCN, $E_T(30) = 45.6$), and methanol (MeOH, $E_T(30) = 55.4$) (Figure 8). The photophysical data are summarized in Table 1. Strong absorption in the visible region was observed for both **1a** and **2a**, with minimal change in the maximum absorption wavelength on increasing solvent polarity (395–412 nm for **1a** and 405–424 nm for **2a**). **2a** showed slightly red-shifted

maximum absorption wavelengths compared to **1a** because of a larger conjugated system. The molar extinction coefficients of **2a** were significantly higher than those of **1a**, for example, 42489 M⁻¹cm⁻¹ for **2a** (entry 8) and 17944 M⁻¹cm⁻¹ for **1a** (entry 3) in DMSO, indicating the significant role of the increased number of conjugated branches in octupolar systems^{42,49}.

Table 1. Photophysical data of compounds **1a** and **2a** in various solvents.

Entry	Compound	Solvent	$\lambda_{\text{abs}}^{\text{a}}$ / nm	ϵ^{b} / M ⁻¹ cm ⁻¹	$\lambda_{\text{fl}}^{\text{c}}$ / nm	$\Delta\nu_{\text{St}}^{\text{d}}$ / cm ⁻¹	$\Phi_{\text{fl}}^{\text{e}}$	τ^{f} / ns
1		toluene	400	16355	537	6378	0.78	3.1
2		CHCl ₃	408	17590	698	10183	0.010	0.36
3	1a	DMSO	412	17944	n.d.	n.d.	n.d.	n.d.
4		MeCN	396	17745	n.d.	n.d.	n.d.	n.d.
5		MeOH	395	17574	n.d.	n.d.	n.d.	n.d.
6		toluene	405	41115	507	4967	0.51	2.2
7		CHCl ₃	415	40012	687	9540	0.016	0.30
8	2a	DMSO	424	42489	n.d.	n.d.	n.d.	n.d.
9		MeCN	407	44149	n.d.	n.d.	n.d.	n.d.
10		MeOH ^g	407	42509	n.d.	n.d.	n.d.	n.d.

^aAbsorption maximum. ^bMolar extinction coefficient (error of ±10–20%). ^cFluorescence maximum. n.d. = not detected or very weak. ^dStokes shift. ^eFluorescence quantum yield measured using an absolute photoluminescence quantum yield spectrometer (error of ±10%). ^fFluorescence lifetime determined using the time-correlated single-photon counting method (error of ±10%). ^gCo-solvent with DMSO (10%).

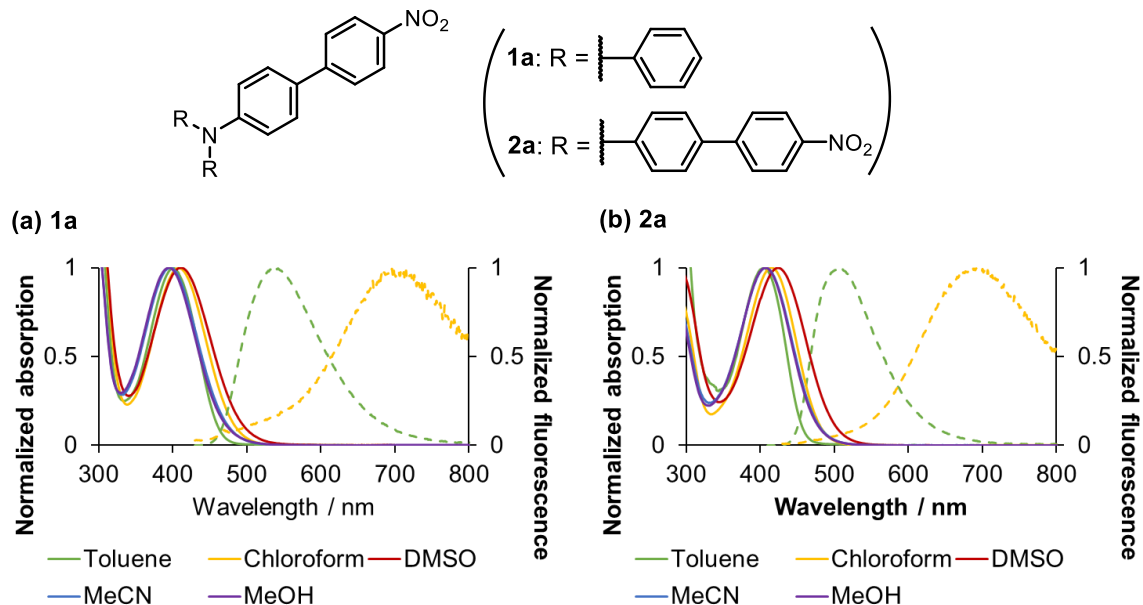


Figure 8. Absorption (full line) and fluorescence (dash line) spectra of compounds **1a** and **2a** in various solvents.

Intense fluorescence emission was observed for both compounds in nonpolar solvent; for example, $\lambda_{fl} = 537$ nm, $\Phi_{fl} = 0.78$ for **1a** (entry 1) and $\lambda_{fl} = 507$ nm, $\Phi_{fl} = 0.51$ for **2a** (entry 6) in toluene. The lower fluorescence quantum yield of **2a** than that of **1a** is possibly due to increased non-radiative processes⁴². The maximum emission wavelength was significantly red-shifted, and the fluorescence quantum yield decreased in medium-polarity solvent (chloroform), $\lambda_{fl} = 698$ nm, $\Phi_{fl} = 0.010$ for **1a** (entry 2) and $\lambda_{fl} = 687$ nm, $\Phi_{fl} = 0.016$ for **2a** (entry 7). In highly polar solvents, their emission was undetectable (entries 3–5 and 8–10). The bathochromic shift in fluorescence maximum and the decrease in fluorescence quantum yield when increasing solvent polarity are typical phenomena found in donor-acceptor molecules with intramolecular charge transfer (ICT) character^{50–52}. Smaller Stokes shift values of **2a** than **1a** implied a less polar structure in the excited state of the octupolar analog.

2.3. 2P absorption properties of **2a**

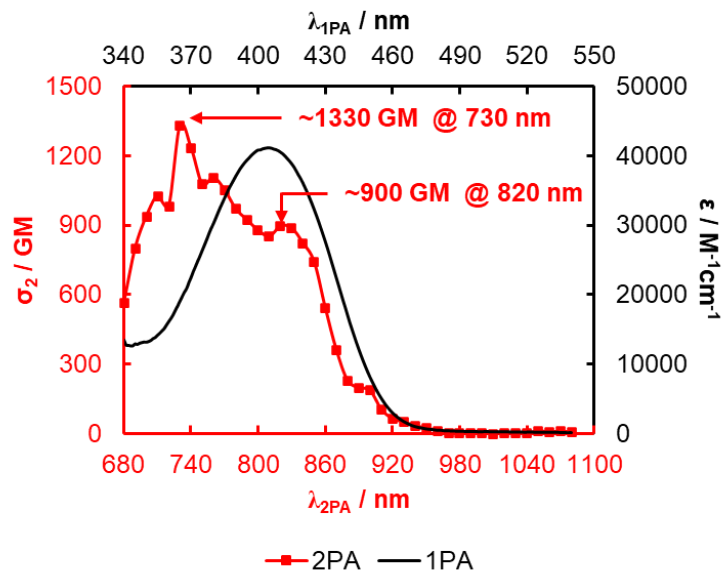


Figure 9. 2P absorption (red line) and 1P absorption (black line) spectra of compound **2a** (1.0×10^{-4} M) in toluene.

The 2P absorption spectrum (Figure 9) of the octupolar molecule **2a** was obtained in toluene using the 2P excitation fluorescence method. The spectrum revealed two 2P absorption maxima at 730 nm ($\sigma_2 = 1330$ GM) and 820 nm ($\sigma_2 = 900$ GM). The maximum with a lower σ_2 value (820 nm) appeared at nearly twice the 1P absorption peak (405 nm), which suggests that the $S_0 \rightarrow S_1$ transition is 2P-allowed in the case of **2a**^{42,53}. On the other hand, the maximum at 730 nm with a larger σ_2 value indicated a predominant contribution of the transition to a higher excited state^{49,52}. It is worth noting that the 2P absorption cross-sections of **2a** showed considerable improvement compared to those of similar-size triphenylamine derivatives^{44,48,49}. These values are equivalent to those of molecules with much larger π -conjugation^{41,42,54}. **2a** exhibited a ratio of 2P absorption cross-

section/molecular weight (σ_2/MW) of 2.2 GM g⁻¹ mol, which aligns with the most efficient molecules^{45,49}. These findings motivated us to develop its EGTA-substituted derivatives of to accomplish the 2P-induced uncaging of Ca²⁺ in NIR region.

2.4. Photophysical properties of 1b–c and 2b–c

Table 2. Photophysical and photochemical data of compounds **1b–c** and **2b–c**.

Entry	Compound	Solvent	$\lambda_{\text{abs}}^{\text{a}}$ / nm	ϵ^{b} / M ⁻¹ cm ⁻¹	K_{d}^{c} / nM	$\Phi_{\text{u}}^{\text{d}}$	σ_2^{e} / GM (λ_{irr} / nm)	$\delta_{\text{u}}^{\text{f}}$ / GM (λ_{irr} / nm)
1	1b	DMSO	400	13607	-	0.005	294 (800)	1.4 (800)
2		MeCN	395	19223	-	0.007	-	-
3	1c	MeOH	403	18276	-	0.004	-	-
4		HEPES buffer (pH 7.4)	405	10387	264	0.003	100 (790)	0.3 (790)
5	2b	DMSO	422	38167	-	0.004	1250 (850)	5.1 (850)
6		MeCN	408	31551	-	0.002	-	-
7	2c	DMSO	421	32836	-	0.007	-	-
8		HEPES buffer (pH 7.4) ^g	428	35970	64	0.008	349 (850)	2.8 (850)

^aAbsorption maximum. ^bMolar extinction coefficient (error ± 10 –20%). ^cDissociation constant determined using Scatchard analysis. ^dUncaging quantum yield (at conversions <10%) irradiated at 405 nm and determined using HPLC and a ferrioxalate actinometer (error ± 10 –20%). ^e2P absorption cross-section determined by comparing with the absolute value of 2-(4-nitrophenyl)benzofuran (error ± 10 –20%). λ_{irr} = Irradiation wavelength. ^f2P uncaging efficiency ($\delta_{\text{u}} = \sigma_2 \times \phi_{\text{u}}$) (error ± 10 –20%). ^gCo-solvent with DMSO (10%).

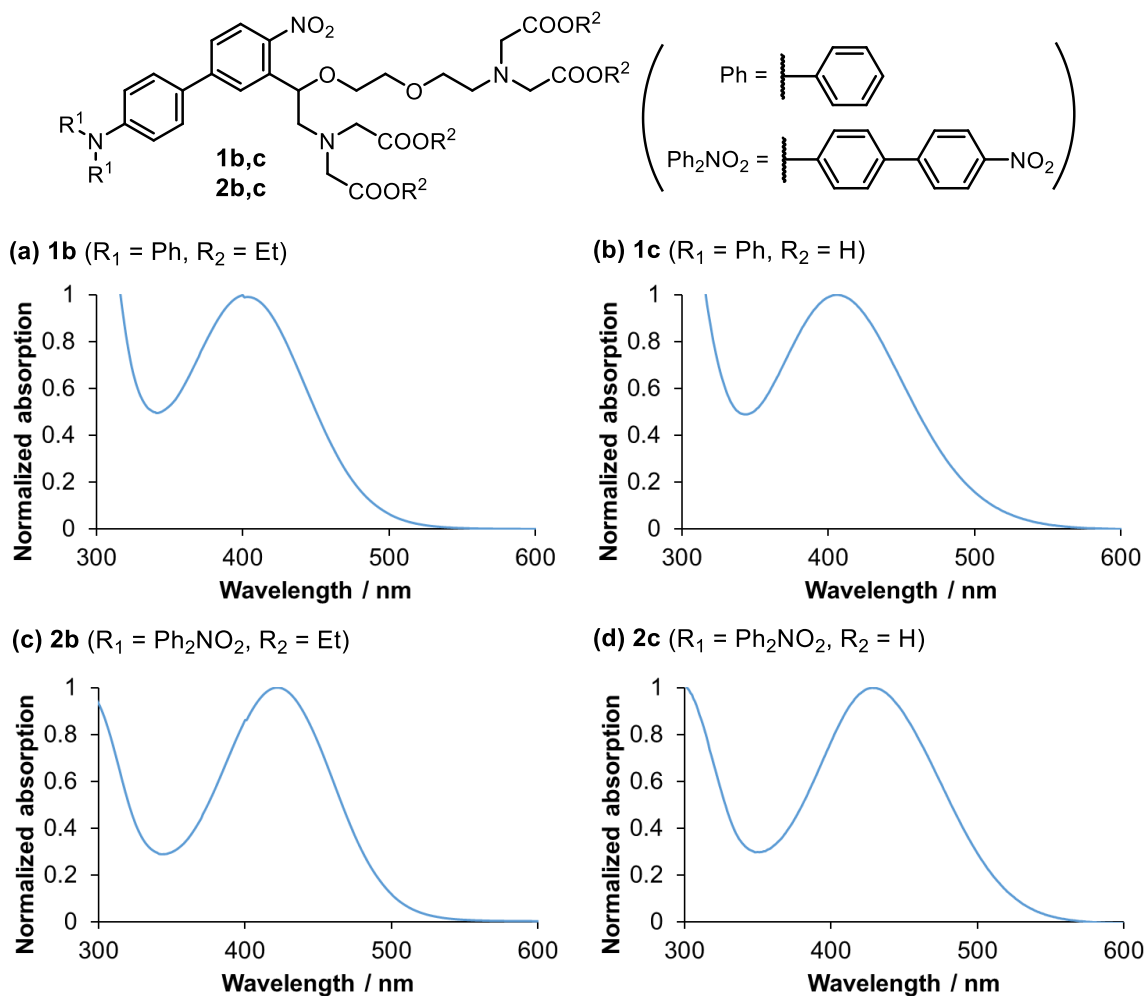


Figure 10. Absorption spectra of **1–2b** in DMSO and **1–2c** in HEPES buffer (pH 7.4).

The absorption spectra of EGTA-substituted derivatives **1b–c** and **2b–c** were measured in various polar solvents, such as DMSO, MeCN, MeOH, and HEPES buffer (pH 7.4) (Figure 10). In the case of **2c**, HEPES buffer with 10% DMSO was used due to its low solubility in water. The solubilities of **1c** in HEPES buffer (pH 7.4) and **2c** in HEPES buffer (pH 7.4, 10% DMSO) were determined to be 2.6 mM and 1.5 mM, respectively (see Experimental section). Both compounds exhibited thermal stability in HEPES buffer at 37 °C (see Experimental section). The photophysical data of **1b–c** and **2b–c** are summarized in Table 2. In general, the

substitution of EGTA unit did not have considerable influence on the maximum absorption wavelengths and molar extinction coefficients of these EGTA-substituted derivatives compared to non-substituted compounds **1a** and **2a**.

2.5. Ca²⁺ binding affinities of 1c and 2c

The Ca²⁺ binding affinities of **1c** and **2c** were assessed by the titration method using fluo-3^{9,55}, a Ca²⁺-sensitive fluorescence dye ($K_d = 500$ nM). This dye generates fluorescence emission upon binding with Ca²⁺, and the fluorescence intensity increases with incremental additions of CaCl₂ (Figures 11a, c). The concentrations of free calcium ions [Ca²⁺]_F were evaluated from the fluorescence intensity at 530 nm. Scatchard analysis (Figures 11b, d) revealed the dissociation constant K_d of 264 nM and 64 nM for **1c** and **2c**, respectively (Table 2). Similar values were recorded for nitrophenyl-substituted EGTA (NP-EGTA)⁹ and PNTP-EGTA¹² derivatives.

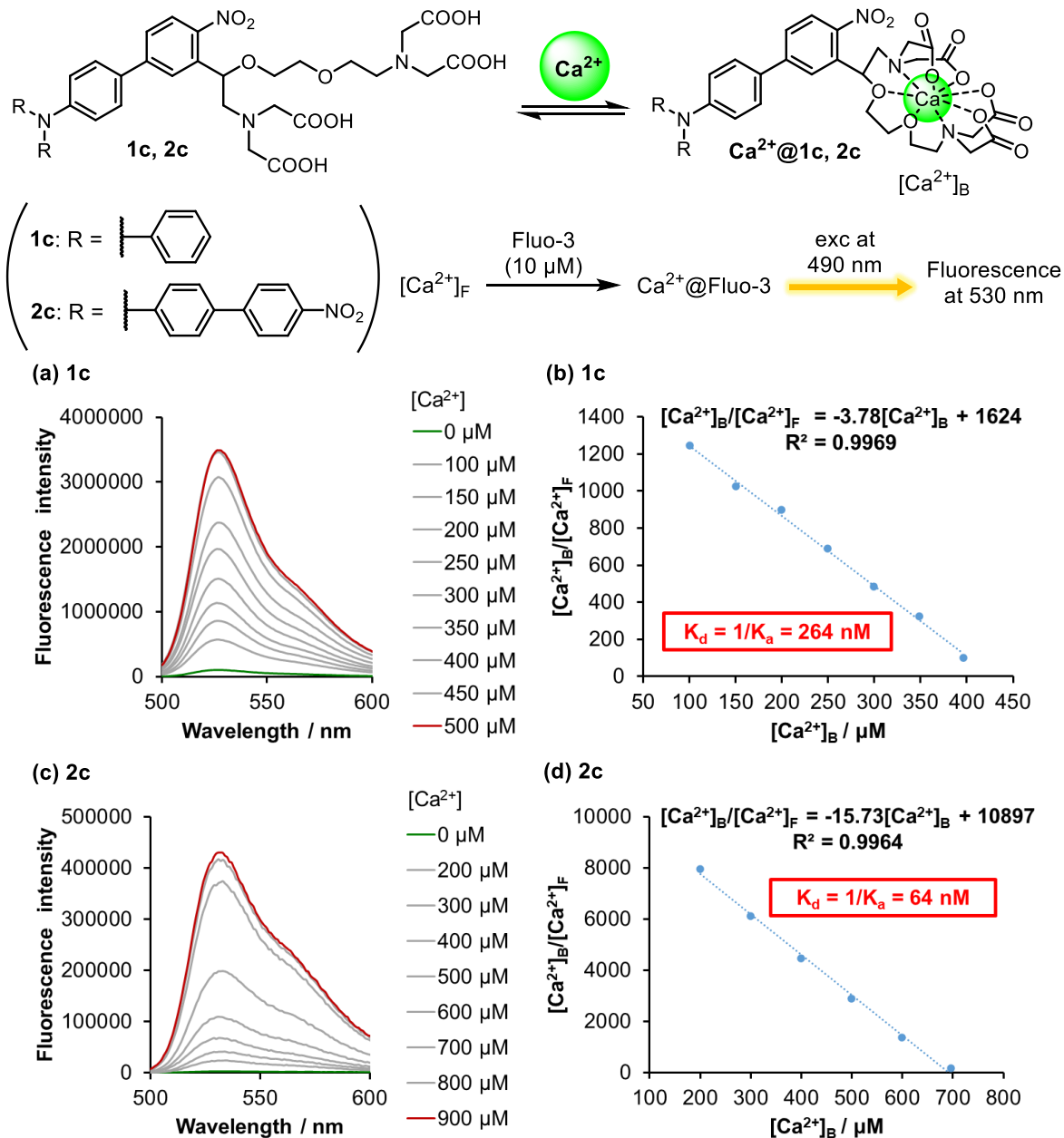


Figure 11. Emission spectra obtained by incremental addition of $CaCl_2$ into solutions of (a) **1c** and (c) **2c** (1.0 mM in HEPES/100 mM KCl, pH 7.4 at 25 °C, 10% DMSO for **2c**) with fluo-3 (10 μ M). Scatchard analyses of (b) **1c** and (d) **2c**. $[Ca^{2+}]_F$: concentration of free Ca^{2+} and $[Ca^{2+}]_B$: concentration of bound Ca^{2+} .

2.6. 1P photoreactions of 1b–c and 2b–c

The 1P photoreactions were carried out in CD₃CN for ethyl ester derivatives **1b** and **2b** (Figure 12) and in CD₃OD for acid derivatives **1c** and **2c** (Figure 13). A 405 nm LED lamp was used as the light source, and the photoreactions were monitored using ¹H NMR spectroscopy (400 MHz).

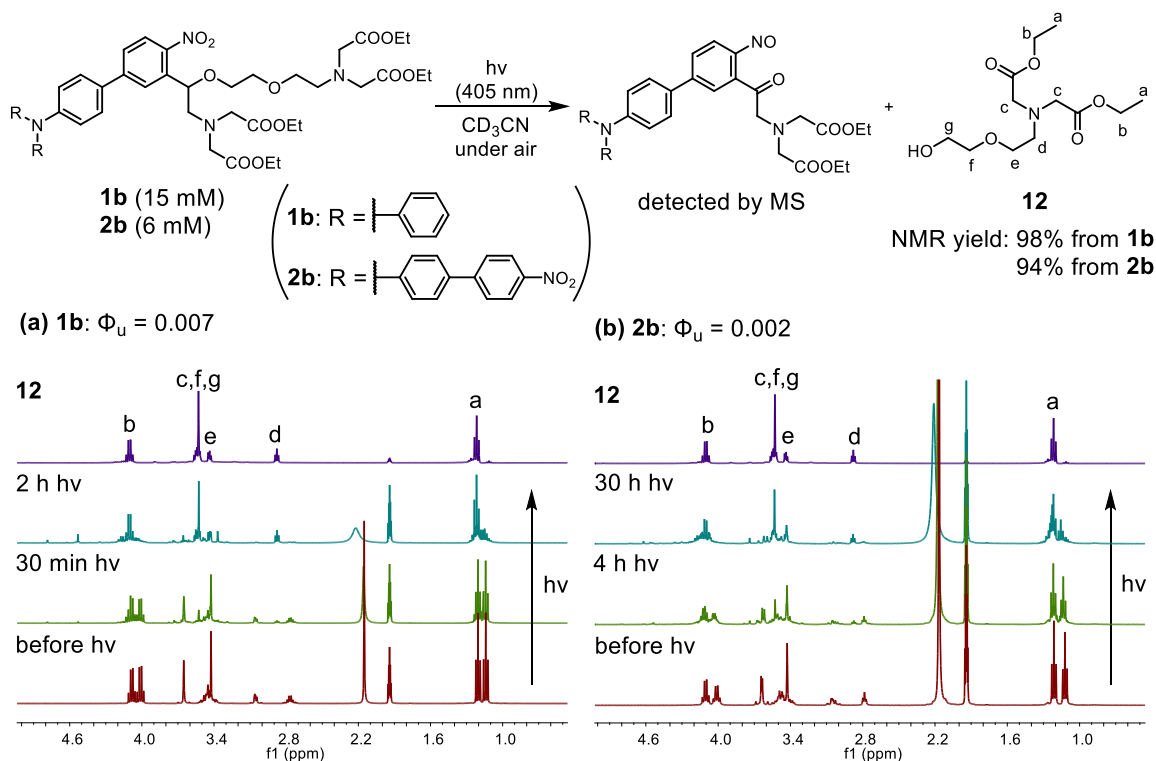


Figure 12. ¹H NMR spectra (400 MHz, 0.5–5.0 ppm) during photolysis at 405 nm in CD₃CN of compounds (a) **1b** and (b) **2b**.

The photodecomposition of **1b–c** and **2b–c** led to the clean release of the fragmentation products **12** and **13**. The chemical yields of **12** and **13**, calculated using triphenylmethane as an NMR standard, were found to be 94–98% and 73–74%, respectively. Even though the nitrosoketone photoproducts were not recognized in the NMR spectra after photolysis

because they are thermally and photochemically unstable, these compounds were detected by mass spectrometry (see Experimental section). The uncaging quantum yields of **1b–c** and **2b–c** (Table 2) were found to be 0.002–0.008, depending on the solvent. Low uncaging quantum yields have been reported for similar oNB PPGs with amino substituents^{12,56}. The substitution of a strong electron-donating amino group and a strong electron-withdrawing nitro group generates the ICT character in the excited state, which hinders the intramolecular hydrogen abstraction of oNB PPG.

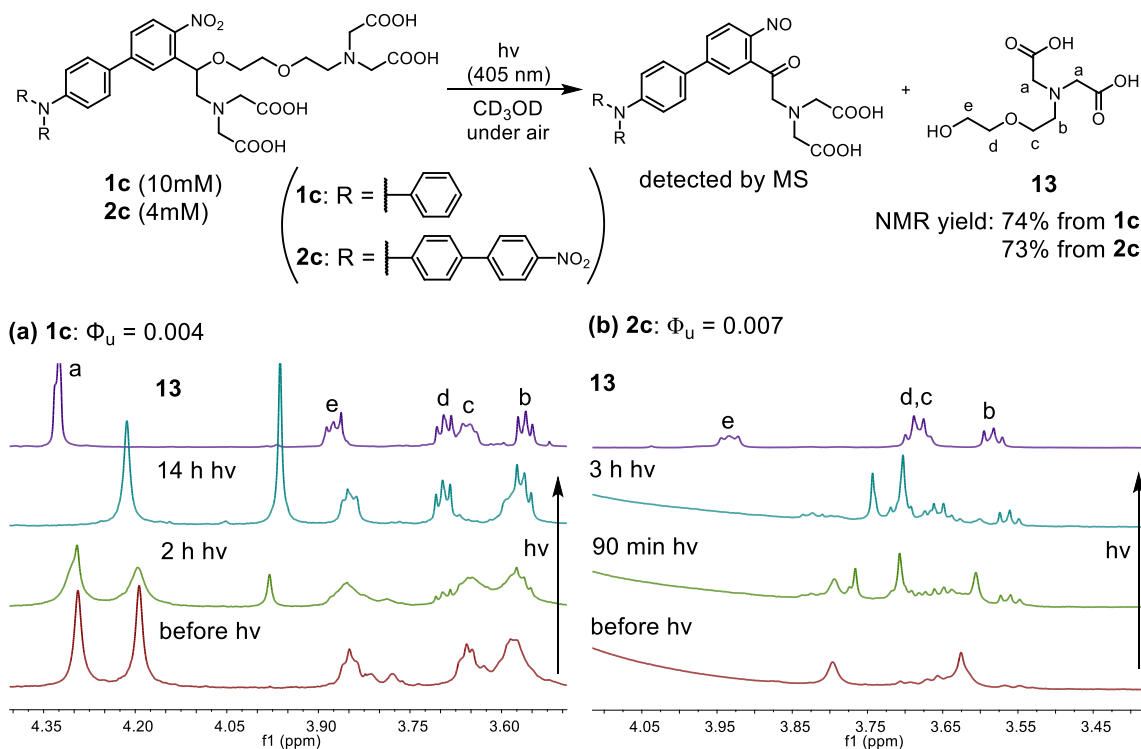


Figure 13. (a) ¹H NMR spectra (400 MHz, 3.5–4.4 ppm) during photolysis at 405 nm in CD₃OD of compound **1c**. (b) ¹H NMR spectra (400 MHz, 3.4–4.1 ppm) during photolysis at 405 nm in CD₃OD/DMSO-d₆ (1:1) of compound **2c**.

2.7. 2P photoreactions of **1b–c** and **2b–c**

2P photoreactions were performed in DMSO for ethyl ester derivatives **1b** and **2b** and in HEPES buffer (pH 7.4) for acid derivatives **1c** and **2c**. The photolysis was carried out at various wavelengths using a femtosecond Ti:sapphire laser (~700 mW) and monitored using HPLC. The decomposition rates of **1b–c** and **2b–c** depended on the irradiation wavelength, as shown in Figures 14a, c and 15a, c. 2P uncaging efficiencies ($\delta_u = \sigma_2 \times \Phi_u$) and 2PA cross-sections σ_2 of these EGTA-substituted compounds were determined by comparing their rate constants with those of 2-(4-nitrophenyl)benzofuran (NPBF)-substituted caged benzoic acid, whose absolute value was reported ($\sigma_2 = 18 \text{ GM at } 720 \text{ nm}$)⁵⁷. The 2P absorption spectra are shown in Figures 14b, d and 15b, d. The maximum values are presented in Table 2.

The octupolar compounds **2b** and **2c** displayed substantial 2P absorption cross-sections (1250 GM at 850 nm and 349 GM at 850 nm, respectively), which aligns with those of the non-substituted molecule **2a**. On the other hand, modest values were observed for the dipolar compounds **1b** and **1c** (294 GM at 800 nm and 100 GM at 790 nm, respectively). The decline of 2P absorption cross-sections in acid derivatives **1c** and **2c** compared to ethyl ester derivatives **1b** and **2b** could be attributed to the protonation of the central nitrogen donor in protic solvent⁵⁸. Subsequently, the 2P uncaging efficiencies of the three-branched molecules **2b** and **2c** (5.1 GM at 850 nm and 2.8 GM at 850 nm, respectively) were greater than those of mono-branched molecules **1b** and **1c** (1.4 GM at 800 nm and 0.3 GM at 790 nm, respectively).

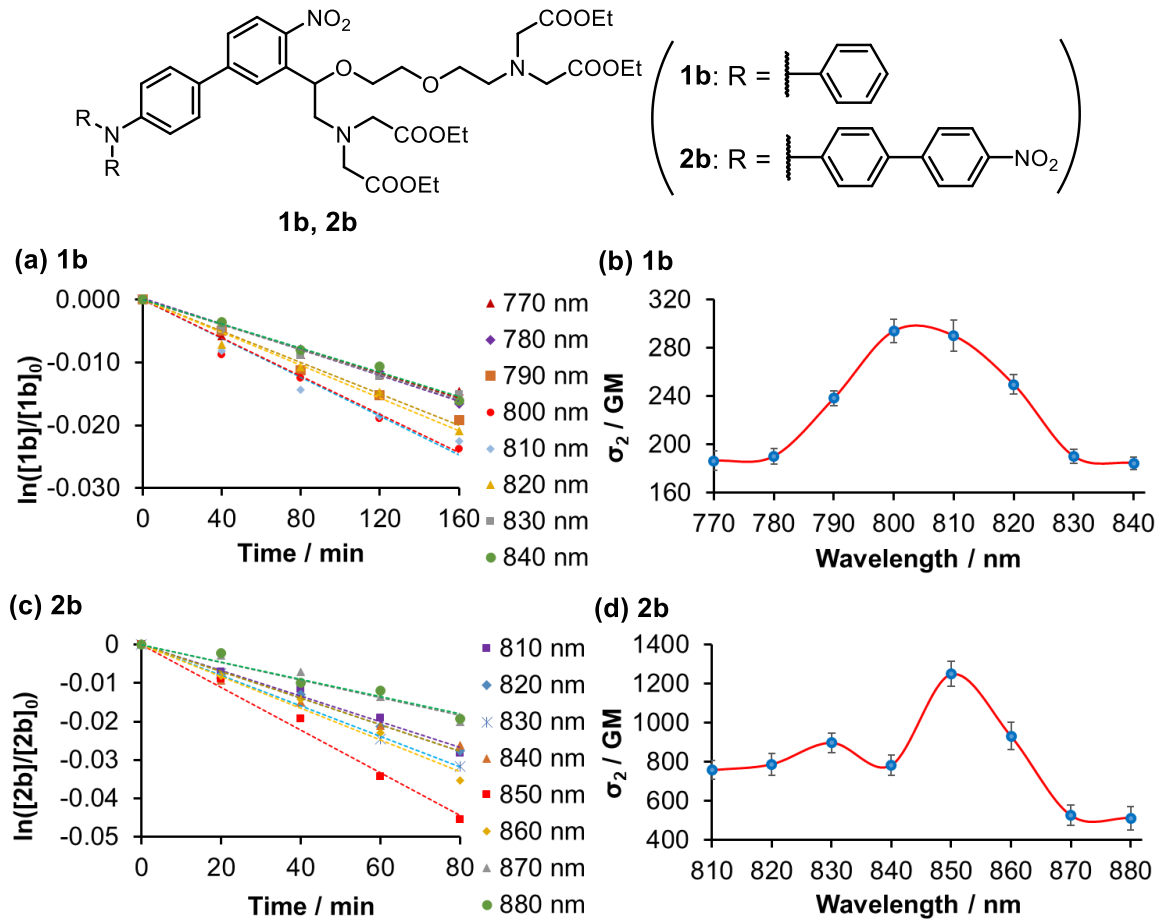


Figure 14. Time profiles of 2P photolysis of (a) **1b** and (c) **2b** in DMSO. 2P absorption spectra of (b) **1b** and (d) **2b**.

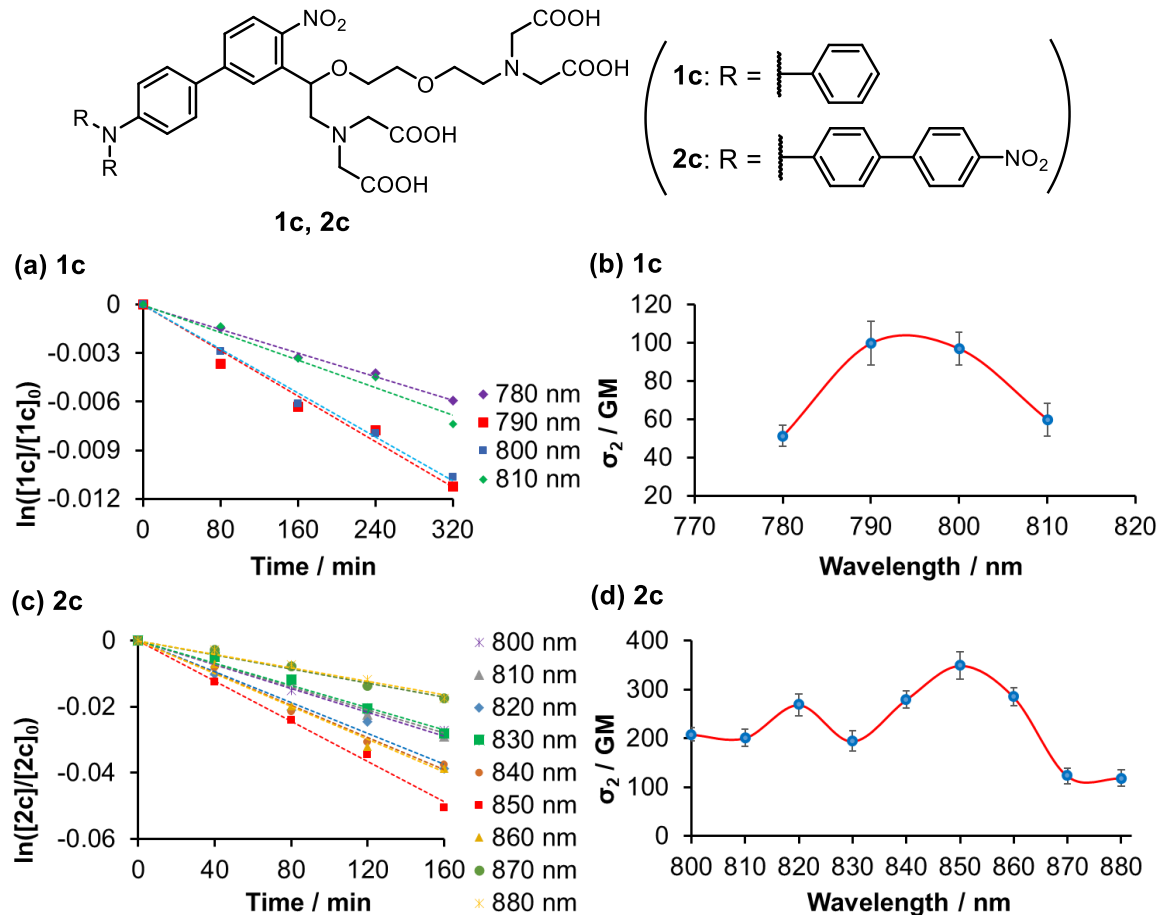


Figure 15. Time profiles of 2P photolysis of (a) **1c** and (c) **2c** in HEPES buffer (pH 7.4). 2P absorption spectra of (b) **1c** and (d) **2c**.

2.8. Uncaging of Ca^{2+} by 1P and 2P excitation

The uncaging of Ca^{2+} by 1P excitation was carried out at 405 nm using an LED lamp. Solutions containing 1.0 mM of either **1c** or **2c**, 100 μM CaCl_2 , and 10 μM fluo-3 in HEPES buffer (100 mM KCl, pH 7.4, 10% DMSO for **2c**) were irradiated and the release of Ca^{2+} was verified by observing the fluorescence emission from Ca^{2+} @fluo-3 (Figure 16). The rise in fluorescence intensity upon irradiation (Figures 16a, c) confirmed the release of Ca^{2+} from Ca^{2+} @**1c** and **2c**. Additionally, the plot of fluorescence intensity at 530 nm versus irradiation

time (Figures 16b, d) demonstrated that the uncaging of Ca^{2+} by 1P excitation from **2c** was faster than that from **1c**.

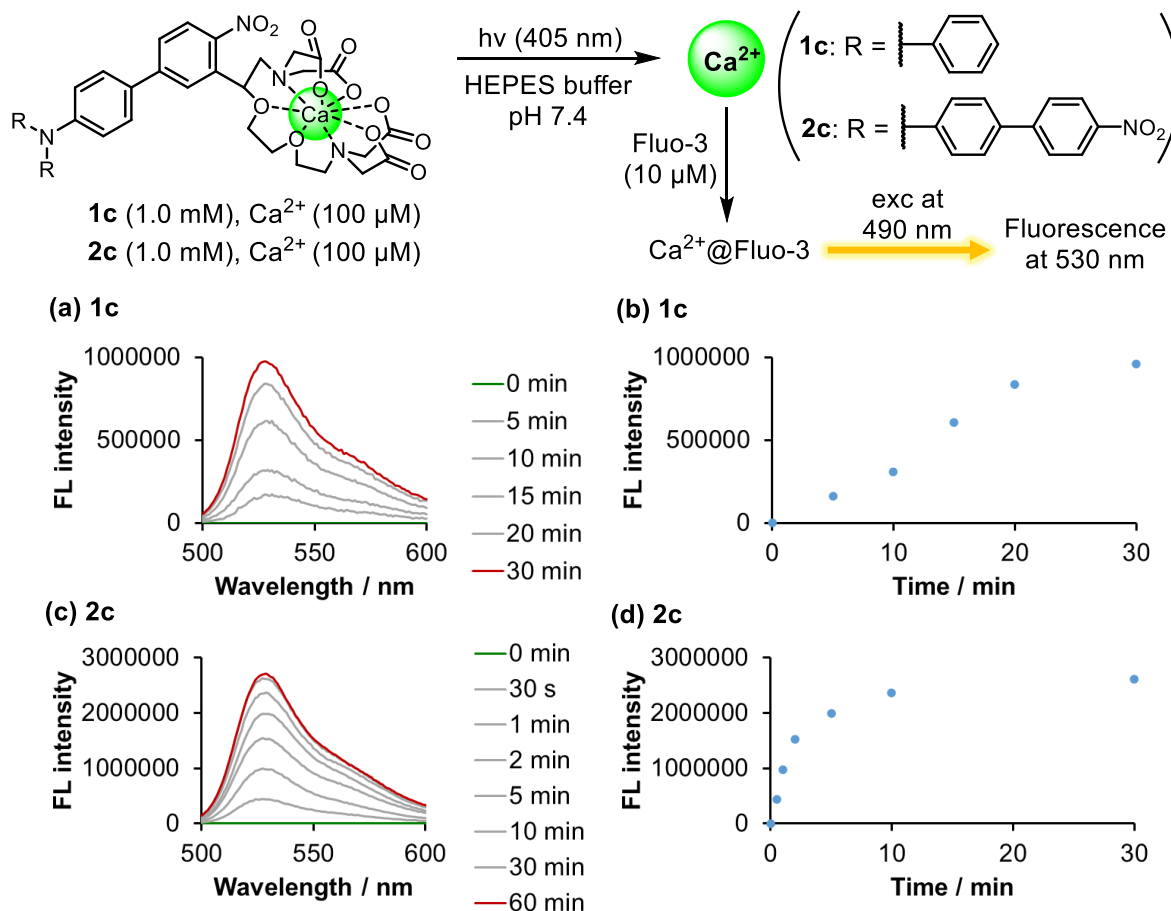


Figure 16. Emission spectra obtained by 405 nm irradiation of solutions containing (a) **1c** (1.0 mM), fluo-3 (10 μM), Ca^{2+} (100 μM) in HEPES buffer (100 mM KCl, pH 7.4); and (c) **2c** (1.0 mM), fluo-3 (10 μM), Ca^{2+} (100 μM) in HEPES buffer (100 mM KCl, pH 7.4, 10% DMSO). Plots of emission intensity at 530 nm vs. irradiation time of (b) **1c**, and (d) **2c**.

The uncaging of Ca^{2+} from Ca^{2+} @**2c** by 2P excitation was carried out at 850 nm using a femtosecond Ti:sapphire laser (~ 700 mW). As depicted in Figure 17, the emission intensity

of $\text{Ca}^{2+}@$ fluo-3 increased during the photolysis, which obviously indicated that Ca^{2+} was successfully released by 2P excitation in the NIR region.

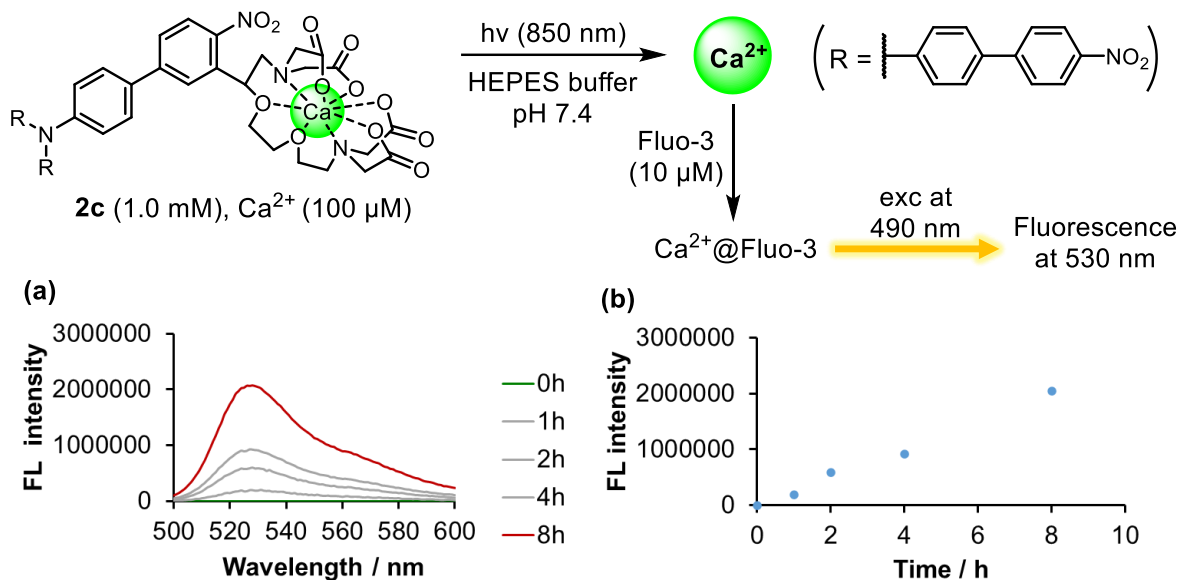


Figure 17. (a) Emission spectra obtained by 850 nm irradiation of solutions containing **2c** (1.0 mM), fluo-3 (10 μM), Ca^{2+} (100 μM) in HEPES buffer (100 mM KCl, pH 7.4, 10% DMSO). (b) Plot of emission intensity at 530 nm vs. irradiation time of **2c**.

2.9. Summary

In this study, we designed and synthesized a novel octupolar chromophore TNBPA **2a**, which consists of a central nitrogen donor and three nitro acceptors attached via biphenylene linkers. This three-branched molecule exhibited significantly large 2P absorption cross-sections, 1330 GM at 730 nm and 900 GM at 820 nm in toluene. With an attractive σ_2/MW value (2.2 GM g^{-1} mol), this compound shows promise as a 2P probe for sensing applications. Moreover, a set of 2P excitable calcium chelators **1b-c** and **2b-c** with dipolar and octupolar structures were synthesized, which showed modest to decent values of 2P absorption cross-

sections (100–1250 GM) and 2P uncaging efficiencies (0.3–5.1 GM). 1P and 2P-induced uncaging of Ca²⁺ was also successfully observed from these calcium chelators.

2.10. Experimental section

General information

Chemical reagents and solvents purchased from commercial suppliers were utilized without additional purification. Silica Gel 60 N (spherical, neutral) with particle sizes of 63–210 μm was used for column chromatography. NMR spectra were recorded using a Bruker ASCEND 400 spectrometer (¹H NMR: 400 MHz, ¹³C NMR: 100 MHz). Chemical shifts (δ) were reported in parts per million (ppm) relative to the residual peak of solvents (CDCl₃: δ 7.26 ppm for ¹H NMR, δ 77.16 ppm for ¹³C NMR; CD₃OD: δ 3.31 ppm for ¹H NMR, δ 49.00 ppm for ¹³C NMR; DMSO-d₆: δ 2.50 ppm for ¹H NMR, δ 39.52 ppm for ¹³C NMR; acetone-d₆: δ 2.05 ppm for ¹H NMR, δ 29.84 ppm for ¹³C NMR). The data was presented in the following format: chemical shift, multiplicity (s = singlet, d = doublet, dd = doublet of doublets, ddd = doublet of doublets of doublets, t = triplet, q = quartet, qd = quartet of doublets, m = multiplet, and br = broad signal), coupling constant J (Hz), and integration. UV-vis spectra were measured with a SHIMADZU UV-3600 Plus spectrophotometer. Fluorescence spectra were measured with a FluoroMax-4 spectrofluorometer. Mass spectrometric data were obtained using a Thermo Fisher Scientific LTQ Orbitrap XL, conducted by the Natural Science Center for Basic Research and Development (N-BARD), Hiroshima University. IR spectra were recorded using a JASCO MCT-6000M spectrometer.

Thermal stability of **1c** and **2c**

Table 3. Thermal stability of **1c** and **2c** in HEPES buffer.

Compound	Solvent	Condition ^a	Decomposition after 24h ^b (%)
1c	HEPES buffer (pH 7.4)	25 °C	1.9 ± 0.1
		37 °C	4.6 ± 0.7
2c	HEPES buffer (pH 7.4, 10% DMSO)	25 °C	1.0 ± 0.3
		37 °C	5.0 ± 0.5

^aUnder air, dark. ^bMonitored by HPLC.

Solubilities of **1c** and **2c**

3.9 mg of compound **1c** and 1.35 mL of HEPES buffer (pH 7.4) were added to a quartz cuvette 5 x 10 mm so that compound **1c** did not dissolve completely. Then, HEPES buffer (pH 7.4) was continuously dropped into the solution, and the procedure was monitored by UV-vis spectroscopic analysis (Figure 18a).

2.3 mg of compound **2c** and 1.05 mL of HEPES buffer (pH 7.4, 10% DMSO) were added to a quartz cuvette 5 x 10 mm so that compound **2c** did not dissolve completely. Then, HEPES buffer (pH 7.4, 10% DMSO) was continuously dropped into the solution, and the procedure was monitored by UV-vis spectroscopic analysis (Figure 18c).

The UV-vis analyses (Figure 18b, d) estimated the solubilities of **1c** and **2c** to be 2.6 and 1.5 mM, respectively.

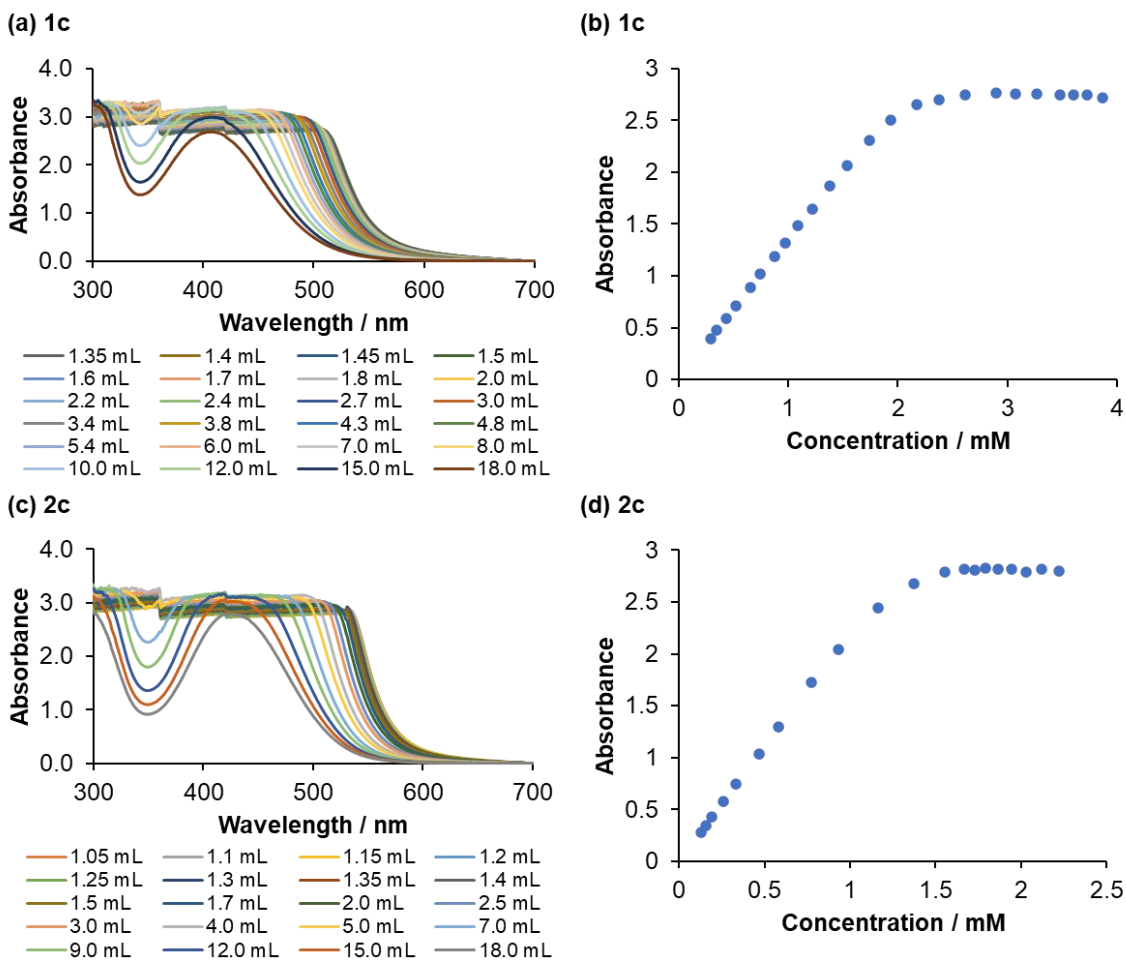


Figure 18. (a) Absorption spectra of **1c** during the addition of HEPES buffer (pH 7.4); b) Plot of absorbance at 530 nm vs. concentration of **1c**; (c) Absorption spectra of **2c** during the addition of HEPES buffer (pH 7.4, 10% DMSO); d) Plot of absorbance at 507 nm vs. concentration of **2c**.

Ca²⁺ binding affinities of **1c** and **2c**

The association constants (K_a) of calcium chelators **1c** and **2c** were determined using the method described in the literature^{9,55}:

$$[\text{Ca}^{2+}]_B/[\text{Ca}^{2+}]_F = K_a ([\text{chelator}]_T - [\text{Ca}^{2+}]_B)$$

Here, $[\text{Ca}^{2+}]_B$ is concentration of Ca²⁺ bound to the chelator, $[\text{Ca}^{2+}]_F$ is concentration of free Ca²⁺, and $[\text{chelator}]_T$ is total concentration of chelator.

$[\text{Ca}^{2+}]_F$ was derived from the fluorescence spectra of fluo-3 ($K_d = 500$ nM), a Ca²⁺-sensitive dye, through titration with CaCl₂ solution:

$$[\text{Ca}^{2+}]_F = K_{d(\text{Fluo-3})} (E_{\text{int}} - E_{\text{min}}) / (E_{\text{max}} - E_{\text{int}})$$

Here, E_{int} is emission intensity at each Ca²⁺ concentration, E_{min} is emission intensity without Ca²⁺, and E_{max} is emission intensity with excess Ca²⁺.

Solutions of chelator (1.0 mM) and fluo-3 (10 μM) in HEPES (10 mM, pH 7.4, 100 mM KCl, 10% DMSO for **2c**) were prepared. The titration with incremental addition of CaCl₂ resulted in emission spectra depicted in Figure 11. The emission intensity at 530 nm remained constant after adding 500 μM and 900 μM of CaCl₂ for **1c** and **2c**, respectively, indicating a saturation point.

Mass spectra of nitrosoketone

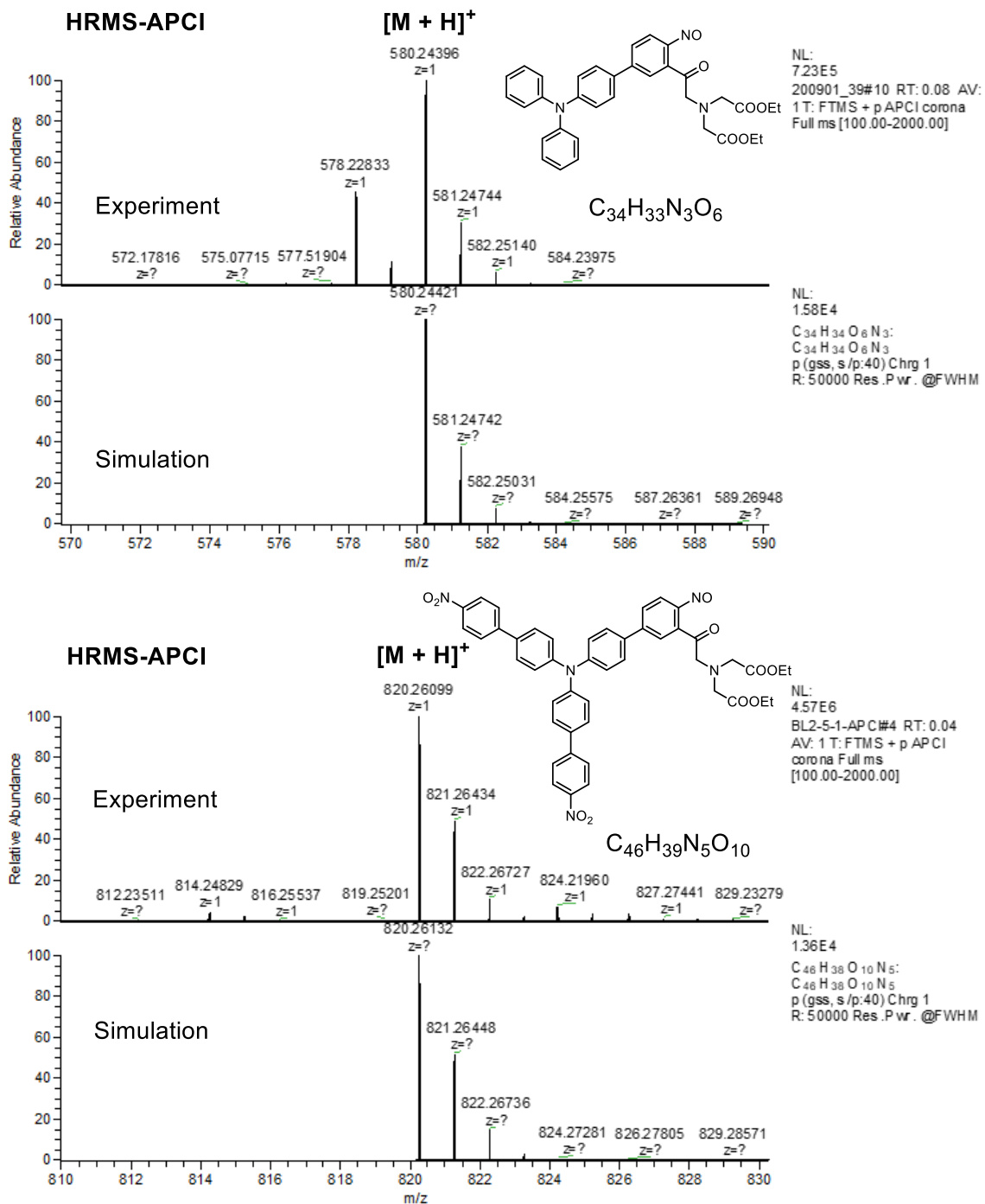
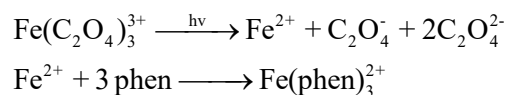


Figure 19. Mass spectra of nitrosoketone.

Chemical actinometer for quantum yield measurement⁵⁹

One of the most reliable and widely used chemical actinometers to measure photon fluxes is ferrioxalate, which, upon irradiation, decomposes according to the following equations:



The number of ferrous ions generated during the photochemical reaction is determined by conversion to the colored tris-phenanthroline complex, which absorbs the light at 510 nm ($\epsilon = 11100 \text{ M}^{-1} \text{ cm}^{-1}$). The complexation between ferric ions and phenanthroline is not considerable, and their complex does not have absorption at 510 nm.

Procedure for measurement:

1. 120 mg of $\text{K}_3[\text{Fe}(\text{C}_2\text{O}_4)_3] \cdot 3\text{H}_2\text{O}$ was dissolved in 20 mL of 0.05 M H_2SO_4 (1).
2. 5 mg of 1,10-phenanthroline monohydrate and 1.12 g of $\text{CH}_3\text{COONa} \cdot 3\text{H}_2\text{O}$ were dissolved in 5 mL of 0.5 M H_2SO_4 (2).
3. 3 mL of solution (1) was taken and irradiated with each light source for specific times. After each irradiation, 0.5 mL of solution (2) was added, and the absorption spectra were measured.
4. The changes in absorbance at 510 nm with respect to irradiation time were used to calculate the amount of light as the equation below:

$$I (\text{mol/s}) = \frac{\text{moles of Fe}^{2+}}{\Phi_\lambda \times t \times F} = \frac{V_1 \times V_3 \times \Delta A_{510}}{10^3 \times V_2 \times l \times \epsilon_{510} \times \Phi_\lambda \times t}$$

V_1 : irradiated volume (3 mL)

V_2 : aliquot of irradiated solution taken for determining ferrous ions (3 mL)

V_3 : final volume (3.5 mL)

ΔA_{510} : absorbance difference between solutions before and after irradiation

l : optical pathlength of irradiation cell (1 cm)

ϵ_{510} : molar extinction coefficient of $\text{Fe}(\text{phen})_3^{2+}$ at 510 nm ($11100 \text{ M}^{-1}\text{cm}^{-1}$)

Φ_λ : quantum yield of ferrous ions generation at the irradiation wavelength ($\Phi_{365} = 1.21$, $\Phi_{405} = 1.14$, $\Phi_{320} = 1.24$)

t : irradiation time

F : mean function of light absorbed by the ferrioxalate solution

Table 4. Photon number of LED lamp 405 nm.

	Time (s)	ΔA_{510}	I (mol/s)	I_{avg} (mol/s)
LED lamp 405 nm	0.5	0.28	1.6×10^{-7}	
	1	0.59	1.6×10^{-7}	1.6×10^{-7}
	1.5	0.86	1.6×10^{-7}	

2P absorption spectrum of 2a

Two-photon-excited fluorescence (2PEF) technique was employed to determine the 2PA spectrum of compound **1** in solution phase using Fluorescein (0.1 N NaOH solution) as the standard^{60,61}. The experimental setup is illustrated in Figure 20. In brief, the excitation light source was a mode-locked Ti:Sapphire laser system (Chameleon Ultra II, Coherent Inc.) which delivers ~140 fs pulses with the repetition rate of 80 MHz and the beam diameter of 2 mm. The wavelength range utilized for this experiment was 680-1080 nm and the intensity level of the excitation beam was carefully controlled by the combination of a $\lambda/2$ wave plate and a polarizer in order to avoid the occurrence of either saturation of absorption or

photodegradation within the tested sample during the measurement. To minimize the effects of re-absorption, the excitation beam was focused as close as possible to the wall of the quartz cell (10 mm×10 mm cuvette) and the 2PEF emission was collected and induced by an optical fiber into a CCD imaging spectrometer (QE-Pro, Ocean Optics) for the spectra recording.

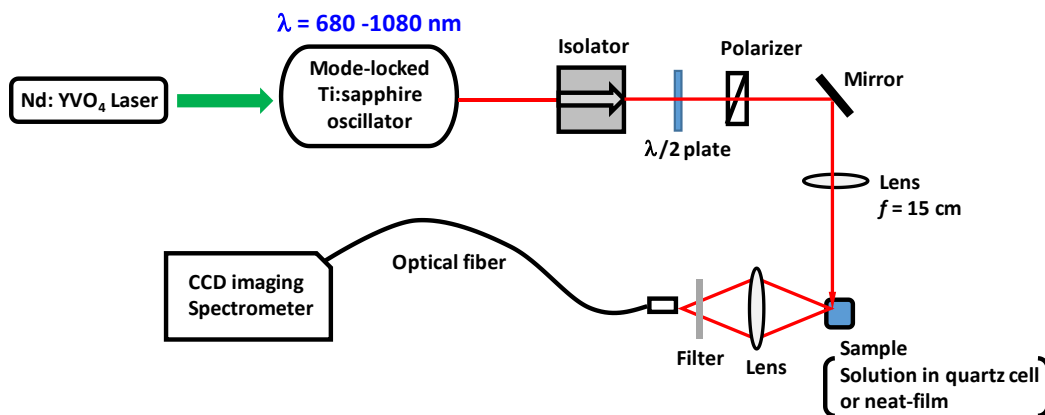


Figure 20. Optical setup for 2PA spectrum measurement.

2P uncaging efficiencies of 1b–c and 2b–c

The mode-locked Ti:sapphire laser (Mai Tai, Spectra Physic Inc.), which delivers ~80 fs pulses with the repetition rate of 80 MHz, was used as the excitation light source for the measurement of 2P uncaging efficiencies of **1b–c** and **2b–c**. The excitation wavelength range performed in these experiments was 770 – 880 nm. Three mirrors and a lens on top of the sample were used to deliver and focus the laser beam on the sample (Figure 21).

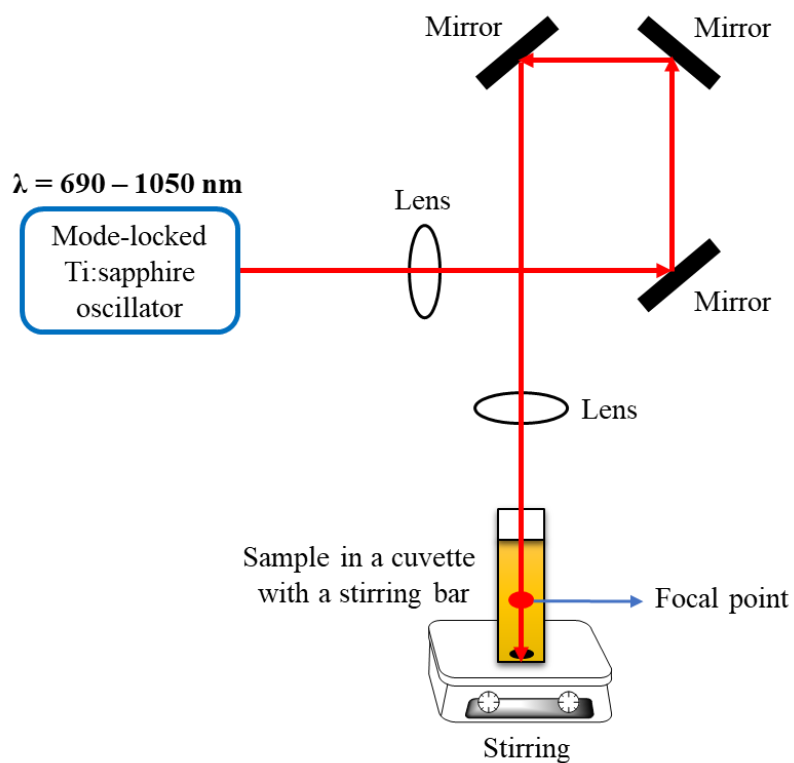
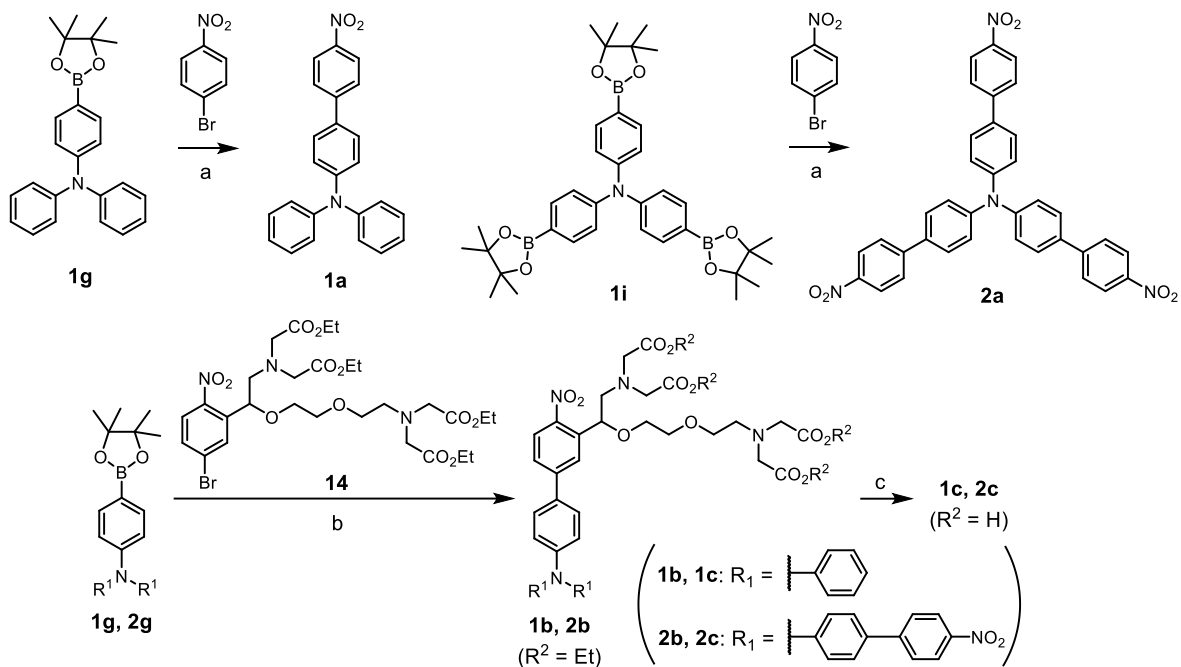


Figure 21. Optical setup for 2P uncaging efficiency measurement.

Synthesis



Reagents and conditions: (a) Pd(PPh₃)₄, K₃PO₄, 1,4-dioxane/H₂O, 80°C, overnight, 80% for **1a** and 82% for **2a**; (b) Pd(PPh₃)₄, K₃PO₄, 1,4-dioxane/H₂O, 60°C, 3h, 77% for **1b** and 63% for **2b**; (c) KOH, MeOH, 60°C, 3h, 92% for **1c**; LiOH.H₂O, THF/EtOH/H₂O, 25°C, overnight, 89% for **2c**.

4'-nitro-N,N-diphenyl-[1,1'-biphenyl]-4-amine⁶² (**1a**). In a round-bottom flask, **1g**⁶³ (1.0 mmol), 1-bromo-4-nitrobenzene (1.5 mmol), Pd(PPh₃)₄ (0.1 mmol) and K₃PO₄ (3.0 mmol) was mixed in 1,4-dioxane/H₂O (2:1, 9.0 mL). The reaction mixture was degassed by bubbling with N₂ and stirred in an oil bath at 80°C for 4h. The solvent was removed under reduced pressure, and the residue was purified by silica gel column chromatography (hexane/EtOAc = 95:5) to give the desired product **1a** (80%) as a red solid. ¹H NMR (400 MHz, CDCl₃) δ

8.27 (d, $J = 8.8$ Hz, 2H), 7.70 (d, $J = 8.8$ Hz, 2H), 7.51 (d, $J = 8.8$ Hz, 2H), 7.34 – 7.27 (m, 4H), 7.18 – 7.12 (m, 6H), 7.12 – 7.07 (m, 2H). mp 155-157 °C.

tris(4'-nitro-[1,1'-biphenyl]-4-yl)amine (**2a**). In a round-bottom flask, compound **1i**⁶⁴ (1.0 mmol), 1-bromo-4-nitrobenzene (4.0 mmol), Pd(PPh₃)₄ (0.1 mmol) and K₃PO₄ (6.0 mmol) was mixed in 1,4-dioxane/H₂O (2:1, 9.0 mL). The reaction mixture was degassed by bubbling with N₂ for 20 min and stirred in an oil bath at 80°C for 4h. The solvent was removed under reduced pressure, and the residue was purified by silica gel column chromatography (hexane/CH₂Cl₂ = 1:2) to give the desired product **2a** (82%) as a red solid. ¹H NMR (400 MHz, CDCl₃) δ 8.30 (d, $J = 8.8$ Hz, 6H), 7.74 (d, $J = 8.8$ Hz, 6H), 7.61 (d, $J = 8.8$ Hz, 6H), 7.30 (d, $J = 8.8$ Hz, 6H). ¹³C {¹H} NMR (100 MHz, CDCl₃) δ 147.8, 147.1, 146.8, 133.9, 128.7, 127.3, 124.9, 124.4. IR (KBr, cm⁻¹) ν 3036, 2444, 1923, 1589, 1509, 1483, 1397, 1332, 1189, 1109, 1004, 854, 829, 755, 728, 693, 655, 553. HRMS (APCI) m/z [M]⁻ calcd for C₃₆H₂₄N₄O₆ 608.1701; found 608.1695. mp > 290°C.

Diethyl 5-(4'-(diphenylamino)-4-nitro-[1,1'-biphenyl]-3-yl)-3,12-bis(2-ethoxy-2-oxoethyl)-6,9-dioxa-3,12-diazatetradecanedioate (**1b**). In a round-bottom flask, compound **14**⁴⁰ (116.1 mg, 0.17 mmol), **1g**⁶³ (1.2 mmol), Pd(PPh₃)₄ (0.1 mmol) and K₃PO₄ (3.0 mmol) was mixed in 1,4-dioxane/H₂O (2:1, 9.0 mL). The reaction mixture was degassed by bubbling with N₂ and stirred in an oil bath at 60°C for 3h. The solvent was removed under reduced pressure, and the residue was purified by silica gel column chromatography (hexane/EtOAc = 2:1) to give the desired product **1b** (77%) as an orange oil. ¹H NMR (400 MHz, CDCl₃) δ 8.05 (d, $J = 8.6$ Hz, 1H), 7.98 (d, $J = 2.0$ Hz, 1H), 7.57 (dd, $J = 8.6, 2.0$ Hz, 1H), 7.53 (d, $J = 8.8$ Hz, 2H), 7.33 – 7.27 (m, 4H), 7.18 – 7.12 (m, 6H), 7.11 – 7.05 (m, 2H), 5.30 (dd, $J = 7.7,$

2.4 Hz, 1H), 4.16 (q, $J = 7.1$ Hz, 4H), 4.09 (q, $J = 7.1$ Hz, 4H), 3.83 – 3.71 (m, 4H), 3.60 – 3.44 (m, 10H), 3.18 – 3.04 (m, 2H), 2.94 – 2.81 (m, 2H), 1.26 (t, $J = 7.1$ Hz, 6H), 1.21 (t, $J = 7.1$ Hz, 6H). $^{13}\text{C}\{^1\text{H}\}$ NMR (100 MHz, CDCl_3) δ 171.8, 171.3, 148.8, 147.3, 146.4, 146.0, 137.6, 131.7, 129.4, 128.1, 126.2, 125.7, 125.5, 125.0, 123.6, 123.0, 78.2, 70.3, 68.9, 61.3, 60.4, 55.9, 55.7, 53.7, 14.3, 14.2. IR (KBr, cm^{-1}) ν 2980, 2906, 2872, 1744, 1590, 1516, 1490, 1331, 1280, 1195, 1095, 1030, 827, 757, 731, 698, 623, 590, 529. HRMS (ESI) m/z [$\text{M} + \text{Na}$] $^+$ calcd for $\text{C}_{46}\text{H}_{56}\text{O}_{12}\text{N}_4\text{Na}$ 879.3787; found 879.3780.

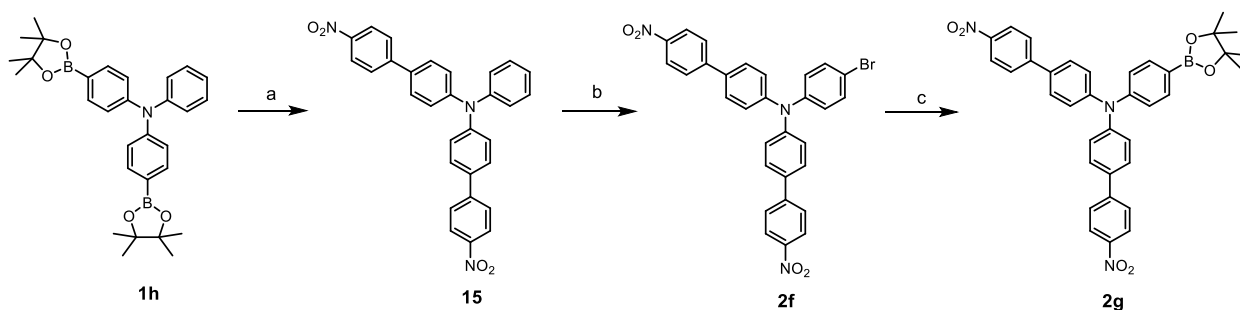
Diethyl 5-(4'-(bis(4'-nitro-[1,1'-biphenyl]-4-yl)amino)-4-nitro-[1,1'-biphenyl]-3-yl)-3,12-bis(2-ethoxy-2-oxoethyl)-6,9-dioxo-3,12-diazatetradecanedioate (**2b**). In a round-bottom flask, compound **14**⁴⁰ (1.0 mmol), **2g** (1.2 mmol), $\text{Pd}(\text{PPh}_3)_4$ (0.1 mmol) and K_3PO_4 (3.0 mmol) was mixed in 1,4-dioxane/ H_2O (2:1, 9.0 mL). The reaction mixture was degassed by bubbling with N_2 and stirred in an oil bath at 60°C for 3h. The solvent was removed under reduced pressure, and the residue was purified by silica gel column chromatography (hexane/ $\text{EtOAc} = 1:1$) to give the desired product **2b** (63%) as a red oil. ^1H NMR (400 MHz, CDCl_3) δ 8.30 (d, $J = 8.8$ Hz, 4H), 8.08 (d, $J = 8.5$ Hz, 1H), 8.02 (d, $J = 1.7$ Hz, 1H), 7.75 (d, $J = 8.8$ Hz, 4H), 7.67 – 7.54 (m, 7H), 7.34 – 7.27 (m, 6H), 5.31 (dd, $J = 7.5, 2.5$ Hz, 1H), 4.16 (q, $J = 7.1$ Hz, 4H), 4.07 (q, $J = 7.1$ Hz, 4H), 3.83 – 3.72 (m, 4H), 3.61 – 3.46 (m, 10H), 3.19 – 3.04 (m, 2H), 2.97 – 2.79 (m, 2H), 1.26 (t, $J = 7.1$ Hz, 6H), 1.19 (t, $J = 7.1$ Hz, 6H). $^{13}\text{C}\{^1\text{H}\}$ NMR (100 MHz, CDCl_3) δ 171.9, 171.4, 147.9, 147.7, 147.0, 146.9, 146.8, 145.7, 137.9, 134.0, 133.7, 128.7, 128.6, 127.3, 126.7, 126.1, 125.7, 125.0, 124.8, 124.4, 78.4, 70.4, 69.1, 61.5, 60.5, 56.0, 55.9, 53.8, 14.41, 14.35. IR (KBr, cm^{-1}) ν 2980, 2905, 2872, 1740,

1591, 1515, 1485, 1340, 1285, 1194, 1110, 1030, 854, 829, 757, 729, 696, 553. HRMS (ESI) m/z $[M + Na]^+$ calcd for $C_{58}H_{62}O_{16}N_6Na$ 1121.4115; found 1121.4102.

3,12-bis(carboxymethyl)-5-(4'-(diphenylamino)-4-nitro-[1,1'-biphenyl]-3-yl)-6,9-dioxo-3,12-diazatetradecanedioic acid (**1c**). To a solution of **1b** (0.1 mmol) in MeOH (10 mL) was added KOH (0.5 mmol), and the reaction mixture was stirred in an oil bath at 60°C for 3h. The solvent was removed under reduced pressure, and the residue was acidified with 1N HCl to pH 1. The dark red solid was collected and dried to give the desired product **1c** (92%). 1H NMR (400 MHz, CD_3OD) δ 8.21 (d, $J = 8.4$ Hz, 1H), 8.06 (s, 1H), 7.87 (d, $J = 8.4$ Hz, 1H), 7.67 (d, $J = 7.9$ Hz, 2H), 7.37 – 7.27 (m, 4H), 7.16 – 7.07 (m, 8H), 5.68 (d, $J = 8.0$ Hz, 1H), 4.52 (s, 4H), 4.24 (s, 4H), 3.99 – 3.58 (m, 10H). $^{13}C\{^1H\}$ NMR (100 MHz, CD_3OD) δ 168.4, 167.2, 149.2, 147.2, 146.6, 146.4, 133.7, 130.8, 129.3, 127.9, 127.0, 126.0, 125.6, 125.0, 123.7, 122.2, 73.8, 69.9, 68.1, 65.4, 59.7, 55.7, 55.3, 55.2. IR (KBr, cm^{-1}) ν 3424, 3033, 2960, 1945, 1737, 1588, 1517, 1490, 1402, 1332, 1282, 1108, 1030, 900, 849, 826, 756, 697, 618, 528. HRMS (APCI) m/z $[M - H]^+$ calcd for $C_{38}H_{41}O_{12}N_4$ 745.2716; found 745.2717. mp 162–164°C.

5-(4'-(bis(4'-nitro-[1,1'-biphenyl]-4-yl)amino)-4-nitro-[1,1'-biphenyl]-3-yl)-3,12-bis(carboxymethyl)-6,9-dioxo-3,12-diazatetradecanedioic acid (**2c**). To a solution of **2b** (0.1 mmol) in THF/EtOH/ H_2O (3:1:1, 10 mL) was added $LiOH \cdot H_2O$ (2.0 mmol), and the reaction mixture was stirred at room temperature overnight. The solution was acidified with 1N HCl to pH 1, and the solvent was removed under reduced pressure. The residue was washed with water, and the orange solid was collected and dried to give the desired product **2c** (89%). 1H NMR (400 MHz, $DMSO-d_6$) δ 8.29 (d, $J = 8.7$ Hz, 4H), 8.10 (d, $J = 8.6$ Hz, 1H), 8.01 (s,

1H), 7.97 (d, $J = 8.7$ Hz, 4H), 7.89 – 7.75 (m, 7H), 7.34 – 7.18 (m, 6H), 5.15 (d, $J = 6.8$ Hz, 1H), 3.53 – 3.35 (m, 14H), 3.06 – 2.94 (m, 2H), 2.80 – 2.66 (m, 2H). $^{13}\text{C}\{^1\text{H}\}$ NMR (100 MHz, DMSO- d_6) δ 173.5, 172.9, 147.7, 147.5, 147.0, 146.7, 146.3, 144.9, 137.4, 133.4, 133.0, 129.1, 127.7, 126.5, 126.4, 126.0, 125.1, 124.8, 124.6, 77.5, 70.0, 69.5, 68.9, 61.1, 56.0, 55.8, 53.7. IR (KBr, cm^{-1}) ν 3423, 3035, 2959, 1921, 1735, 1591, 1516, 1484, 1341, 1285, 1196, 1110, 1005, 899, 854, 828, 757, 727, 695, 554. HRMS (ESI) m/z $[\text{M} - \text{H}]^-$ calcd for $\text{C}_{50}\text{H}_{45}\text{O}_{16}\text{N}_6$ 985.2898; found 985.2883. mp 157–159°C.



Reagents and conditions: (a) $\text{Pd}(\text{PPh}_3)_4$, K_3PO_4 , 1,4-dioxane/ H_2O , 80°C, 4h, 61% for **15**; (b) NBS, DMF, 0–25°C, overnight, 97% for **2f**; (c) bis(pinacolato)diboron, AcOK, $\text{Pd}(\text{dppf})\text{Cl}_2$, 1,4-dioxane, 80°C, overnight, 94% for **2g**.

4'-nitro-N-(4'-nitro-[1,1'-biphenyl]-4-yl)-N-phenyl-[1,1'-biphenyl]-4-amine (**15**). In a round-bottom flask, **1h**⁶⁵ (1.0 mmol), 1-bromo-4-nitrobenzene (2.5 mmol), $\text{Pd}(\text{PPh}_3)_4$ (0.1 mmol) and K_3PO_4 (4.5 mmol) was mixed in 1,4-dioxane/ H_2O (2:1, 9 mL). The reaction mixture was degassed by bubbling with N_2 and stirred in an oil bath at 80°C for 4h. The solvent was removed under reduced pressure, and the residue was purified by silica gel column chromatography (hexane/ $\text{CH}_2\text{Cl}_2 = 2:1$) to give the desired product **15** (61%) as a red solid. ^1H NMR (400 MHz, CDCl_3) δ 8.29 (d, $J = 8.8$ Hz, 4H), 7.72 (d, $J = 8.8$ Hz, 4H),

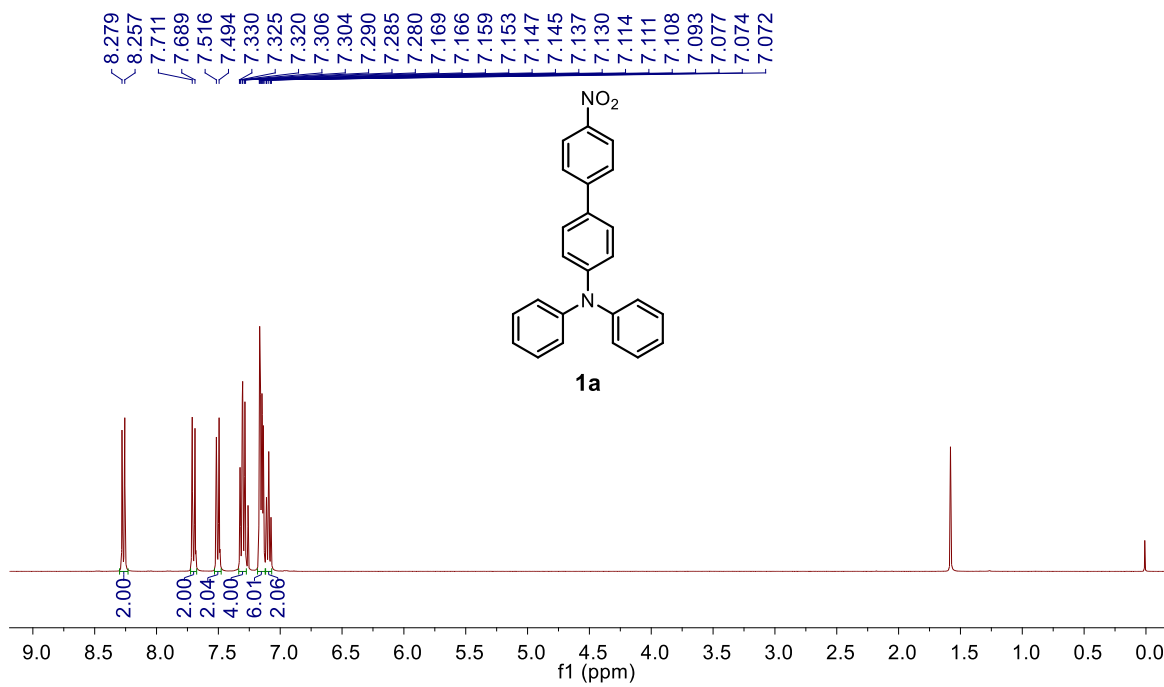
7.55 (d, $J = 8.8$ Hz, 4H), 7.38 – 7.33 (m, 2H), 7.26 – 7.19 (m, 6H), 7.18 – 7.14 (m, 1H). $^{13}\text{C}\{^1\text{H}\}$ NMR (100 MHz, CDCl_3) δ 148.2, 146.8, 146.7, 132.8, 129.7, 128.3, 127.0, 125.7, 124.5, 124.2, 124.0. HRMS (APCI) m/z $[\text{M} + \text{H}]^+$ calcd for $\text{C}_{30}\text{H}_{22}\text{O}_4\text{N}_3$ 488.1605; found 488.1603.

N-(4-bromophenyl)-4'-nitro-N-(4'-nitro-[1,1'-biphenyl]-4-yl)-[1,1'-biphenyl]-4-amine (**2f**). To a solution of **15** (1.0 mmol) in DMF (100 mL) at 0°C was added NBS (1.0 mmol) portionwise. The reaction mixture was stirred at room temperature overnight. The solution was quenched with ice water and extracted with EtOAc. The organic layer was washed with water, dried over Na_2SO_4 and the solvent was removed under reduced pressure to give the desired product **2f** (97%) as a red solid. ^1H NMR (400 MHz, CDCl_3) δ 8.29 (d, $J = 8.8$ Hz, 4H), 7.72 (d, $J = 8.8$ Hz, 4H), 7.56 (d, $J = 8.8$ Hz, 4H), 7.44 (d, $J = 8.8$ Hz, 2H), 7.22 (d, $J = 8.8$ Hz, 4H), 7.08 (d, $J = 8.8$ Hz, 2H). $^{13}\text{C}\{^1\text{H}\}$ NMR (100 MHz, CDCl_3) δ 147.7, 146.8, 146.7, 145.9, 133.3, 132.7, 128.5, 127.1, 126.7, 124.24, 124.23, 116.9. IR (KBr, cm^{-1}) ν 3034, 1590, 1509, 1484, 1399, 1340, 1285, 1191, 1109, 1073, 1005, 959, 854, 824, 756, 733, 724, 708, 692, 655, 559, 518. HRMS (APCI) m/z $[\text{M}]^-$ calcd for $\text{C}_{30}\text{H}_{20}\text{O}_4\text{N}_3\text{Br}$ 565.0643; found 565.0640. mp $230\text{--}232^\circ\text{C}$.

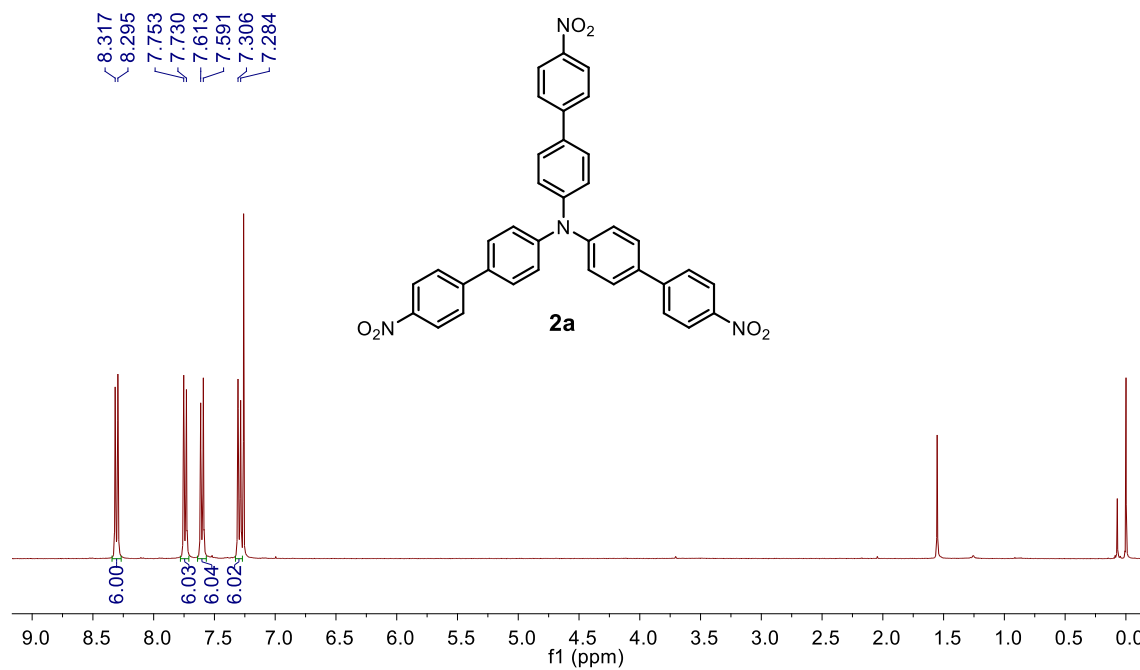
4'-nitro-N-(4'-nitro-[1,1'-biphenyl]-4-yl)-N-(4-(4,4,5,5-tetramethyl-1,3,2-dioxaborolan-2-yl)phenyl)-[1,1'-biphenyl]-4-amine (**2g**). In a round-bottom flask, **2f** (1.0 mmol), bis(pinacolato)diboron (1.2 mmol), AcOK (4.5 mmol) and $\text{Pd}(\text{dppf})\text{Cl}_2$ (0.1 mmol) was mixed in 1,4-dioxane (10 mL). The reaction mixture was degassed by bubbling with N_2 and stirred in an oil bath at 80°C overnight. The reaction mixture was filtered, and the filtrate was removed under reduced pressure. The residue was purified by silica gel column

chromatography (hexane/EtOAc = 10:1) to give the desired product **2g** (94%) as an orange solid. ^1H NMR (400 MHz, CDCl_3) δ 8.29 (d, $J = 8.8$ Hz, 4H), 7.77 (d, $J = 8.8$ Hz, 2H), 7.73 (d, $J = 8.8$ Hz, 4H), 7.56 (d, $J = 8.8$ Hz, 4H), 7.24 (d, $J = 8.8$ Hz, 4H), 7.16 (d, $J = 8.8$ Hz, 2H), 1.36 (s, 12H). $^{13}\text{C}\{^1\text{H}\}$ NMR (100 MHz, CDCl_3) δ 149.4, 147.9, 146.8, 136.2, 133.3, 128.4, 127.1, 124.7, 124.2, 123.7, 83.8, 67.1, 24.9. IR (KBr, cm^{-1}) ν 2976, 1593, 1516, 1485, 1389, 1340, 1284, 1191, 1144, 1109, 1088, 1005, 962, 855, 834, 757, 729, 695, 662, 557, 530. HRMS (APCI) m/z $[\text{M} + \text{H}]^+$ calcd for $\text{C}_{36}\text{H}_{33}\text{O}_6\text{N}_3\text{B}$ 614.2457; found 614.2459. mp 184–186°C.

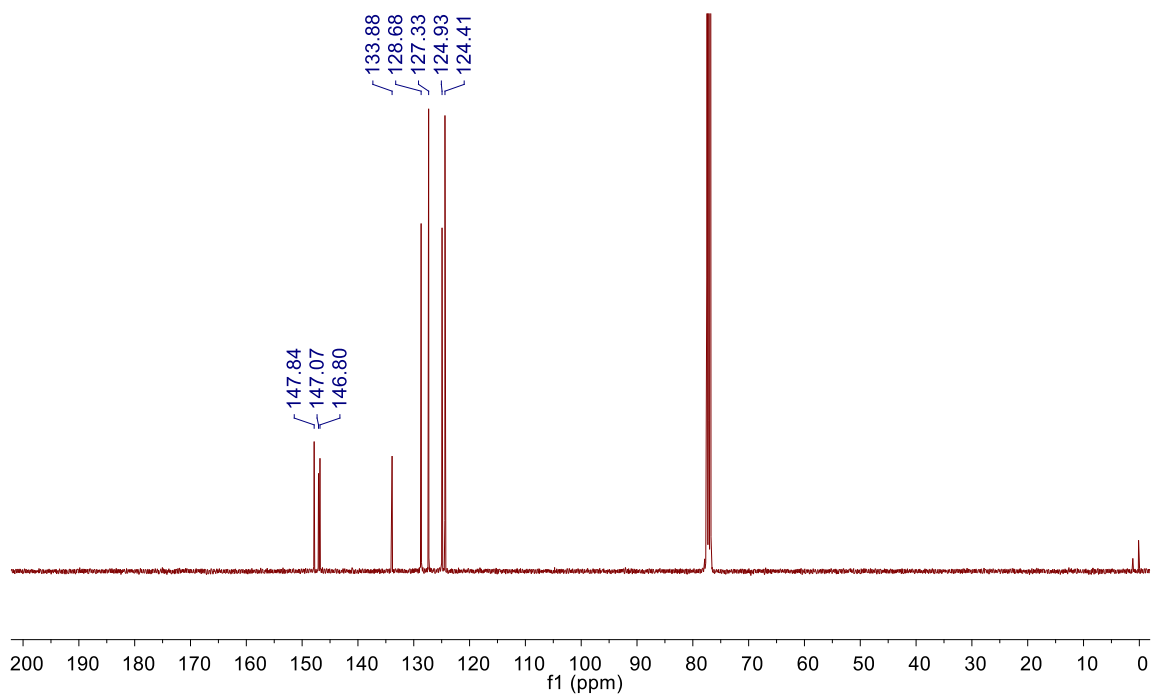
^1H NMR (400MHz, CDCl_3)



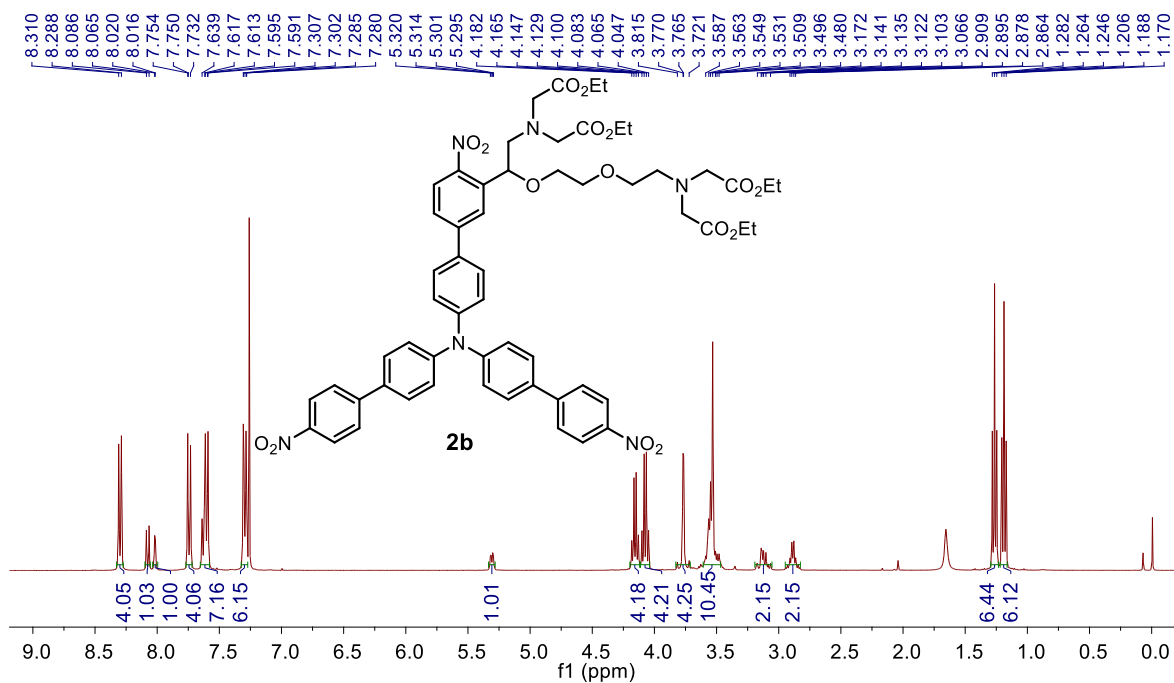
^1H NMR (400MHz, CDCl_3)



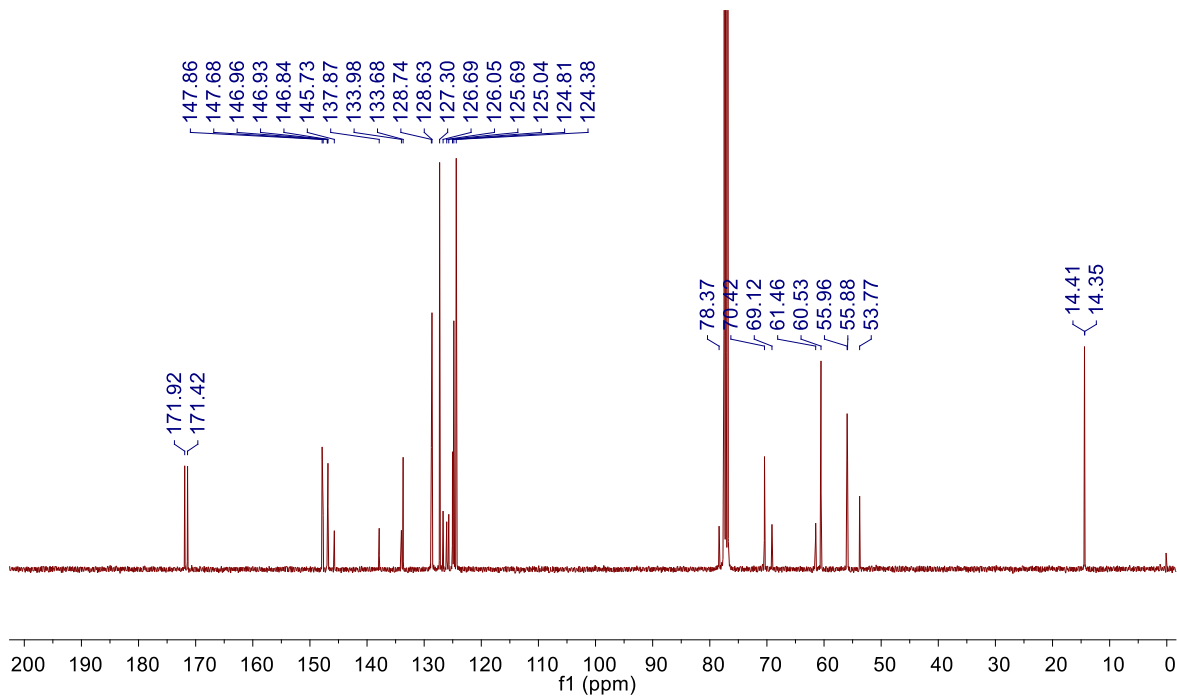
$^{13}\text{C}\{^1\text{H}\}$ NMR (100MHz, CDCl_3)



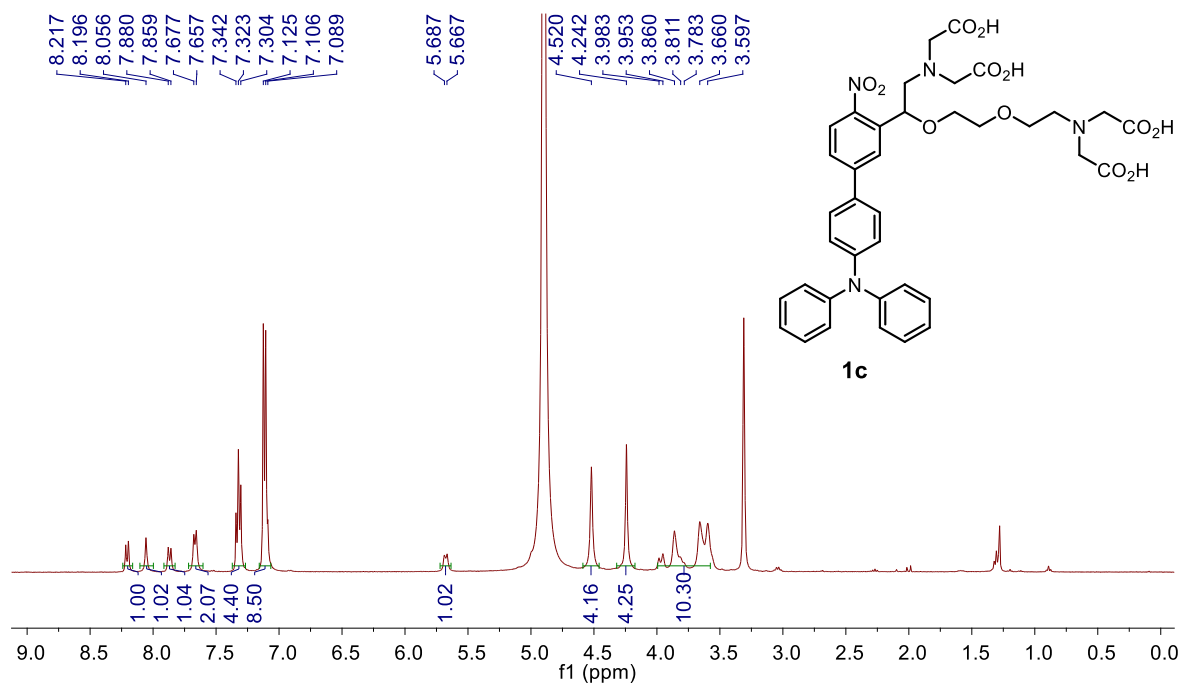
^1H NMR (400MHz, CDCl_3)



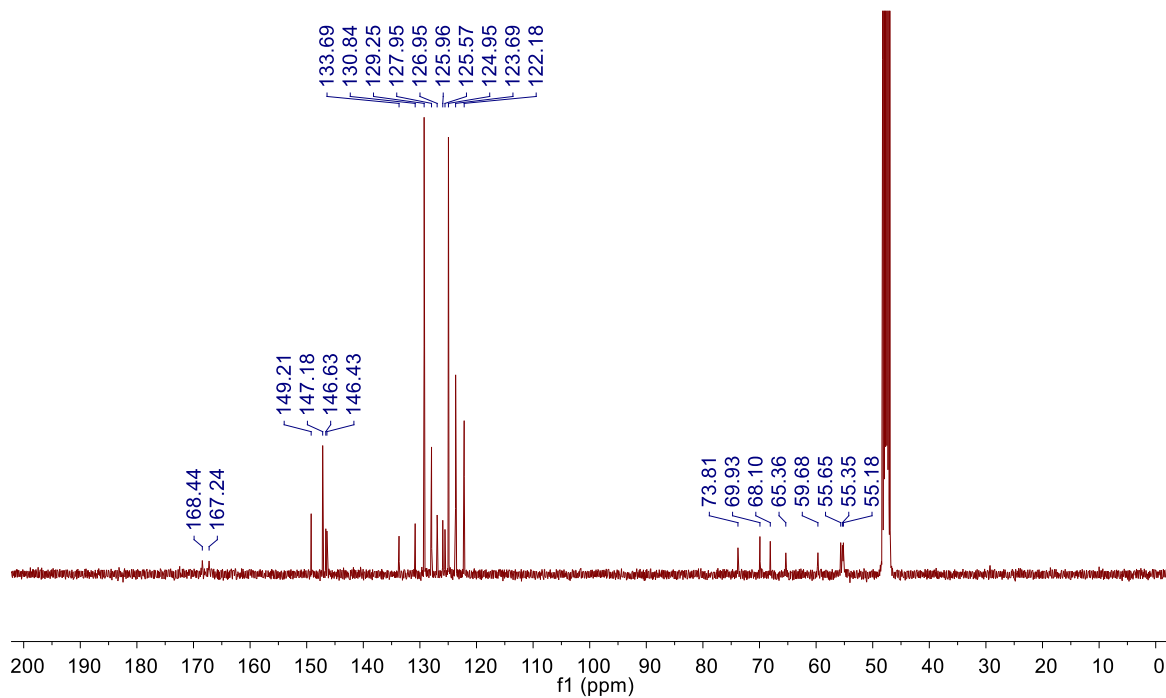
$^{13}\text{C}\{^1\text{H}\}$ NMR (100MHz, CDCl_3)



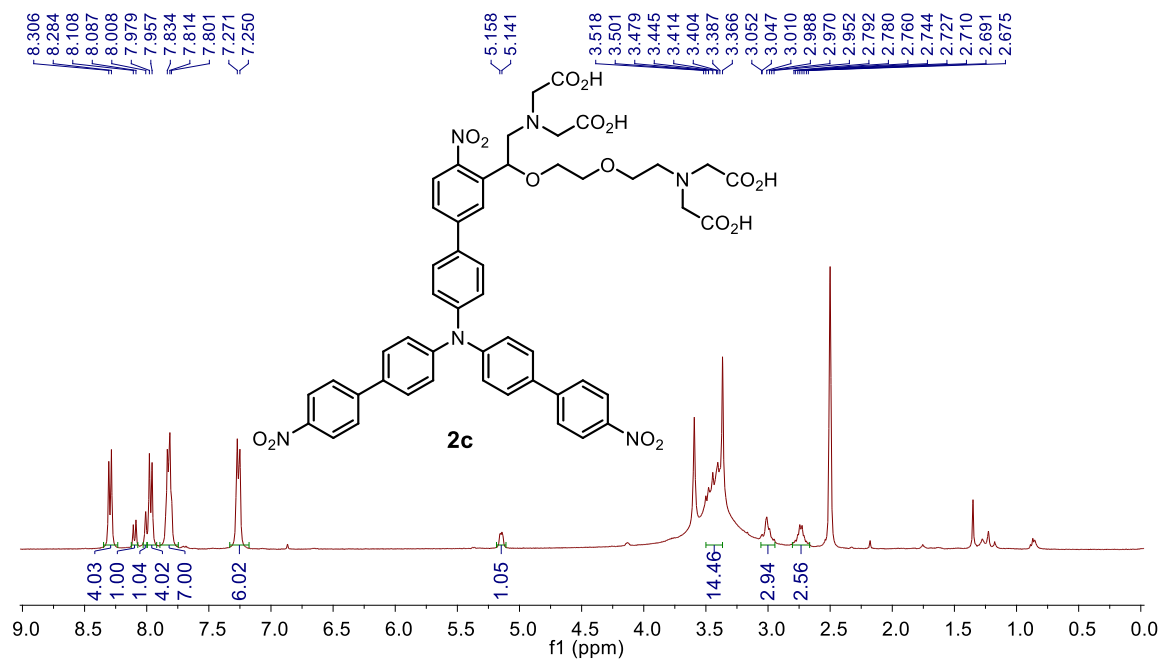
^1H NMR (400MHz, CD_3OD)



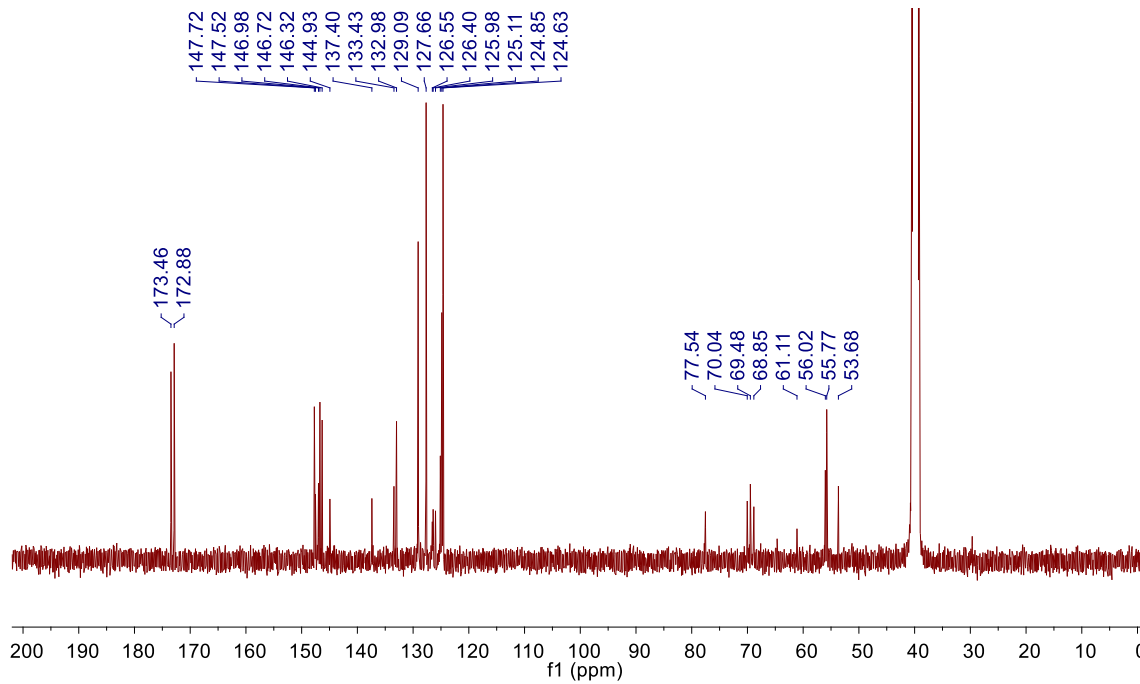
$^{13}\text{C}\{^1\text{H}\}$ NMR (100MHz, CD_3OD)



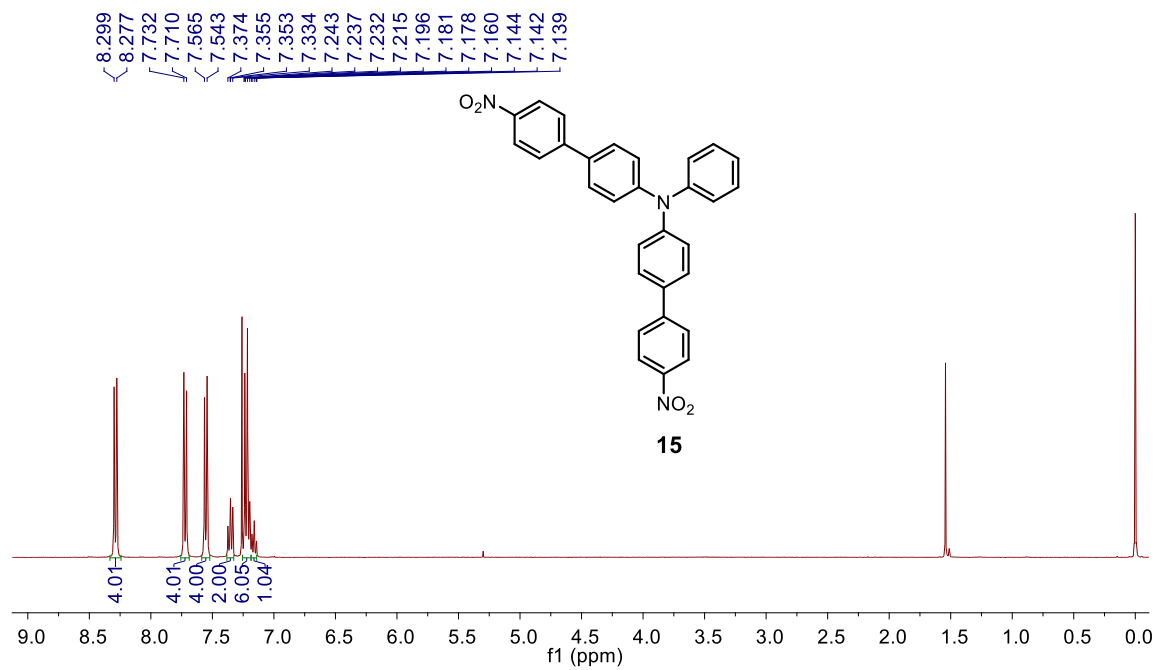
^1H NMR (400MHz, DMSO- d_6)



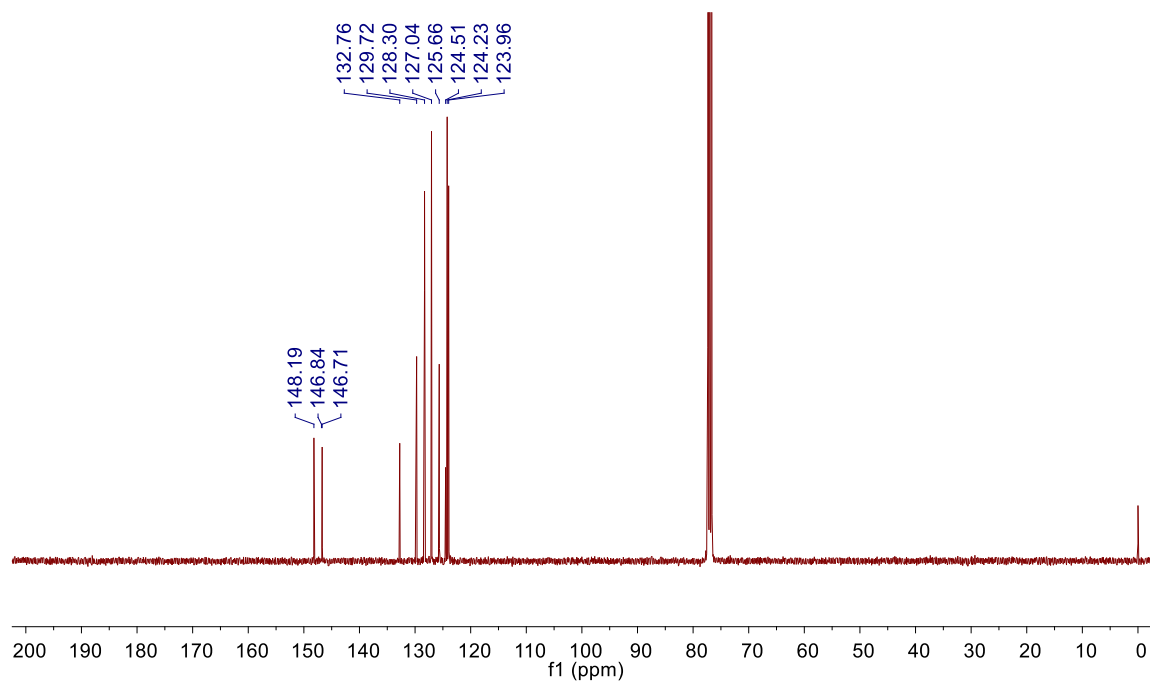
$^{13}\text{C}\{^1\text{H}\}$ NMR (100MHz, DMSO- d_6)



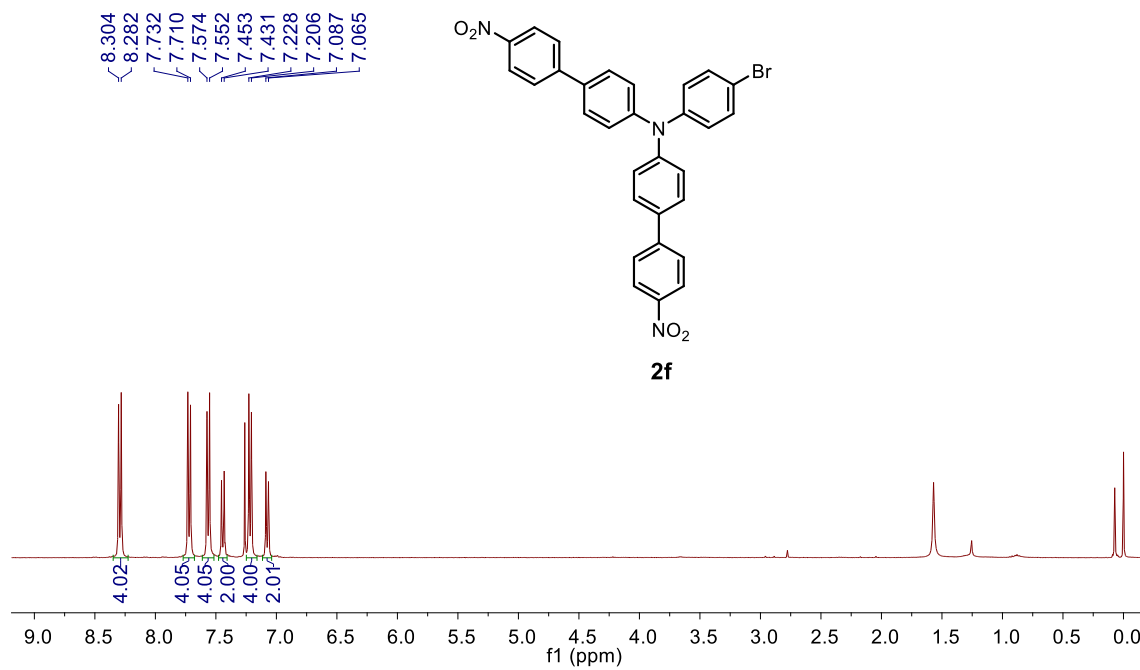
^1H NMR (400MHz, CDCl_3)



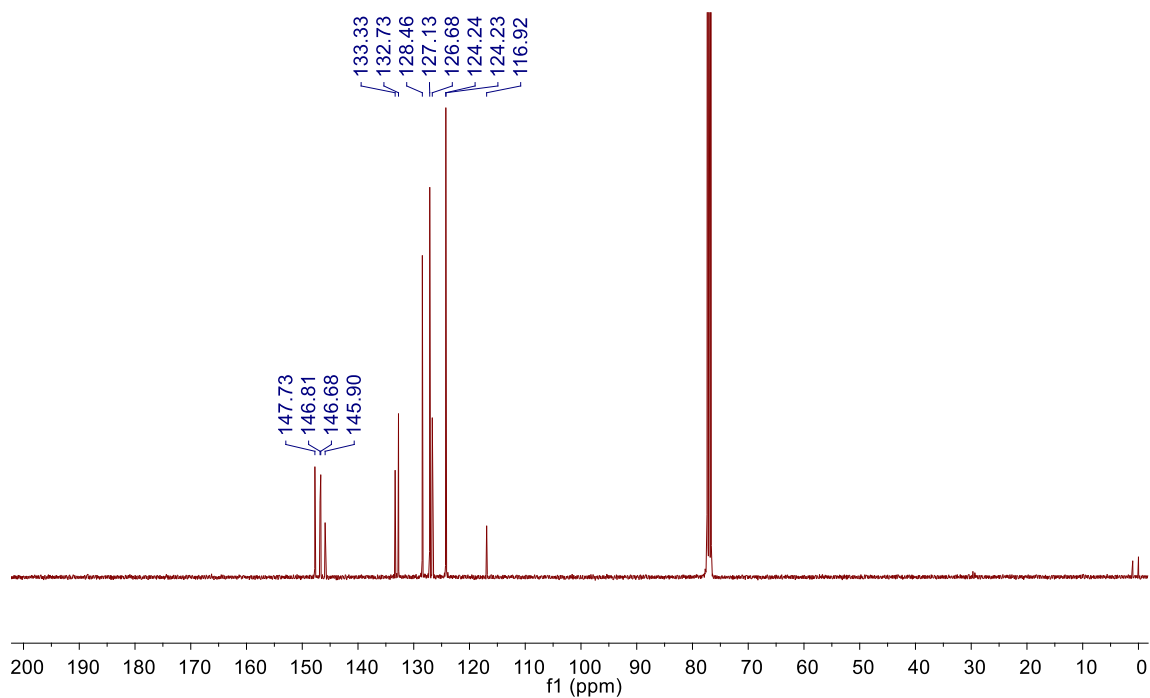
$^{13}\text{C}\{^1\text{H}\}$ NMR (100MHz, CDCl_3)



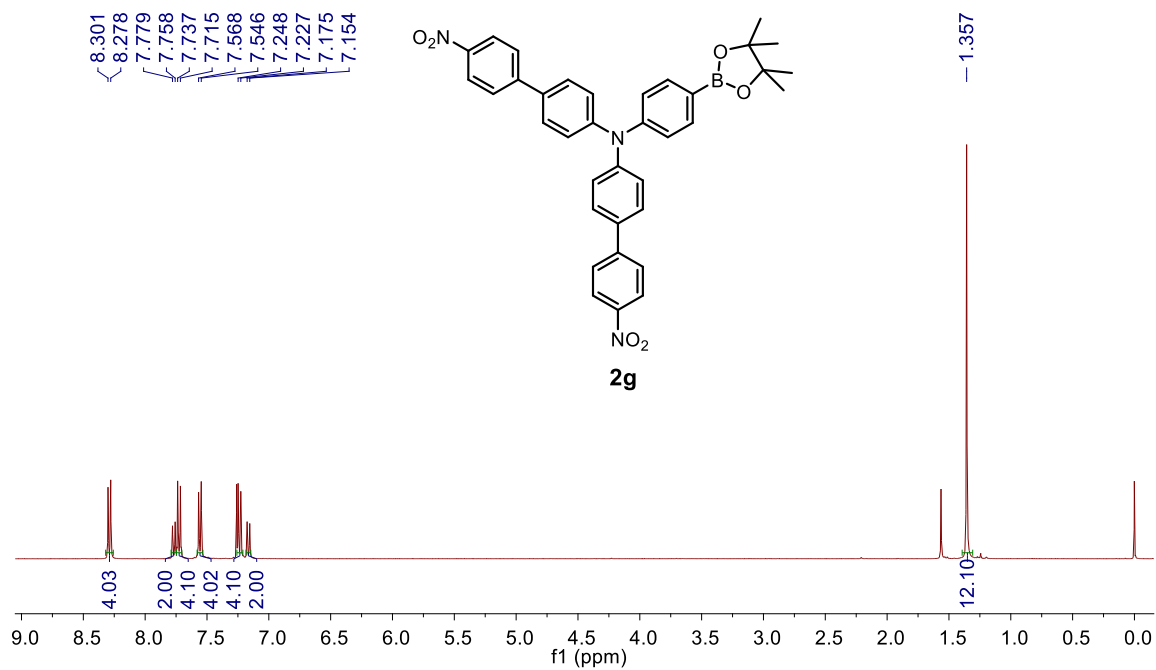
^1H NMR (400MHz, CDCl_3)



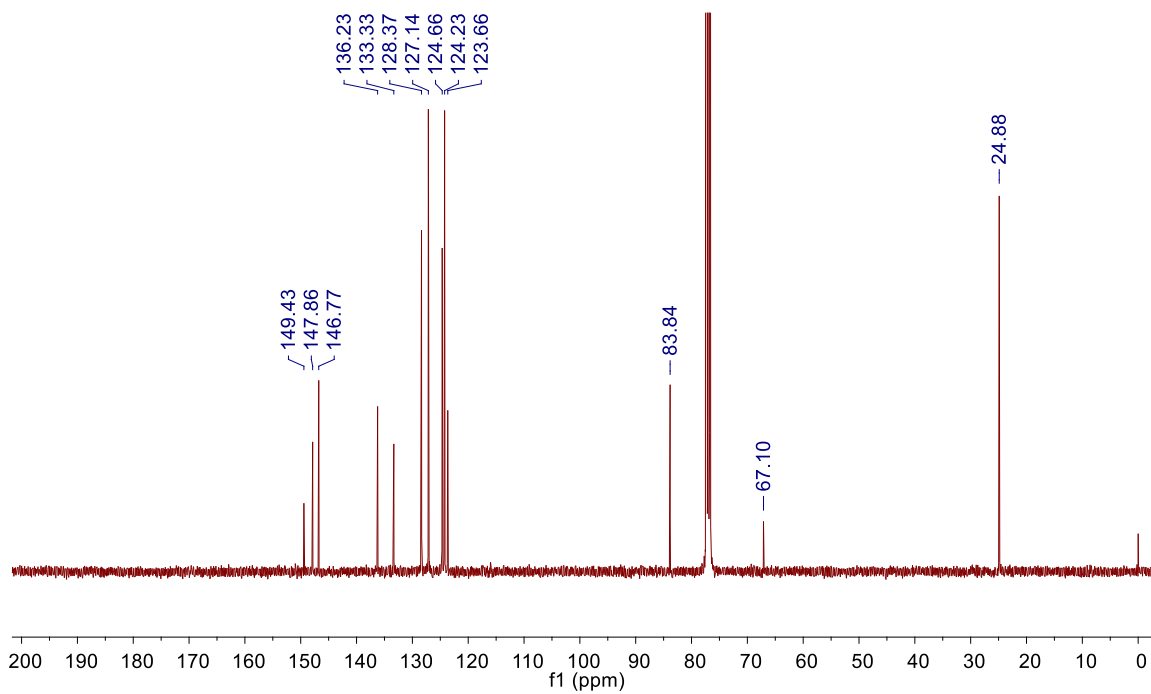
$^{13}\text{C}\{^1\text{H}\}$ NMR (100MHz, CDCl_3)



^1H NMR (400MHz, CDCl_3)



$^{13}\text{C}\{^1\text{H}\}$ NMR (100MHz, CDCl_3)



Chapter 3

Substituent effects on the uncaging quantum yield of amino-substituted nitrobiphenyl units

3.1. Introduction

Ortho-nitrobenzyl (oNB) (Figure 2) is still a general platform for molecular engineering to optimize PPGs with desirable characters. Recently, there have been many endeavors to develop *o*-NB scaffolds^{39,40,56,57,66–71} that can be excited in the visible and near-infrared (NIR) region (Figure 22a) to minimize the cytotoxicity caused by high-energy photons such as ultraviolet region light (~300 nm). However, the bathochromic shifts of absorption maxima sometimes negatively affect the quantum yield (Φ_u) of uncaging reaction^{5,56}. This is also the case we encountered when developing the octupolar chromophore TNBPA, as shown in Chapter 2. Although an exceptional 2P cross-section was revealed for the parent chromophore, low uncaging quantum yields ($\Phi_u \sim 0.004\text{--}0.008$) prevent further applications in biological studies. At least 0.02 of Φ_u has been suggested for practical PPGs³.

In this study, we attempted to shed light on factors that govern the photo-deprotection quantum yield Φ_u and find solutions to enhance the yield of nitrobiphenyl scaffolds with amino substituents as electron donors^{40,72–74}, whose push-pull system induces a large transition dipole moment and high 2P response in NIR region. Using diphenylamine-substituted derivatives **1** as the parent system, we carried out a systematic study on substituent effect (Figure 22b): extending the π -conjugation at diphenylamine unit, compounds **3** and **4**, along with adding extra electron-donating/withdrawing groups, compounds **5** and **2**, cyclizing the diphenylamine unit, compounds **6–8**, and changing the relative position of nitro group and amino group from para to meta position, compounds **9–11**. First, we examined the variation of uncaging quantum yield Φ_u for 2P-responsive chromophores. Then, some molecular engineering was conducted to improve quantum efficiency by modulating the

intramolecular charge-transfer (ICT) character, which was discussed as a feasible explanation for low Φ_u of several oNB PPGs^{12,56,75,76}. These substituent effects were investigated on the photophysical properties of the chromophores themselves **1a–11a** ($R^2 = H$), and photochemical reactions of the model oNB-type caged alcohols **1d–11d** ($R^2 = CH(CH_3)OCH_2CH_2OCH_2CH_3$). This alcohol moiety can be easily detected by NMR analysis and can increase the solubility of the chromophores in organic solvents and water. Quantum chemical calculations were also performed to provide insights into the characteristics of the lowest excited states for the newly designed compounds.

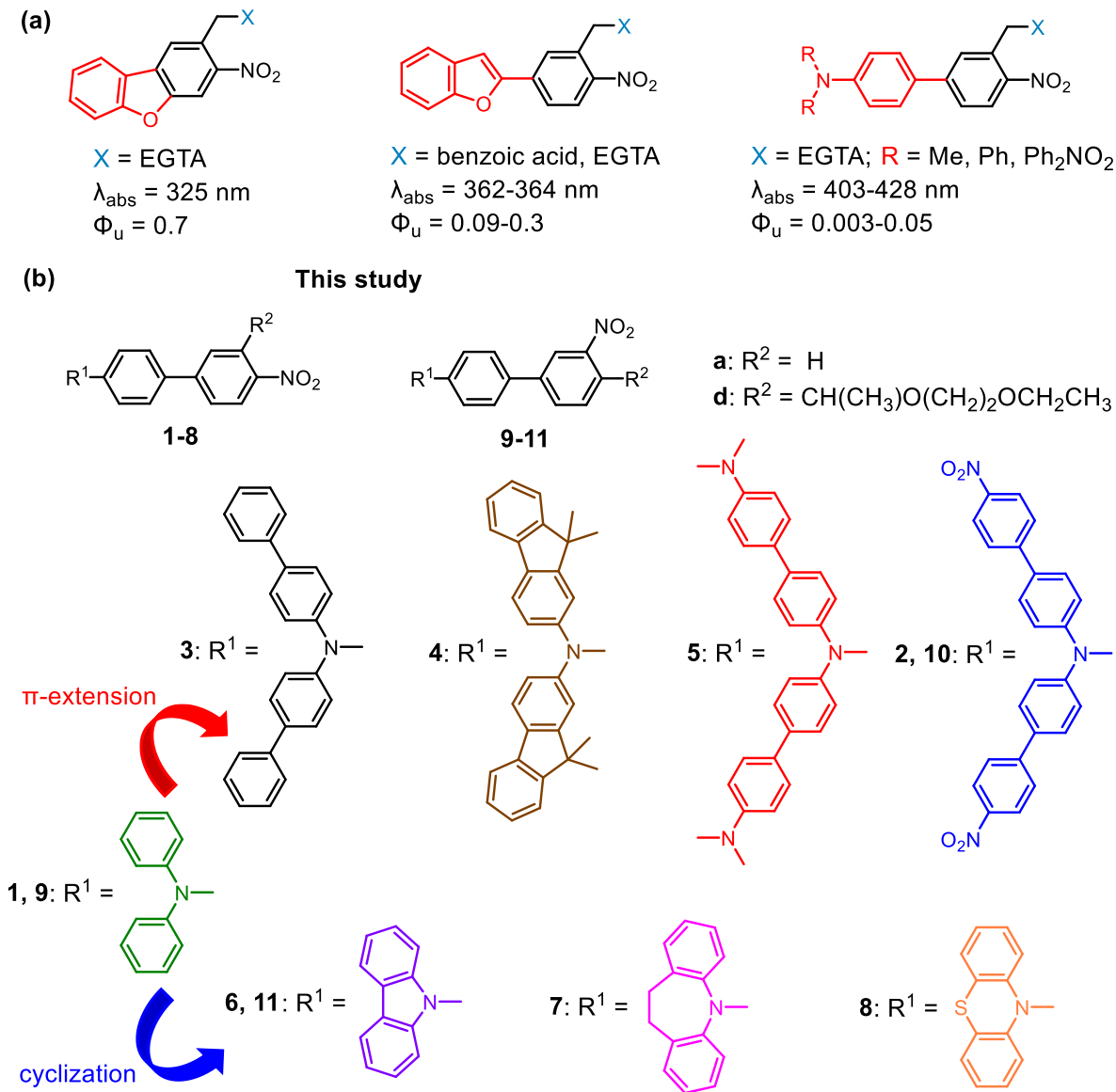


Figure 22. (a) Examples of red-shifted oNB PPGs; (b) Molecular designs of this study.

3.2. Photophysical properties

Absorption and fluorescence spectra of the chromophores without the leaving group **1a**–**11a** ($R^2 = \text{H}$) were measured in various solvents with different polarities: toluene ($E_{\text{T}}(30) = 33.9$), chloroform (CHCl_3 , $E_{\text{T}}(30) = 39.1$), and dimethyl sulfoxide (DMSO, $E_{\text{T}}(30) = 45.1$) (Figures 23 and 24). The photophysical data are summarized in Table 5.

Table 5. Photophysical data of **1a–11a** in various solvents.

Entry	Compound	Solvent	$\lambda_{\text{abs}}^{\text{a}}$ / nm	ϵ^{b} / $\text{M}^{-1}\text{cm}^{-1}$	$\lambda_{\text{onset}}^{\text{c}}$ / nm	$\lambda_{\text{fl}}^{\text{d}}$ / nm	λ_{0-0}^{e} / nm	$\Delta\nu_{\text{st}}^{\text{f}}$ / cm^{-1}	$\Phi_{\text{fl}}^{\text{g}}$	τ^{h} / ns
1	1a	toluene	400	16355	462	537	464	6378	0.78	3.1
2		CHCl_3	408	17590	482	698	488	10183	0.010	0.36
3		DMSO	412	17944	492	n.d.	n.d.	n.d.	n.d.	n.d.
4	3a	toluene	410	21242	472	551	476	6241	0.71	3.8
5		CHCl_3	419	21659	495	n.d.	n.d.	n.d.	n.d.	n.d.
6		DMSO	419	19308	503	n.d.	n.d.	n.d.	n.d.	n.d.
7	4a	toluene	423	17077	490	573	495	6189	0.58	4.0
8		CHCl_3	433	15787	517	n.d.	n.d.	n.d.	n.d.	n.d.
9		DMSO	433	16870	523	n.d.	n.d.	n.d.	n.d.	n.d.
10	5a	toluene	431	14079	505	641	522	7601	0.029	1.1
11		CHCl_3	435	16237	524	n.d.	n.d.	n.d.	n.d.	n.d.
12		DMSO	436	16665	536	n.d.	n.d.	n.d.	n.d.	n.d.
13	2a	toluene	405	41115	457	507	453	4967	0.51	2.2
14		CHCl_3	415	40012	483	687	493	9540	0.016	0.30
15		DMSO	424	42489	498	n.d.	n.d.	n.d.	n.d.	n.d.
16	6a	toluene	340	14623	411	n.d.	n.d.	n.d.	n.d.	n.d.
17		CHCl_3	341	13316	420	n.d.	n.d.	n.d.	n.d.	n.d.
18		DMSO	341	14320	425	n.d.	n.d.	n.d.	n.d.	n.d.
19	7a	toluene	394	19525	452	511	451	5811	0.62	2.3
20		CHCl_3	403	18537	475	647	504	9358	0.053	0.42
21		DMSO	409	19478	486	702	507	10205	0.011	0.06
22	8a	toluene	359	5377	444	n.d.	n.d.	n.d.	n.d.	n.d.
23		CHCl_3	363	5040	458	n.d.	n.d.	n.d.	n.d.	n.d.
24		DMSO	366	5940	466	n.d.	n.d.	n.d.	n.d.	n.d.
25	9a	toluene	338	21924	378	562	437	11792	0.027	5.3
26		CHCl_3	338	22085	379	n.d.	n.d.	n.d.	n.d.	n.d.
27		DMSO	338	23303	379	n.d.	n.d.	n.d.	n.d.	n.d.
28	10a	toluene	394	27313	456	511	455	5811	0.54	2.8
29		CHCl_3	405	26508	480	685	492	10093	0.014	0.21
30		DMSO	412	28952	498	n.d.	n.d.	n.d.	n.d.	n.d.
31	11a	toluene	314	15909	352	n.d.	n.d.	n.d.	n.d.	n.d.
32		CHCl_3	314	15609	353	n.d.	n.d.	n.d.	n.d.	n.d.
33		DMSO	314	14994	354	n.d.	n.d.	n.d.	n.d.	n.d.

^aAbsorption maximum at the lowest-energy allowed absorption band. ^bMolar extinction coefficient (error ± 10 – 20%). ^cOnset wavelength. ^dFluorescence maximum. n.d. = not detected or very weak. ^e0-0 wavelength. ^fStokes shift. ^gFluorescence quantum yield measured using absolute photoluminescence quantum yield spectrometer (error $\pm 10\%$). ^hFluorescence lifetime determined using time-correlated single-photon counting method (error $\pm 10\%$).

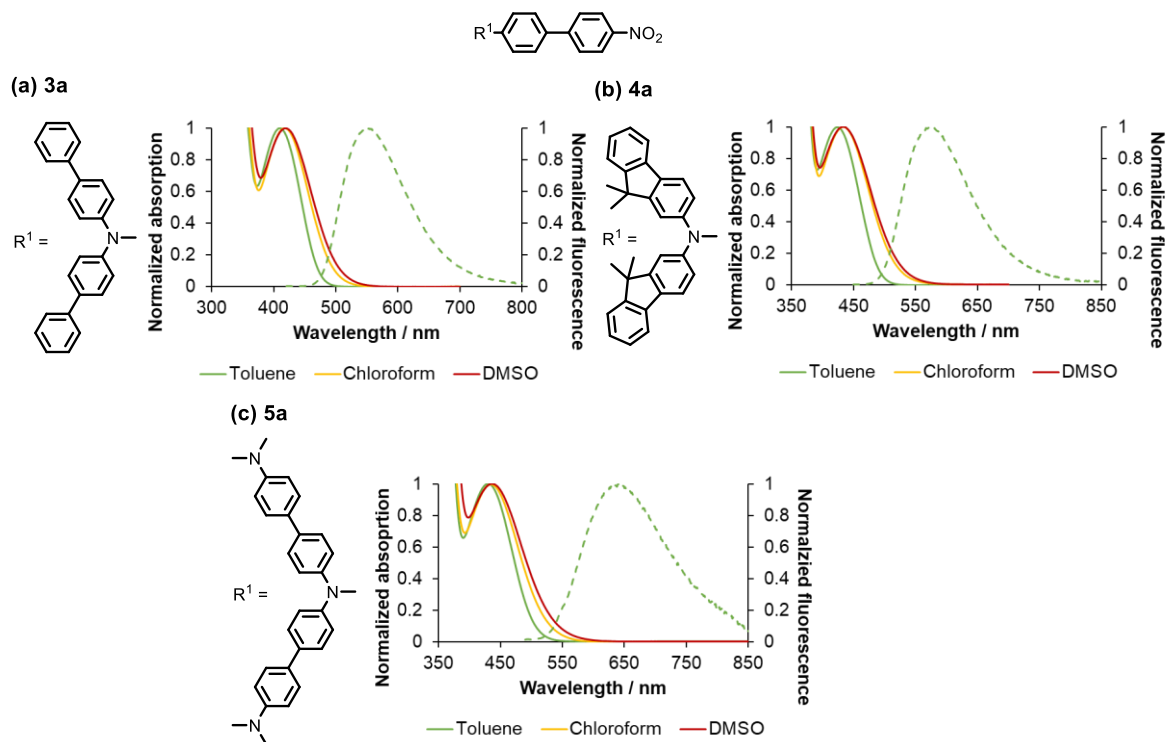


Figure 23. Absorption (full line) and fluorescence (dash line) spectra of **3a–5a** in various solvents.

The para derivatives with π -extended conjugation **1a–5a** showed broad absorption bands in the visible range ($\lambda_{\text{abs}} > 400$ nm) (Figures 23 and 24). The absorption behaviors of these compounds can be observed more clearly if we consider their onset wavelength values (Table 5), which were determined from the intersection between the baseline and a tangent line on the inflection point for the low-energy side of the absorption band. Compounds **1a–5a** exhibited bathochromic shifts of ~ 30 – 40 nm with the increase in solvent polarity, e.g., $\lambda_{\text{onset}} = 462$ nm (entry 1), 482 nm (entry 2), 492 nm (entry 3) for **1a** in toluene, CHCl_3 , and DMSO, respectively. Adding one phenyl ring at each side of the diphenylamine unit led to bathochromic shifts of ~ 10 nm for **3a** compared to **1a**, e.g., $\lambda_{\text{onset}} = 462$ nm (entry 1) and 472

nm (entry 4) for **1a** and **3a**, respectively, in toluene. Restricting the torsion around the phenyl-phenyl bond or introducing an electron-donating group (EDG) at both ends of dibiphenylamine produced additional shifts of 20–30 nm for **4a** and **5a**, e.g., $\lambda_{\text{onset}} = 472$ nm (entry 4), 490 nm (entry 7) and 505 nm (entry 10) for **3a–5a**, respectively, in toluene. Conversely, functionalizing dibiphenylamine with electron-withdrawing group (EWG) induced hypsochromic shifts of 5–15 nm for **2a**, e.g., $\lambda_{\text{onset}} = 472$ nm (entry 4) and 457 nm (entry 13) for **3a** and **2a**, respectively, in toluene. The molar extinction coefficients at absorption maxima of these compounds fall within the range of 14000–21000 $\text{M}^{-1}\text{cm}^{-1}$, except for significantly higher values of **2a** ($\sim 40000 \text{ M}^{-1}\text{cm}^{-1}$). The elevation in absorptivity of **2a** most likely resulted from the character of octupolar systems, in which the molar extinction coefficients increase with the number of dipolar branches^{42,52,77}. Compounds **1a–4a** exhibited intense emission bands in nonpolar toluene, $\lambda_{\text{fl}} = 537$ nm (entry 1), 551 nm (entry 4), 573 nm (entry 7) and 507 nm (entry 13) for **1a–4a**, respectively, with decent fluorescence quantum yields ($\Phi_{\text{fl}} \sim 0.51–0.78$), while the emission from **5a** displayed much weaker intensity, $\lambda_{\text{fl}} = 641$ nm, $\Phi_{\text{fl}} = 0.029$ (entry 10). Increasing solvent polarity induced apparent bathochromic shifts of fluorescence maxima associated with considerable decreases in fluorescence quantum yields, $\lambda_{\text{fl}} = 698$ nm, $\Phi_{\text{fl}} = 0.010$ (entry 2) and $\lambda_{\text{fl}} = 687$ nm, $\Phi_{\text{fl}} = 0.016$ (entry 14) for **1a** and **2a**, respectively, in CHCl_3 , or even sufficiently suppressed the emission from these compounds (entries 3, 5–6, 8–9, 11–12, and 15). Together with large Stokes shift values (5000–10000 cm^{-1}), these results are consistent with those found in push-pull molecules with strong ICT characteristics in the excited state^{78–80}. The suppression of

fluorescence in polar solvents could be ascribed to the formation of a twisted ICT state, which is highly stabilized in polar solvents and principally nonemissive⁸¹.

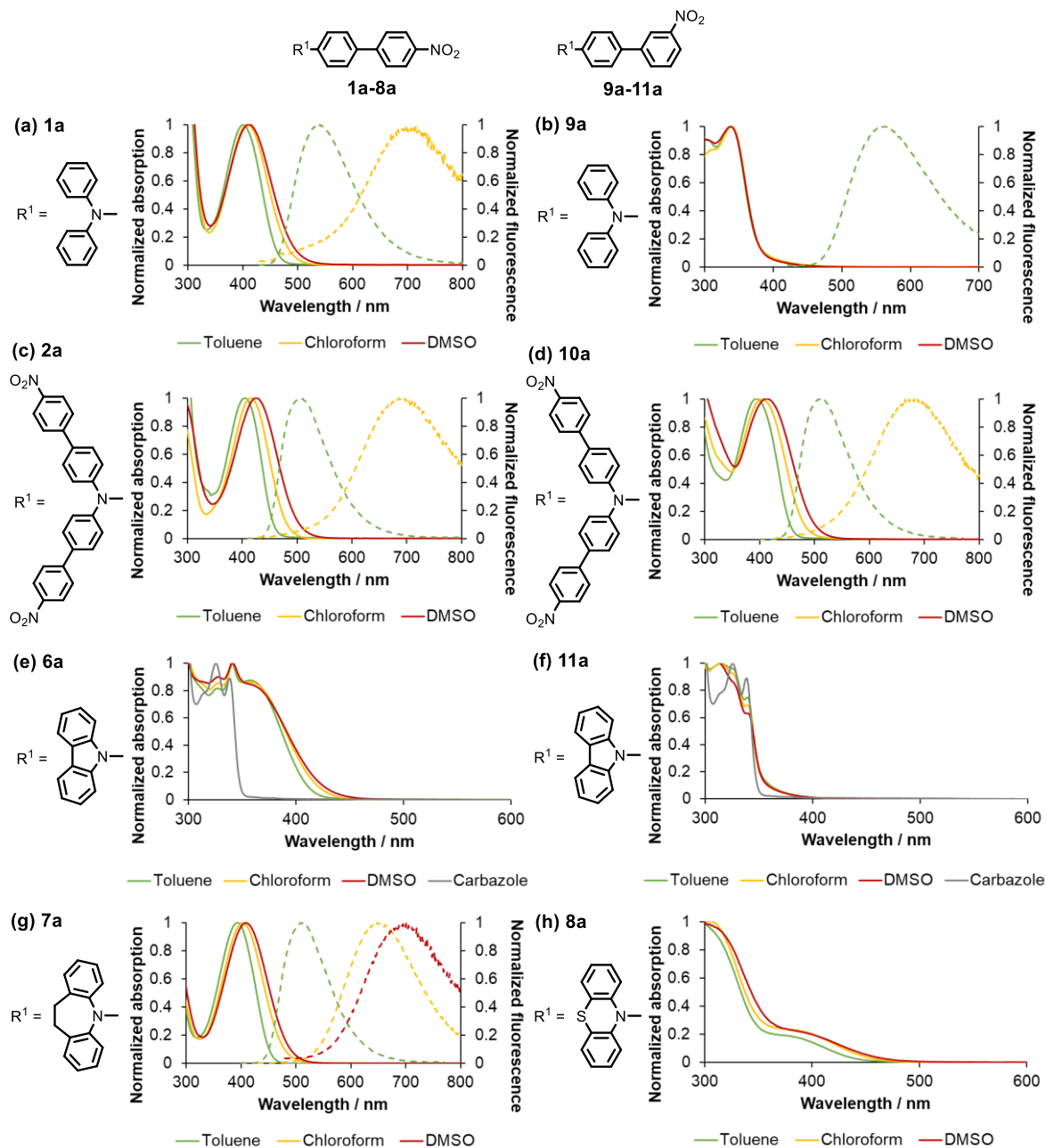


Figure 24. Absorption (full line) and fluorescence (dash line) spectra of **1a**, **2a** and **6a–11a** in various solvents.

On the other hand, the para derivatives with cyclic substituents **6a–8a** demonstrated rather divergent features (Figure 24). Cyclization of diphenylamine into carbazole in **6a**, iminodibenzyl in **7a**, and phenothiazine in **8a** caused hypsochromic shifts in their absorption bands compared to **1a**. The absorption spectra of **6a** exhibited vibrational structures, which may originate from the carbazole unit. Compounds **6a–8a** showed blue shifts of 50–70 nm, ~10 nm, and ~20 nm, respectively, in comparison with **1a**, e.g., $\lambda_{\text{onset}} = 492$ nm (entry 3), 425 nm (entry 18), 486 nm (entry 21) and 466 nm (entry 24) for **1a** and **6a–8a**, respectively, in DMSO. Compounds **6a** and **8a** exhibited only slight bathochromic shifts of 10–20 nm with solvent polarity, while the shifts from **7a** (~30 nm) were similar to those from **1a–5a**. The molar extinction coefficients at absorption maxima of **6a** and **7a** (14000–19000 $\text{M}^{-1}\text{cm}^{-1}$) were comparable to those of **1a** (~17000 $\text{M}^{-1}\text{cm}^{-1}$), while much lower values were obtained for **8a** (~5000 $\text{M}^{-1}\text{cm}^{-1}$). The absorption maximum of **8a** (~360 nm, Table 5) was estimated from the onset wavelength value by assuming that the onset wavelength is at 10% peak height of the maximum wavelength⁸². Compound **7a** exhibited a strong CT emission in toluene, $\lambda_{\text{fl}} = 511$ nm with $\Phi_{\text{fl}} = 0.62$ (entry 19), which significantly red-shifted and became weakened in higher-polarity solvents, e.g., $\lambda_{\text{fl}} = 702$ nm with $\Phi_{\text{fl}} = 0.011$ in DMSO (entry 21). No emission corresponding to the CT state was observed for **6a** and **8a**. Fluorescence quenching of these two compounds could be due to their lowest excited singlet states S_1 being dominated by the forbidden local $n-\pi^*$ transition within the nitro group, which accelerates non-radiative decay processes such as internal conversion or intersystem crossing⁸³. Thus, the cyclization diminished CT character in the S_1 state of **6a** and **8a** but had no noticeable effect on **7a**.

Altering the relative position between the nitro group and the amino group to the meta also caused hypsochromic shifts in the absorption spectra of meta derivatives (Figure 24) compared to those of the para analogs. For example, diphenylamine-substituted **9a** and carbazole-substituted **11a** exhibited shifts of 80–110 nm and 60–70 nm, respectively, e.g., $\lambda_{\text{onset}} = 492$ nm (entry 3, for **1a**), 379 nm (entry 27, for **9a**), 425 nm (entry 18, for **6a**) and 354 nm (entry 33, for **11a**) in DMSO. Changes from bis(nitrobiphenyl)amine-substituted **10a** were negligible, e.g., $\lambda_{\text{onset}} = 483$ nm (entry 14, for **2a**) and 480 nm (entry 29, for **10a**) in CHCl_3 . Bathochromic shifts of ~40 nm with solvent polarity were observed for **10a**. However, no variation with solvents was found for **9a** and **11a**. Compounds **10a** and **11a** showed identical fluorescent properties to their para analogs: a CT emission for **10a** (entries 28–30) and no emission for **11a** (entries 31–33). On the other hand, the fluorescence from **9a** in toluene, $\lambda_{\text{fl}} = 562$ nm with $\Phi_{\text{fl}} = 0.027$ (entry 25), displayed considerably weaker intensity than that from **1a**. While other compounds showed consistency between onset wavelength and 0-0 wavelength determined from the intersection between absorption and emission spectra, a large deviation was noted for **9a** in toluene (Table 5). This indicated that the absorption band at 340 nm and emission band at 560 nm of **9a** in toluene likely originated from different excited states; in other words, the absorption band at 340 nm is attributed to the transition to higher excited states. The same phenomenon may also be observed in the absorption of **11a**. The slanting signals starting from ~390 nm and ~360 nm in the absorption spectra of **9a** and **11a** (Figure 24), respectively, possibly correspond to the excitation to the S_1 state. The forbidden transition between ground state S_0 and S_1 state could be the reason for the low fluorescence quantum yield of **9a**.

3.3. Photoreactions

Photoreactions of the model oNB-type caged alcohols **1d–11d** ($R^2 = \text{CH}(\text{CH}_3)\text{OCH}_2\text{CH}_2\text{OCH}_2\text{CH}_3$) were carried out in air-saturated DMSO at $\sim 23^\circ\text{C}$ using 405 nm LED lamp (± 20 nm, 7.8×10^{-7} mol s^{-1}) for compounds **2d–5d** and **10d**, 365 nm LED lamp (± 20 nm, 3.3×10^{-7} mol s^{-1}) for compounds **1d** and **6d–9d**, and 320 nm Xenon lamp with a monochromator (± 10 nm, 2.8×10^{-9} mol s^{-1}) for compound **11d**. The data are summarized in Table 6. The choices of light sources were to comply with the absorption of each compound. The absorption spectra of these caged derivatives (Figure 25) exhibited slight hypsochromic shifts compared to those of their chromophores ($R^2 = \text{H}$), although the molar extinction coefficients remained more or less unaffected.

Table 6. Photophysical and photochemical data of **1d–11d** in DMSO.

Compound	$\lambda_{\text{abs}}^{\text{a}}$ / nm	ϵ^{b} / $\text{M}^{-1}\text{cm}^{-1}$	$\lambda_{\text{onset}}^{\text{c}}$ / nm	Chemical yields ^d of 2-EE / %	$\Phi_{\text{u}}(\lambda_{\text{irr}})^{\text{e}}$	$\epsilon \times \Phi_{\text{u}}^{\text{f}}$
1d	399	13310	481	82	0.02 (365)	266
3d	401	13996	491	86	0.004 (405)	56
4d	415	17888	510	88	0.002 (405)	36
5d	420	15246	519	82	0.002 (405)	30
2d	420	35114	496	86	0.002 (405)	70
6d	342	13888	419	80	0.2 (365)	2778
7d	399	13175	479	80	0.02 (365)	264
8d	361	4870	449	86	0.1 (365)	487
9d	339	20736	383	88	0.01 (365)	207
10d	412	28265	498	89	<0.001 (405)	<28
11d	312	14602	356	87	0.2 (320)	2920

^aAbsorption maximum at the lowest-energy allowed absorption band. ^bMolar extinction coefficient (error ± 10 – 20%). ^cOnset wavelength. ^dPhotoreactions of caged alcohols were carried out in DMSO- d_6 and monitored by ^1H NMR spectroscopy. Chemical yields of 2-EE

(2-ethoxyethanol) were determined using triphenylmethane as NMR standard (error ± 10 –20%). ^eUncaging quantum yields (at conversions $< 10\%$) were determined using HPLC and a ferrioxalate actinometer (error ± 10 –20%). λ_{irr} = irradiation wavelength. ^fUncaging cross-section.

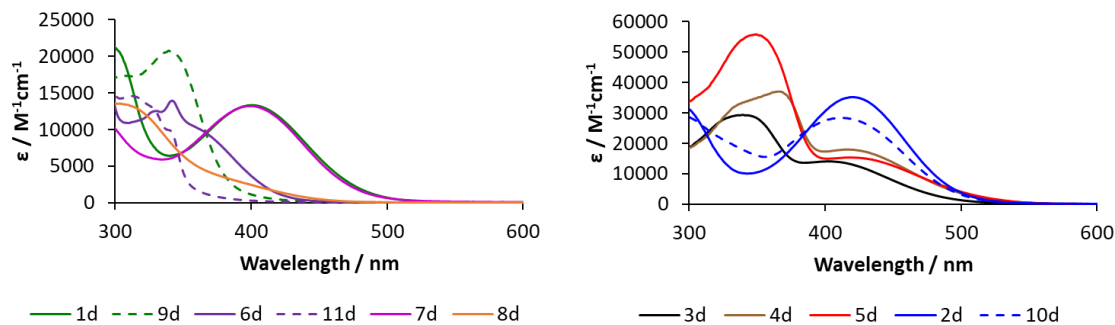


Figure 25. Absorption spectra of **1d–11d** in DMSO.

Firstly, the photoreactions of caged alcohols (5–9 mM) in air-saturated DMSO- d_6 monitored by ^1H NMR spectroscopy (400 MHz) (Figures 26–28) showed the release of 2-ethoxyethanol (2-EE) with chemical yields of 80–90%, which were determined using triphenylmethane as NMR standard. Interestingly, an intermediate was observed in the ^1H NMR spectra during the photolysis of these caged alcohols. The formation of 2-EE and a nitrosoketone by-product (confirmed by mass spectrometry) were detected from the intermediate. The lifetime of the intermediate varied significantly with the amino substituents. We temporarily assigned this intermediate to the hemiacetal **C** (Figure 2). Formation of the similar hemiacetal **C** from the parent oNB has been proved by time-resolved infrared (TR-IR) spectroscopy¹⁹. The nitrosoketone photoproducts exhibited red-shifted absorption spectra in comparison with the corresponding oNB caged alcohols (see Experimental section).

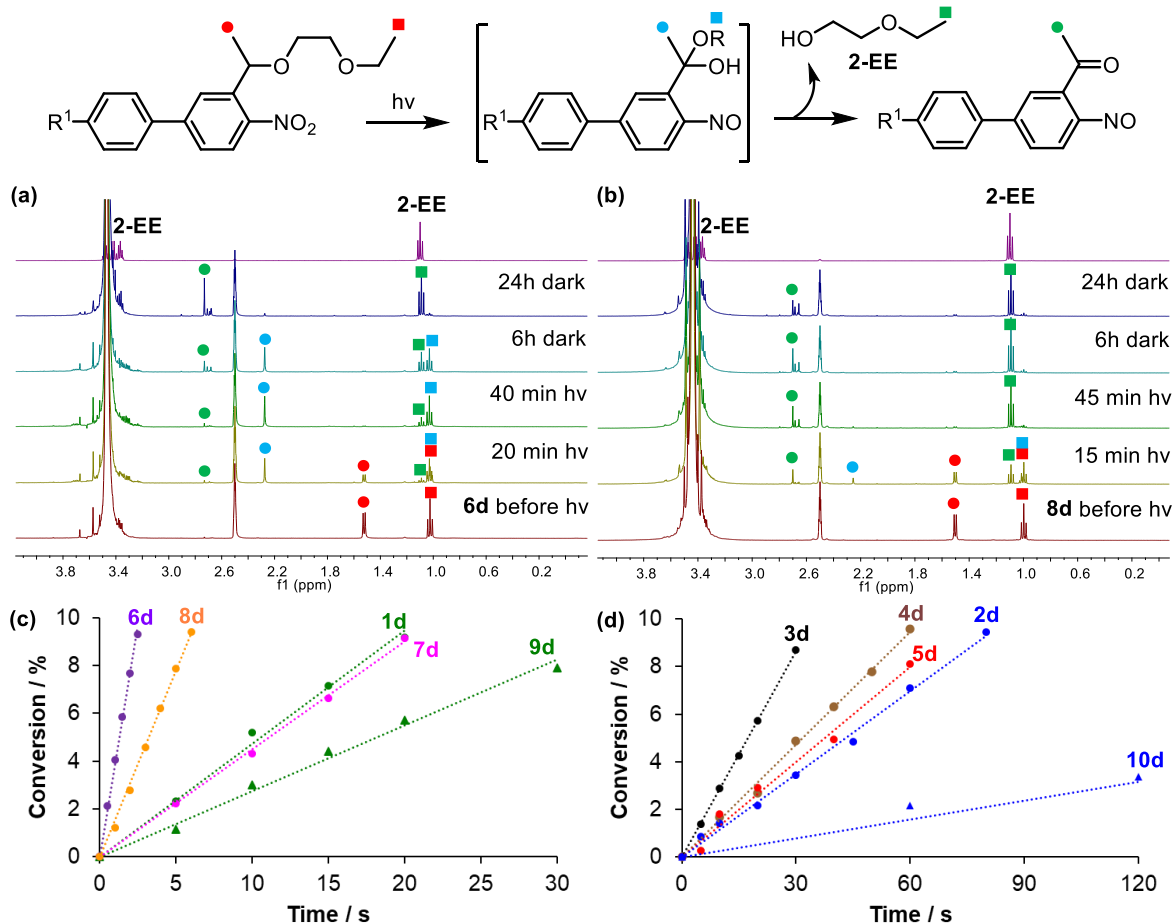


Figure 26. ^1H NMR spectra (400 MHz, 0–4 ppm) during photolysis in air-saturated $\text{DMSO-}d_6$ ($\sim 23^\circ\text{C}$) at 365 nm (LED lamp, $3.3 \times 10^{-7} \text{ mol s}^{-1}$) of (a) **6d** (8 mM) and (b) **8d** (8 mM) compared with ^1H NMR spectra of an authentic sample of 2-ethoxyethanol (2-EE). The samples after photolysis were kept in the dark for 1 day to follow the thermal decomposition of the intermediate. The peak of methyl protons (blue square) of the intermediate overlapped with that of the caged alcohol (red square). Time profile of photolysis (<10% of conversion) in air-saturated DMSO ($\sim 23^\circ\text{C}$) at (c) 365 nm (LED lamp, $3.3 \times 10^{-7} \text{ mol s}^{-1}$) and (d) 405 nm (LED lamp, $7.8 \times 10^{-7} \text{ mol s}^{-1}$) monitored by HPLC (ODS-3, $3\mu\text{m}$, acetonitrile 100%).

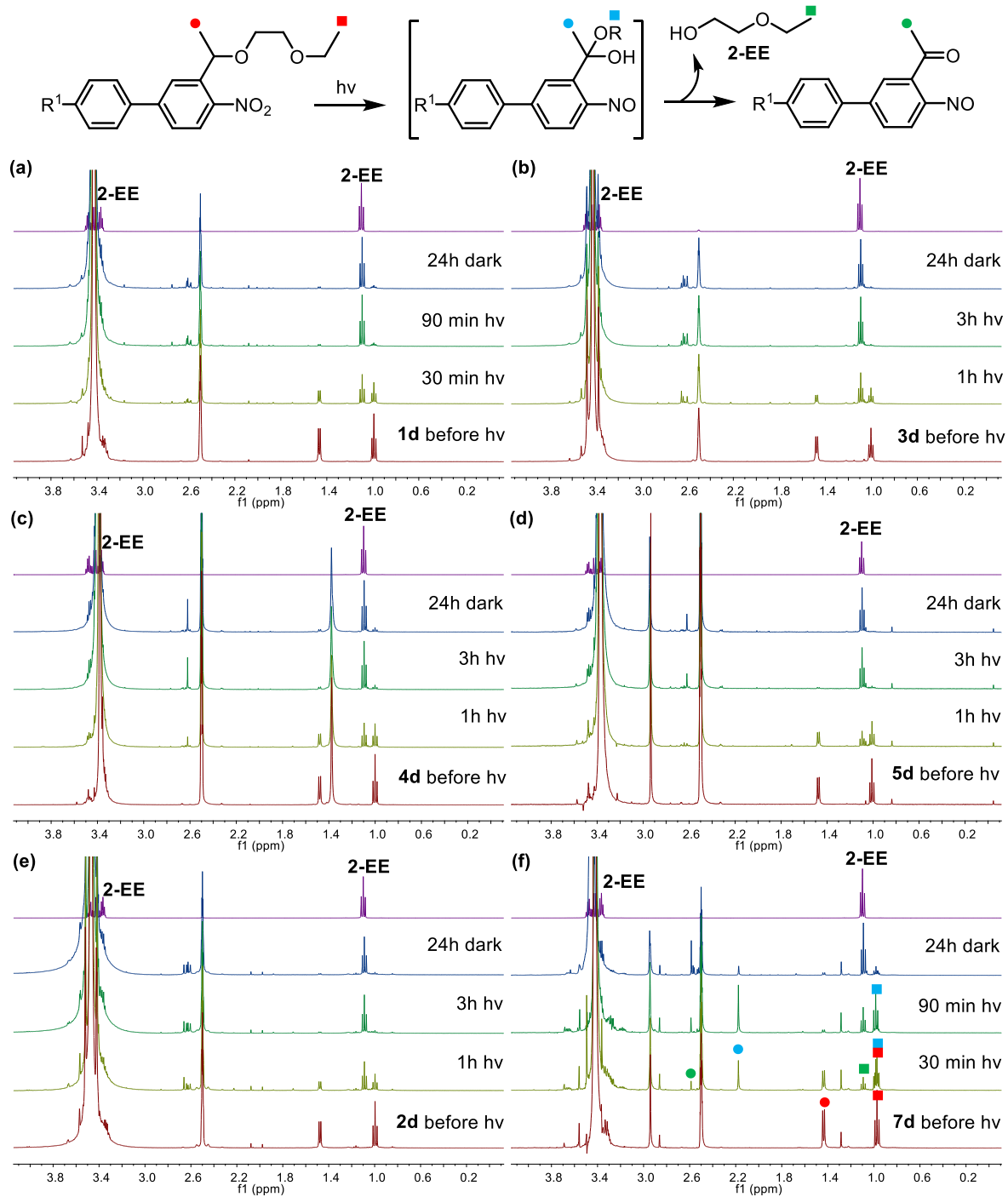


Figure 27. ¹H NMR spectra (400 MHz, 0–4 ppm) during photolysis in air-saturated DMSO-d₆ (~23°C) at 365 nm (LED lamp, $3.3 \times 10^{-7} \text{ mol s}^{-1}$) of (a) **1d** (8 mM) and (f) **7d** (8 mM); at 405 nm (LED lamp, $7.8 \times 10^{-7} \text{ mol s}^{-1}$) of (b) **3d** (6 mM), (c) **4d** (6 mM), (d) **5d** (5 mM)

and (e) **2d** (6 mM) compared with ^1H NMR spectra of an authentic sample of 2-ethoxyethanol (2-EE). The samples after photolysis were kept in the dark for 1 day to follow the thermal decomposition of the intermediate.

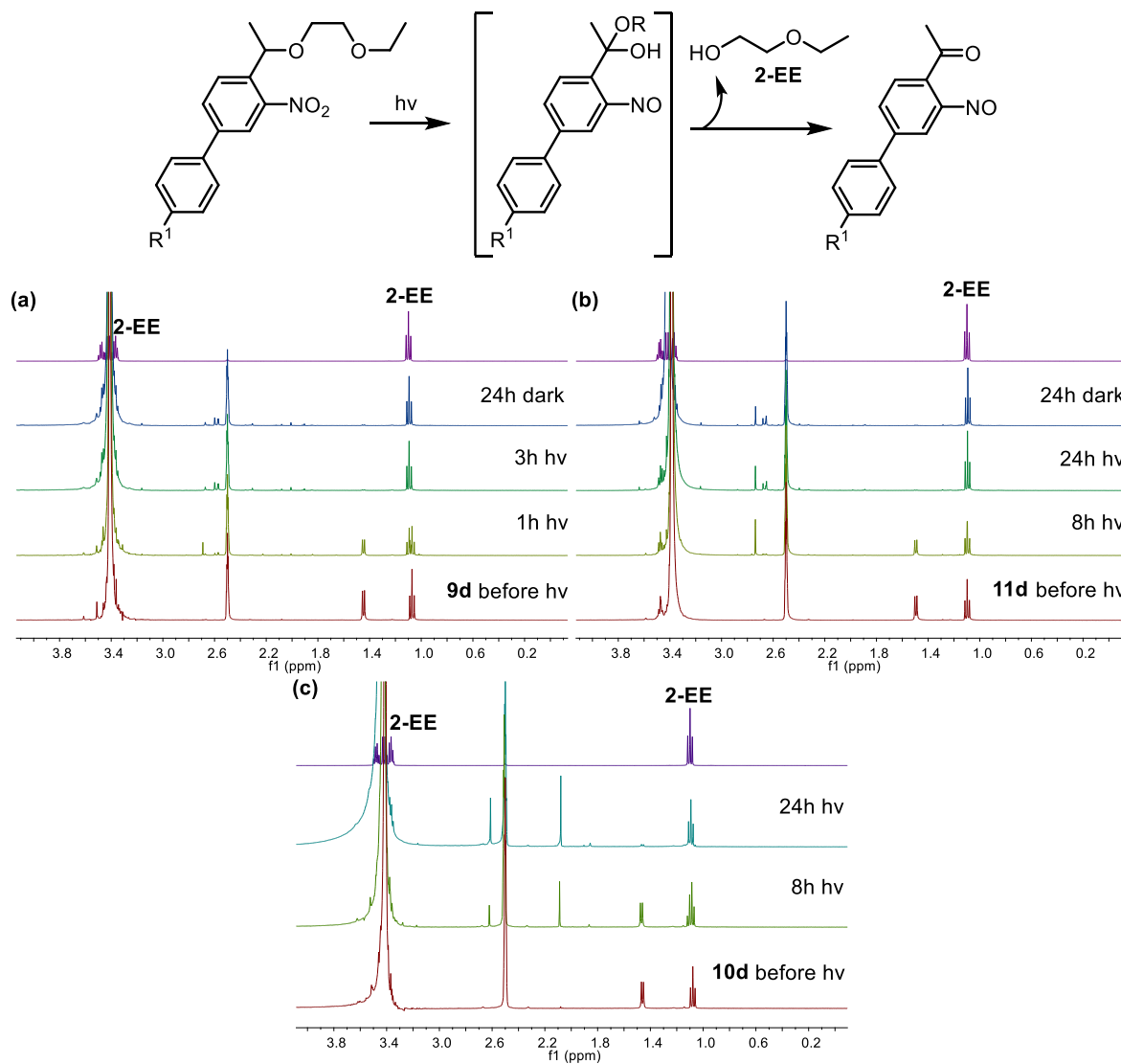


Figure 28. ^1H NMR spectra (400 MHz, 0–4 ppm) during photolysis in air-saturated DMSO- d_6 ($\sim 23^\circ\text{C}$) at 365 nm (LED lamp, $3.3 \times 10^{-7} \text{ mol s}^{-1}$) of (a) **9d** (8 mM); at 320 nm (Xenon lamp with a monochromator, $2.8 \times 10^{-9} \text{ mol s}^{-1}$) of (b) **11d** (8 mM); and at 405 nm (LED lamp, $7.8 \times 10^{-7} \text{ mol s}^{-1}$) of (c) **10d** (6 mM) compared with ^1H NMR spectra of an authentic

sample of 2-ethoxyethanol (2-EE). The samples after photolysis were kept in the dark for 1 day to follow the thermal decomposition of the intermediate.

The photochemical decomposition of caged alcohols in air-saturated DMSO was monitored by HPLC (ODS-3, 3 μ m, acetonitrile 100%) (Figures 26c, d), and the quantum yields (at conversions <10%) (Table 6) were determined using a ferrioxalate actinometer (see Experimental section). There was no significant difference in decomposition rates under air, oxygen, and argon (see Experimental section), indicating the uncaging process of these oNB derivatives occurred mainly from the S₁ state or a short-live T₁ state. The molecular designs that may enhance 2P response **2d**–**5d** suffer from the sacrifice of photoreaction quantum yield. Particularly, extending diphenylamine into dibiphenylamine decreased the uncaging quantum yield by five times ($\Phi_u = 0.02$ and 0.004 for **1d** and **3d**, respectively), while torsional restriction around phenyl-phenyl bond and EDG/EWG attachment additionally reduced this parameter by half ($\Phi_u = 0.002$ for **2d**, **4d** and **5d**). In contrast, the quantum efficiency increased when using the cyclic diphenylamine unit. While **7d** showed a similar quantum yield ($\Phi_u = 0.02$) to that of **1d**, significantly improved uncaging quantum yields ($\Phi_u = 0.2$ and 0.1) were observed for **6d** and **8d**, respectively. On the other hand, the meta derivatives displayed various behaviors, in which **11d** gave comparable quantum efficiency ($\Phi_u = 0.2$) to **6d**, **9d** gave slightly less efficient value ($\Phi_u = 0.01$) than **1d**, but **10d** having NO₂ groups at the dibiphenylamine moiety hardly reacted to light irradiation ($\Phi_u < 0.001$). Briefly, we succeeded in developing three new chromophores that proceeded uncaging with sufficient quantum yields, namely, carbazole-substituted **6d**, **11d**, and phenothiazine-substituted **8d** by the cyclization strategy.

In general, the quantum efficiencies tend to decrease with bathochromic shifts of absorption bands, as seen in the extended π -conjugated systems **2d–4d**, which followed the trend reported in the literature and was consistent with the energy gap law^{5,84}. However, the significantly ineffective photoreaction of bis(nitrobiphenyl)amine-substituted **2d** and **10d** may result from their unique character of lowest excited states, which is clarified below by quantum chemical calculations. In addition, we also found a close relationship between ICT character and uncaging quantum yield, as molecules with no emission from the CT state (**6d**, **8d**, and **11d**) are those with high photo-reactivities. Changing the relative position between the nitro group and the amino group (**9d–11d**) did not give any desirable effect on modulating the ICT characteristics and quantum efficiency.

3.4. Quantum chemical calculations

To provide insights into the substituent effects on characters of lowest excited states and photoreaction quantum efficiencies, we performed density functional theory (DFT) and time-dependent (TD) DFT calculations at the M06-2X/6-31G(d) level of theory in vacuum and DMSO (SMD method) for caged alcohols **1d'–11d'** with the leaving group -OCH₂CH₂OCH₂CH₃ replaced by -OCH₃. Table 7 summarizes computed results for the ground state S₀ and the lowest excited single state S₁, including energy of highest occupied molecular orbital (HOMO) and lowest unoccupied molecular orbital (LUMO), HOMO-LUMO gap and dipole moment for S₀; absorption wavelength, oscillator strength, dipole moment, contribution percentage of HOMO-LUMO transition and overall transition type determined from natural transition orbital (NTO) for S₁.

Table 7. Computational data of ground state S_0 and lowest excited single state S_1 for **1d'**–**11d'** at (TD)-M062X/6-31g(d) in vacuum and DMSO (SMD method).

Compound	S_0				S_1				Transition ^h
	E_{HOMO}^a / eV	E_{LUMO}^b / eV	$\Delta E_{\text{H-L}}^c$ / eV	μ^d / D	λ_{cal}^e / nm	f^f	μ^d / D	H-L^g / %	
1d'	-6.35 (-6.24)	-0.98 (-1.00)	5.37 (5.24)	5.3 (6.3)	324 (334)	0.61 (0.74)	16.5 (22.7)	62 (67)	CT
3d'	-6.25 (-6.14)	-1.01 (-0.99)	5.24 (5.15)	5.1 (6.0)	331 (339)	0.82 (0.93)	18.1 (21.9)	67 (66)	CT
4d'	-6.08 (-6.00)	-1.02 (-1.01)	5.06 (4.99)	5.3 (6.0)	342 (349)	0.83 (0.92)	19.1 (22.6)	70 (67)	CT
5d'	-5.81 (-5.80)	-0.90 (-1.00)	4.91 (4.80)	8.3 (9.5)	342 (351)	0.89 (0.94)	25.3 (29.4)	66 (62)	CT
2d'	-6.75 (-6.25)	-1.57 (-1.41)	5.17 (4.84)	2.2 (2.5)	337 (362)	0.97 (1.09)	10.7 (13.2)	81 (81)	CT
6d'	-6.73 (-6.68)	-1.17 (-1.05)	5.56 (5.63)	3.1 (3.7)	313 (315)	0.14 (0.21)	4.1 (7.3)	11 (13)	LE
7d'	-6.35 (-6.32)	-1.38 (-1.28)	4.97 (5.04)	3.8 (4.5)	338 (328)	0.20 (0.27)	25.0 (28.5)	77 (72)	CT
8d'	-6.61 (-6.50)	-0.89 (-0.97)	5.72 (5.53)	6.6 (8.1)	316 (325)	0.27 (0.61)	9.2 (19.2)	26 (52)	LE, (CT)
9d'	-6.29 (-6.23)	-1.07 (-1.12)	5.22 (5.11)	3.8 (4.5)	316 (325)	0.13 (0.20)	14.7 (24.1)	52 (79)	CT
10d'	-6.69 (-6.24)	-1.54 (-1.40)	5.15 (4.84)	5.7 (7.0)	338 (363)	0.96 (1.11)	13.7 (17.6)	79 (81)	CT
11d'	-6.68 (-6.67)	-1.00 (-0.90)	5.67 (5.77)	3.8 (5.2)	309 (309)	0.01 (0.01)	3.1 (4.8)	0	LE

Values in parentheses were calculated in DMSO (SMD method). ^aHOMO energy. ^bLUMO energy. ^cHOMO-LUMO gap. ^dDipole moment (Debye). ^eCalculated absorption wavelength. ^fOscillator strength. ^gContribution percentage of HOMO-LUMO (charge-transfer) transition in S_1 state. ^hOverall transition type. LE = locally excited, CT = charge transfer.

The optimized ground-state structures of all compounds exhibited twist angles of $\sim 35^\circ$ between the phenyl rings. HOMOs of these compounds were localized on amino parts and their adjacent phenyl rings. In contrast, LUMOs were localized on the nitrophenyl part of oNB units, except for those of **2d'** and **10d'** whose LUMOs were found on two peripheral

nitrophenyl moieties (see Experimental section). As a result, there were large differences in LUMO energies of **2d'** and **10d'** (−1.57 and −1.54 eV in vacuum, respectively) compared to other compounds, e.g., −0.98 eV for **1d'** in vacuum. HOMO energies, on the other hand, varied with amino substituents and corresponded to their electron donor strength. Extending π -conjugation along with torsional restriction and EDG attachment increased the donor strength of amino substituents and also the HOMO energies of **3d'**–**5d'** (−6.35, −6.25, −6.08 and −5.81 eV for **1d'** and **3d'**–**5d'**, respectively, in vacuum), which subsequently reduced their HOMO-LUMO gaps (5.37, 5.24, 5.06 and 4.91 eV for **1d'** and **3d'**–**5d'**, respectively, in vacuum). Functionalization with EWG decreased the donor strength and HOMO energies in **2d'** and **10d'** (−6.75 and −6.69 eV, respectively, in vacuum). However, due to their different behaviors in LUMOs, it is not straightforward to compare HOMO-LUMO gaps of these two compounds with those of others. In contrast, the cyclic form did not change the energy of HOMO in **7d'** (−6.35 eV in vacuum) compared to that in **1d'** but resulted in considerably lower HOMO energies of **6d'**, **8d'**, and **11d'** (−6.73 eV, −6.61 eV, and −6.68 eV, respectively, in vacuum), which suggested carbazole and phenothiazine are weak donors. The aromatic character of carbazole lowered the donor ability, while the cyclic structure of phenothiazine reduced the interaction of lone pair on nitrogen atom with the rest of the molecule⁸⁵. The decreases in HOMO energies of **6d'**, **8d'**, and **11d'**, thus, expanded their HOMO-LUMO gaps (5.56, 5.72, and 5.67 eV, respectively, in vacuum). Altering relative position between the amino group and the nitro group, however, had no significant effect on the energy of HOMO, LUMO, and HOMO-LUMO gap, e.g., 5.37 and 5.22 eV for **1d'** and **9d'**, respectively, in vacuum.

The TD-M062X/6-31g(d) calculation using optimized ground state geometries predicted hypsochromic shift of the absorption spectra for all compounds compared to experimental spectra. In particular, 60–70 nm shifts in absorption maxima were observed for **1d'**–**5d'**, **7d'**, and **10d'**, e.g., calculated 334 nm, observed 399 nm for **1d'** in DMSO. Similar results in the prediction of absorption spectra for strong push-pull molecules using TD-M062X/6-31g(d) level of theory were also found in previous studies¹². It is difficult to precisely evaluate the shifts in **6d'**, **8d'**, **9d'**, and **11d'** because of the uncertainty in determining the absorption maxima related to the S₁ state in their experimental spectra. Relatively, oscillator strengths computed for **7d'** and **9d'** (0.20 and 0.13, respectively, in vacuum) could be ascribed to the lack of overlap between the frontier orbitals of these two compounds compared to others. In contrast, those computed for **6d'**, **8d'**, and **11d'** (0.14, 0.27, and 0.01, respectively, in vacuum) conceivably resulted from the contribution of forbidden n–π* excitation. These findings agree with the small absorption related to the S₁ state in the experimental spectra of **8d**, **9d**, and **11d** (Figure 24). Computation in DMSO (SMD method) tends to overestimate the CT transition in the case of **8d'**.

Investigations of the transitions contributing to the lowest excited singlet state S₁ of the designed oNB molecules provided valuable information regarding their quantum efficiencies. HOMO-LUMO transition, which corresponds to CT transition from the donor (amino part) to the acceptor (nitro part), contributed significantly (50–80%) to the S₁ states of **1d'**–**5d'**, **7d'**, **9d'**, and **10d'** (Table 7). In contrast, it covered only 11% (13% in DMSO) and 25% (52% in DMSO) of the transitions responsible for S₁ states of **6d'** and **8d'**, respectively, and was not even found in those of **11d'**. Minor contribution of CT transition to the S₁ states of

6d', **8d'**, and **11d'** implied that they are dominated by the forbidden local $n-\pi^*$ excitation within the nitro group. This explained the considerably low oscillator strength for **11d'**, while slightly higher values for **6d'** and **8d'** were probably due to some contribution from the allowed CT transition. NTO pictures obviously describe the excitation character of these compounds (Figures 29 and 30). Since the $n-\pi^*$ transition is crucial to trigger the intramolecular hydrogen abstraction process⁷⁶, which is the first step in photo-uncaging of oNB PPGs and important in determining their uncaging quantum yield (Figure 2), the absence of its contribution to the lowest excited states caused inefficiency in photoreactions. While there was no noticeable difference in the dipole moment at ground state for all compounds (Table 7), the vast increase in this parameter upon excitation for **1d'**–**5d'**, **7d'**, **9d'**, and **10d'**, e.g., 8.3 D at S_0 and 25.3 D at S_1 for **4d'** in vacuum, suggested the existence of strong CT character at S_1 state of these derivatives. The substitution of strong EDGs increased HOMO energy, which subsequently reduced HOMO-LUMO gap, stabilized the CT transition, and switched it to the lowest excited state. Functionalization with strong EWGs as in **2d'** and **10d'**, however, induced electron migration towards the branches instead of the oNB moiety upon excitation, which substantially suppressed the uncaging quantum efficiency. Altering the relative position between donor and acceptor had almost no effect on the HOMO-LUMO gap. However, the cyclic structure of the donor might bring about the reversed effect, which decreased HOMO energy, destabilized HOMO-LUMO (CT) transition, and preserved the local excitation character at the lowest excited state, as observed in **6d'**, **8d'**, and **11d'**.

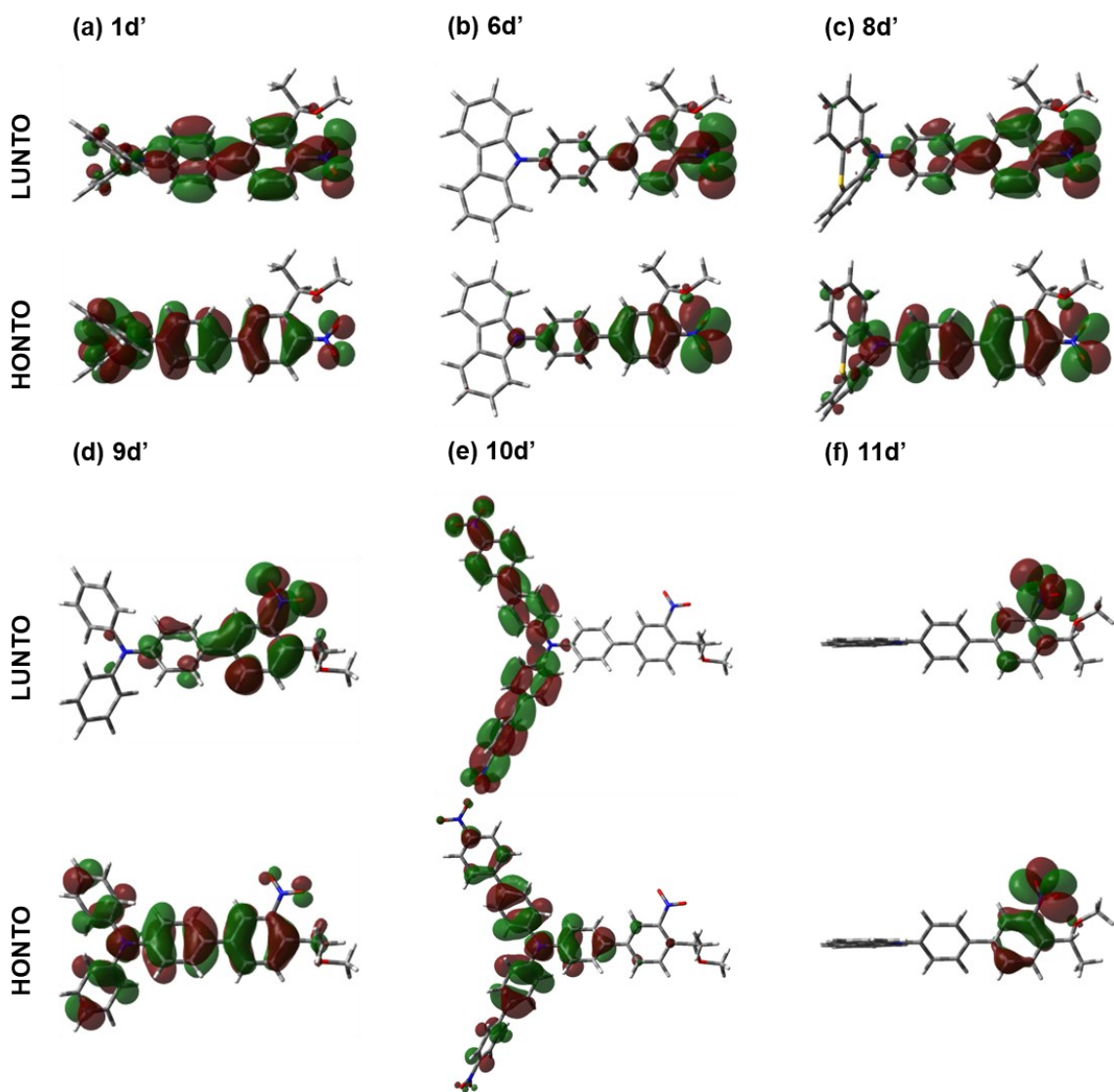


Figure 29. Natural transition orbitals (NTOs) for the lowest excited single state S_1 calculated at TD-M062X/6-31g(d) level of theory in DMSO (SMD method).

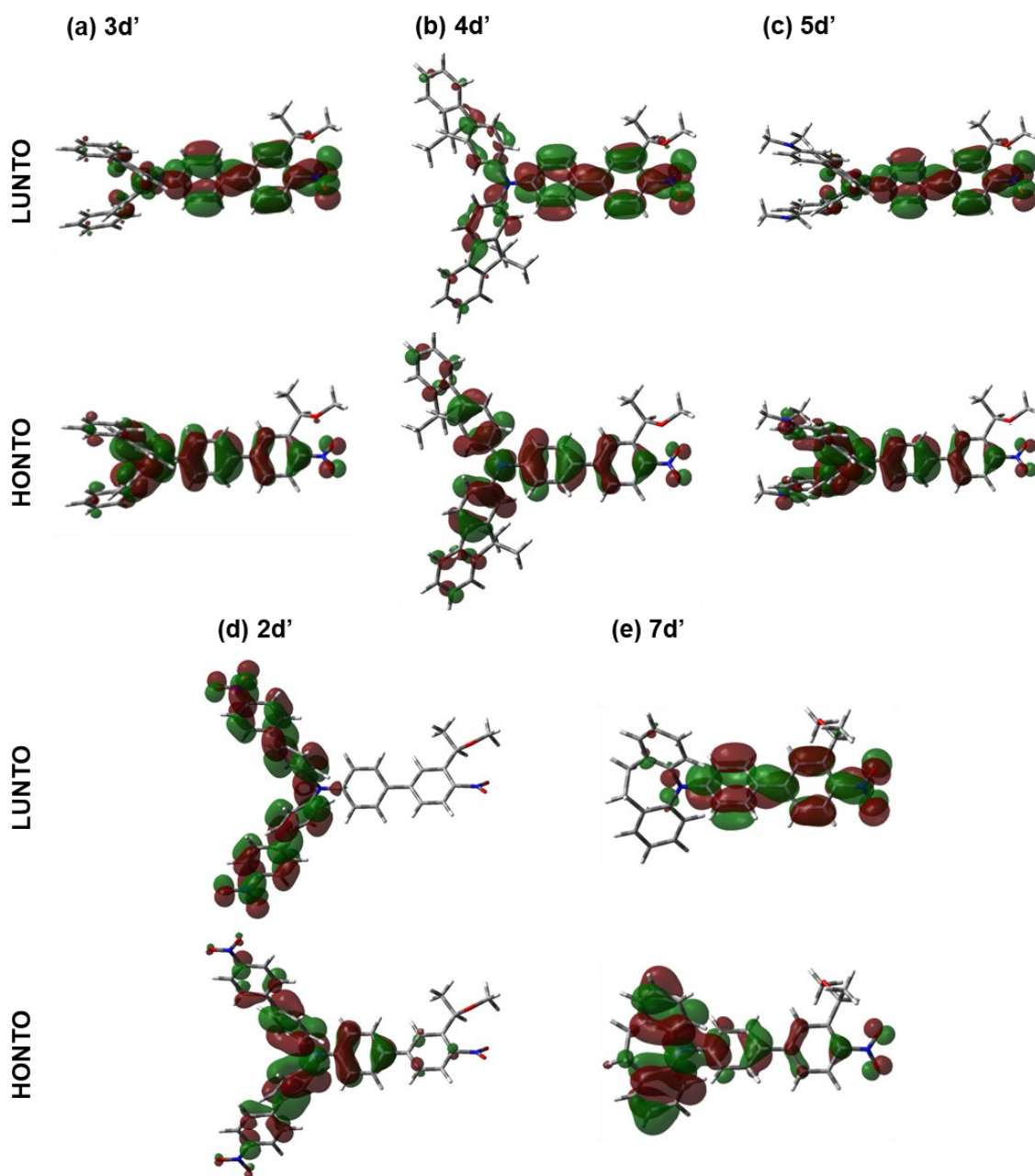


Figure 30. Natural transition orbitals (NTOs) for the lowest excited single state S_1 calculated at TD-M062X/6-31g(d) level of theory in DMSO (SMD method).

3.5. Summary

In this study, we designed and synthesized a series of nitrobiphenyl chromophores by varying amino substituents as electron donors and their relative position to the nitro group. These substituent effects were investigated on the uncaging quantum yield of oNB PPG. In this manner, we developed new nitrobiphenyl scaffolds substituted by carbazole and phenothiazine units **6d**, **11d**, and **8d**, whose uncaging quantum yields were observed to be 0.2, 0.2, and 0.1, respectively, rendering them potential compounds for future biological experiments. The quantum chemical calculations, which predict the character of the lowest excited states, can serve as a valuable tool to predict the quantum efficiencies of oNB PPGs.

3.6. Experimental section

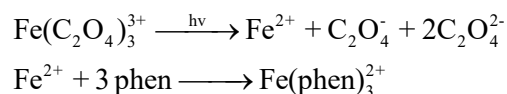
General information

Chemical reagents and solvents purchased from commercial suppliers were utilized without additional purification. Silica Gel 60 N (spherical, neutral) with particle sizes of 63–210 μm was used for column chromatography. NMR spectra were recorded using a Bruker ASCEND 400 spectrometer (^1H NMR: 400 MHz, ^{13}C NMR: 100 MHz). Chemical shifts (δ) were reported in parts per million (ppm) relative to the residual peak of solvents (CDCl_3 : δ 7.26 ppm for ^1H NMR, δ 77.16 ppm for ^{13}C NMR; CD_3OD : δ 3.31 ppm for ^1H NMR, δ 49.00 ppm for ^{13}C NMR; $\text{DMSO}-d_6$: δ 2.50 ppm for ^1H NMR, δ 39.52 ppm for ^{13}C NMR; acetone- d_6 : δ 2.05 ppm for ^1H NMR, δ 29.84 ppm for ^{13}C NMR). The data was presented in the following format: chemical shift, multiplicity (s = singlet, d = doublet, dd = doublet of doublets, ddd = doublet of doublets of doublets, t = triplet, q = quartet, qd = quartet of doublets, m = multiplet, and br = broad signal), coupling constant J (Hz), and integration.

UV-vis spectra were measured with a SHIMADZU UV-3600 Plus spectrophotometer. Fluorescence spectra were measured with a FluoroMax-4 spectrofluorometer. Mass spectrometric data were obtained using a Thermo Fisher Scientific LTQ Orbitrap XL, conducted by the Natural Science Center for Basic Research and Development (N-BARD), Hiroshima University. IR spectra were recorded using a JASCO MCT-6000M spectrometer.

Chemical actinometer for quantum yield measurement⁵⁹

One of the most reliable and widely used chemical actinometers to measure photon fluxes is ferrioxalate, which, upon irradiation, decomposes according to the following equations:



The number of ferrous ions generated during the photochemical reaction is determined by conversion to the colored tris-phenanthroline complex, which absorbs the light at 510 nm ($\epsilon = 11100 \text{ M}^{-1} \text{ cm}^{-1}$). The complexation between ferric ions and phenanthroline is not considerable, and their complex does not have absorption at 510 nm.

Procedure for measurement:

1. 120 mg of $\text{K}_3[\text{Fe}(\text{C}_2\text{O}_4)_3] \cdot 3\text{H}_2\text{O}$ was dissolved in 20 mL of 0.05 M H_2SO_4 (1).
2. 5 mg of 1,10-phenanthroline monohydrate and 1.12 g of $\text{CH}_3\text{COONa} \cdot 3\text{H}_2\text{O}$ were dissolved in 5 mL of 0.5 M H_2SO_4 (2).
3. 3 mL of solution (1) was taken and irradiated with each light source for specific times. After each irradiation, 0.5 mL of solution (2) was added, and the absorption spectra were measured.

4. The changes in absorbance at 510 nm with respect to irradiation time were used to calculate the amount of light as the equation below:

$$I (\text{mol/s}) = \frac{\text{moles of Fe}^{2+}}{\Phi_{\lambda} \times t \times F} = \frac{V_1 \times V_3 \times \Delta A_{510}}{10^3 \times V_2 \times l \times \epsilon_{510} \times \Phi_{\lambda} \times t}$$

V_1 : irradiated volume (3 mL)

V_2 : aliquot of irradiated solution taken for determining ferrous ions (3 mL)

V_3 : final volume (3.5 mL)

ΔA_{510} : absorbance difference between solutions before and after irradiation

l : optical pathlength of irradiation cell (1 cm)

ϵ_{510} : molar extinction coefficient of $\text{Fe}(\text{phen})_3^{2+}$ at 510 nm ($11100 \text{ M}^{-1}\text{cm}^{-1}$)

Φ_{λ} : quantum yield of ferrous ions generation at the irradiation wavelength ($\Phi_{365} = 1.21$, $\Phi_{405} = 1.14$, $\Phi_{320} = 1.24$)

t : irradiation time

F : mean function of light absorbed by the ferrioxalate solution

Table 8. Photon number of LED lamp 365 nm, LED lamp 405 nm and Xenon lamp 320 nm.

	Time (s)	ΔA_{510}	I (mol/s)	I_{avg} (mol/s)
LED lamp 365 nm	0.5	0.63	3.3×10^{-7}	
	1	1.27	3.3×10^{-7}	3.3×10^{-7}
	1.5	1.90	3.3×10^{-7}	
LED lamp 405 nm	0.2	0.56	7.8×10^{-7}	
	0.4	1.11	7.9×10^{-7}	7.8×10^{-7}
	0.6	1.70	7.8×10^{-7}	
Xenon lamp 320 nm	30	0.33	2.8×10^{-9}	
	60	0.65	2.8×10^{-9}	2.8×10^{-9}
	90	0.97	2.7×10^{-9}	

Measurement of uncaging quantum yield

Photoreactions of caged alcohols (3.0 mL, 0.4–0.6 mM, Abs at $\lambda_{\text{irr}} > 3$) were carried out in air-saturated DMSO at $\sim 23^\circ\text{C}$ using 405 nm LED lamp (± 20 nm, 7.8×10^{-7} mol s^{-1}) for compounds **2d–5d** and **10d**, 365 nm LED lamp (± 20 nm, 3.3×10^{-7} mol s^{-1}) for compounds **1b** and **6d–9d**, and 320 nm Xenon lamp with a monochromator (± 10 nm, 2.8×10^{-9} mol s^{-1}) for compound **11d**. The consumption of caged alcohols was monitored using HPLC (ODS-3, 3 μm , MeCN 100%), and the conversion rate was determined by fitting a trendline over the first 10% of conversion.

The quantum yield of uncaging was determined using the following equation:

$$\text{Quantum yield } \Phi_u = \frac{\text{conversion rate } k \text{ (s}^{-1}\text{)} \times \text{concentration } C \text{ (M)} \times \text{volume } V \text{ (L)}}{\text{photon number } I \text{ (mol s}^{-1}\text{)} \times 100}$$

Table 9. Conversion rate and quantum yield of caged alcohols **1d–11d** in DMSO.

Compound	Concentration / mM	Photon number / mol s^{-1}	Conversion rate / s^{-1}	Quantum yield Φ_u
1d	0.6	3.3×10^{-7}	0.4599	0.02
3d	0.4	7.8×10^{-7}	0.2824	0.004
4d	0.4	7.8×10^{-7}	0.1575	0.002
5d	0.4	7.8×10^{-7}	0.1351	0.002
2d	0.4	7.8×10^{-7}	0.1164	0.002
6d	0.6	3.3×10^{-7}	3.8199	0.2
7d	0.6	3.3×10^{-7}	0.4534	0.02
8d	0.6	3.3×10^{-7}	1.5525	0.1
9d	0.6	3.3×10^{-7}	0.2750	0.01
10d	0.4	7.8×10^{-7}	0.0264	<0.001
11d	0.6	2.8×10^{-9}	0.0304	0.2

Photoreactions in Ar-saturated and O₂-saturated DMSO

Photoreactions of **1d** and **6d** (3.0 mL, 0.6 mM, Abs at $\lambda_{\text{irr}} > 3$) were carried out in Ar-saturated and O₂-saturated DMSO at ~23°C (solutions were purged with Ar and O₂ gas by bubbling for 20 minutes) using 365 nm LED lamp (± 20 nm, 3.3×10^{-7} mol s⁻¹). Comparable decomposition rates were observed under air, oxygen, and argon, indicating that the uncaging process of these oNB derivatives occurred primarily from the S₁ state or a short-lived T₁ state.

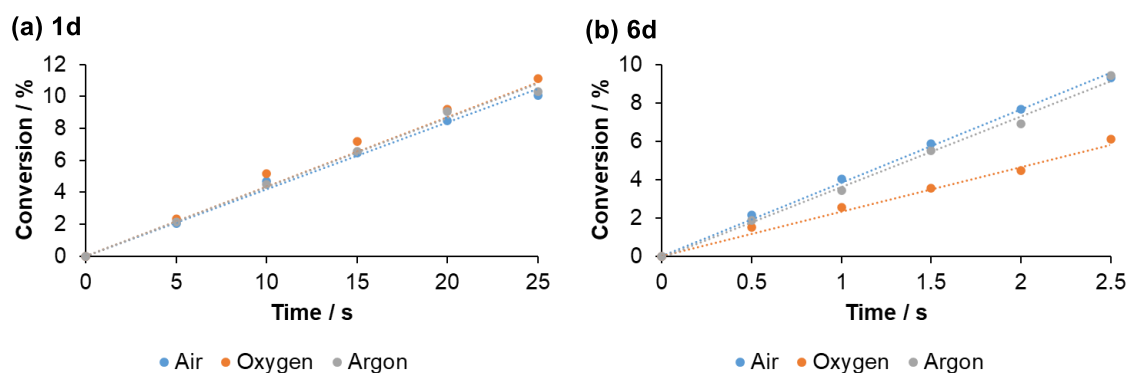


Figure 31. Time profile of photolysis (<10% conversion) in air-saturated, Ar-saturated and O₂-saturated DMSO.

Absorption spectra of nitrosoketone

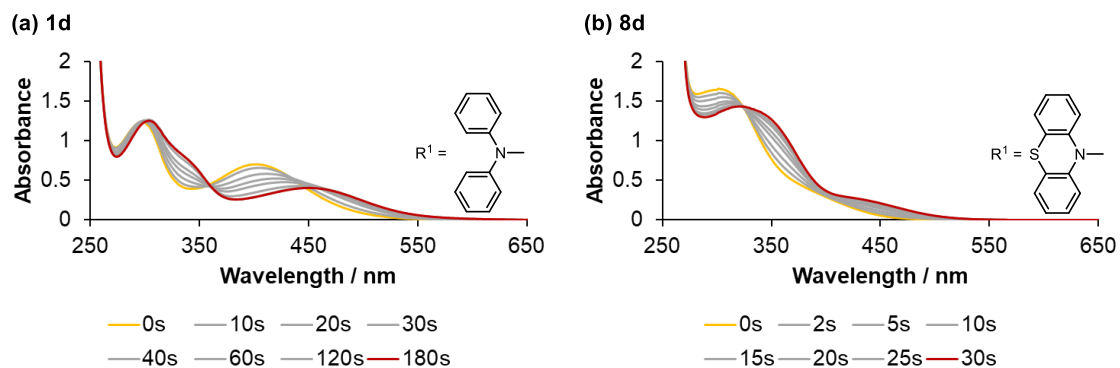
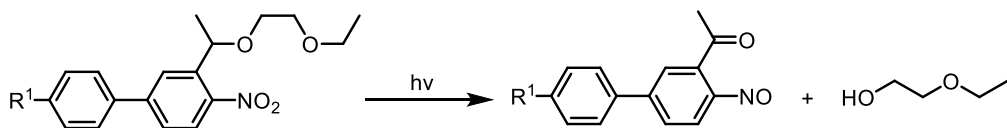


Figure 32. Absorption spectra during photolysis of (a) **1d** (0.06 mM) and (b) **8d** (0.12 mM) in air-saturated DMSO ($\sim 23^\circ\text{C}$) at 365 nm (LED lamp, $3.3 \times 10^{-7} \text{ mol s}^{-1}$). The absorption spectra after photolysis (red line) can be assigned to those of nitrosoketone photoproducts.

Mass spectra of nitrosoketone

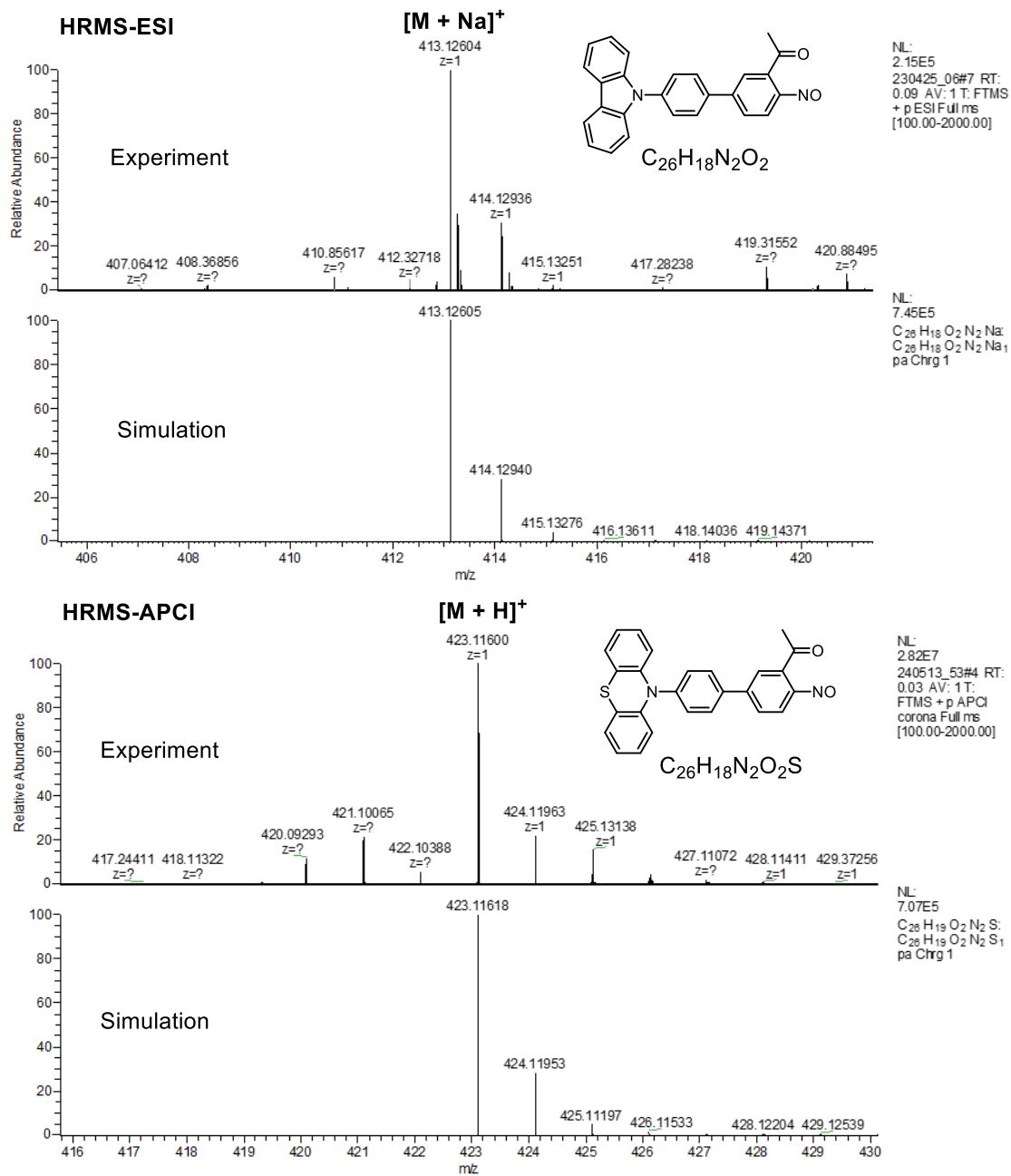


Figure 33. Mass spectra of nitrosoketone.

Quantum chemical calculations

Density functional theory (DFT) and time-dependent (TD) DFT calculations were performed using Gaussian 09 packages⁸⁶. Ground state geometries were optimized at the M062X/6-31g(d) level of theory in gas phase and DMSO (SMD model). The energy minimum structures were confirmed by vibrational frequency analysis at the same level of theory. Number of imaginary frequencies, energies (in Hartree), and Cartesian coordinates (in Å) of computed geometries were listed below. Properties related to the lowest excited single state S_1 were obtained at the TD-M062X/6-31g(d) level of theory in gas phase and DMSO (SMD model) using the optimized ground state geometries.

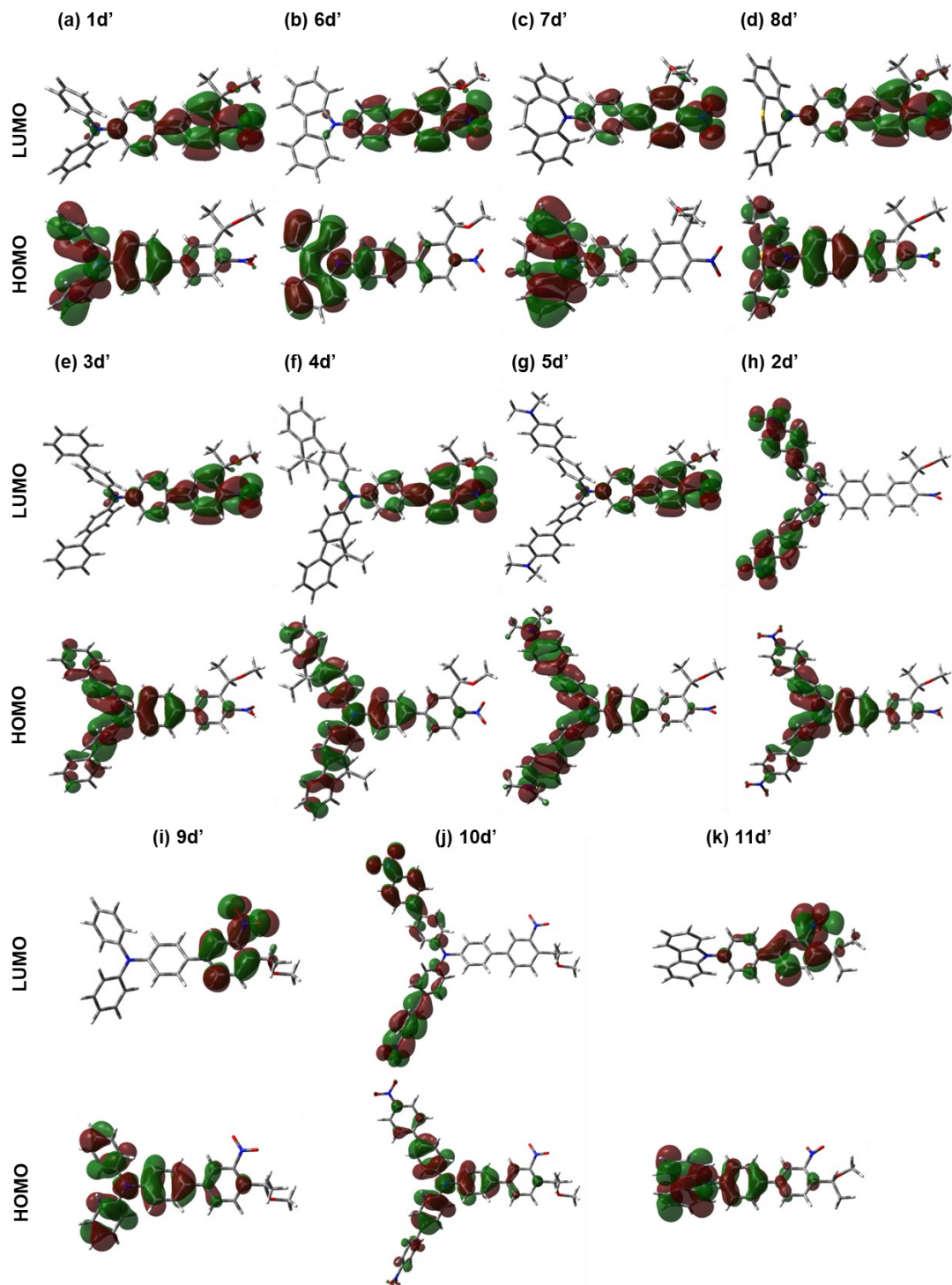
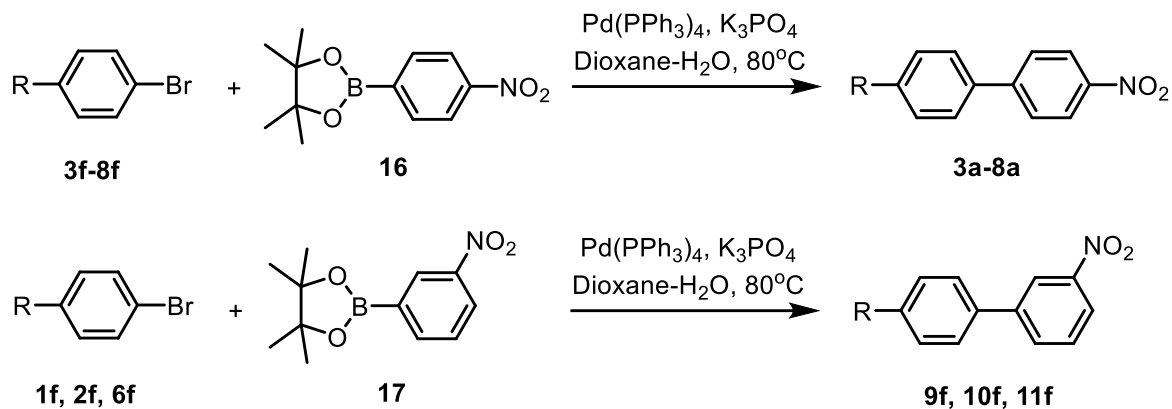


Figure 34. Frontier molecular orbitals calculated using the M062X/6-31g(d) level of theory in DMSO (SMD model).

Synthesis

Compounds **3f**⁸⁷, **4f**⁸⁸, **6f**⁸⁹, **7f**⁹⁰, **8f**⁹¹, and **6g**⁹² were synthesized according to procedures reported in the literature and confirmed by ¹H NMR spectra.

General procedure for syntheses of **3a–11a**



In a round-bottom flask, **3f** (1.0 mmol), **16**⁹³ (1.2 mmol), Pd(PPh₃)₄ (0.10 mmol) and K₃PO₄ (3.0 mmol) was mixed in 1,4-dioxane/H₂O (2:1, 9 mL). The reaction mixture was degassed by bubbling with N₂ and stirred at 80°C in an oil bath for 4h. The solvent was removed under reduced pressure, and the residue was purified by silica gel column chromatography to give the desired product **3a**.

N,N-di([1,1'-biphenyl]-4-yl)-4'-nitro-[1,1'-biphenyl]-4-amine (**3a**). Hexane/CH₂Cl₂ = 2:1. Orange solid (83%). ¹H NMR (400 MHz, CDCl₃) δ 8.29 (d, *J* = 8.8 Hz, 2H), 7.73 (d, *J* = 8.8 Hz, 2H), 7.63 – 7.58 (m, 4H), 7.58 – 7.53 (m, 6H), 7.49 – 7.42 (m, 4H), 7.39 – 7.32 (m, 2H), 7.28 – 7.24 (m, 6H). ¹³C{¹H} NMR (100 MHz, CDCl₃) δ 148.7, 147.1, 146.7, 146.5, 140.6, 136.6, 132.2, 129.0, 128.3, 128.2, 127.2, 127.1, 126.9, 125.2, 124.3, 123.5. IR (KBr, cm⁻¹) ν 1592, 1510, 1483, 1335, 1281, 1189, 1109, 1004, 855, 835, 764, 741, 721, 693, 553. HRMS (APCI) *m/z* [M + H]⁺ calcd for C₃₆H₂₇N₂O₂ 519.2067; found 519.2065. mp 232–235°C.

N-(9,9-dimethyl-9H-fluoren-2-yl)-9,9-dimethyl-*N*-(4'-nitro-[1,1'-biphenyl]-4-yl)-9H-fluoren-2-amine (**4a**). Hexane/CH₂Cl₂ = 2:1. Red solid (82%). ¹H NMR (400 MHz, acetone-d₆) δ 8.31 (d, *J* = 9.0 Hz, 2H), 7.97 (d, *J* = 9.0 Hz, 2H), 7.83 – 7.74 (m, 6H), 7.54 – 7.48 (m, 2H), 7.40 (d, *J* = 2.0 Hz, 2H), 7.37 – 7.23 (m, 6H), 7.18 – 7.14 (m, 2H), 1.44 (s, 12H). ¹³C{¹H} NMR (100 MHz, acetone-d₆) δ 156.2, 154.5, 149.9, 147.8, 147.6, 147.5, 139.6, 135.9, 132.3, 129.1, 128.0, 127.8, 127.7, 124.9, 124.8, 123.7, 123.5, 121.9, 120.5, 120.3, 47.6, 27.3. IR (KBr, cm⁻¹) ν 1591, 1515, 1484, 1448, 1339, 1109, 855, 828, 755, 736. HRMS (APCI) *m/z* [M + H]⁺ calcd for C₄₂H₃₅N₂O₂ 599.2693; found 599.2694. mp 142–146°C.

*N*⁴-(4'-(dimethylamino)-[1,1'-biphenyl]-4-yl)-*N*^{4'},*N*^{4'}-dimethyl-*N*⁴-(4'-nitro-[1,1'-biphenyl]-4-yl)-[1,1'-biphenyl]-4,4'-diamine (**5a**). Hexane/CH₂Cl₂ = 1:2. Red solid (76%). ¹H NMR (400 MHz, CDCl₃) δ 8.27 (d, *J* = 8.9 Hz, 2H), 7.71 (d, *J* = 8.9 Hz, 2H), 7.55 – 7.47 (m, 10H), 7.25 – 7.18 (m, 6H), 6.81 (d, *J* = 8.9 Hz, 4H), 3.00 (s, 12H). ¹³C{¹H} NMR (100 MHz, CDCl₃) δ 149.9, 149.0, 147.3, 146.5, 145.3, 136.8, 131.3, 128.7, 128.2, 127.5, 127.2, 126.9, 125.5, 124.3, 122.7, 113.0, 40.7. IR (KBr, cm⁻¹) ν 1608, 1590, 1498, 1443, 1334, 1285, 1186, 1109, 810, 755. HRMS (APCI) *m/z* [M + H]⁺ calcd for C₄₀H₃₇N₄O₂ 605.2911; found 605.2913. mp 137–139°C.

9-(4'-nitro-[1,1'-biphenyl]-4-yl)-9H-carbazole (**6a**). Hexane/CH₂Cl₂ = 4:1. Yellow solid (89%). ¹H NMR (400 MHz, CDCl₃) δ 8.37 (d, *J* = 8.8 Hz, 2H), 8.17 (d, *J* = 8.0 Hz, 2H), 7.86 (t, *J* = 8.7 Hz, 4H), 7.73 (d, *J* = 8.8 Hz, 2H), 7.51 – 7.42 (m, 4H), 7.36 – 7.29 (m, 2H). ¹³C{¹H} NMR (100 MHz, CDCl₃) δ 147.5, 146.7, 140.8, 138.7, 137.8, 129.0, 128.0, 127.7, 126.3, 124.5, 123.8, 120.6, 120.5, 109.9. IR (KBr, cm⁻¹) ν 1592, 1517, 1451, 1337, 1230,

858, 830, 754, 722, 687, 653. HRMS (APCI) m/z $[M + H]^+$ calcd for $C_{24}H_{17}N_2O_2$ 365.1285; found 365.1284. mp > 250°C.

5-(4'-nitro-[1,1'-biphenyl]-4-yl)-10,11-dihydro-5*H*-dibenzo[*b,f*]azepine (7a).

Hexane/ CH_2Cl_2 = 4:1. Yellow solid (71%). 1H NMR (400 MHz, acetone- d_6) δ 8.24 (d, J = 9.0 Hz, 2H), 7.84 (d, J = 9.0 Hz, 2H), 7.59 (d, J = 9.0 Hz, 2H), 7.46 (dd, J = 7.6, 1.5 Hz, 2H), 7.40 – 7.27 (m, 6H), 6.65 (d, J = 9.0 Hz, 2H), 3.02 (s, 4H). $^{13}C\{^1H\}$ NMR (100 MHz, acetone- d_6) δ 150.9, 148.1, 147.0, 144.0, 139.1, 132.1, 130.6, 129.0, 128.5, 128.2, 128.1, 127.1, 124.9, 113.9, 31.3. IR (KBr, cm^{-1}) ν 1589, 1510, 1485, 1448, 1336, 1287, 1200, 1109, 855, 821, 771, 754, 641. HRMS (ESI) m/z $[M + Na]^+$ calcd for $C_{26}H_{20}N_2O_2Na$ 415.1417; found 415.1414. mp 176–179°C.

10-(4'-nitro-[1,1'-biphenyl]-4-yl)-10*H*-phenothiazine (8a). Hexane/ CH_2Cl_2 = 4:1. Orange solid (82%). 1H NMR (400 MHz, $CDCl_3$) δ 8.34 (d, J = 8.9 Hz, 2H), 7.80 (d, J = 8.8 Hz, 4H), 7.47 (d, J = 8.6 Hz, 2H), 7.12 (dd, J = 7.5, 1.6 Hz, 2H), 6.99 – 6.88 (m, 4H), 6.46 (dd, J = 8.0, 1.3 Hz, 2H). $^{13}C\{^1H\}$ NMR (100 MHz, $CDCl_3$) δ 147.4, 146.7, 143.8, 142.8, 137.5, 129.6, 129.2, 127.9, 127.4, 127.1, 124.4, 123.5, 123.0, 118.0. IR (KBr, cm^{-1}) ν 1590, 1510, 1485, 1459, 1335, 1301, 1259, 1236, 1105, 1041, 917, 855, 826, 747, 646, 617. HRMS (APCI) m/z $[M + H]^+$ calcd for $C_{24}H_{17}N_2O_2S$ 397.1005; found 397.1007. mp > 250°C.

3'-nitro-*N,N*-diphenyl-[1,1'-biphenyl]-4-amine (9a). Hexane/ CH_2Cl_2 = 4:1. Yellow solid (89%). 1H NMR (400 MHz, $CDCl_3$) δ 8.42 (s, 1H), 8.14 (d, J = 8.0 Hz, 1H), 7.88 (d, J = 7.8 Hz, 1H), 7.57 (t, J = 8.0 Hz, 1H), 7.49 (d, J = 8.5 Hz, 2H), 7.34 – 7.26 (m, 4H), 7.19 – 7.12 (m, 6H), 7.11 – 7.04 (m, 2H). $^{13}C\{^1H\}$ NMR (100 MHz, $CDCl_3$) δ 148.9, 148.5, 147.4, 142.4, 132.5, 131.9, 129.7, 129.5, 127.9, 124.9, 123.6, 123.4, 121.5, 121.4. IR (KBr, cm^{-1}) ν 1590,

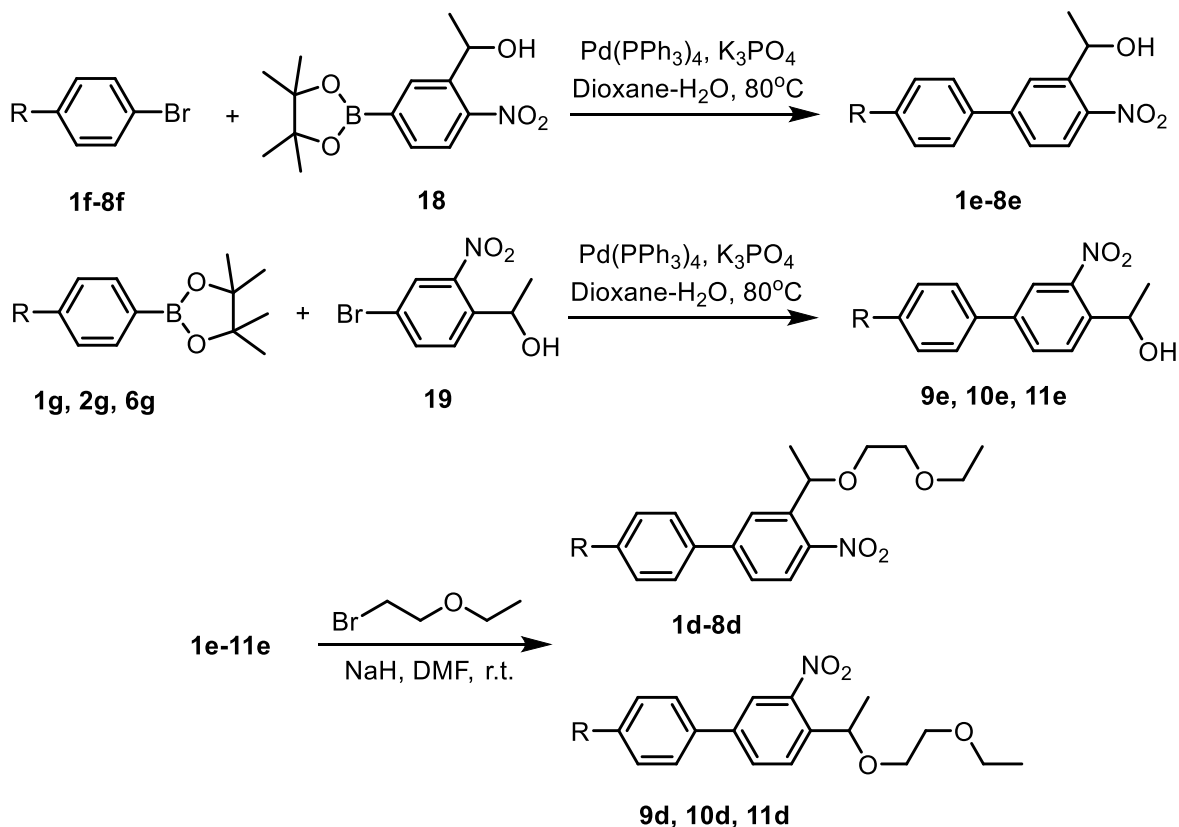
1531, 1513, 1489, 1348, 1281, 835, 804, 755, 697, 512. HRMS (ESI) m/z $[M + Na]^+$ calcd for $C_{24}H_{18}N_2O_2Na$ 389.1260; found 389.1261. mp 122–124°C.

3'-nitro-*N,N*-bis(4'-nitro-[1,1'-biphenyl]-4-yl)-[1,1'-biphenyl]-4-amine (10a).

Hexane/ CH_2Cl_2 = 1:2. Orange solid (74%). 1H NMR (400 MHz, $CDCl_3$) δ 8.46 (t, J = 2.0 Hz, 1H), 8.30 (d, J = 8.9 Hz, 4H), 8.20 (ddd, J = 8.2, 2.2, 0.9 Hz, 1H), 7.92 (ddd, J = 7.8, 1.6, 1.0 Hz, 1H), 7.74 (d, J = 8.9 Hz, 4H), 7.66 – 7.55 (m, 7H), 7.33 – 7.26 (m, 6H). $^{13}C\{^1H\}$ NMR (100 MHz, $CDCl_3$) δ 149.0, 147.9, 147.4, 146.9, 146.8, 142.2, 134.0, 133.6, 132.7, 130.0, 128.6, 128.4, 127.3, 125.2, 124.7, 124.4, 122.0, 121.7. IR (KBr, cm^{-1}) ν 1733, 1590, 1511, 1483, 1341, 1285, 1192, 1109, 855, 829, 779, 754, 722, 696. HRMS (APCI) m/z $[M + H]^+$ calcd for $C_{36}H_{25}N_4O_6$ 609.1769; found 609.1763. mp > 250°C.

9-(3'-nitro-[1,1'-biphenyl]-4-yl)-9*H*-carbazole (11a). Hexane/ CH_2Cl_2 = 4:1. Yellow solid (89%). 1H NMR (400 MHz, $CDCl_3$) δ 8.57 (t, J = 1.9 Hz, 1H), 8.27 (ddd, J = 8.2, 2.2, 0.9 Hz, 1H), 8.17 (d, J = 7.7 Hz, 2H), 8.03 (ddd, J = 7.7, 1.7, 1.0 Hz, 1H), 7.88 (d, J = 8.5 Hz, 2H), 7.75 – 7.67 (m, 3H), 7.51 – 7.42 (m, 4H), 7.35 – 7.29 (m, 2H). $^{13}C\{^1H\}$ NMR (100 MHz, $CDCl_3$) δ 148.8, 141.8, 140.7, 138.1, 137.5, 132.9, 130.0, 128.6, 127.5, 126.2, 123.6, 122.4, 121.9, 120.5, 120.3, 109.8. IR (KBr, cm^{-1}) ν 1604, 1517, 1478, 1451, 1348, 1228, 1172, 876, 837, 805, 780, 751, 724, 682. HRMS (APCI) m/z $[M + H]^+$ calcd for $C_{24}H_{17}N_2O_2$ 365.1285; found 365.1287. mp 156–160°C.

General procedure for syntheses of **1d–11d**



Step 1:

Synthesis of **1e–8e**: In a round-bottom flask, **1f** (1.0 mmol), **18** (1.2 mmol), $\text{Pd}(\text{PPh}_3)_4$ (0.10 mmol) and K_3PO_4 (3.0 mmol) was mixed in 1,4-dioxane/ H_2O (2:1, 9 mL). The reaction mixture was degassed by bubbling with N_2 and stirred at 80°C in an oil bath for 4h. The solvent was removed under reduced pressure, and the residue was purified by silica gel column chromatography to give the desired product **1e**.

Synthesis of **9e–11e**: In a round-bottom flask, **1g** (1.2 mmol), **19** (1.0 mmol), $\text{Pd}(\text{PPh}_3)_4$ (0.10 mmol) and K_3PO_4 (3.0 mmol) was mixed in 1,4-dioxane/ H_2O (2:1, 9 mL). The reaction mixture was degassed by bubbling with N_2 and stirred at 80°C in an oil bath for 4h. The

solvent was removed under reduced pressure, and the residue was purified by silica gel column chromatography to give the desired product **9e**.

1-(4'-(diphenylamino)-4-nitro-[1,1'-biphenyl]-3-yl)ethan-1-ol (**1e**). Hexane/EtOAc = 9:1. Red oil (89%). ¹H NMR (400 MHz, CDCl₃) δ 8.04 (d, *J* = 2.0 Hz, 1H), 8.01 (d, *J* = 8.6 Hz, 1H), 7.57 (dd, *J* = 8.5, 2.1 Hz, 1H), 7.52 (d, *J* = 8.7 Hz, 2H), 7.34 – 7.26 (m, 4H), 7.19 – 7.11 (m, 6H), 7.12 – 7.06 (m, 2H), 5.54 (q, *J* = 6.3 Hz, 1H), 2.43 (br, 1H), 1.62 (d, *J* = 6.3 Hz, 3H). ¹³C{¹H} NMR (100 MHz, CDCl₃) δ 148.9, 147.3, 146.3, 145.9, 142.1, 131.9, 129.6, 128.2, 125.7, 125.5, 125.3, 125.1, 123.8, 123.0, 66.0, 24.4. IR (KBr, cm⁻¹) ν 3557, 3035, 2977, 1589, 1514, 1488, 1330, 1282, 1180, 1105, 1074, 825, 755, 736, 698, 529. HRMS (ESI) *m/z* [M + Na]⁺ calcd for C₂₆H₂₂N₂O₃Na 433.1523; found 433.1520.

1-(4'-(di([1,1'-biphenyl]-4-yl)amino)-4-nitro-[1,1'-biphenyl]-3-yl)ethan-1-ol (**3e**). Hexane/EtOAc = 4:1. Red solid (89%). ¹H NMR (400 MHz, CDCl₃) δ 8.06 (d, *J* = 2.0 Hz, 1H), 8.04 (d, *J* = 8.5 Hz, 1H), 7.67 – 7.49 (m, 11H), 7.48 – 7.41 (m, 4H), 7.37 – 7.30 (m, 2H), 7.27 – 7.24 (m, 6H), 5.55 (q, *J* = 6.4 Hz, 1H), 2.36 (br, 1H), 1.63 (d, *J* = 6.3 Hz, 3H). ¹³C{¹H} NMR (100 MHz, CDCl₃) δ 148.6, 146.5, 146.3, 146.1, 142.1, 140.6, 136.5, 132.5, 129.0, 128.4, 128.2, 127.2, 126.9, 125.9, 125.6, 125.5, 125.1, 123.7, 66.1, 24.4. IR (KBr, cm⁻¹) ν 3030, 2925, 2855, 1597, 1514, 1484, 1323, 1294, 1188, 1107, 909, 830, 763, 733, 698. HRMS (APCI) *m/z* [M + H]⁺ calcd for C₃₈H₃₁N₂O₃ 563.2329; found 563.2323. mp 89–92°C.

1-(4'-(bis(9,9-dimethyl-9*H*-fluoren-2-yl)amino)-4-nitro-[1,1'-biphenyl]-3-yl)ethan-1-ol (**4e**). Hexane/EtOAc = 4:1. Red solid (76%). ¹H NMR (400 MHz, acetone-*d*₆) δ 8.24 (d, *J* = 2.1 Hz, 1H), 8.01 (d, *J* = 8.5 Hz, 1H), 7.82 – 7.71 (m, 7H), 7.54 – 7.48 (m, 2H), 7.40 (d, *J* = 1.9 Hz, 2H), 7.37 – 7.23 (m, 6H), 7.15 (dd, *J* = 8.2, 2.1 Hz, 2H), 5.51 – 5.44 (m, 1H), 4.66

(d, $J = 4.3$ Hz, 1H), 1.54 (d, $J = 6.3$ Hz, 3H), 1.44 (s, 12H). $^{13}\text{C}\{^1\text{H}\}$ NMR (100 MHz, acetone- d_6) δ 156.1, 154.4, 149.6, 147.8, 146.8, 146.1, 144.3, 139.6, 135.7, 132.9, 129.0, 128.0, 127.7, 126.0, 125.8, 124.6, 124.0, 123.5, 121.8, 120.4, 120.1, 65.7, 47.5, 27.3, 25.6. IR (KBr, cm^{-1}) ν 3568, 2960, 2923, 2860, 1599, 1580, 1513, 1459, 1448, 1342, 1311, 1276, 827, 779, 759, 736. HRMS (ESI) m/z $[\text{M} + \text{Na}]^+$ calcd for $\text{C}_{44}\text{H}_{38}\text{N}_2\text{O}_3\text{Na}$ 665.2775; found 665.2775. mp 138–142°C.

1-(4'-(bis(4'-(dimethylamino)-[1,1'-biphenyl]-4-yl)amino)-4-nitro-[1,1'-biphenyl]-3-yl)ethan-1-ol (**5e**). Hexane/ $\text{CH}_2\text{Cl}_2 = 1:2$. Red solid (76%). ^1H NMR (400 MHz, CDCl_3) δ 8.04 (d, $J = 1.9$ Hz, 1H), 8.01 (d, $J = 8.5$ Hz, 1H), 7.60 – 7.46 (m, 11H), 7.25 – 7.17 (m, 6H), 6.81 (d, $J = 8.8$ Hz, 4H), 5.52 (q, $J = 6.2$ Hz, 1H), 3.00 (s, 12H), 2.51 (br, 1H), 1.62 (d, $J = 6.3$ Hz, 3H). $^{13}\text{C}\{^1\text{H}\}$ NMR (100 MHz, CDCl_3) δ 149.8, 148.8, 146.3, 145.7, 145.2, 142.1, 136.5, 131.5, 128.7, 128.1, 127.4, 127.1, 125.6, 125.5, 125.3, 125.2, 122.7, 112.9, 65.9, 40.6, 24.3. IR (KBr, cm^{-1}) ν 3030, 2975, 1607, 1498, 1444, 1322, 1284, 1226, 1185, 1167, 1107, 1063, 945, 812, 528. HRMS (ESI) m/z $[\text{M} + \text{H}]^+$ calcd for $\text{C}_{42}\text{H}_{41}\text{N}_4\text{O}_3$ 649.3173; found 649.3174. mp 133–136°C.

1-(4'-(bis(4'-nitro-[1,1'-biphenyl]-4-yl)amino)-4-nitro-[1,1'-biphenyl]-3-yl)ethan-1-ol (**2e**). Hexane/ $\text{CH}_2\text{Cl}_2 = 1:2$. Red solid (85%). ^1H NMR (400 MHz, CDCl_3) δ 8.30 (d, $J = 8.9$ Hz, 4H), 8.08 (d, $J = 2.0$ Hz, 1H), 8.05 (d, $J = 8.5$ Hz, 1H), 7.74 (d, $J = 8.9$ Hz, 4H), 7.65 – 7.56 (m, 7H), 7.29 (d, $J = 8.7$ Hz, 6H), 5.57 (q, $J = 6.2$ Hz, 1H), 2.36 (br, 1H), 1.64 (d, $J = 6.3$ Hz, 3H). $^{13}\text{C}\{^1\text{H}\}$ NMR (100 MHz, CDCl_3) δ 147.8, 147.7, 146.9, 146.8, 146.3, 145.9, 142.2, 134.0, 133.7, 128.7, 128.6, 127.3, 126.0, 125.7, 125.6, 125.0, 124.8, 124.4, 66.0, 24.6. IR (KBr, cm^{-1}) ν 3546, 3038, 2928, 1590, 1513, 1483, 1337, 1285, 1192, 1109, 855, 827,

755, 732, 695. HRMS (APCI) m/z $[M]^-$ calcd for $C_{38}H_{28}N_4O_7$ 652.1964; found 652.1970. mp 144–148°C.

1-(4'-(9*H*-carbazol-9-yl)-4-nitro-[1,1'-biphenyl]-3-yl)ethan-1-ol (**6e**). Hexane/EtOAc = 4:1. Yellow solid (80%). 1H NMR (400 MHz, $CDCl_3$) δ 8.21 – 8.13 (m, 3H), 8.08 (d, J = 8.5 Hz, 1H), 7.87 (d, J = 8.4 Hz, 2H), 7.74 – 7.65 (m, 3H), 7.53 – 7.40 (m, 4H), 7.33 (t, J = 7.3 Hz, 2H), 5.58 (q, J = 6.3 Hz, 1H), 2.31 (br, 1H), 1.67 (d, J = 6.3 Hz, 3H). ^{13}C $\{^1H\}$ NMR (100 MHz, $CDCl_3$) δ 146.6, 145.7, 142.2, 140.7, 138.4, 137.8, 128.9, 127.5, 126.4, 126.20, 126.16, 125.5, 123.7, 120.5, 120.4, 109.8, 65.9, 24.6. IR (KBr, cm^{-1}) ν 3057, 1604, 1518, 1478, 1451, 1335, 1229, 1174, 1106, 1072, 1018, 910, 868, 829, 751, 725. HRMS (APCI) m/z $[M]^-$ calcd for $C_{26}H_{20}N_2O_3$ 408.1479; found 408.1480. mp 78–82°C.

1-(4'-(10,11-dihydro-5*H*-dibenzo[*b,f*]azepin-5-yl)-4-nitro-[1,1'-biphenyl]-3-yl)ethan-1-ol (**7e**). Hexane/EtOAc = 4:1. Red oil (76%). 1H NMR (400 MHz, acetone- d_6) δ 8.13 (d, J = 2.1 Hz, 1H), 7.95 (d, J = 8.6 Hz, 1H), 7.66 (dd, J = 8.6, 2.2 Hz, 1H), 7.56 (d, J = 9.0 Hz, 2H), 7.48 – 7.44 (m, 2H), 7.40 – 7.27 (m, 6H), 6.66 (d, J = 9.0 Hz, 2H), 5.48 – 5.42 (m, 1H), 4.58 (d, J = 4.2 Hz, 1H), 3.03 (s, 4H), 1.50 (d, J = 6.3 Hz, 3H). ^{13}C $\{^1H\}$ NMR (100 MHz, acetone- d_6) δ 150.6, 146.6, 146.2, 144.2, 144.0, 139.0, 132.0, 130.5, 128.7, 128.5, 128.4, 128.1, 125.7, 125.3, 125.2, 113.8, 65.7, 31.3, 25.6. IR (KBr, cm^{-1}) ν 3435, 3034, 2976, 2927, 1595, 1579, 1514, 1488, 1449, 1322, 1267, 1198, 1107, 821, 778, 759. HRMS (ESI) m/z $[M + Na]^+$ calcd for $C_{28}H_{24}N_2O_3Na$ 459.1679; found 459.1679.

1-(4-nitro-4'-(10*H*-phenothiazin-10-yl)-[1,1'-biphenyl]-3-yl)ethan-1-ol (**8e**). Hexane/EtOAc = 4:1. Orange solid (83%). 1H NMR (400 MHz, $CDCl_3$) δ 8.14 (d, J = 2.0 Hz, 1H), 8.07 (d, J = 8.5 Hz, 1H), 7.82 (d, J = 8.4 Hz, 2H), 7.68 (dd, J = 8.5, 2.0 Hz, 1H),

7.47 (d, $J = 8.4$ Hz, 2H), 7.11 (dd, $J = 7.4, 1.7$ Hz, 2H), 6.99 – 6.84 (m, 4H), 6.43 (dd, $J = 8.0, 1.3$ Hz, 2H), 5.57 (q, $J = 6.3$ Hz, 1H), 2.41 (br, 1H), 1.65 (d, $J = 6.3$ Hz, 3H). $^{13}\text{C}\{^1\text{H}\}$ NMR (100 MHz, CDCl_3) δ 146.6, 145.7, 143.8, 142.4, 142.2, 137.8, 129.6, 129.5, 127.2, 127.1, 126.4, 126.2, 125.5, 123.3, 122.4, 117.7, 65.9, 24.6. IR (KBr, cm^{-1}) ν 3436, 3062, 2975, 2928, 1605, 1588, 1515, 1461, 1443, 1342, 1309, 1259, 1105, 911, 829, 746. HRMS (ESI) m/z $[\text{M} + \text{Na}]^+$ calcd for $\text{C}_{26}\text{H}_{20}\text{N}_2\text{O}_3\text{SNa}$ 463.1087; found 463.1088. mp 134–136°C.

1-(4'-(diphenylamino)-3-nitro-[1,1'-biphenyl]-4-yl)ethan-1-ol (**9e**). Hexane/EtOAc = 9:1. Orange oil (83%). ^1H NMR (400 MHz, CDCl_3) δ 8.08 (d, $J = 1.7$ Hz, 1H), 7.90 – 7.80 (m, 2H), 7.47 (d, $J = 8.7$ Hz, 2H), 7.33 – 7.26 (m, 4H), 7.18 – 7.11 (m, 6H), 7.11 – 7.04 (m, 2H), 5.44 (q, $J = 6.3$ Hz, 1H), 2.35 (br, 1H), 1.61 (d, $J = 6.4$ Hz, 3H). $^{13}\text{C}\{^1\text{H}\}$ NMR (100 MHz, CDCl_3) δ 148.5, 148.4, 147.4, 141.1, 138.9, 131.6, 131.4, 129.5, 128.2, 127.8, 125.0, 123.6, 123.4, 122.1, 65.6, 24.3. IR (KBr, cm^{-1}) ν 3435, 3035, 2974, 2928, 1708, 1591, 1514, 1488, 1351, 1331, 1280, 1105, 1072, 826, 754, 697. HRMS (APCI) m/z $[\text{M}]^-$ calcd for $\text{C}_{26}\text{H}_{22}\text{N}_2\text{O}_3$ 410.1636; found 410.1638.

1-(4'-(bis(4'-nitro-[1,1'-biphenyl]-4-yl)amino)-3-nitro-[1,1'-biphenyl]-4-yl)ethan-1-ol (**10e**). Hexane/ CH_2Cl_2 = 1:2. Red solid (78%). ^1H NMR (400 MHz, CDCl_3) δ 8.30 (d, $J = 8.8$ Hz, 4H), 8.12 (d, $J = 1.7$ Hz, 1H), 7.94 – 7.84 (m, 2H), 7.74 (d, $J = 8.8$ Hz, 4H), 7.62 – 7.55 (m, 6H), 7.29 (d, $J = 8.6$ Hz, 6H), 5.47 (q, $J = 6.3$ Hz, 1H), 2.34 (s, 1H), 1.62 (d, $J = 6.4$ Hz, 3H). $^{13}\text{C}\{^1\text{H}\}$ NMR (100 MHz, CDCl_3) δ 148.4, 147.9, 147.3, 146.9, 146.8, 140.7, 139.4, 133.6, 133.5, 131.6, 128.6, 128.4, 128.3, 127.2, 125.2, 124.7, 124.3, 122.3, 65.6, 24.4. IR (KBr, cm^{-1}) ν 3037, 2928, 1590, 1513, 1483, 1341, 1285, 1189, 1109, 855, 827, 793, 755,

733, 693, 656. HRMS (APCI) m/z $[M]^-$ calcd for $C_{38}H_{28}N_4O_7$ 652.1964; found 652.1975. mp 128–132°C.

1-(4'-(9*H*-carbazol-9-yl)-3-nitro-[1,1'-biphenyl]-4-yl)ethan-1-ol (**1e**). Hexane/EtOAc = 4:1. Yellow solid (85%). 1H NMR (400 MHz, $CDCl_3$) δ 8.23 (s, 1H), 8.17 (d, $J = 7.6$ Hz, 2H), 8.01 – 7.95 (m, 2H), 7.84 (d, $J = 8.6$ Hz, 2H), 7.71 (d, $J = 8.6$ Hz, 2H), 7.51 – 7.41 (m, 4H), 7.35 – 7.29 (m, 2H), 5.51 (qd, $J = 6.3, 3.8$ Hz, 1H), 2.34 (d, $J = 3.7$ Hz, 1H), 1.66 (d, $J = 6.4$ Hz, 3H). $^{13}C\{^1H\}$ NMR (100 MHz, $CDCl_3$) δ 148.3, 140.7, 140.5, 140.0, 138.1, 137.2, 131.9, 128.5, 128.4, 127.6, 126.2, 123.6, 122.7, 120.5, 120.3, 109.8, 65.6, 24.4. IR (KBr, cm^{-1}) ν 3056, 2977, 1604, 1518, 1451, 1351, 1318, 1229, 1172, 1104, 1069, 830, 794, 751, 724. HRMS (APCI) m/z $[M + H]^+$ calcd for $C_{26}H_{21}N_2O_3$ 409.1547; found 409.1542. mp 148–150°C.

Step 2: To a solution of **1e** (1.0 mmol) and NaH (8.0 mmol) in dry DMF (10 mL) at 0°C was added 2-bromoethyl ethyl ether (8.0 mmol) dropwise. The temperature was slowly raised to room temperature, and the reaction mixture was stirred overnight. The reaction mixture was diluted with ethyl acetate and washed with water. The organic layer was dried over Na_2SO_4 , and the solvent was removed under reduced pressure. The residue was purified by silica gel column chromatography to give the desired product **1d**.

3'-(1-(2-ethoxyethoxy)ethyl)-4'-nitro-*N,N*-diphenyl-[1,1'-biphenyl]-4-amine (**1d**). Hexane/EtOAc = 9:1. Red oil (82%). 1H NMR (400 MHz, $CDCl_3$) δ 8.06 (d, $J = 2.0$ Hz, 1H), 8.04 (d, $J = 8.6$ Hz, 1H), 7.61 – 7.51 (m, 3H), 7.34 – 7.26 (m, 4H), 7.19 – 7.10 (m, 6H), 7.11 – 7.04 (m, 2H), 5.19 (q, $J = 6.3$ Hz, 1H), 3.65 – 3.44 (m, 6H), 1.58 (d, $J = 6.3$ Hz, 3H), 1.15 (t, $J = 7.0$ Hz, 3H). $^{13}C\{^1H\}$ NMR (100 MHz, $CDCl_3$) δ 148.8, 147.4, 146.6, 146.3, 141.2,

132.1, 129.6, 128.3, 125.57, 125.55, 125.5, 125.1, 123.7, 123.2, 74.0, 70.0, 68.8, 66.8, 24.0, 15.3. IR (KBr, cm^{-1}) ν 3035, 2974, 2867, 1590, 1514, 1489, 1329, 1283, 1180, 1106, 875, 825, 754, 698, 619, 526. HRMS (ESI) m/z $[\text{M} + \text{Na}]^+$ calcd for $\text{C}_{30}\text{H}_{30}\text{N}_2\text{O}_4\text{Na}$ 505.2098; found 505.2093.

N,N-di([1,1'-biphenyl]-4-yl)-3'-(1-(2-ethoxyethoxy)ethyl)-4'-nitro-[1,1'-biphenyl]-4-amine (**3d**). Hexane/EtOAc = 4:1. Red oil (80%). ^1H NMR (400 MHz, CDCl_3) δ 8.09 (d, $J = 2.1$ Hz, 1H), 8.05 (d, $J = 8.6$ Hz, 1H), 7.64 – 7.57 (m, 7H), 7.55 (d, $J = 8.7$ Hz, 4H), 7.48 – 7.41 (m, 4H), 7.37 – 7.31 (m, 2H), 7.28 – 7.23 (m, 6H), 5.20 (q, $J = 6.3$ Hz, 1H), 3.66 – 3.44 (m, 6H), 1.59 (d, $J = 6.3$ Hz, 3H), 1.16 (t, $J = 7.0$ Hz, 3H). ^{13}C $\{^1\text{H}\}$ NMR (100 MHz, CDCl_3) δ 148.5, 146.6, 146.2, 141.3, 140.6, 136.5, 132.6, 128.9, 128.4, 128.2, 127.2, 126.9, 125.7, 125.6, 125.5, 125.1, 123.7, 74.0, 70.0, 68.9, 66.8, 24.0, 15.3. IR (KBr, cm^{-1}) ν 3030, 2974, 2866, 1713, 1597, 1514, 1484, 1323, 1294, 1180, 1106, 875, 831, 763, 731, 698. HRMS (APCI) m/z $[\text{M} + \text{H}]^+$ calcd for $\text{C}_{42}\text{H}_{39}\text{N}_2\text{O}_4$ 635.2904; found 635.2905.

N-(9,9-dimethyl-9*H*-fluoren-2-yl)-*N*-(3'-(1-(2-ethoxyethoxy)ethyl)-4'-nitro-[1,1'-biphenyl]-4-yl)-9,9-dimethyl-9*H*-fluoren-2-amine (**4d**). Hexane/EtOAc = 4:1. Red solid (81%). ^1H NMR (400 MHz, acetone- d_6) δ 8.16 (d, $J = 2.1$ Hz, 1H), 8.08 (d, $J = 8.6$ Hz, 1H), 7.82 (dd, $J = 8.6, 2.1$ Hz, 1H), 7.81 – 7.71 (m, 6H), 7.54 – 7.46 (m, 2H), 7.40 (d, $J = 2.0$ Hz, 2H), 7.37 – 7.22 (m, 6H), 7.15 (dd, $J = 8.2, 2.1$ Hz, 2H), 5.15 (q, $J = 6.3$ Hz, 1H), 3.61 – 3.37 (m, 6H), 1.53 (d, $J = 6.3$ Hz, 3H), 1.44 (s, 12H), 1.07 (t, $J = 7.0$ Hz, 3H). ^{13}C $\{^1\text{H}\}$ NMR (100 MHz, acetone- d_6) δ 156.2, 154.5, 149.8, 147.8, 147.7, 146.5, 141.8, 139.7, 135.8, 132.8, 129.1, 128.0, 127.7, 126.4, 126.14, 126.07, 124.7, 123.8, 123.5, 121.9, 120.5, 120.2, 74.4, 70.8, 69.5, 66.9, 47.6, 27.3, 24.1, 15.6. IR (KBr, cm^{-1}) ν 2961, 2863, 1599, 1580, 1514, 1448,

1344, 1312, 1106, 876, 827, 779, 758, 736, 569. HRMS (ESI) m/z $[M + Na]^+$ calcd for $C_{48}H_{46}N_2O_4Na$ 737.3350; found 737.3351. mp 98–102°C.

N^4 -(4'-(dimethylamino)-[1,1'-biphenyl]-4-yl)- N^4 -(3'-(1-(2-ethoxyethoxy)ethyl)-4'-nitro-[1,1'-biphenyl]-4-yl)- N^4,N^4 -dimethyl-[1,1'-biphenyl]-4,4'-diamine (**5d**). Hexane/ CH_2Cl_2 = 1:2. Red solid (82%). 1H NMR (400 MHz, $CDCl_3$) δ 8.09 (d, J = 1.8 Hz, 1H), 8.05 (d, J = 8.6 Hz, 1H), 7.62 – 7.54 (m, 3H), 7.54 – 7.44 (m, 8H), 7.25 – 7.16 (m, 6H), 6.82 (d, J = 8.7 Hz, 4H), 5.21 (q, J = 6.2 Hz, 1H), 3.67 – 3.44 (m, 6H), 3.01 (s, 12H), 1.60 (d, J = 6.3 Hz, 3H), 1.17 (t, J = 7.0 Hz, 3H). ^{13}C $\{^1H\}$ NMR (100 MHz, $CDCl_3$) δ 149.9, 148.8, 146.5, 146.4, 145.4, 141.2, 136.6, 131.7, 128.8, 128.2, 127.5, 127.2, 125.5, 125.3, 122.9, 113.0, 74.0, 70.0, 68.8, 66.8, 40.7, 24.0, 15.3. IR (KBr, cm^{-1}) ν 2865, 1733, 1608, 1499, 1444, 1323, 1296, 1186, 1106, 946, 812, 528. HRMS (ESI) m/z $[M + H]^+$ calcd for $C_{46}H_{49}N_4O_4$ 721.3748; found 721.3752. mp 198–202°C.

3'-(1-(2-ethoxyethoxy)ethyl)-4'-nitro- N,N -bis(4'-nitro-[1,1'-biphenyl]-4-yl)-[1,1'-biphenyl]-4-amine (**2d**). Hexane/ CH_2Cl_2 = 1:2. Red solid (89%). 1H NMR (400 MHz, $CDCl_3$) δ 8.30 (d, J = 8.8 Hz, 4H), 8.11 (d, J = 2.0 Hz, 1H), 8.06 (d, J = 8.5 Hz, 1H), 7.74 (d, J = 8.9 Hz, 4H), 7.68 – 7.57 (m, 7H), 7.32 – 7.27 (m, 6H), 5.20 (q, J = 6.3 Hz, 1H), 3.67 – 3.43 (m, 6H), 1.59 (d, J = 6.3 Hz, 3H), 1.16 (t, J = 7.0 Hz, 3H). ^{13}C $\{^1H\}$ NMR (100 MHz, $CDCl_3$) δ 147.7, 147.5, 146.8, 146.73, 146.70, 145.8, 141.2, 134.0, 133.4, 128.6, 128.5, 127.1, 125.8, 125.7, 125.4, 124.9, 124.6, 124.2, 73.8, 69.9, 68.7, 66.6, 23.8, 15.2. IR (KBr, cm^{-1}) ν 2976, 2868, 1591, 1515, 1483, 1341, 1286, 1192, 1109, 855, 829, 755, 733, 554. HRMS (ESI) m/z $[M + NH_4]^+$ calcd for $C_{42}H_{40}N_5O_8$ 742.2871; found 742.2880. mp 84–86°C.

9-(3'-(1-(2-ethoxyethoxy)ethyl)-4'-nitro-[1,1'-biphenyl]-4-yl)-9*H*-carbazole (**6d**). Hexane/EtOAc = 9:1. Yellow solid (81%). ¹H NMR (400 MHz, CDCl₃) δ 8.23 (d, *J* = 2.1 Hz, 1H), 8.17 (d, *J* = 7.7 Hz, 2H), 8.12 (d, *J* = 8.5 Hz, 1H), 7.92 (d, *J* = 8.6 Hz, 2H), 7.75 – 7.67 (m, 3H), 7.51 – 7.41 (m, 4H), 7.36 – 7.29 (m, 2H), 5.23 (q, *J* = 6.3 Hz, 1H), 3.74 – 3.44 (m, 6H), 1.63 (d, *J* = 6.3 Hz, 3H), 1.19 (t, *J* = 7.0 Hz, 3H). ¹³C{¹H} NMR (100 MHz, CDCl₃) δ 147.5, 145.8, 141.4, 140.8, 138.5, 138.0, 129.1, 127.6, 126.6, 126.3, 126.2, 125.5, 123.7, 120.6, 120.4, 109.9, 74.0, 70.1, 69.0, 66.9, 24.0, 15.3. IR (KBr, cm⁻¹) ν 2974, 2867, 1604, 1518, 1478, 1451, 1334, 1229, 1174, 1105, 914, 876, 830, 751, 724, 671. HRMS (ESI) *m/z* [M + Na]⁺ calcd for C₃₀H₂₈N₂O₄Na 503.1941; found 503.1938. mp 112–116°C.

5-(3'-(1-(2-ethoxyethoxy)ethyl)-4'-nitro-[1,1'-biphenyl]-4-yl)-10,11-dihydro-5*H*-dibenzo[*b,f*]azepine (**7d**). Hexane/EtOAc = 9:1. Red oil (83%). ¹H NMR (400 MHz, CDCl₃) δ 8.04 – 7.94 (m, 2H), 7.51 (dd, *J* = 8.6, 2.1 Hz, 1H), 7.48 – 7.40 (m, 4H), 7.31 – 7.24 (m, 6H), 6.68 (d, *J* = 9.0 Hz, 2H), 5.18 (q, *J* = 6.3 Hz, 1H), 3.61 – 3.39 (m, 6H), 3.02 (s, 4H), 1.55 (d, *J* = 6.3 Hz, 3H), 1.13 (t, *J* = 7.0 Hz, 3H). ¹³C{¹H} NMR (100 MHz, CDCl₃) δ 149.9, 146.7, 146.1, 143.1, 141.2, 138.3, 131.2, 129.9, 128.1, 127.8, 127.6, 127.4, 125.5, 125.0, 124.9, 113.2, 74.0, 70.0, 68.8, 66.8, 30.9, 23.9, 15.2. IR (KBr, cm⁻¹) ν 2926, 1596, 1580, 1515, 1488, 1449, 1322, 1198, 1106, 875, 821, 778, 757, 646. HRMS (ESI) *m/z* [M + Na]⁺ calcd for C₃₂H₃₂N₂O₄Na 531.2254; found 531.2255.

10-(3'-(1-(2-ethoxyethoxy)ethyl)-4'-nitro-[1,1'-biphenyl]-4-yl)-10*H*-phenothiazine (**8d**). Hexane/EtOAc = 9:1. Yellow solid (80%). ¹H NMR (400 MHz, CDCl₃) δ 8.18 (d, *J* = 2.1 Hz, 1H), 8.10 (d, *J* = 8.5 Hz, 1H), 7.88 (d, *J* = 8.6 Hz, 2H), 7.68 (dd, *J* = 8.5, 2.1 Hz, 1H), 7.47 (d, *J* = 8.6 Hz, 2H), 7.09 (dd, *J* = 7.4, 1.7 Hz, 2H), 6.96 – 6.84 (m, 4H), 6.39 (dd, *J* =

8.0, 1.3 Hz, 2H), 5.20 (q, $J = 6.3$ Hz, 1H), 3.69 – 3.44 (m, 6H), 1.61 (d, $J = 6.3$ Hz, 3H), 1.17 (t, $J = 7.0$ Hz, 3H). $^{13}\text{C}\{^1\text{H}\}$ NMR (100 MHz, CDCl_3) δ 147.4, 145.7, 143.9, 142.3, 141.3, 138.0, 130.0, 129.7, 127.2, 127.0, 126.5, 126.3, 125.5, 123.2, 122.0, 117.3, 73.9, 70.1, 68.9, 66.8, 24.0, 15.3. IR (KBr, cm^{-1}) ν 2974, 2867, 1589, 1516, 1461, 1443, 1345, 1309, 1259, 1105, 875, 830, 746. HRMS (ESI) m/z $[\text{M} + \text{Na}]^+$ calcd for $\text{C}_{30}\text{H}_{28}\text{N}_2\text{O}_4\text{SNa}$ 535.1662; found 535.1661. mp 128–130°C.

4'-(1-(2-ethoxyethoxy)ethyl)-3'-nitro-*N,N*-diphenyl-[1,1'-biphenyl]-4-amine (**9d**). Hexane/EtOAc = 9:1. Yellow oil (87%). ^1H NMR (400 MHz, CDCl_3) δ 8.08 (d, $J = 1.4$ Hz, 1H), 7.87 – 7.78 (m, 2H), 7.47 (d, $J = 8.7$ Hz, 2H), 7.32 – 7.26 (m, 4H), 7.21 – 7.10 (m, 6H), 7.10 – 7.04 (m, 2H), 5.08 (q, $J = 6.3$ Hz, 1H), 3.63 – 3.40 (m, 6H), 1.57 (d, $J = 6.4$ Hz, 3H), 1.21 (t, $J = 7.0$ Hz, 3H). $^{13}\text{C}\{^1\text{H}\}$ NMR (100 MHz, CDCl_3) δ 149.1, 148.4, 147.5, 141.1, 138.0, 131.8, 131.5, 129.6, 128.5, 127.8, 125.0, 123.6, 123.4, 122.0, 73.7, 69.9, 68.7, 66.8, 23.8, 15.3. IR (KBr, cm^{-1}) ν 2924, 2855, 1591, 1515, 1486, 1461, 1352, 1279, 1105, 885, 825, 794, 754, 697, 511. HRMS (ESI) m/z $[\text{M} + \text{NH}_4]^+$ calcd for $\text{C}_{30}\text{H}_{34}\text{N}_3\text{O}_4$ 500.2544; found 500.2546.

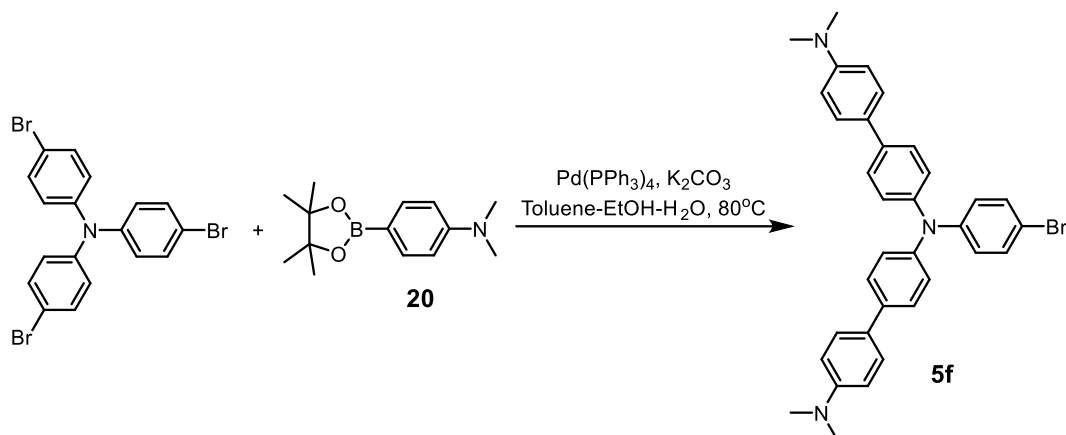
4'-(1-(2-ethoxyethoxy)ethyl)-3'-nitro-*N,N*-bis(4'-nitro-[1,1'-biphenyl]-4-yl)-[1,1'-biphenyl]-4-amine (**10d**). Hexane/ CH_2Cl_2 = 1:2. Red solid (82%). ^1H NMR (400 MHz, CDCl_3) δ 8.30 (d, $J = 8.8$ Hz, 4H), 8.12 (d, $J = 1.6$ Hz, 1H), 7.91 – 7.84 (m, 2H), 7.74 (d, $J = 8.8$ Hz, 4H), 7.63 – 7.54 (m, 6H), 7.29 (d, $J = 8.6$ Hz, 6H), 5.10 (q, $J = 6.3$ Hz, 1H), 3.63 – 3.42 (m, 6H), 1.58 (d, $J = 6.3$ Hz, 3H), 1.21 (t, $J = 7.0$ Hz, 3H). $^{13}\text{C}\{^1\text{H}\}$ NMR (100 MHz, CDCl_3) δ 149.1, 147.9, 147.3, 147.0, 146.8, 140.7, 138.6, 133.9, 133.6, 131.6, 128.7, 128.6, 128.3, 127.3, 125.3, 124.7, 124.4, 122.2, 73.7, 69.9, 68.8, 66.8, 23.8, 15.3. IR (KBr, cm^{-1}) ν

2975, 2867, 1590, 1513, 1483, 1340, 1285, 1188, 1108, 855, 828, 794, 755, 733, 694, 553.

HRMS (ESI) m/z $[M + Na]^+$ calcd for $C_{42}H_{36}N_4O_8Na$ 747.2425; found 747.2430. mp 91–95°C.

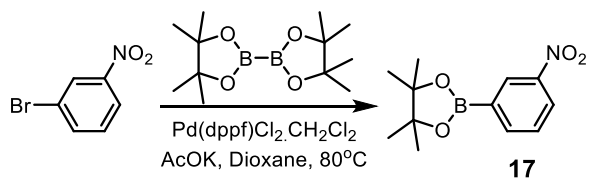
9-(4'-(1-(2-ethoxyethoxy)ethyl)-3'-nitro-[1,1'-biphenyl]-4-yl)-9*H*-carbazole (11d).

Hexane/EtOAc = 9:1. Yellow oil (85%). 1H NMR (400 MHz, $CDCl_3$) δ 8.24 (s, 1H), 8.17 (d, $J = 7.7$ Hz, 2H), 7.99 – 7.92 (m, 2H), 7.84 (d, $J = 8.4$ Hz, 2H), 7.71 (d, $J = 8.4$ Hz, 2H), 7.51 – 7.41 (m, 4H), 7.36 – 7.28 (m, 2H), 5.15 (q, $J = 6.3$ Hz, 1H), 3.67 – 3.45 (m, 6H), 1.62 (d, $J = 6.3$ Hz, 3H), 1.24 (t, $J = 7.0$ Hz, 3H). ^{13}C $\{^1H\}$ NMR (100 MHz, $CDCl_3$) δ 149.0, 140.7, 140.4, 139.1, 138.1, 137.4, 131.9, 128.8, 128.5, 127.6, 126.2, 123.6, 122.6, 120.5, 120.3, 109.8, 73.7, 69.9, 68.8, 66.7, 23.8, 15.3. IR (KBr, cm^{-1}) ν 2974, 2866, 1604, 1519, 1479, 1451, 1354, 1318, 1229, 1172, 1105, 830, 795, 751, 724, 533. HRMS (ESI) m/z $[M + Na]^+$ calcd for $C_{30}H_{28}N_2O_4Na$ 503.1941; found 503.1937.

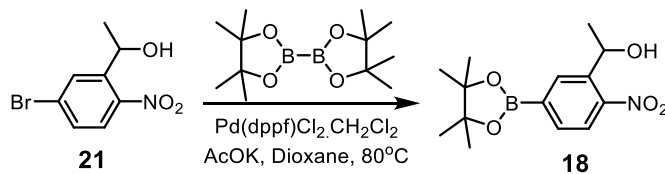


In a round-bottom flask, tris(4-bromophenyl)amine⁹⁴ (1.0 mmol), **20**⁹⁵ (2.0 mmol), Pd(PPh₃)₄ (0.10 mmol) and K₂CO₃ (4.0 mmol) was mixed in toluene/EtOH/H₂O (2:1:1, 8 mL). The reaction mixture was degassed by bubbling with N₂ and stirred at 80°C in an oil bath for 4h. The solvent was removed under reduced pressure, and the residue was purified by silica gel column chromatography (hexane/CH₂Cl₂ = 2:1) to give the desired product **5f** as a red solid (41%).

*N*⁴-(4-bromophenyl)-*N*⁴-(4'-(dimethylamino)-[1,1'-biphenyl]-4-yl)-*N*⁴,*N*⁴-dimethyl-[1,1'-biphenyl]-4,4'-diamine (**5f**). ¹H NMR (400 MHz, CDCl₃) δ 7.51 – 7.44 (m, 8H), 7.34 (d, *J* = 8.9 Hz, 2H), 7.13 (d, *J* = 8.6 Hz, 4H), 7.02 (d, *J* = 8.9 Hz, 2H), 6.82 (d, *J* = 8.4 Hz, 4H), 3.00 (s, 12H). ¹³C{¹H} NMR (100 MHz, CDCl₃) δ 149.7, 147.1, 145.5, 136.2, 132.2, 128.8, 127.4, 127.1, 125.0, 124.8, 114.5, 113.0, 40.7. IR (KBr, cm⁻¹) ν 3028, 2884, 1608, 1498, 1442, 1353, 1317, 1286, 1224, 1165, 1068, 1009, 944, 809, 718, 513. HRMS (ESI) *m/z* [M + H]⁺ calcd for C₃₄H₃₃N₃Br 562.1852; found 562.1854. mp 210–214°C.

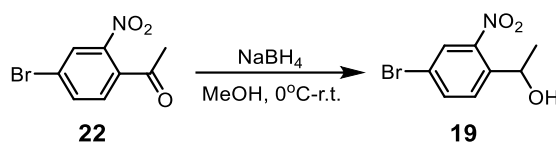


In a round-bottom flask, 1-bromo-3-nitrobenzene (1.0 mmol), bis(pinacolato)diboron (1.2 mmol), AcOK (3.0 mmol) and Pd(dppf)Cl₂·CH₂Cl₂ (0.05 mmol) was mixed in 1,4-dioxane (4 mL). The reaction mixture was degassed by bubbling with N₂ and stirred at 80°C in an oil bath overnight. The reaction mixture was filtered, and the filtrate was removed under reduced pressure. The residue was purified by silica gel column chromatography (hexane/EtOAc = 4:1) to give the desired product **17** as a white solid (84%). ¹H NMR (400 MHz, CDCl₃) δ 8.64 (s, 1H), 8.32 – 8.27 (m, 1H), 8.12 – 8.07 (m, 1H), 7.57 – 7.51 (m, 1H), 1.37 (s, 12H). Data are in agreement with those reported in the literature⁹⁶.



In a round-bottom flask, compound **21**⁵⁷ (1.0 mmol), bis(pinacolato)diboron (1.2 mmol), AcOK (3.0 mmol) and Pd(dppf)Cl₂·CH₂Cl₂ (0.05 mmol) was mixed in 1,4-dioxane (4 mL). The reaction mixture was degassed by bubbling with N₂ and stirred at 80°C in an oil bath overnight. The reaction mixture was filtered, and the filtrate was removed under reduced pressure. The residue was purified by silica gel column chromatography (hexane/EtOAc = 4:1) to give the desired product **18** as a white solid (85%).

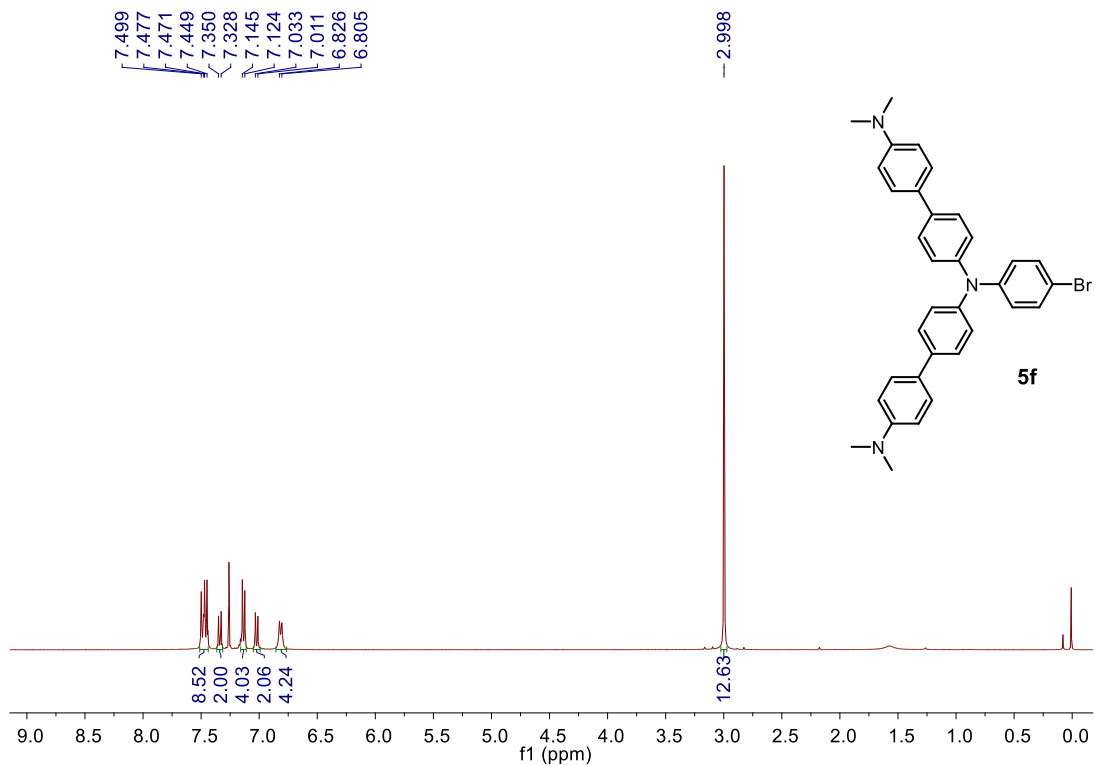
1-(2-nitro-5-(4,4,5,5-tetramethyl-1,3,2-dioxaborolan-2-yl)phenyl)ethan-1-ol (**18**). ^1H NMR (400 MHz, CDCl_3) δ 8.22 (s, 1H), 7.83 (s, 2H), 5.41 – 5.35 (m, 1H), 2.27 (d, $J = 4.1$ Hz, 1H), 1.60 (d, $J = 6.4$ Hz, 3H), 1.36 (s, 12H). $^{13}\text{C}\{^1\text{H}\}$ NMR (100 MHz, CDCl_3) δ 149.8, 139.6, 134.4, 134.1, 123.2, 84.7, 65.7, 25.0, 24.9, 24.4. IR (KBr, cm^{-1}) ν 3513, 2979, 1524, 1346, 1291, 1140, 1103, 963, 833, 710. HRMS (ESI) m/z $[\text{M} + \text{Na}]^+$ calcd for $\text{C}_{14}\text{H}_{20}\text{BNO}_5\text{Na}$ 316.1327; found 316.1331. mp 70–74°C.



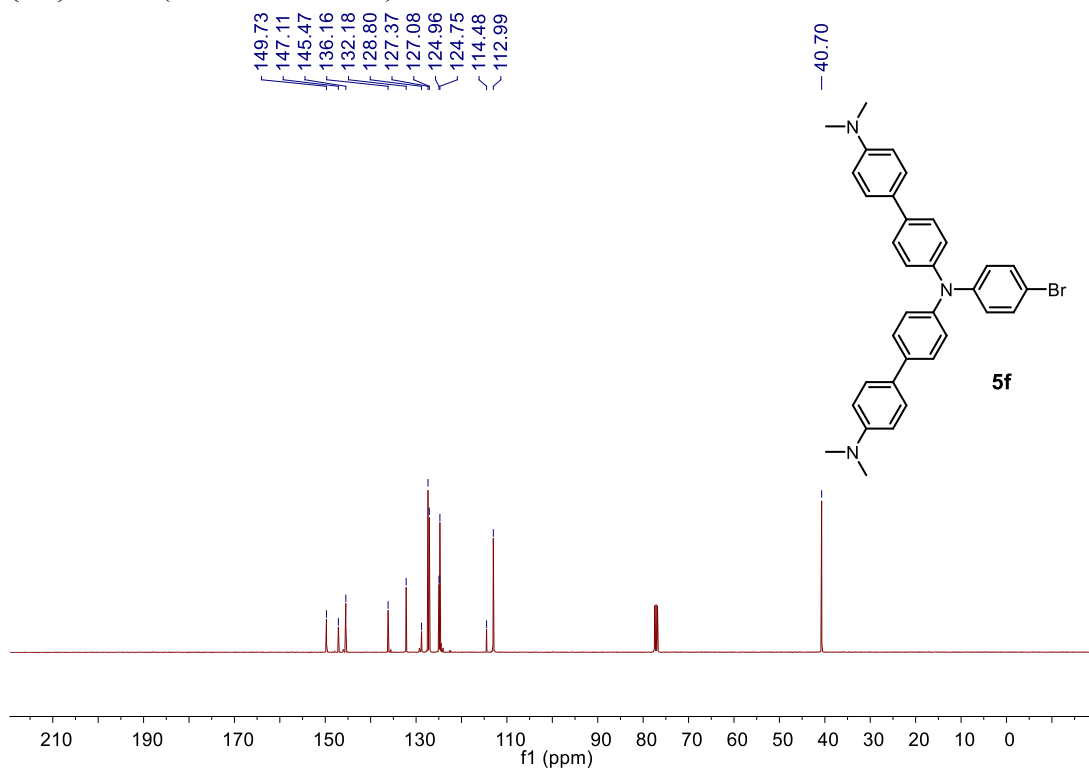
To a solution of compound **22**⁹⁷ (1.0 mmol) in methanol (10 mL) at 0°C was added NaBH_4 (1.2 mmol) portionwise. The temperature was slowly raised to room temperature, and the reaction mixture was stirred for 1h. Methanol was removed under reduced pressure, and the residue was dissolved in CH_2Cl_2 and washed with water. The organic layer was dried over Na_2SO_4 , and the solvent was removed under reduced pressure to give the desired product **19** as a yellow oil (98%) without further purification.

1-(4-bromo-2-nitrophenyl)ethan-1-ol (**19**). ^1H NMR (400 MHz, CDCl_3) δ 8.05 (d, $J = 1.7$ Hz, 1H), 7.80 – 7.72 (m, 2H), 5.40 (q, $J = 6.3$ Hz, 1H), 2.19 (br, 1H), 1.55 (d, $J = 6.4$ Hz, 3H). $^{13}\text{C}\{^1\text{H}\}$ NMR (100 MHz, CDCl_3) δ 148.1, 140.2, 136.7, 129.4, 127.2, 121.2, 65.4, 24.4. IR (KBr, cm^{-1}) ν 3392, 1530, 1349, 1276, 1088, 1067, 1010, 898, 835, 777, 547. HRMS (APCI) m/z $[\text{M}]^-$ calcd for $\text{C}_8\text{H}_8\text{BrNO}_3$ 244.9693; found 244.9699.

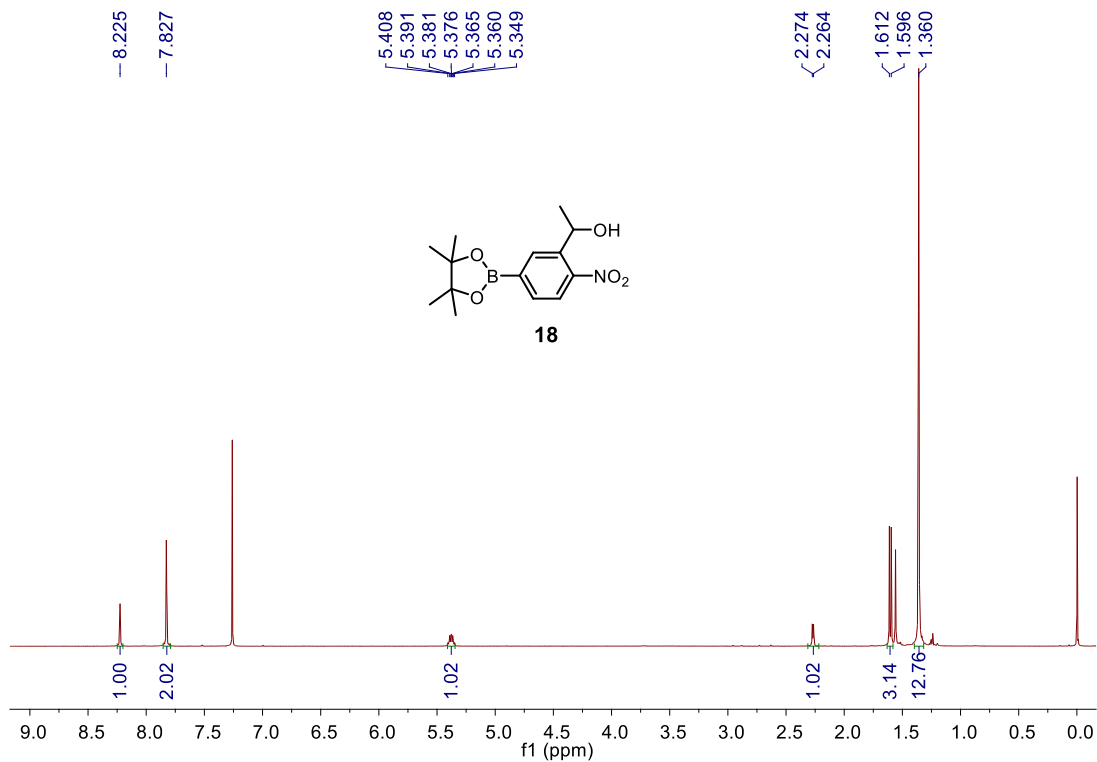
^1H NMR (400MHz, CDCl_3)



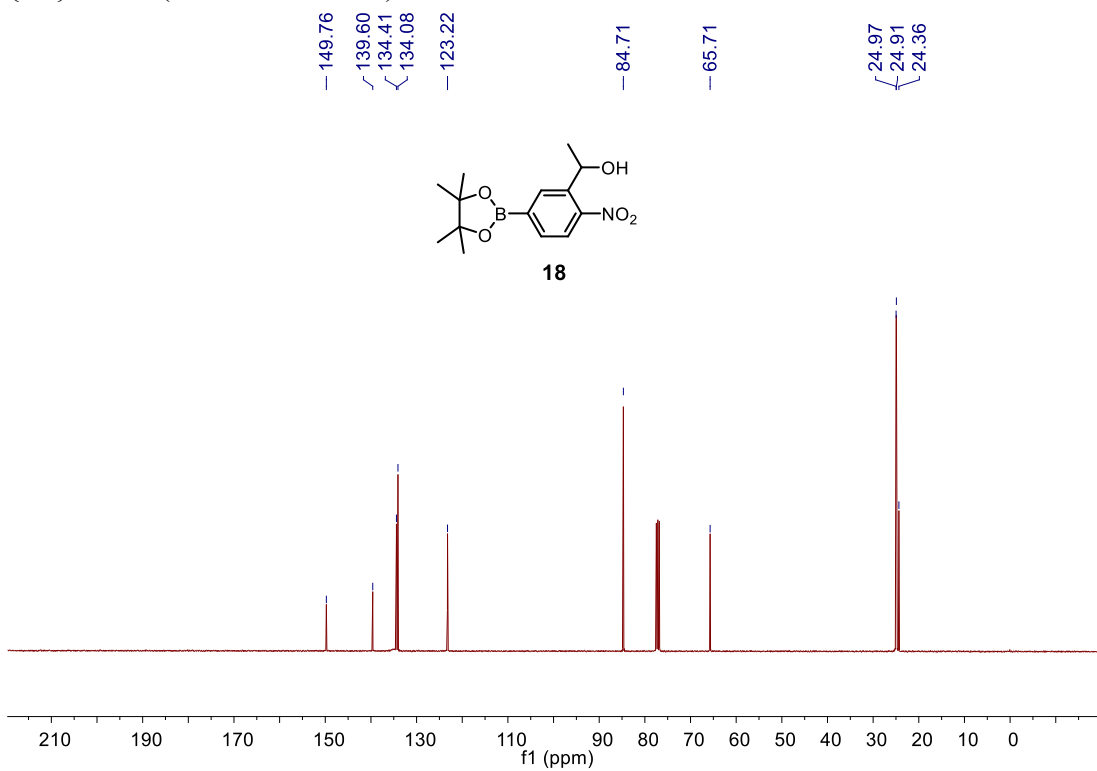
$^{13}\text{C}\{^1\text{H}\}$ NMR (100MHz, CDCl_3)



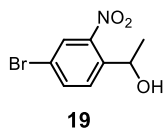
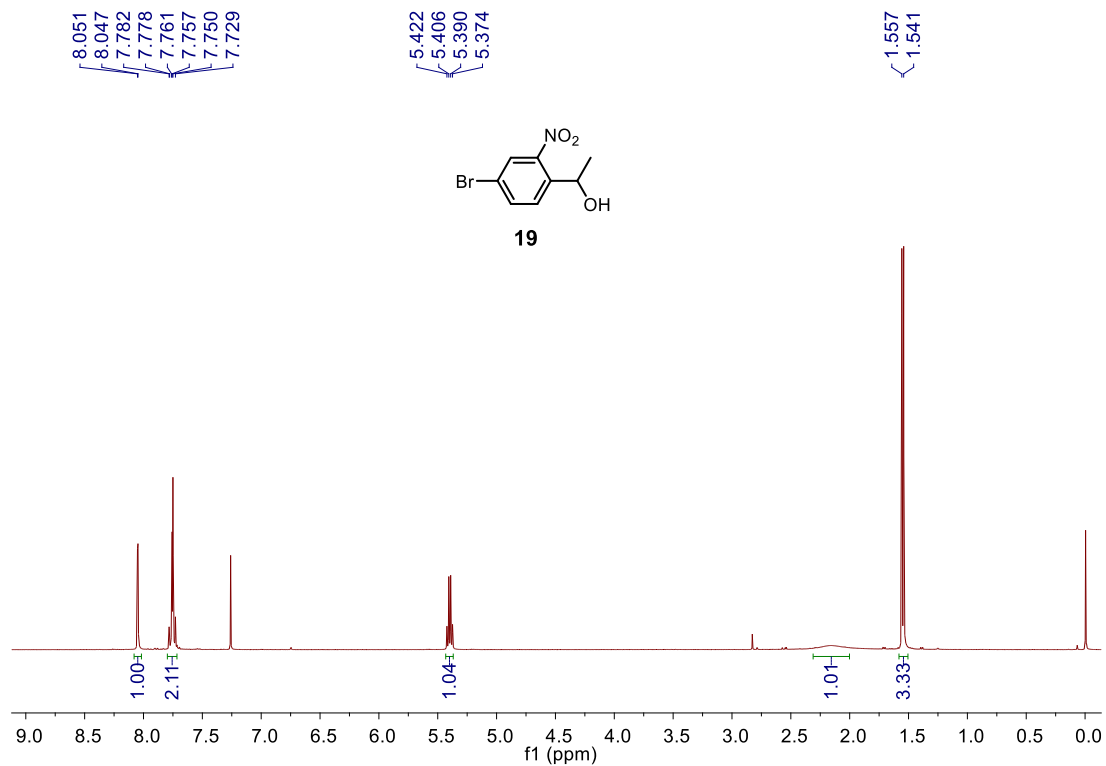
^1H NMR (400MHz, CDCl_3)



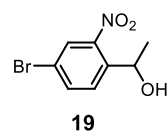
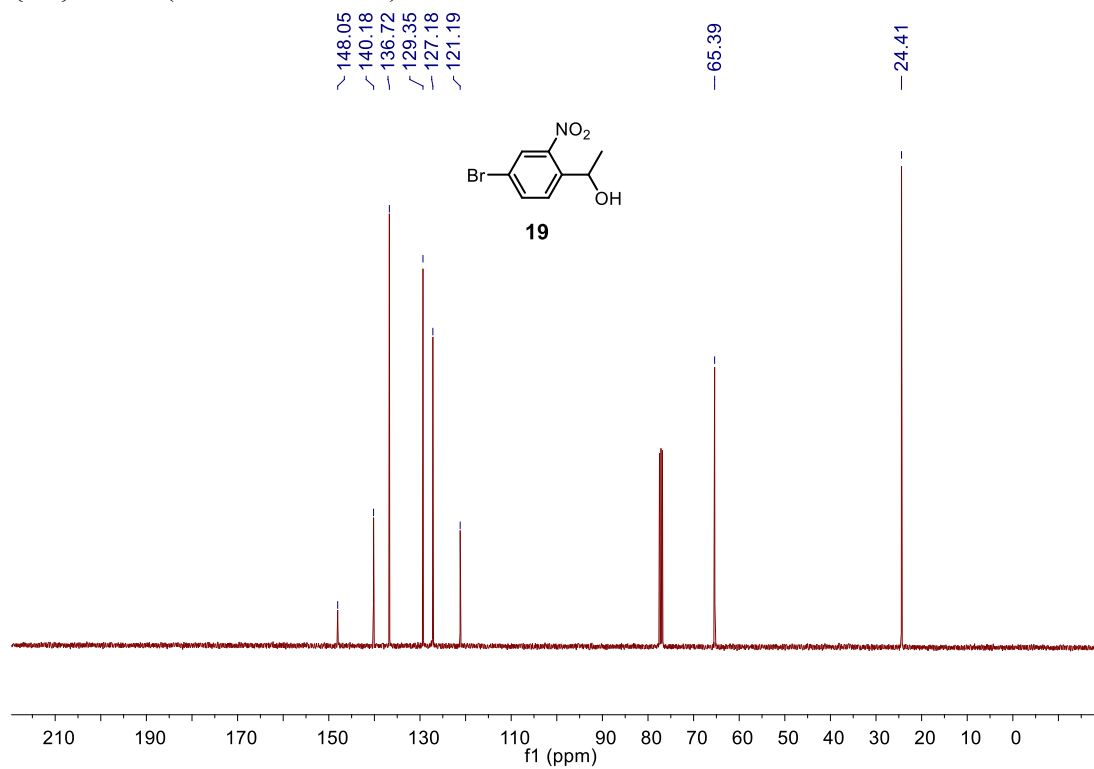
$^{13}\text{C}\{^1\text{H}\}$ NMR (100MHz, CDCl_3)



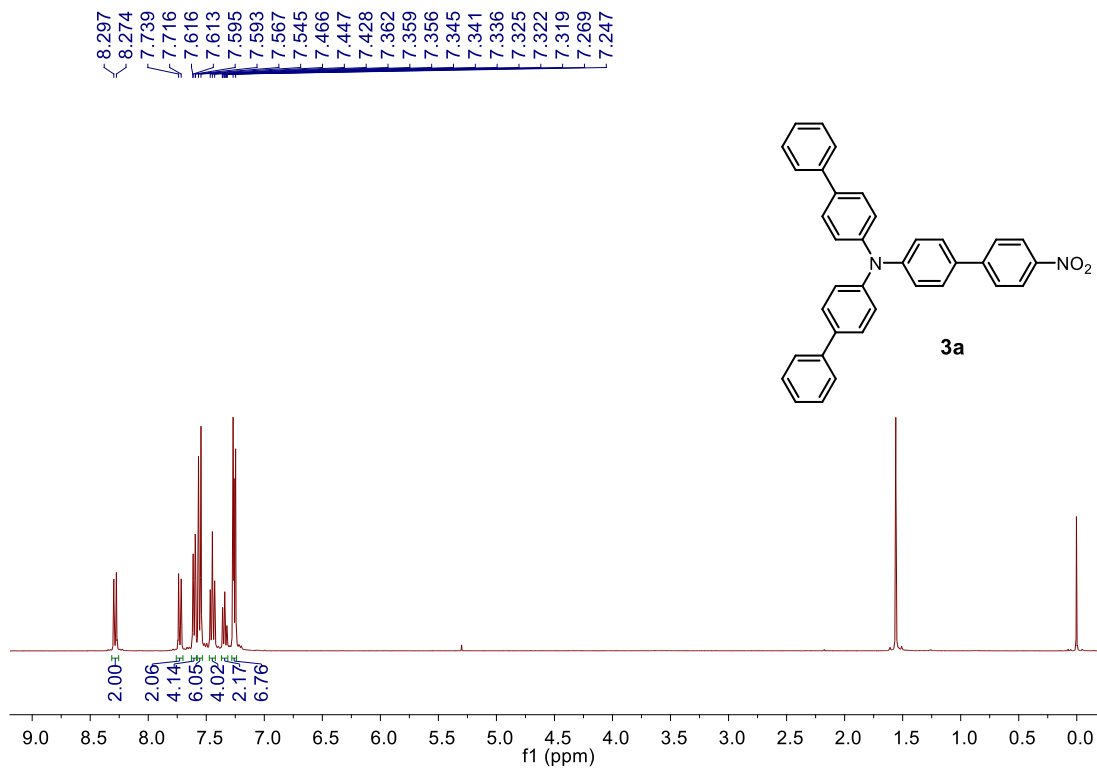
^1H NMR (400MHz, CDCl_3)



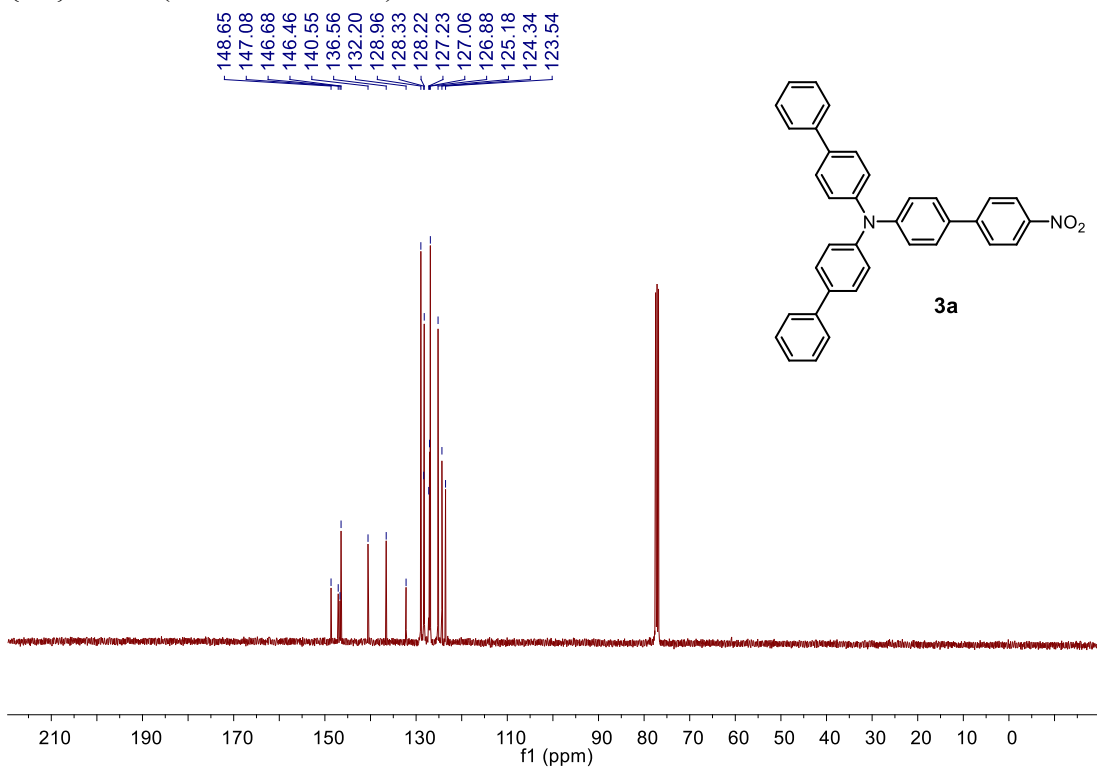
$^{13}\text{C}\{^1\text{H}\}$ NMR (100MHz, CDCl_3)



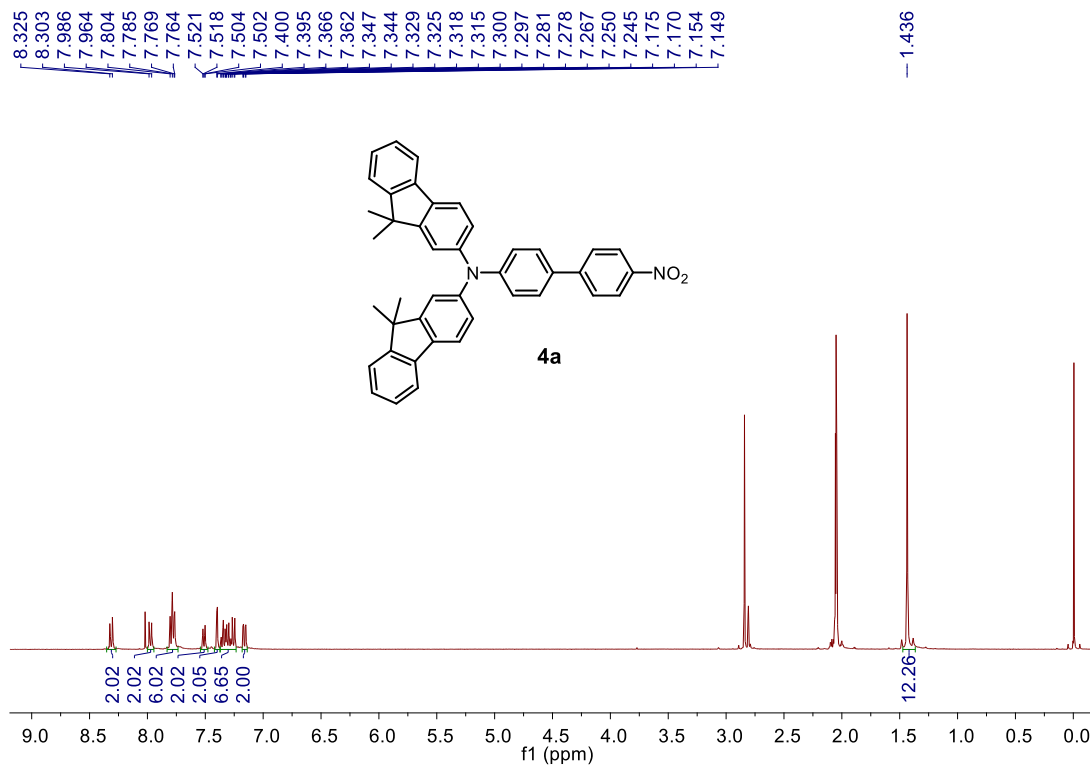
^1H NMR (400MHz, CDCl_3)



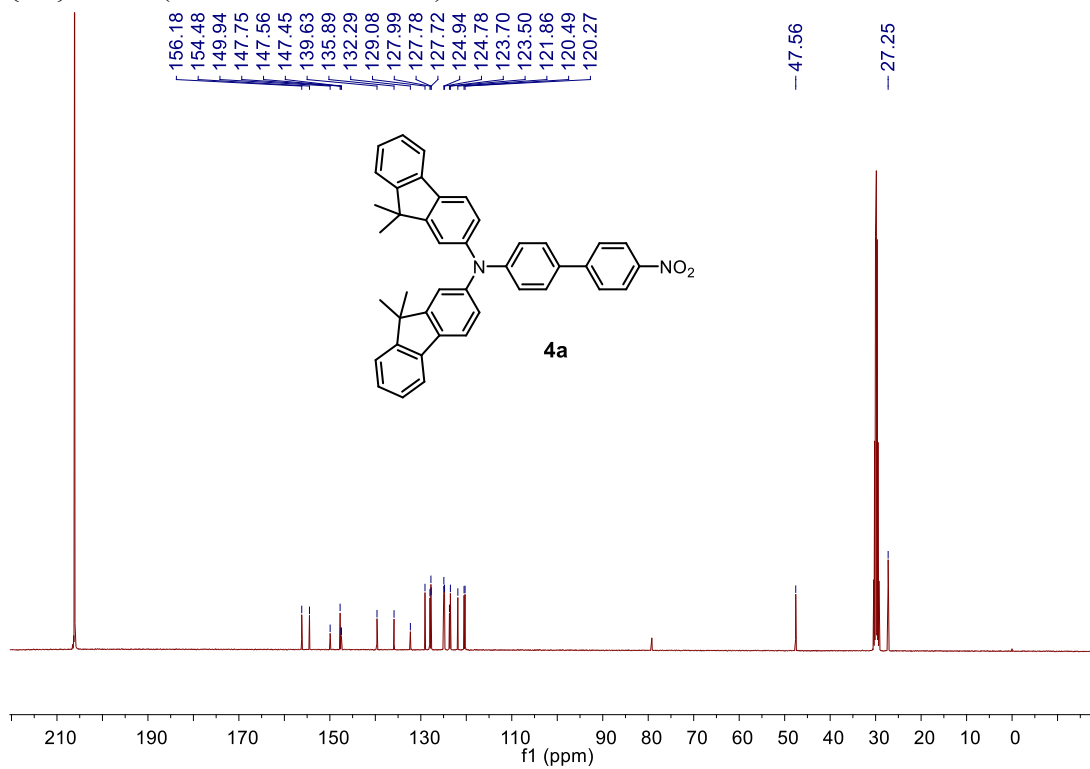
$^{13}\text{C}\{^1\text{H}\}$ NMR (100MHz, CDCl_3)



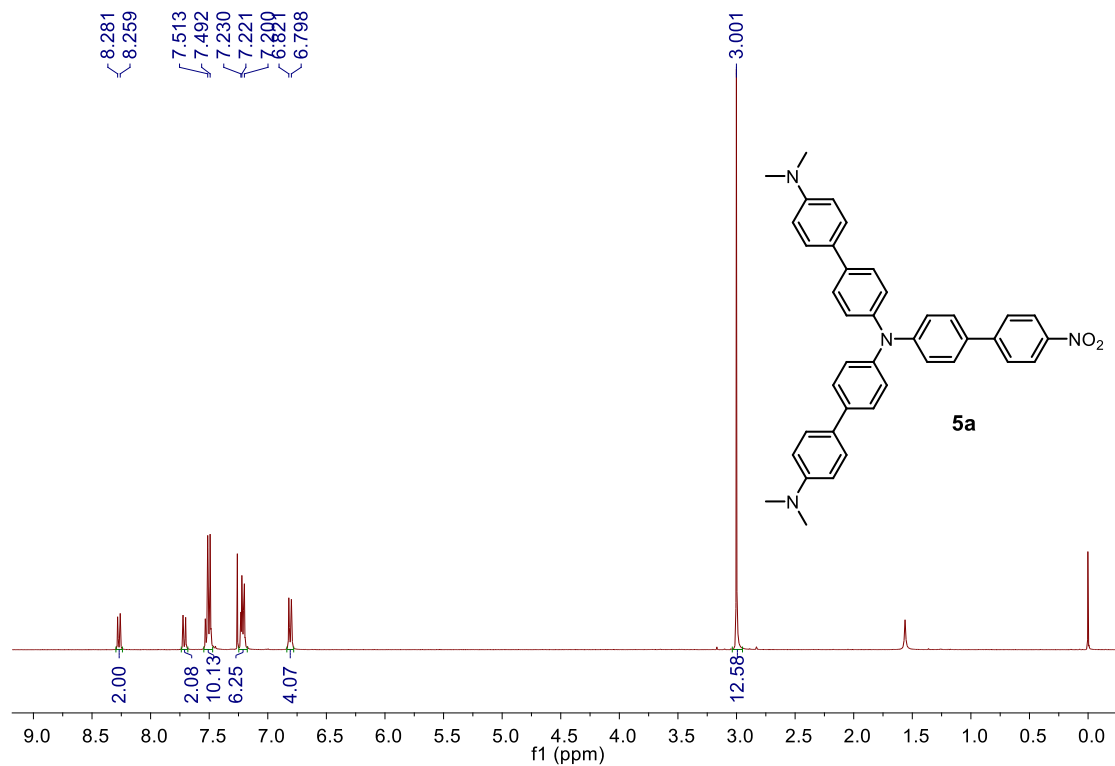
^1H NMR (400MHz, acetone- d_6)



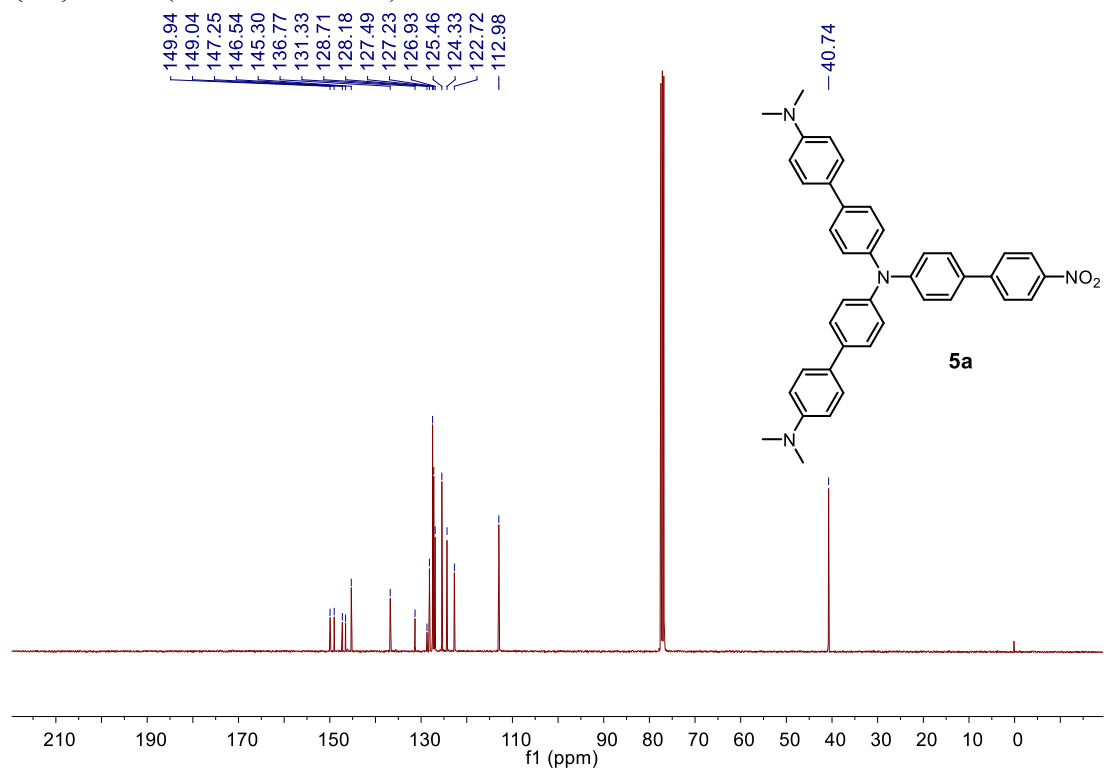
$^{13}\text{C}\{^1\text{H}\}$ NMR (100MHz, acetone- d_6)



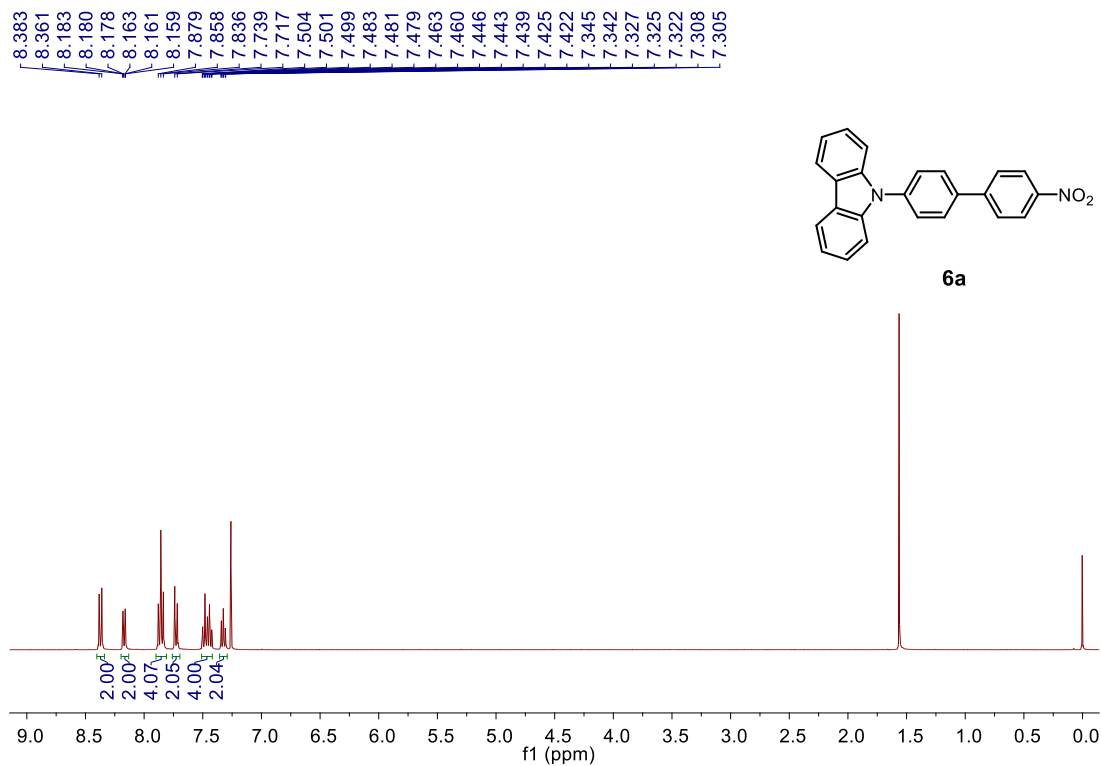
^1H NMR (400MHz, CDCl_3)



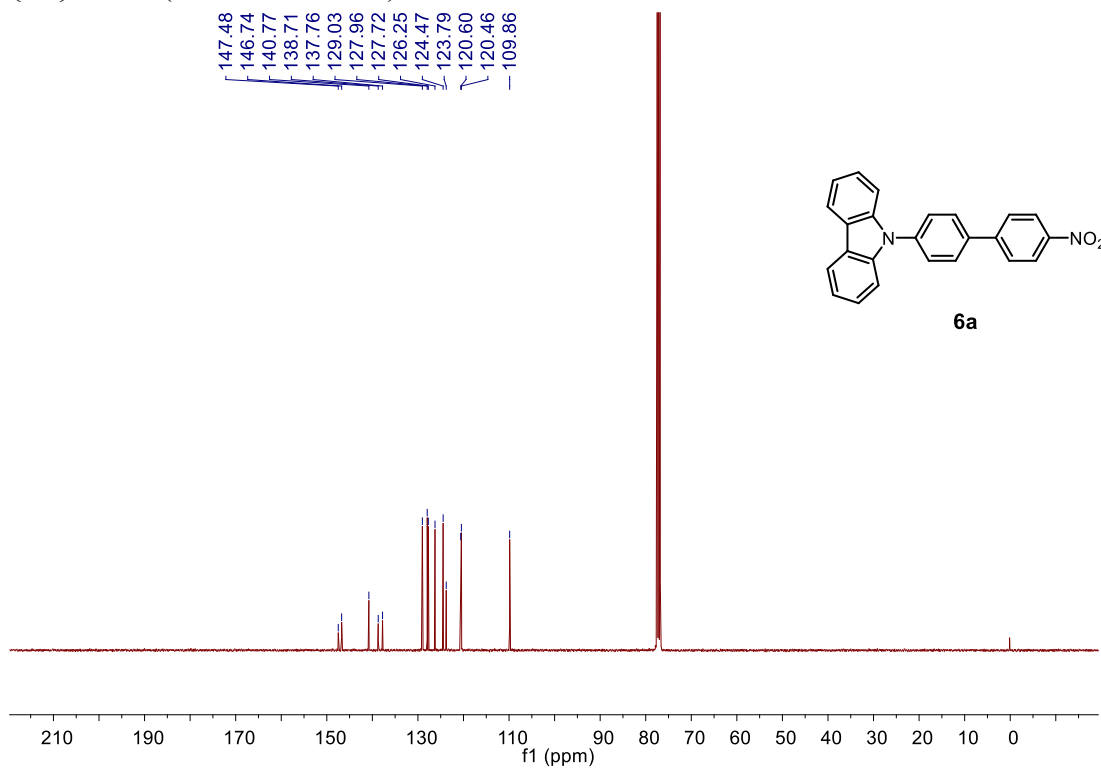
$^{13}\text{C}\{^1\text{H}\}$ NMR (100MHz, CDCl_3)



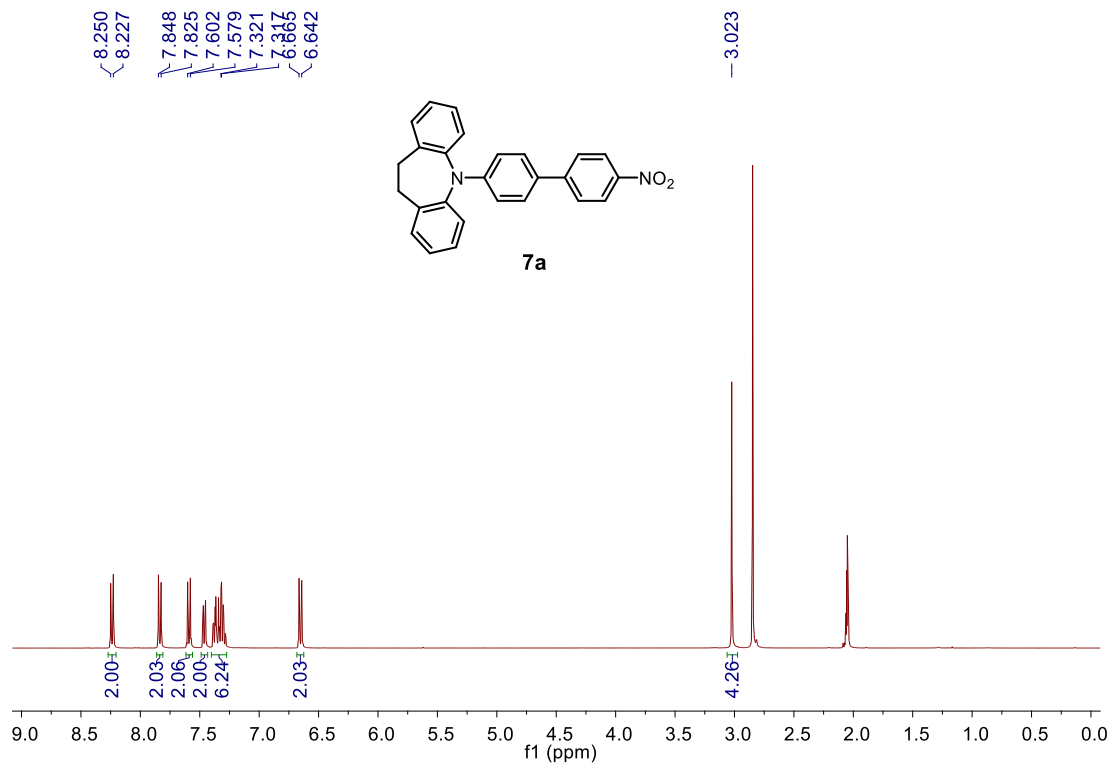
^1H NMR (400MHz, CDCl_3)



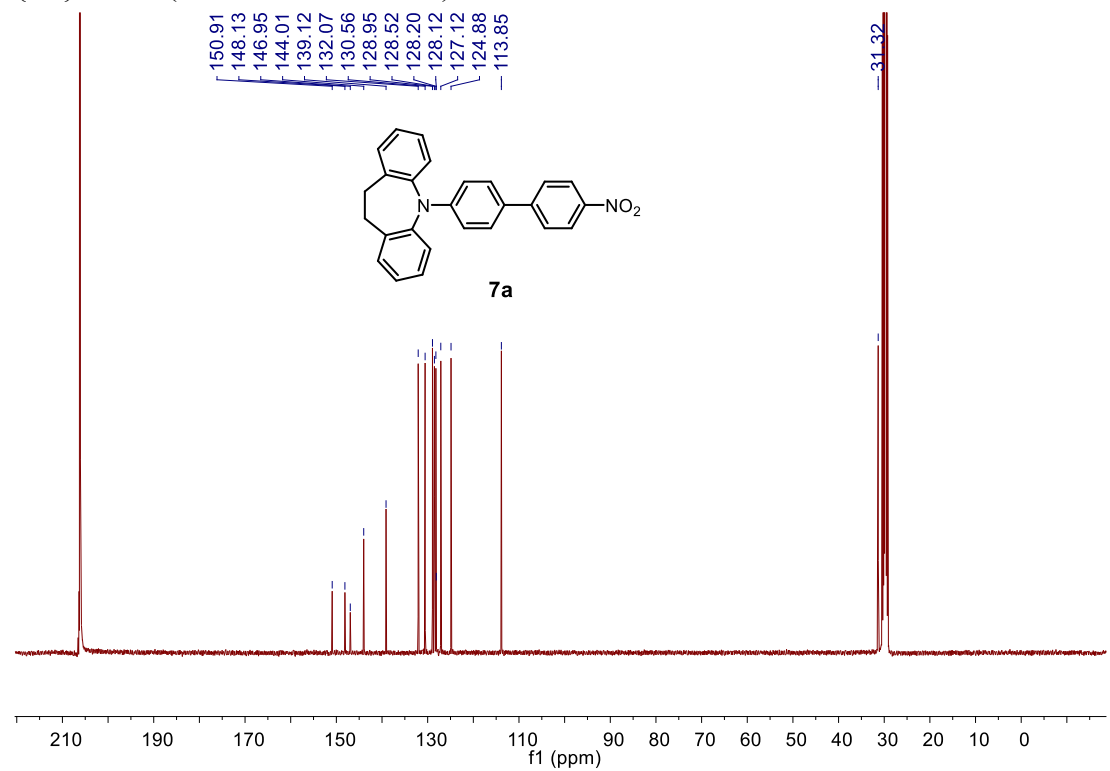
$^{13}\text{C}\{^1\text{H}\}$ NMR (100MHz, CDCl_3)



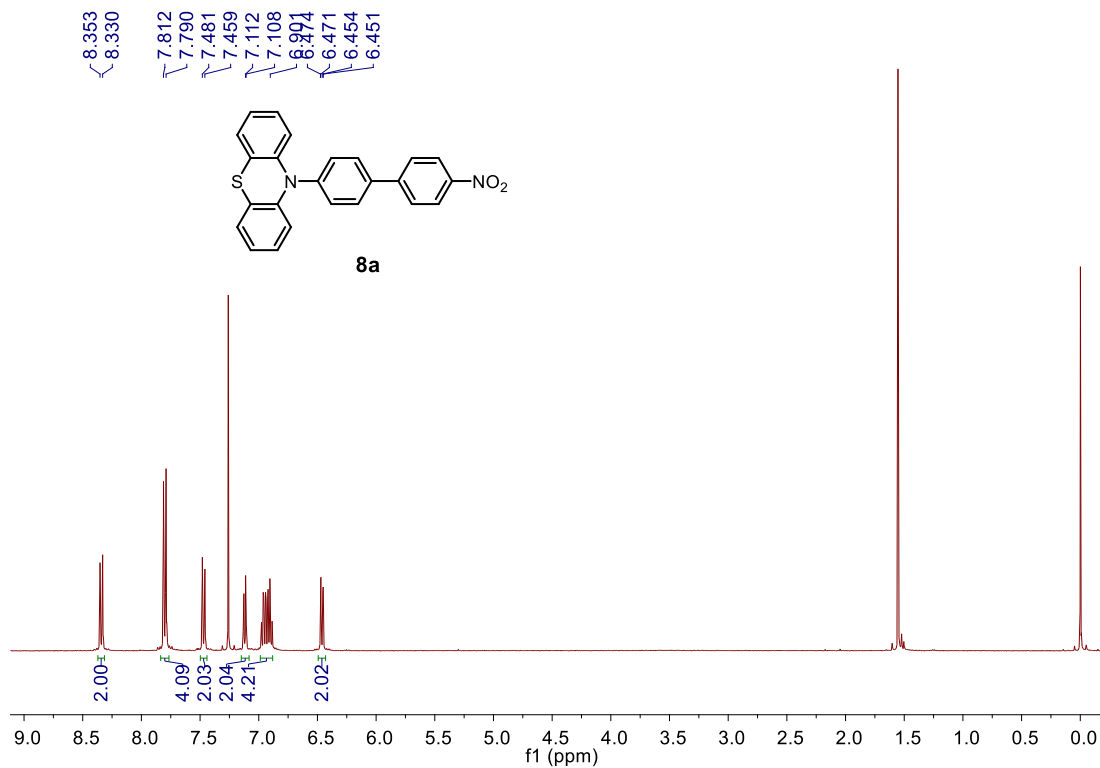
^1H NMR (400MHz, acetone- d_6)



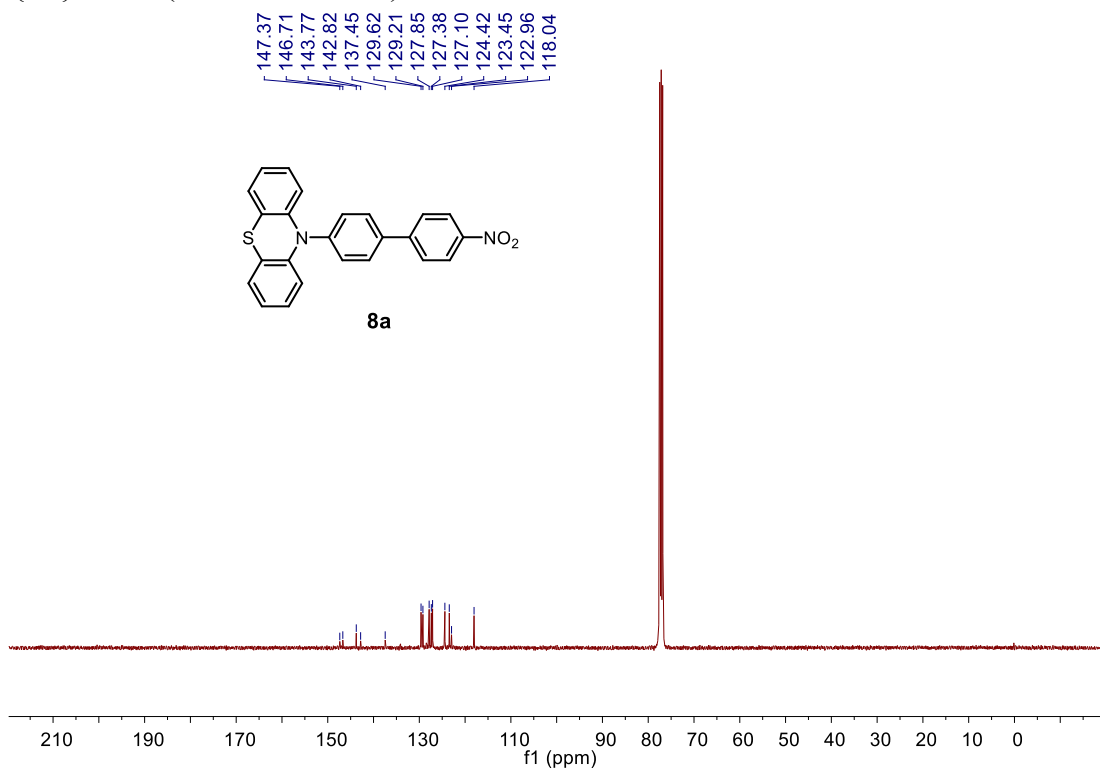
$^{13}\text{C}\{^1\text{H}\}$ NMR (100MHz, acetone- d_6)



^1H NMR (400MHz, CDCl_3)

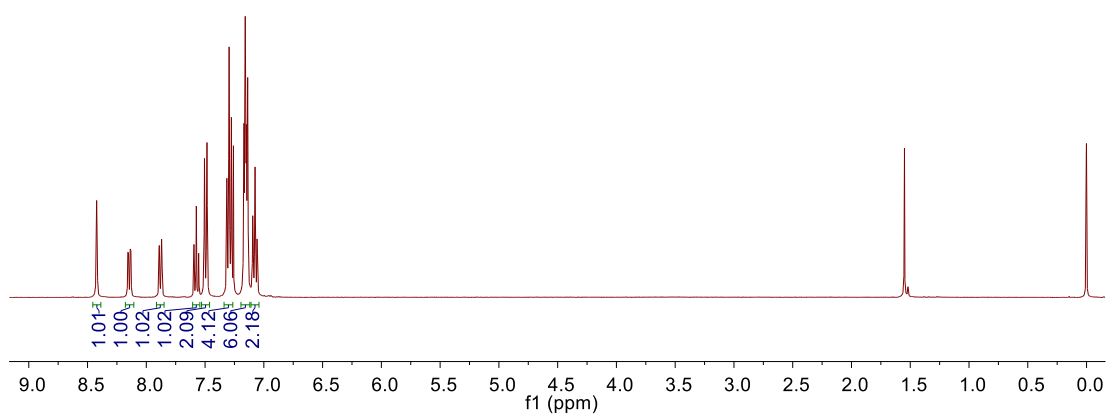
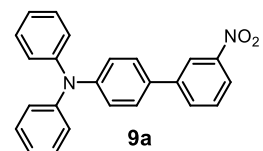


$^{13}\text{C}\{^1\text{H}\}$ NMR (100MHz, CDCl_3)



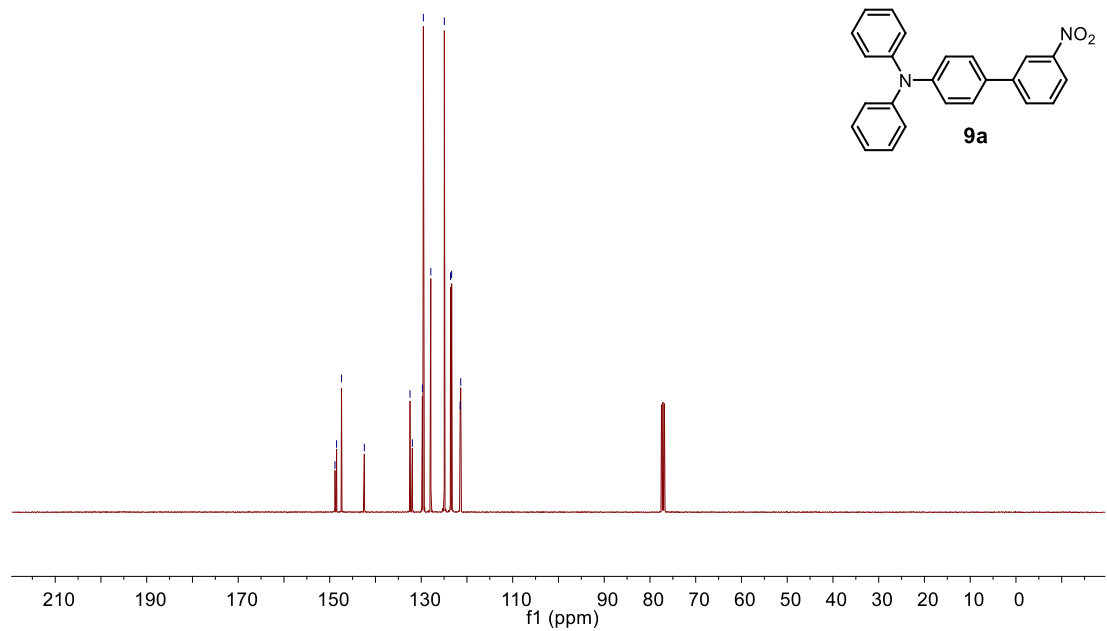
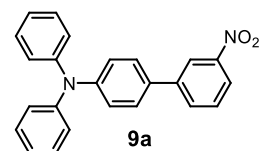
^1H NMR (400MHz, CDCl_3)

8.422
8.157
8.154
8.152
8.137
8.134
8.131
7.889
7.870
7.594
7.574
7.554
7.505
7.484
7.315
7.295
7.276
7.169
7.158
7.157
7.148
7.137
7.094
7.092
7.074
7.058
7.056

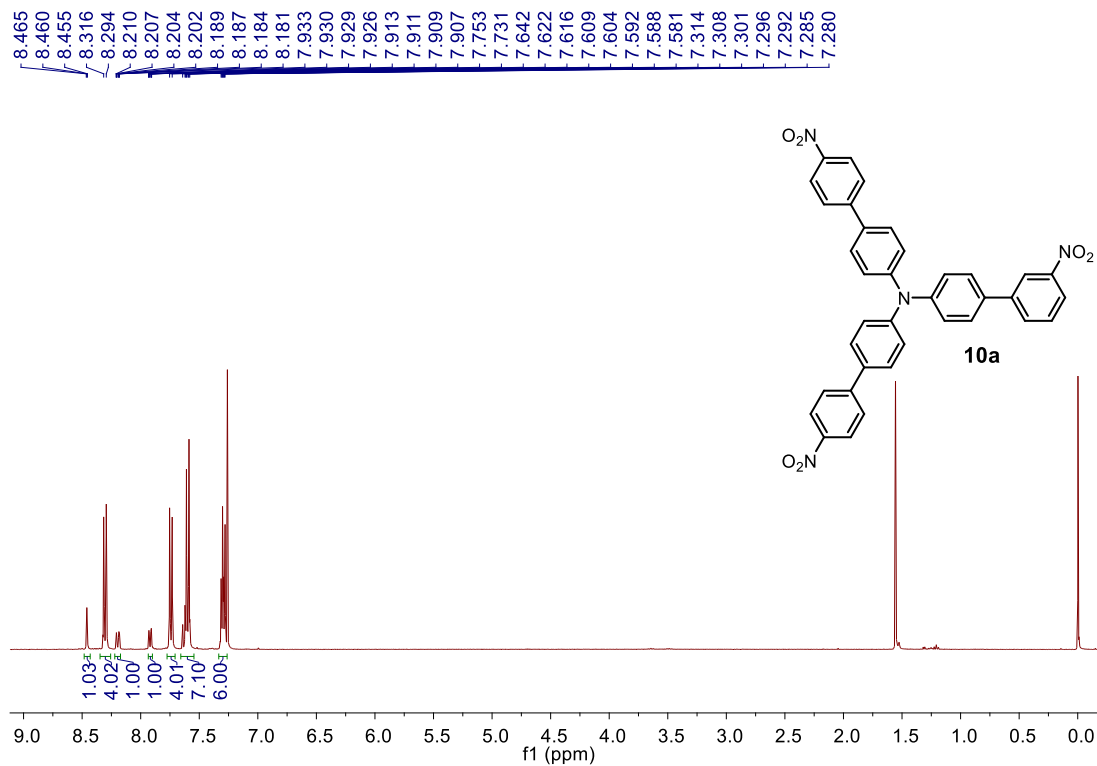


$^{13}\text{C}\{^1\text{H}\}$ NMR (100MHz, CDCl_3)

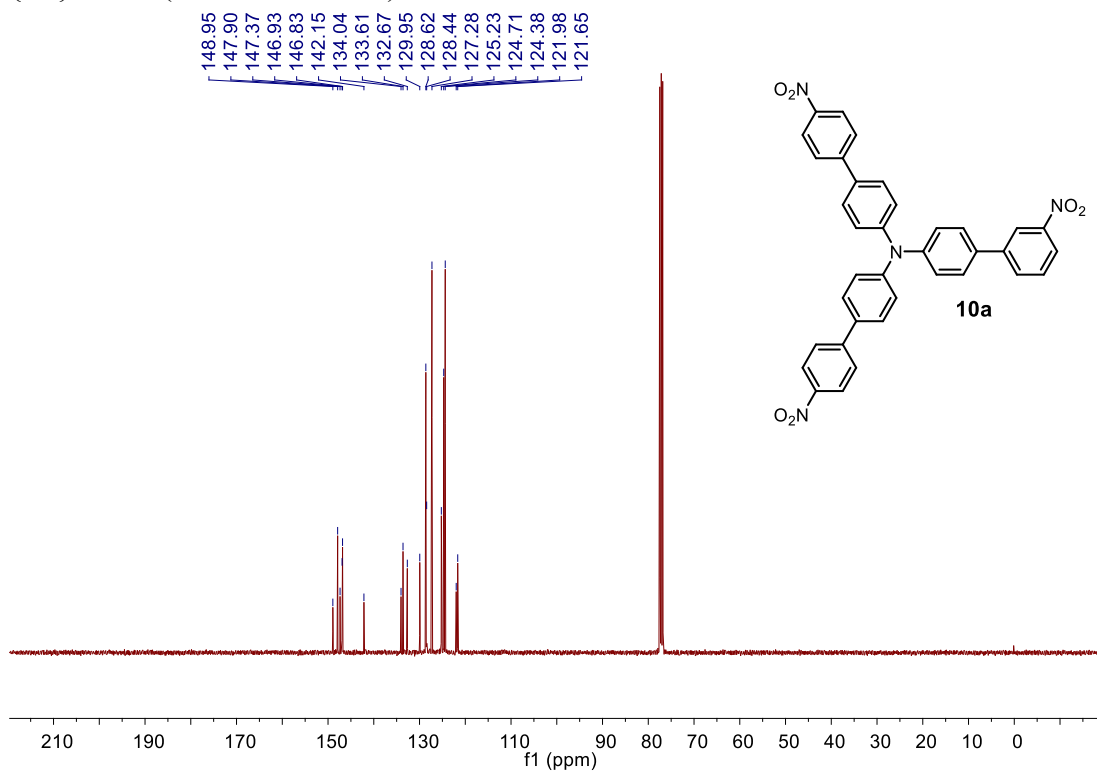
148.85
148.50
147.41
142.43
132.45
131.93
129.74
129.53
127.90
124.94
123.59
123.35
121.48
121.36



^1H NMR (400MHz, CDCl_3)

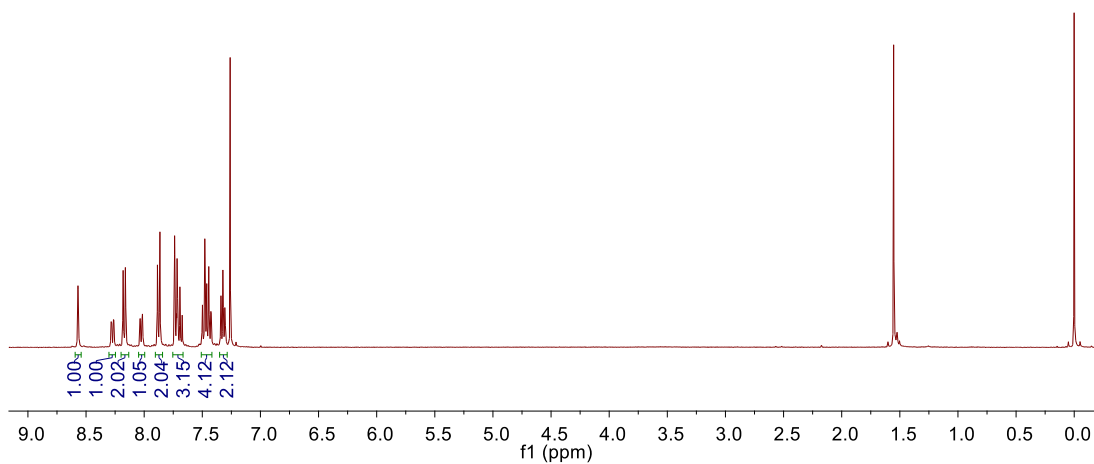
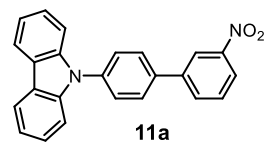


$^{13}\text{C}\{^1\text{H}\}$ NMR (100MHz, CDCl_3)



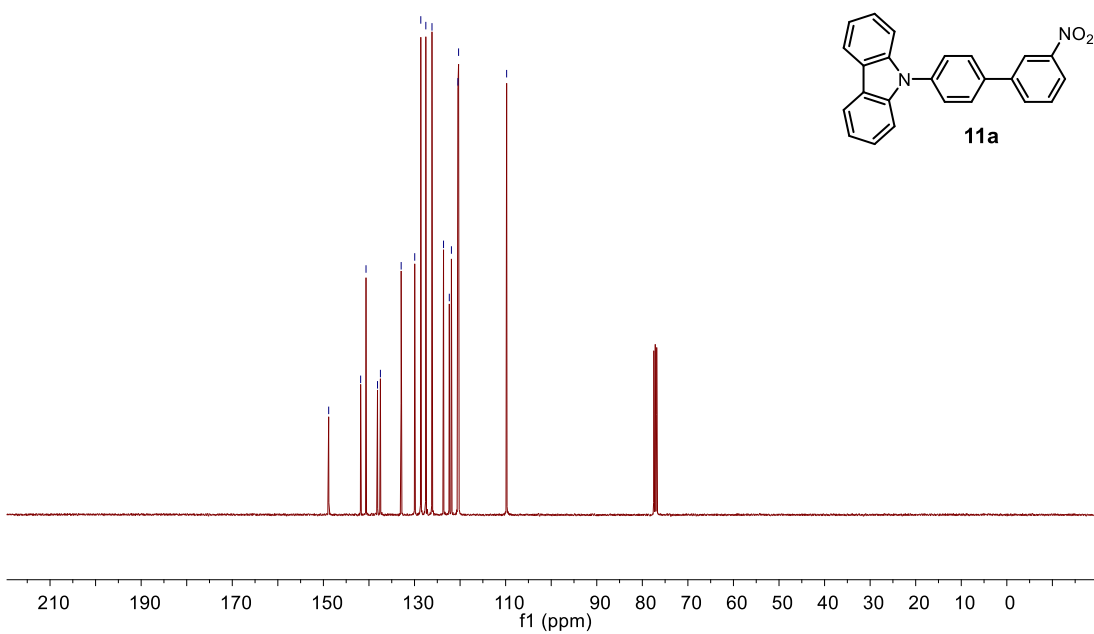
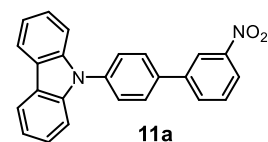
^1H NMR (400MHz, CDCl_3)

8.574
8.569
8.564
8.287
8.285
8.281
8.279
8.266
8.264
8.261
8.259
8.181
8.162
8.038
8.036
8.034
8.032
8.019
8.016
8.015
8.012
7.886
7.864
7.738
7.733
7.722
7.717
7.713
7.693
7.673
7.499
7.478
7.464
7.462
7.447
7.444
7.427
7.424
7.343
7.339
7.323
7.320
7.306
7.303

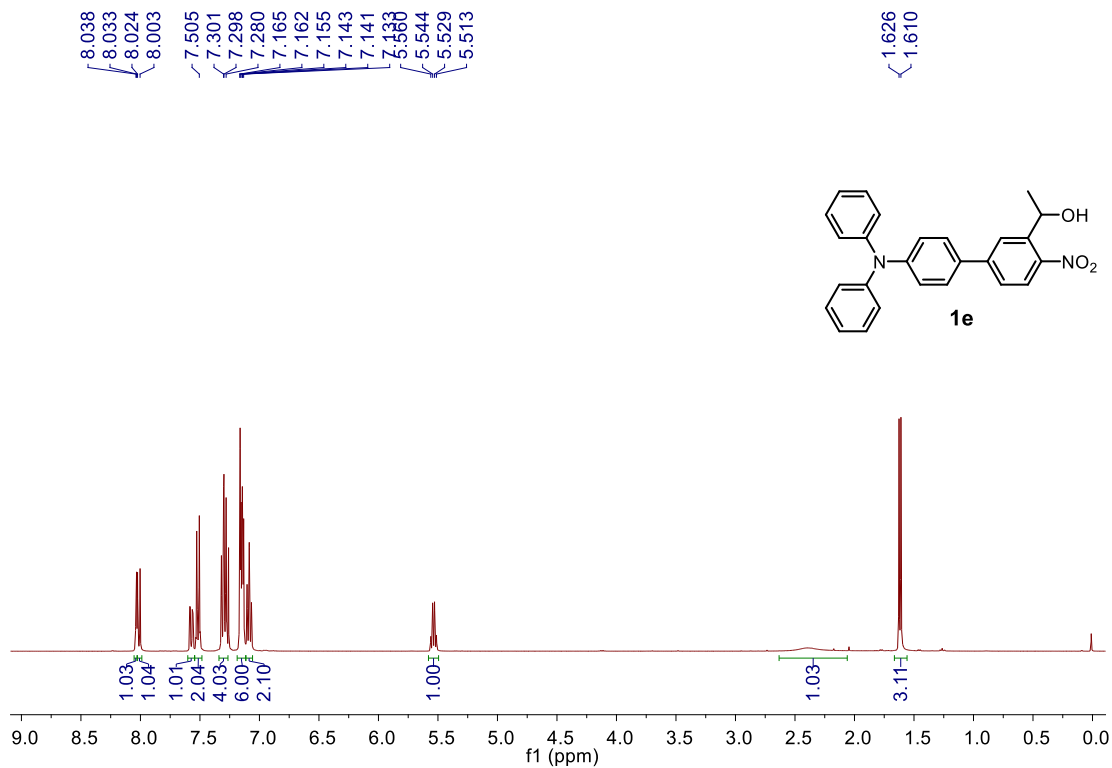


$^{13}\text{C}\{^1\text{H}\}$ NMR (100MHz, CDCl_3)

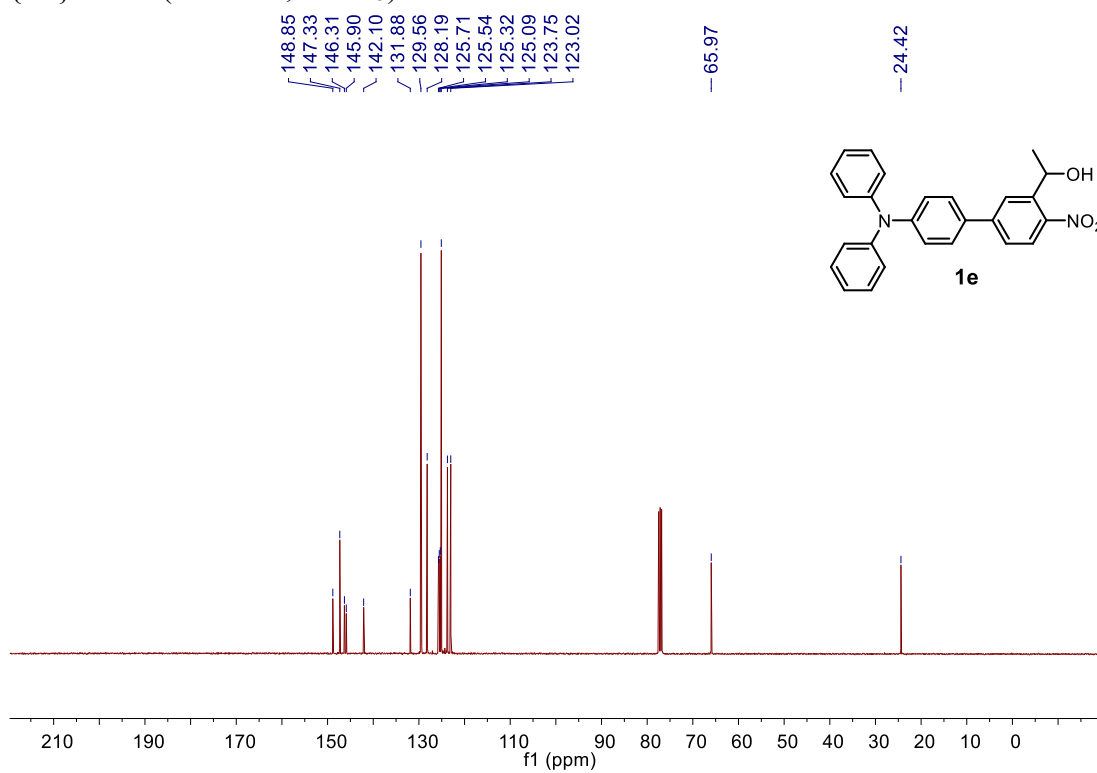
148.84
141.83
140.65
138.12
137.48
132.93
129.96
128.62
127.52
126.17
123.63
122.37
121.90
120.48
120.33
109.78



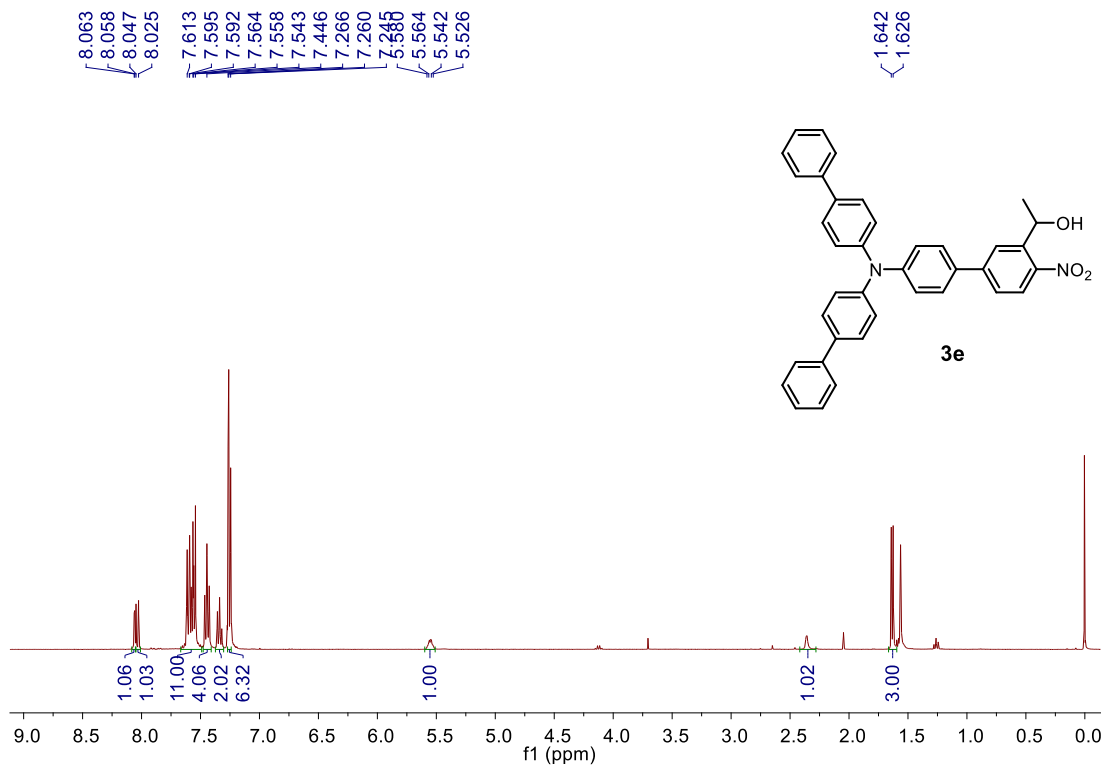
^1H NMR (400MHz, CDCl_3)



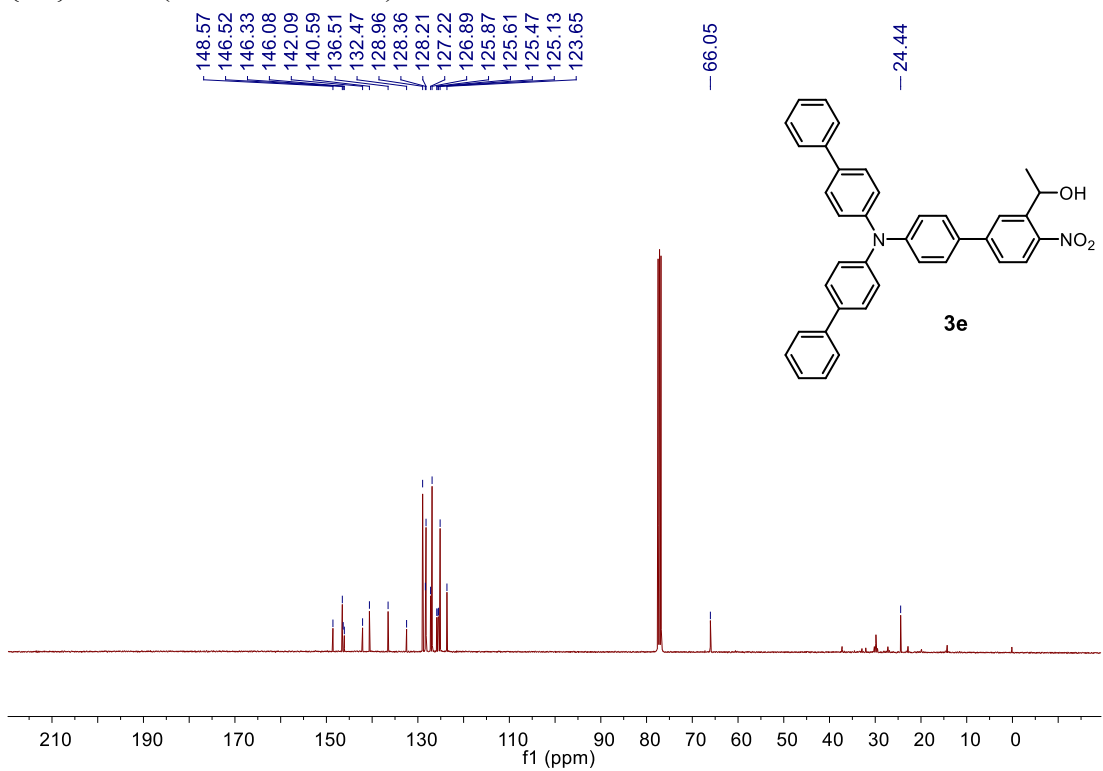
$^{13}\text{C}\{^1\text{H}\}$ NMR (100MHz, CDCl_3)



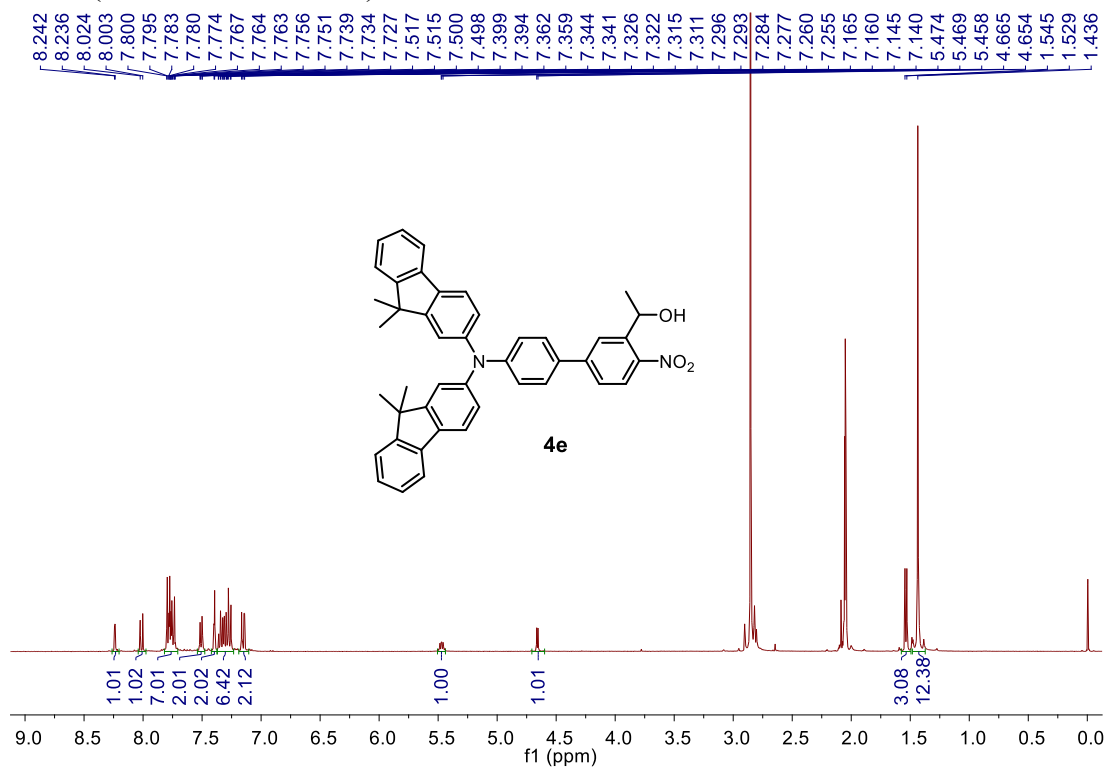
^1H NMR (400MHz, CDCl_3)



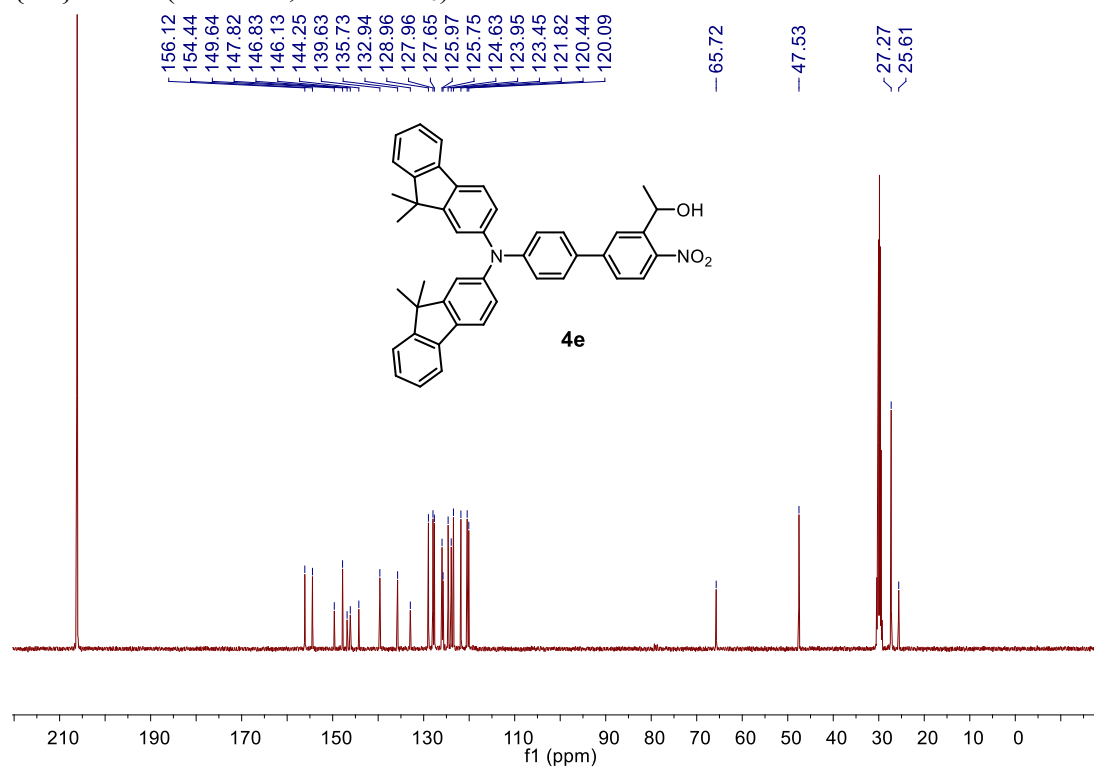
$^{13}\text{C}\{^1\text{H}\}$ NMR (100MHz, CDCl_3)



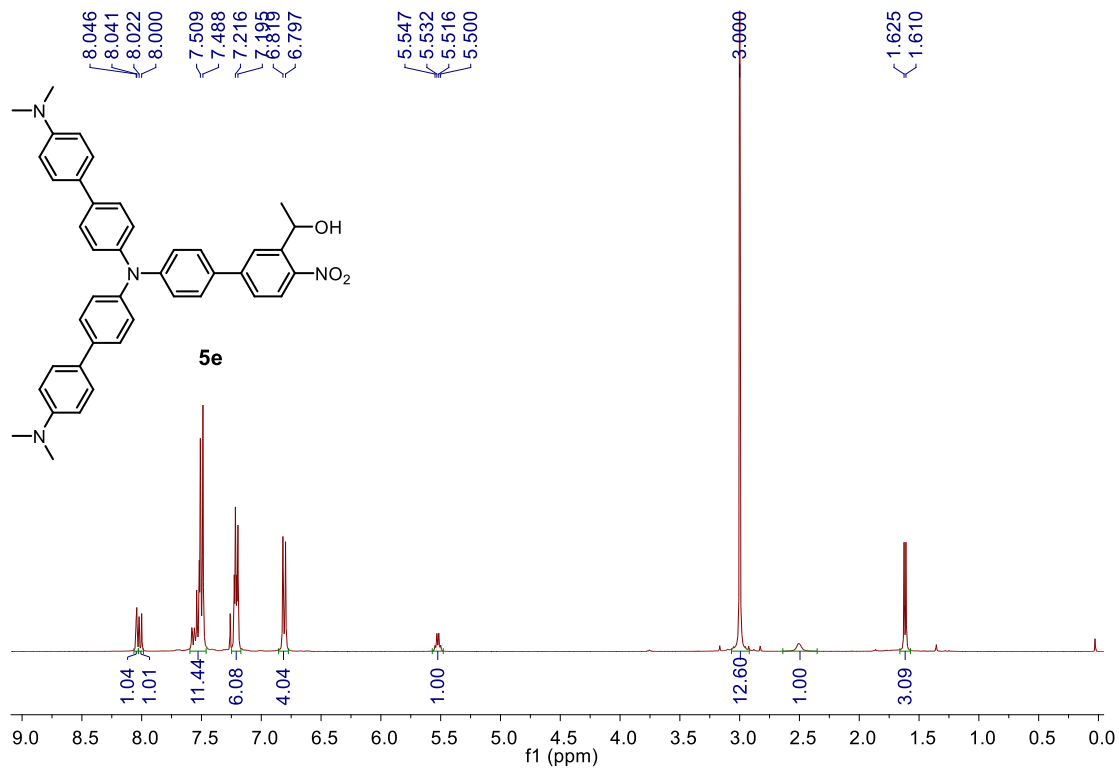
^1H NMR (400MHz, acetone- d_6)



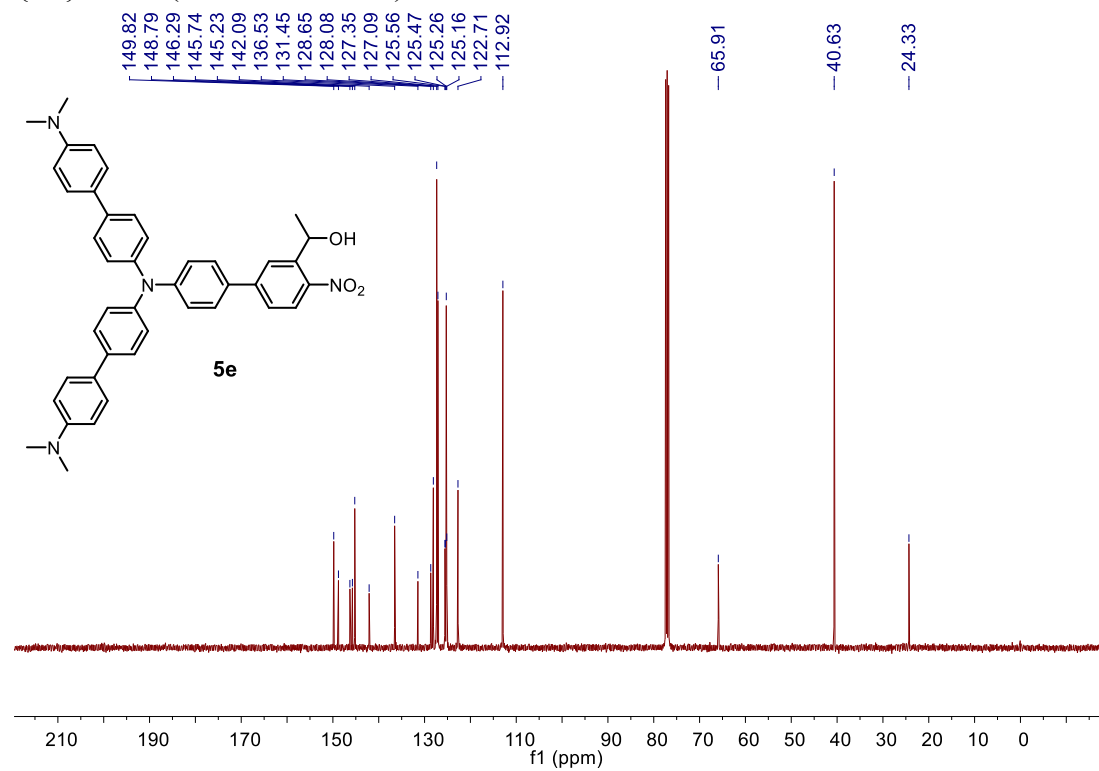
$^{13}\text{C}\{^1\text{H}\}$ NMR (100MHz, acetone- d_6)



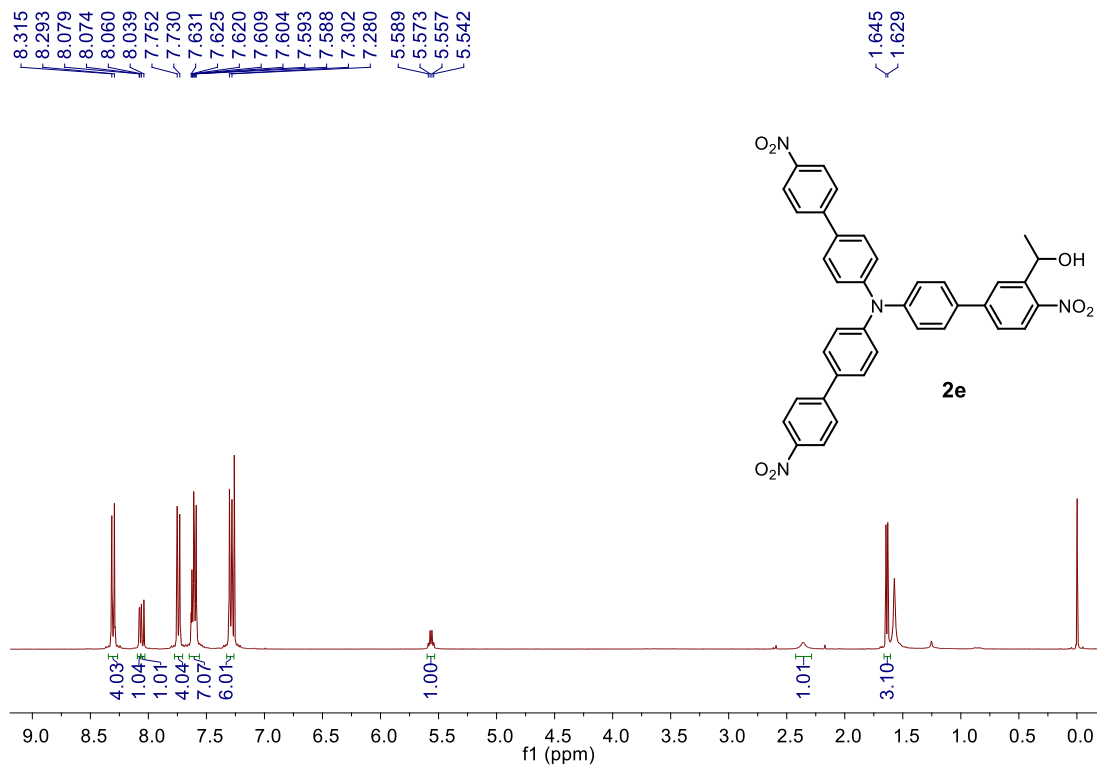
^1H NMR (400MHz, CDCl_3)



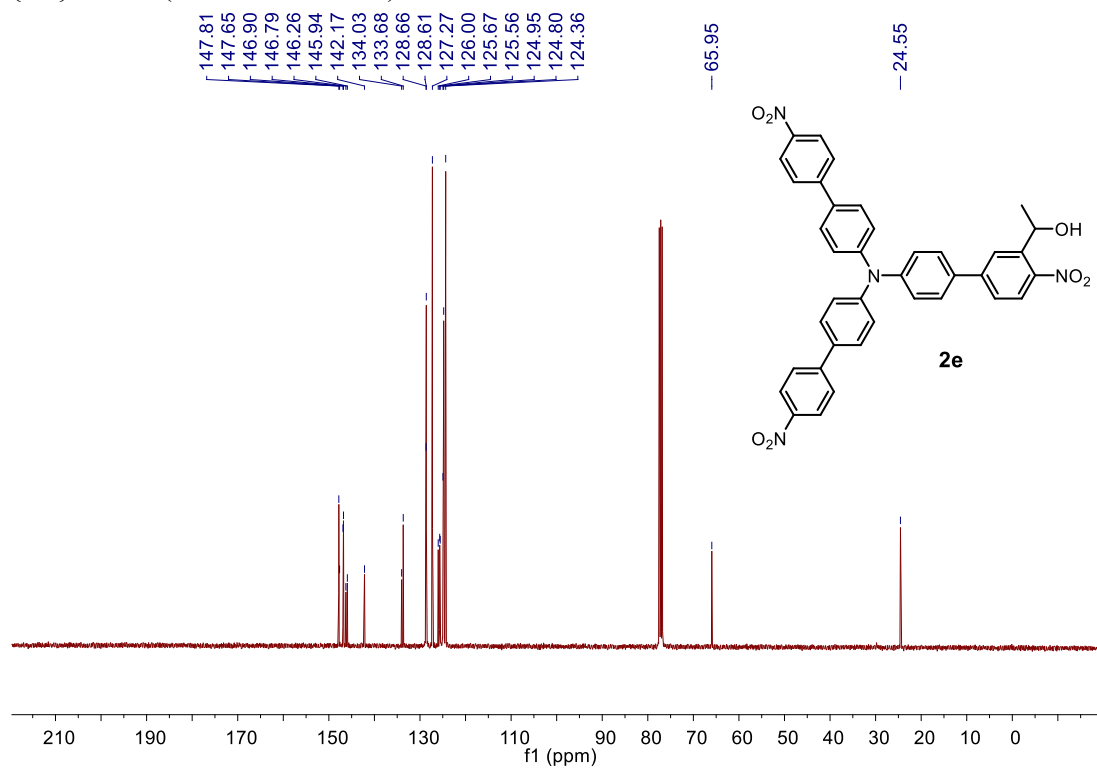
$^{13}\text{C}\{^1\text{H}\}$ NMR (100MHz, CDCl_3)



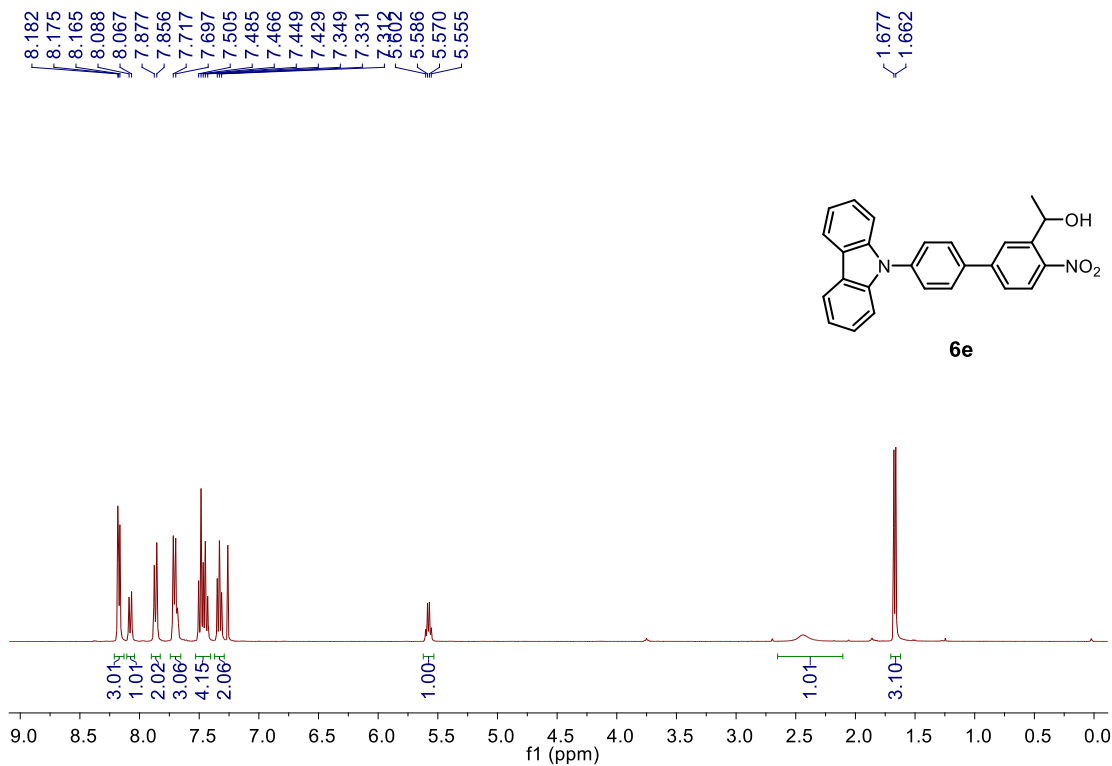
^1H NMR (400MHz, CDCl_3)



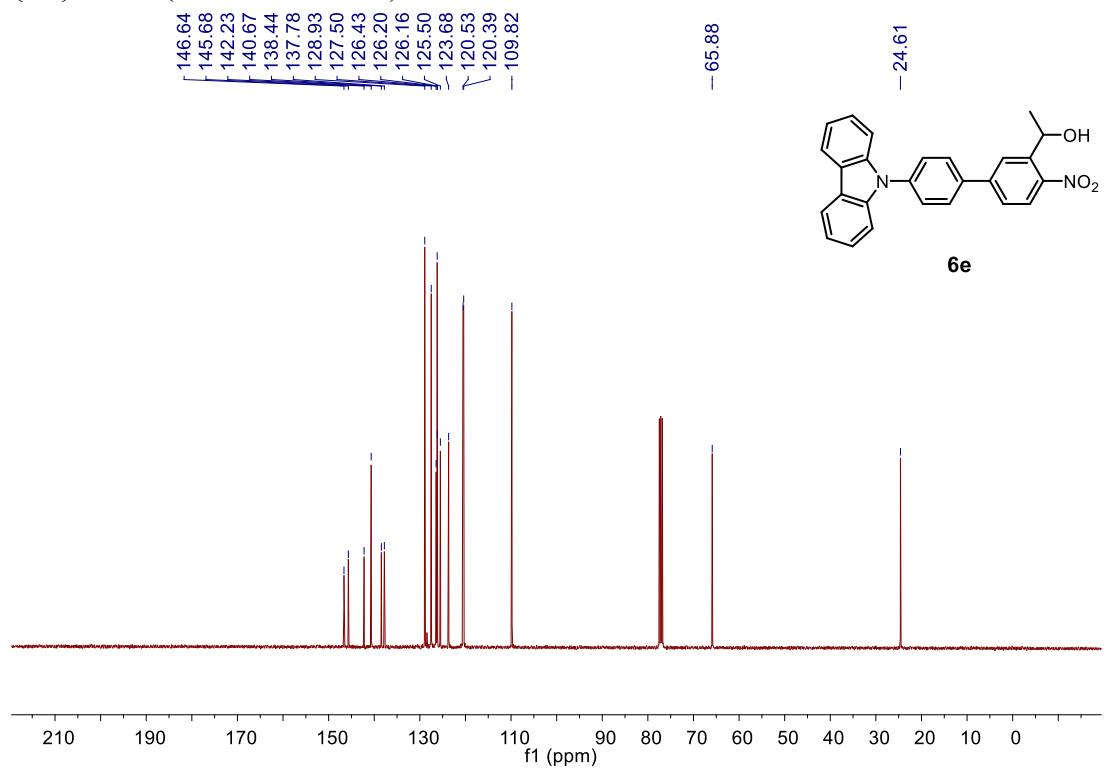
$^{13}\text{C}\{^1\text{H}\}$ NMR (100MHz, CDCl_3)



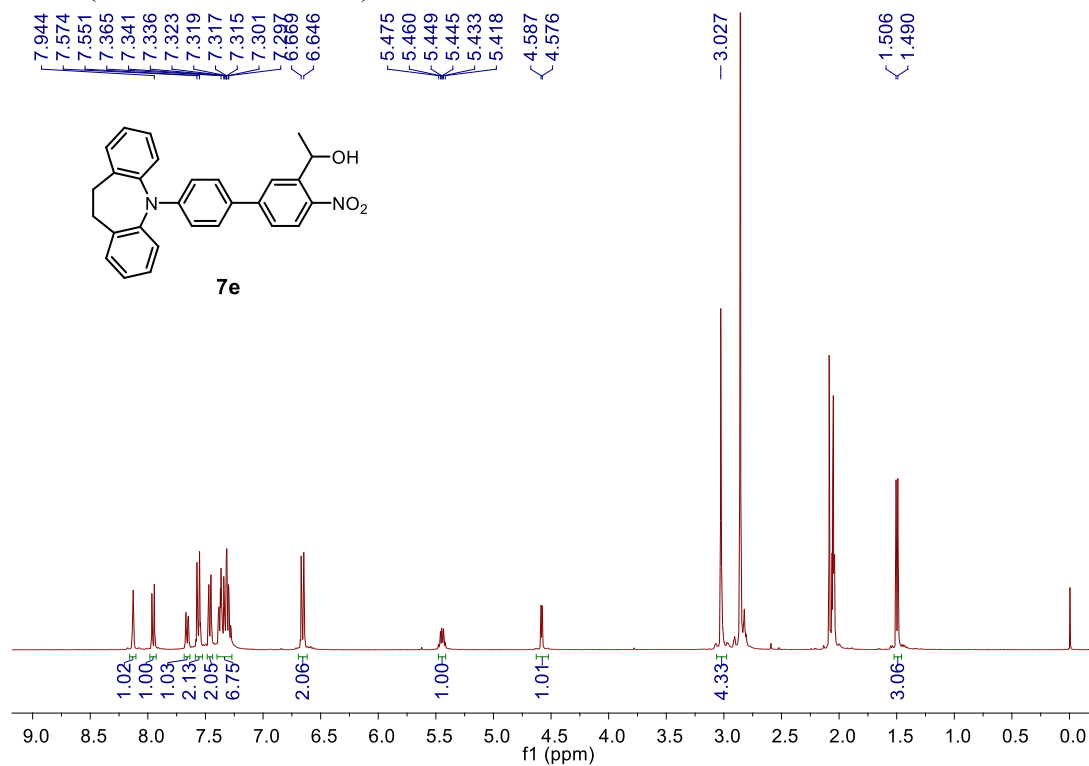
^1H NMR (400MHz, CDCl_3)



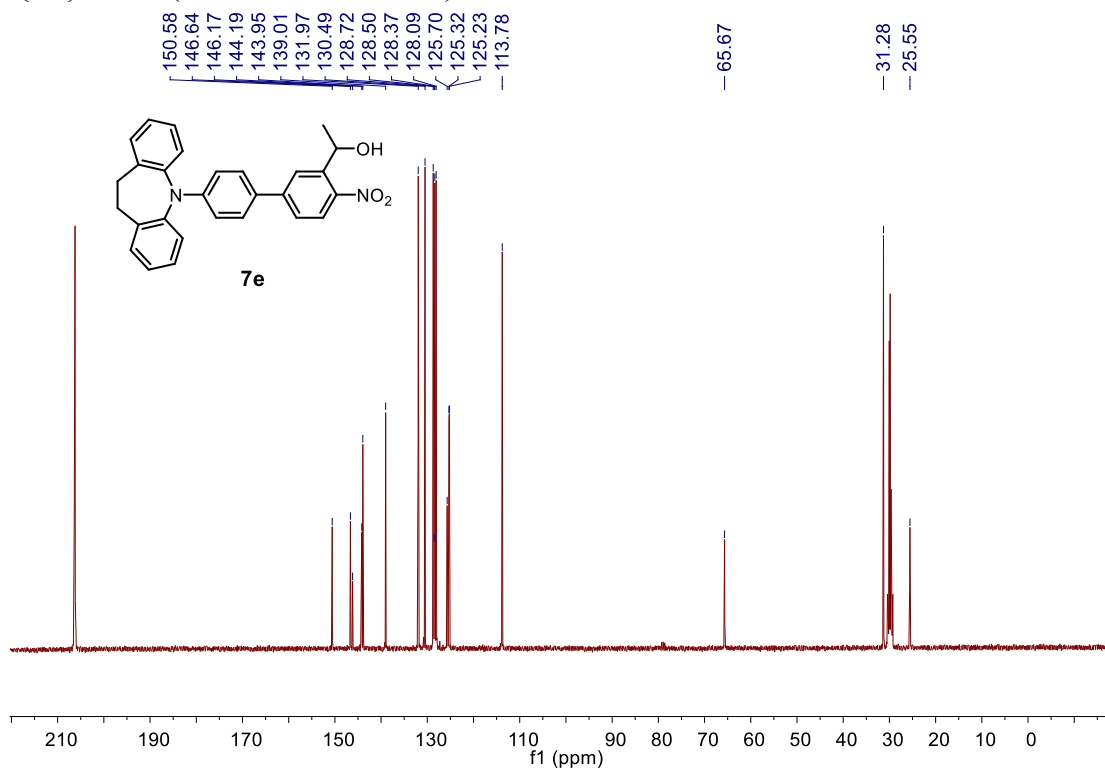
$^{13}\text{C}\{^1\text{H}\}$ NMR (100MHz, CDCl_3)



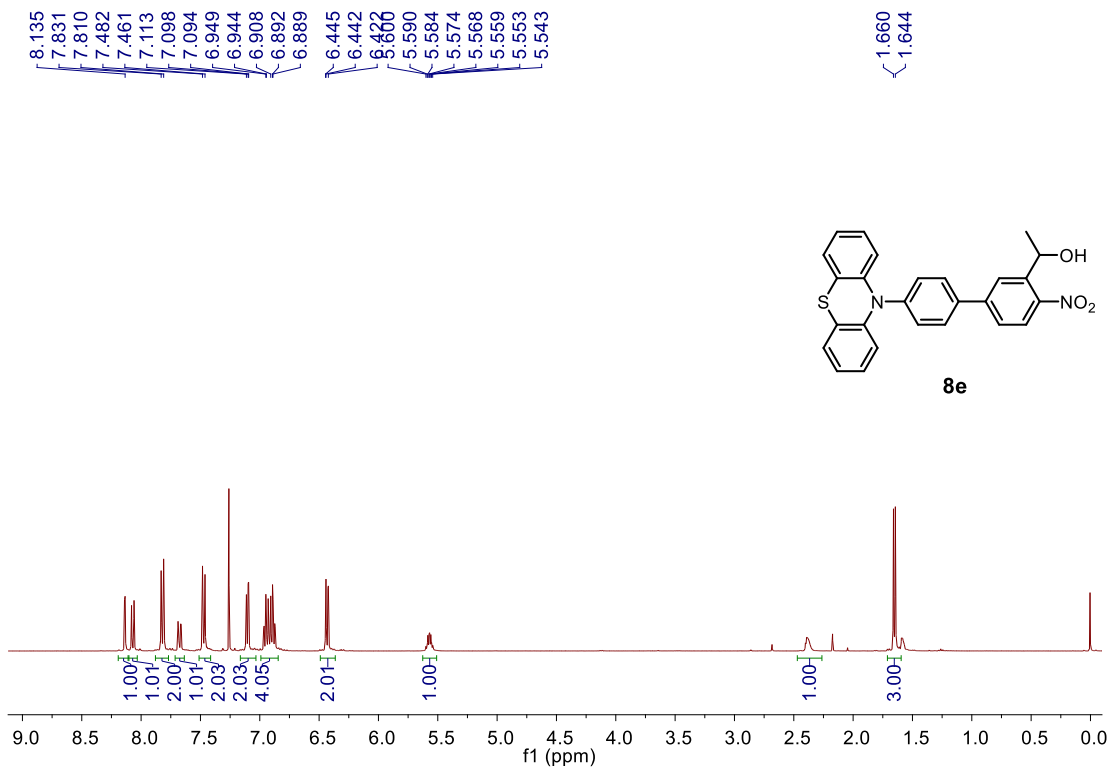
^1H NMR (400MHz, acetone- d_6)



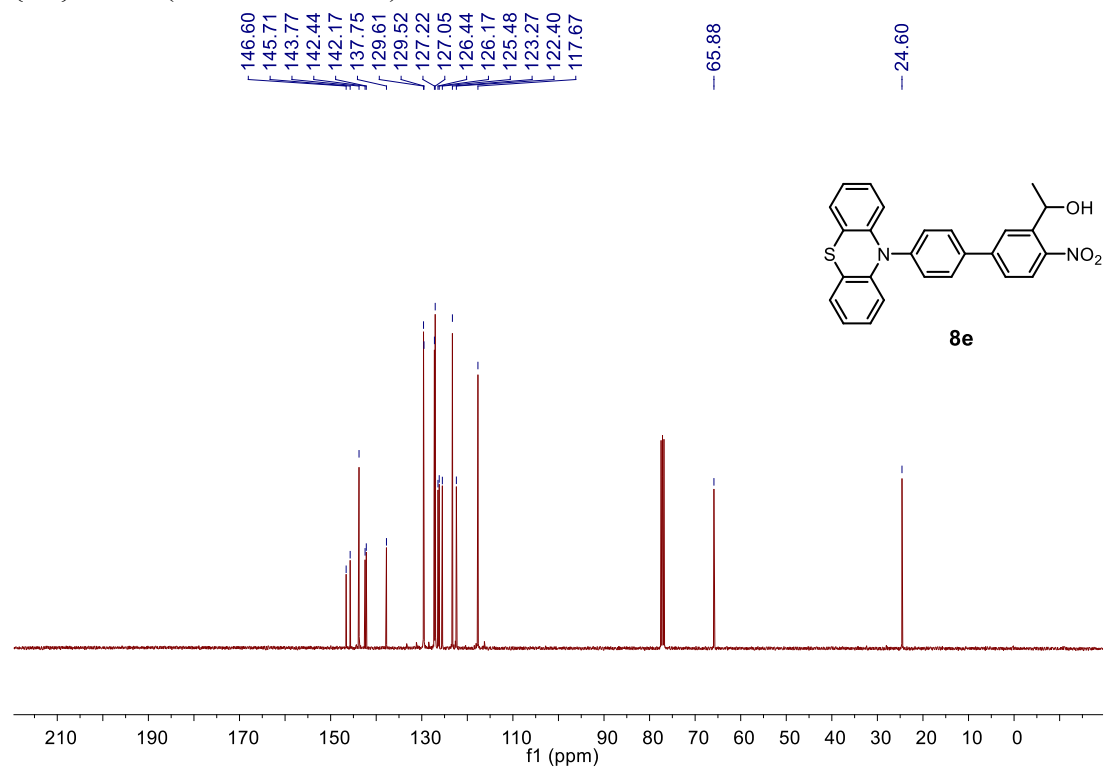
$^{13}\text{C}\{^1\text{H}\}$ NMR (100MHz, acetone- d_6)



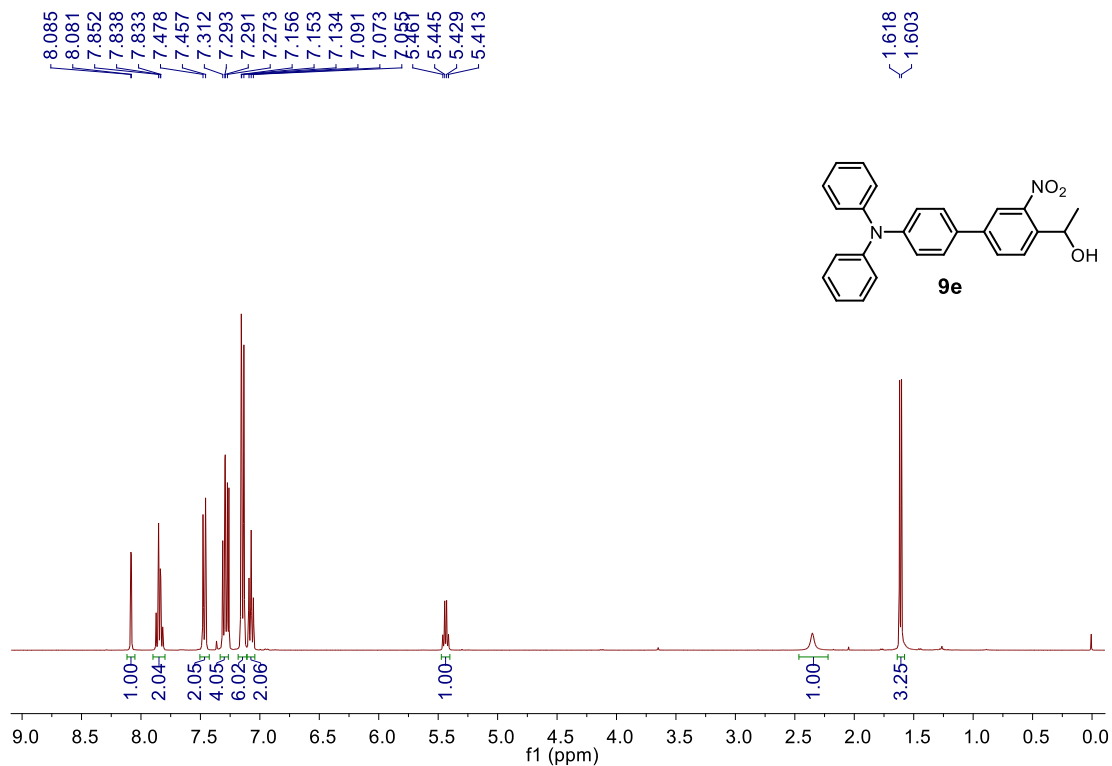
^1H NMR (400MHz, CDCl_3)



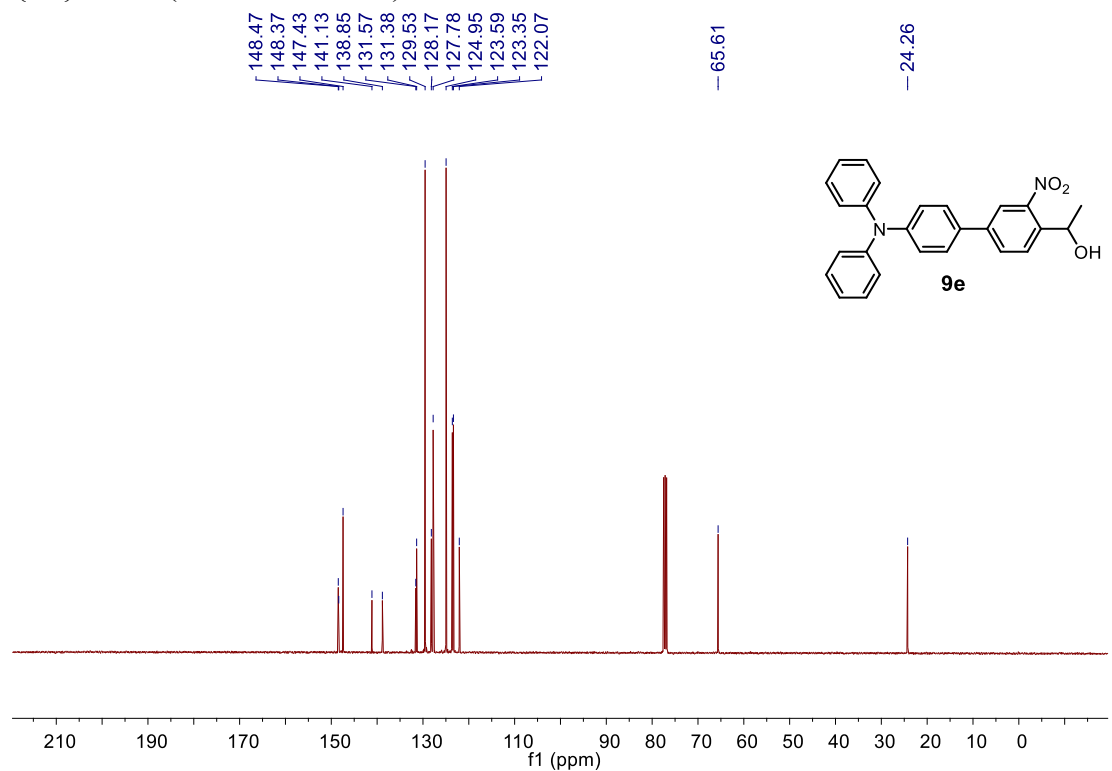
$^{13}\text{C}\{^1\text{H}\}$ NMR (100MHz, CDCl_3)



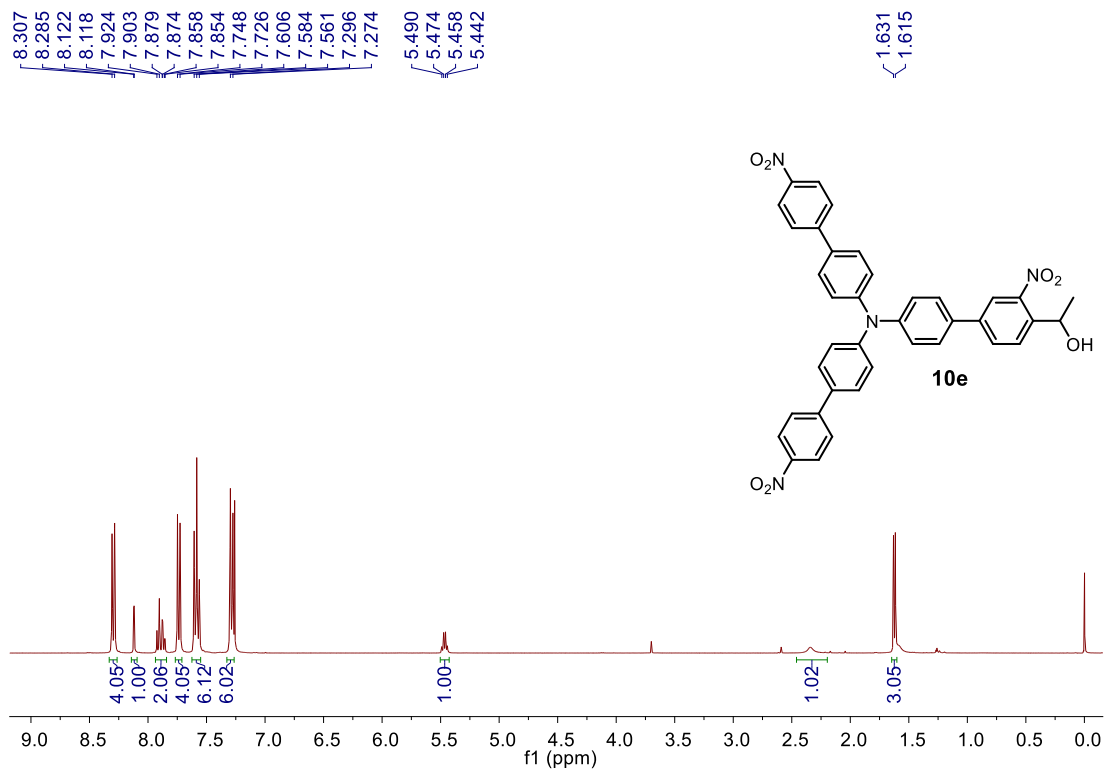
^1H NMR (400MHz, CDCl_3)



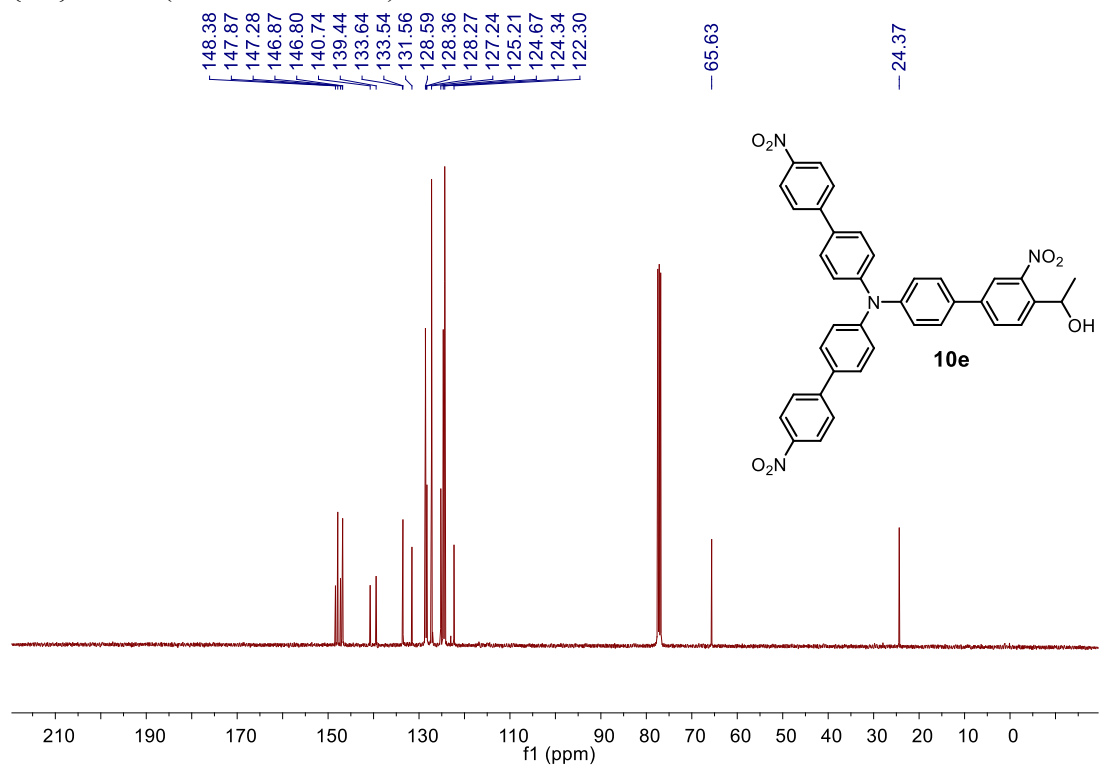
$^{13}\text{C}\{^1\text{H}\}$ NMR (100MHz, CDCl_3)



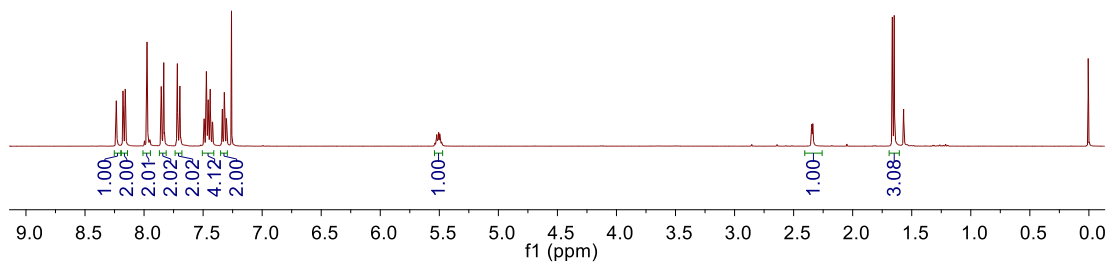
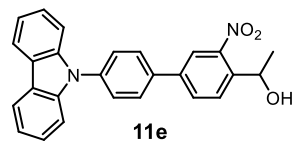
^1H NMR (400MHz, CDCl_3)



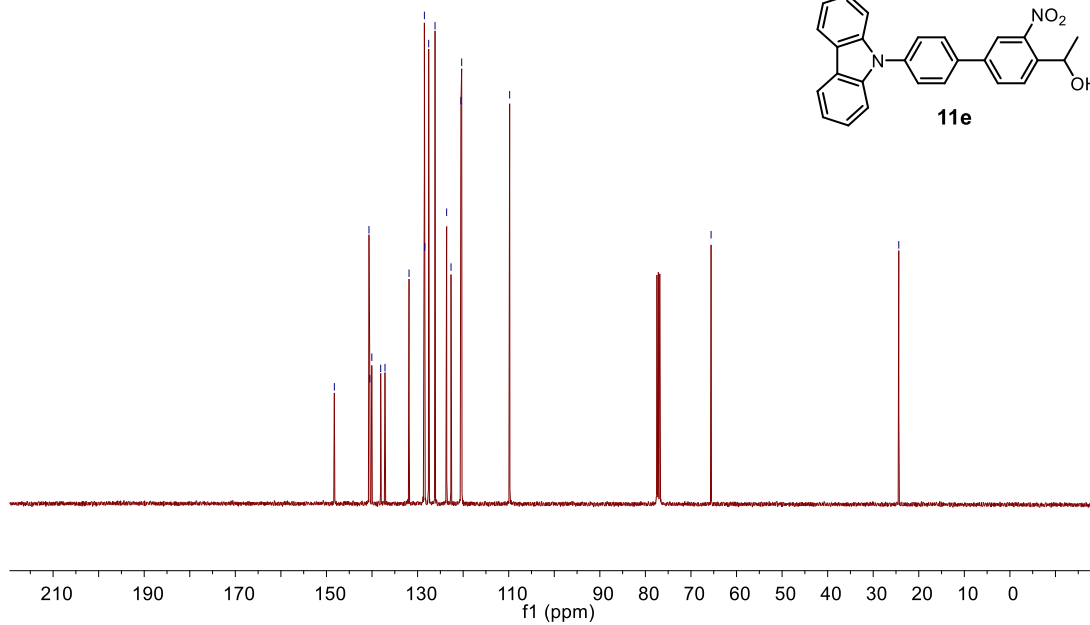
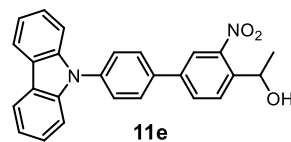
$^{13}\text{C}\{^1\text{H}\}$ NMR (100MHz, CDCl_3)



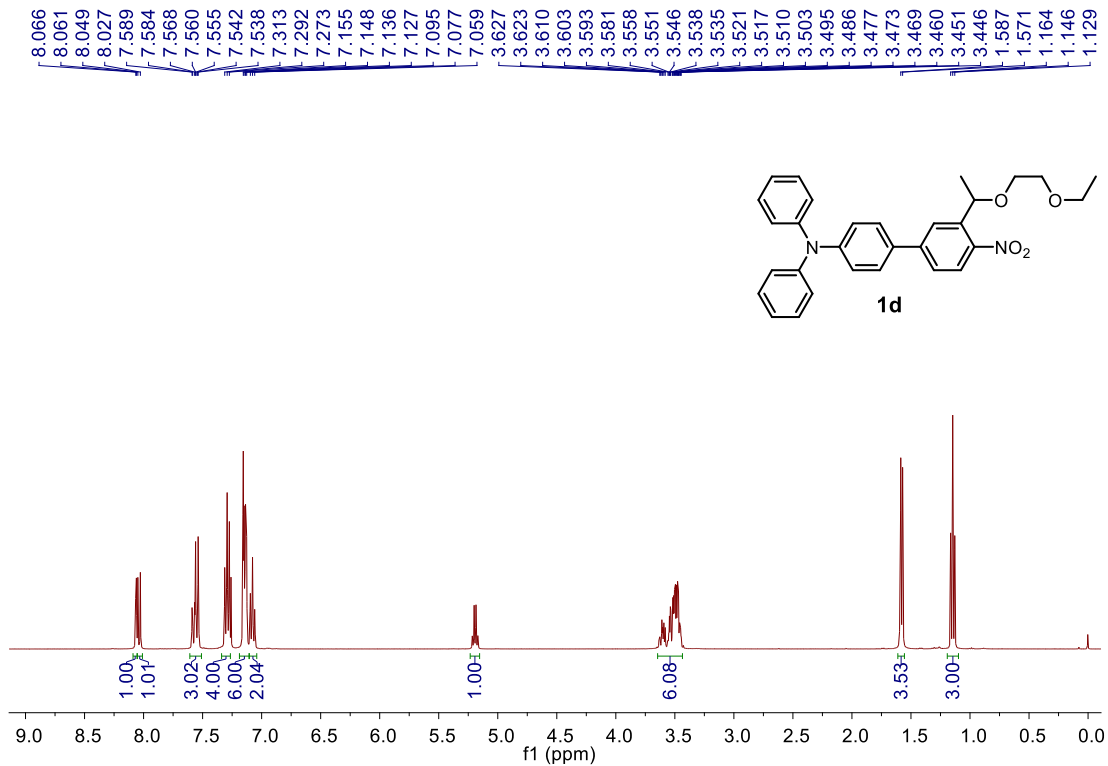
^1H NMR (400MHz, CDCl_3)



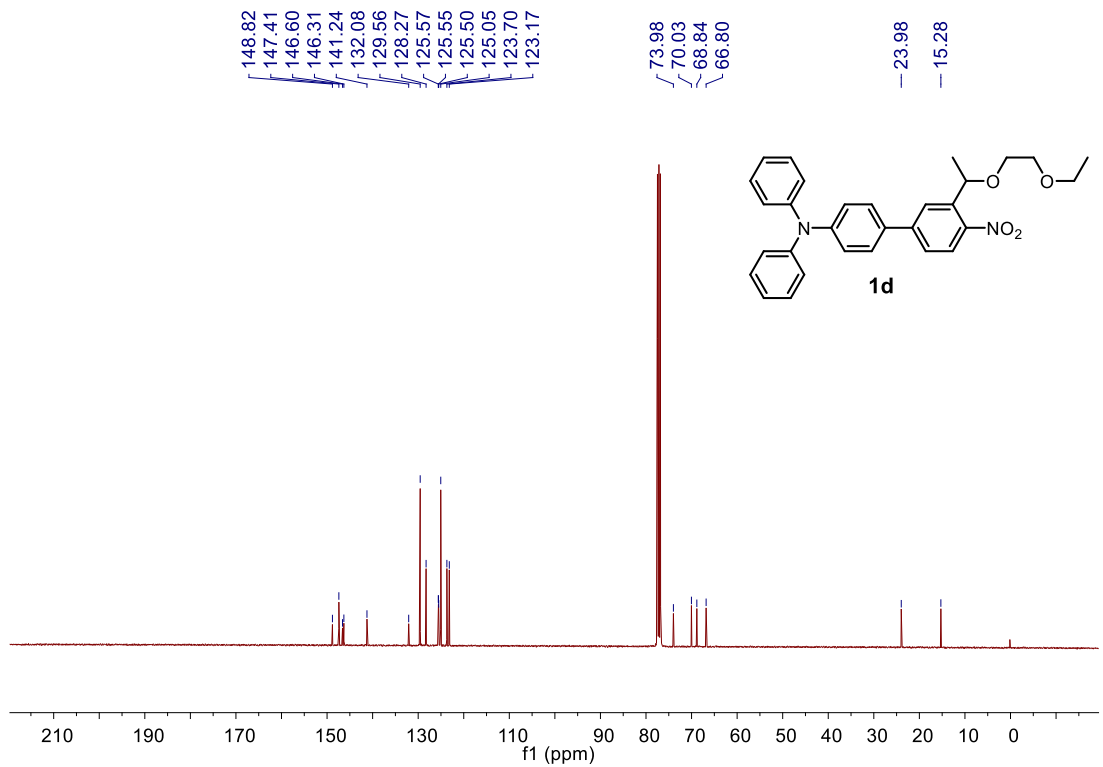
$^{13}\text{C}\{^1\text{H}\}$ NMR (100MHz, CDCl_3)



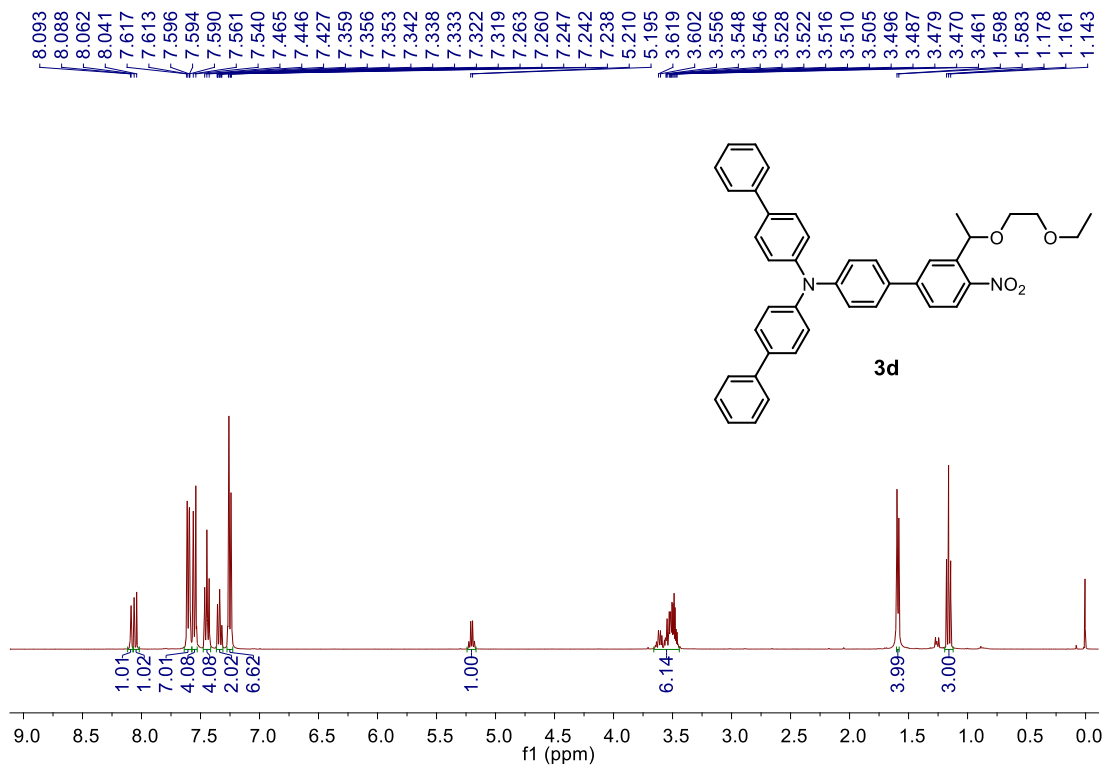
^1H NMR (400MHz, CDCl_3)



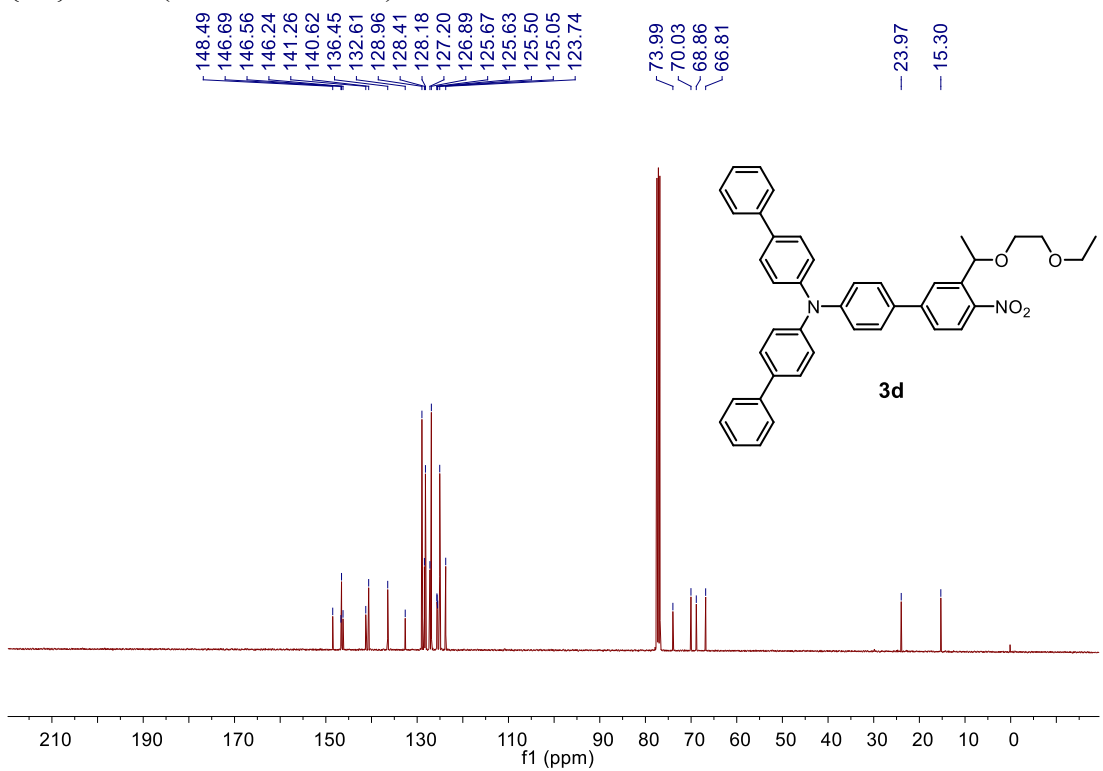
$^{13}\text{C}\{^1\text{H}\}$ NMR (100MHz, CDCl_3)



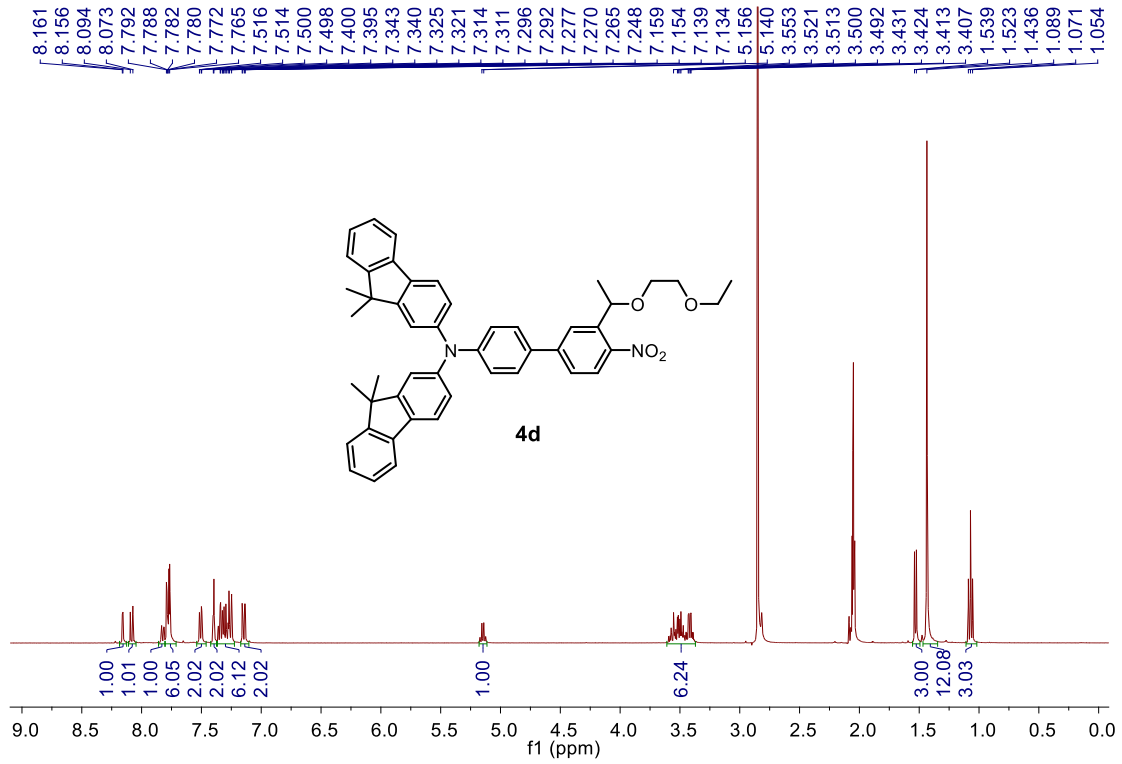
^1H NMR (400MHz, CDCl_3)



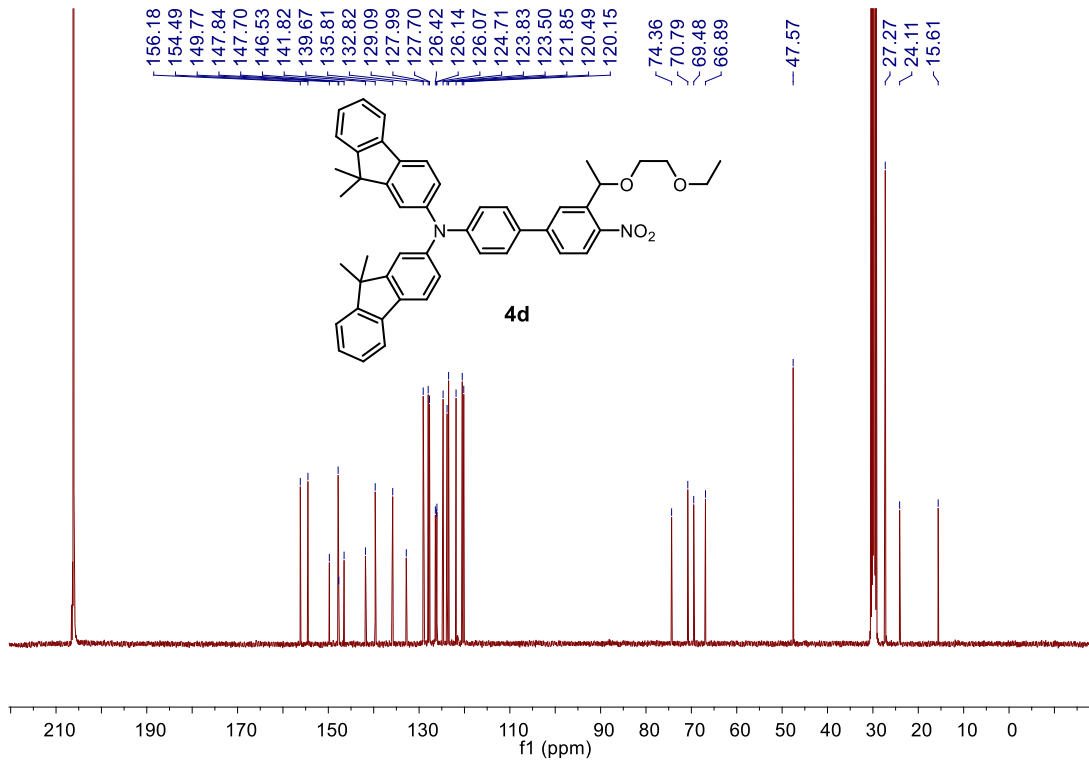
$^{13}\text{C}\{^1\text{H}\}$ NMR (100MHz, CDCl_3)



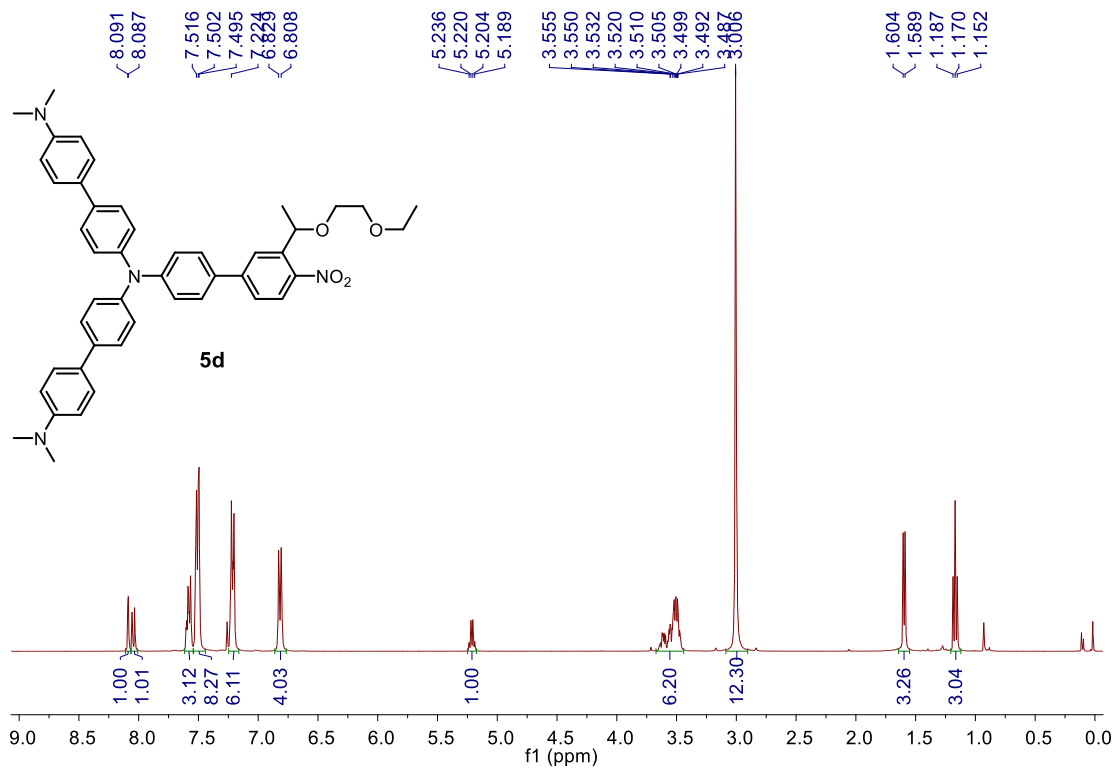
¹H NMR (400MHz, acetone-d₆)



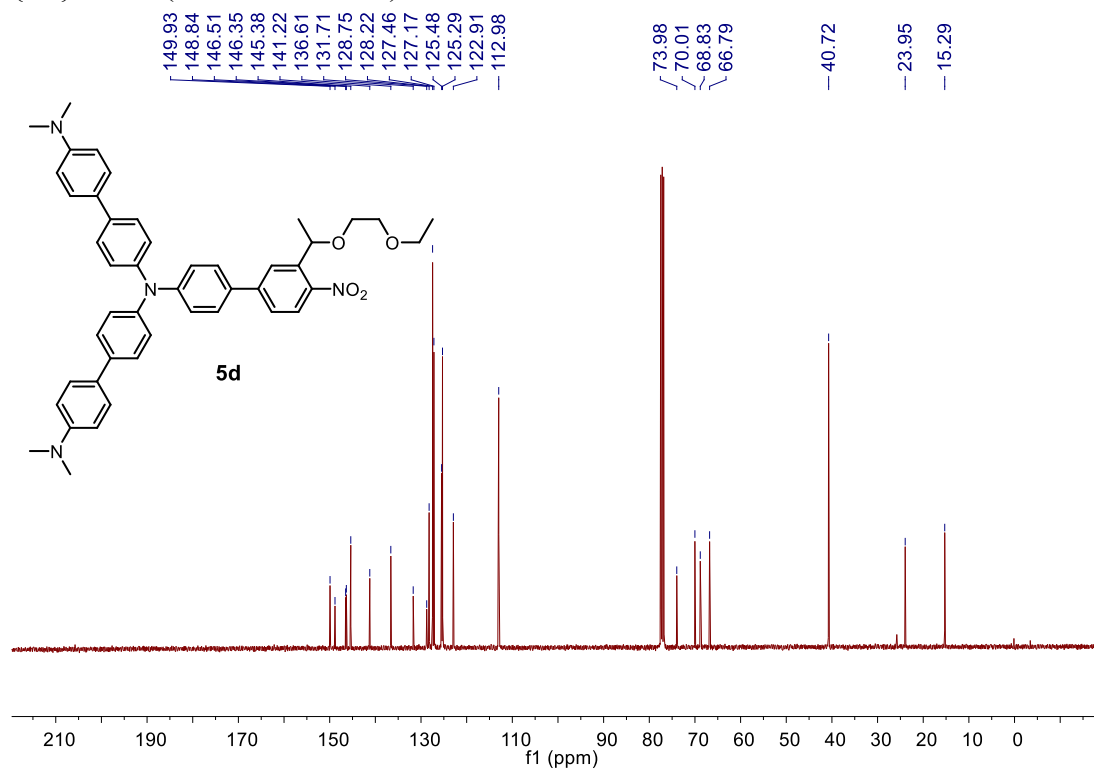
¹³C{¹H} NMR (100MHz, acetone-d₆)



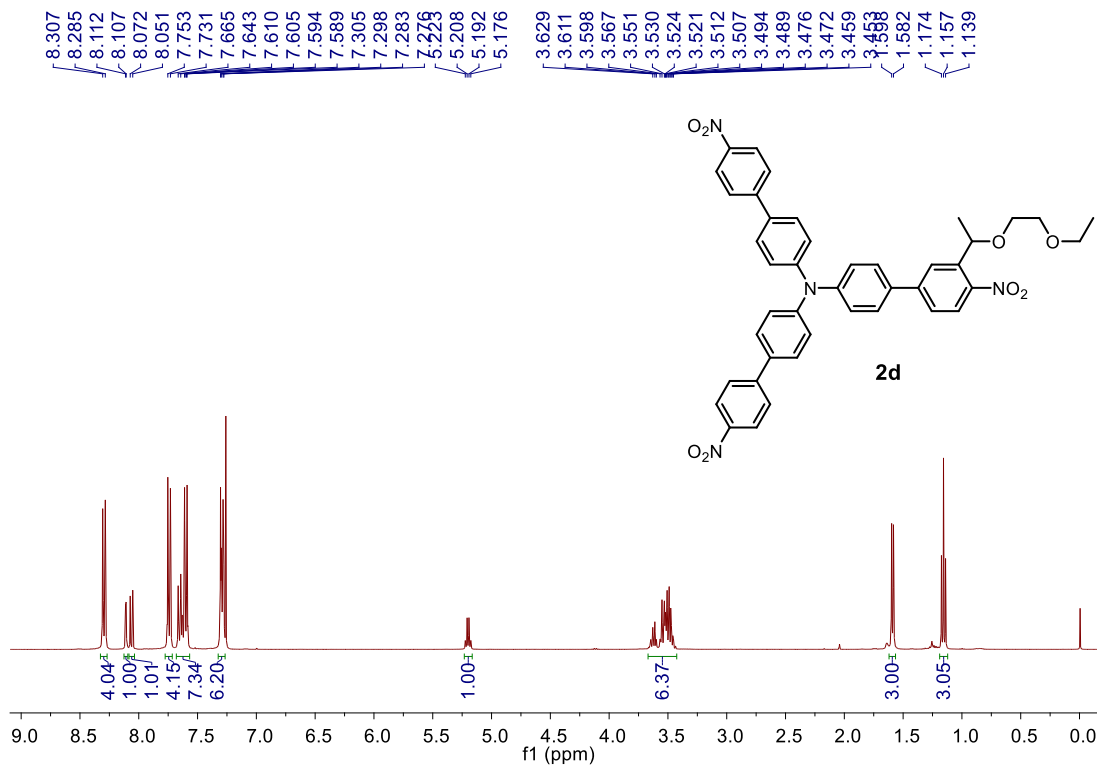
^1H NMR (400MHz, CDCl_3)



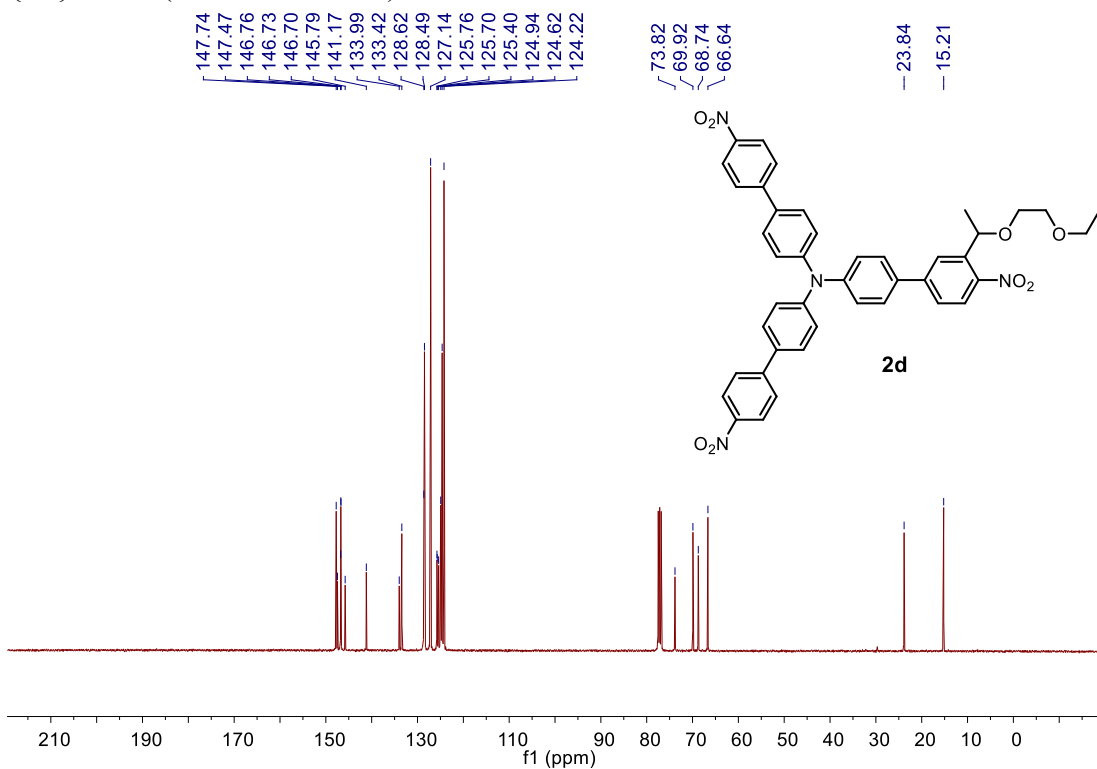
$^{13}\text{C}\{^1\text{H}\}$ NMR (100MHz, CDCl_3)



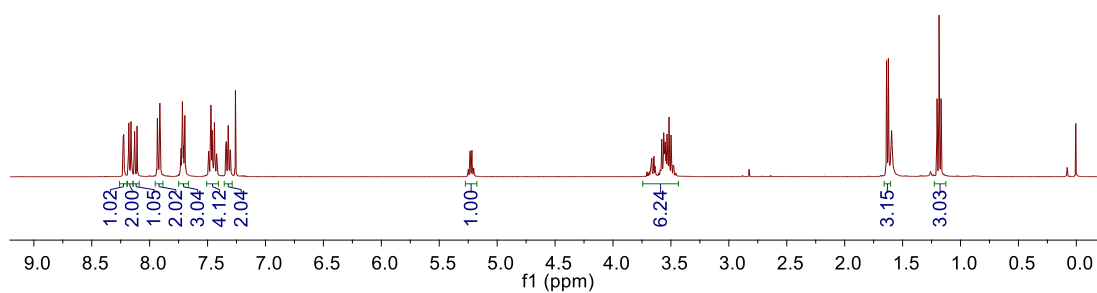
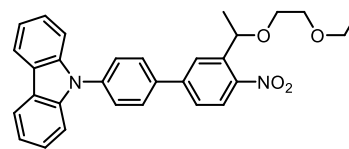
^1H NMR (400MHz, CDCl_3)



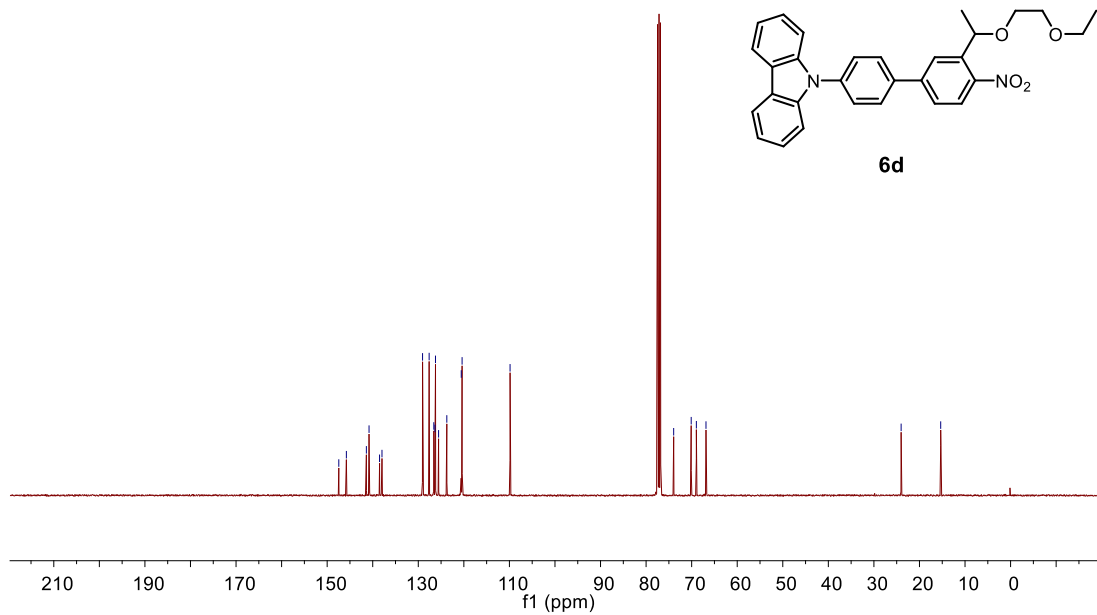
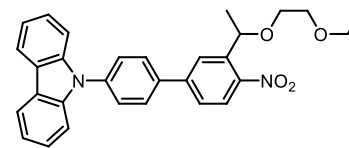
$^{13}\text{C}\{^1\text{H}\}$ NMR (100MHz, CDCl_3)



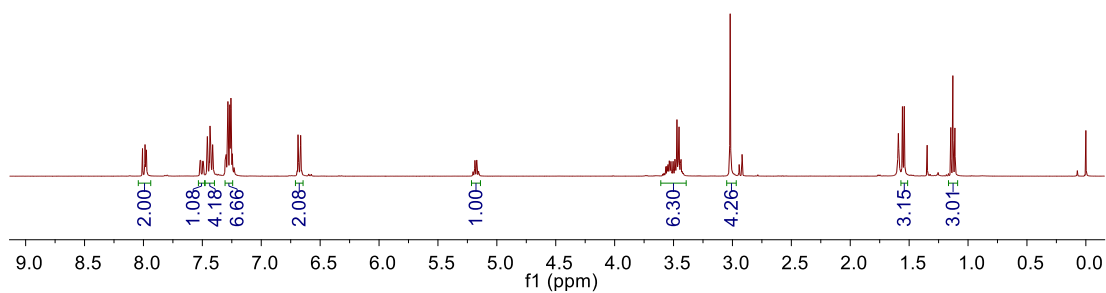
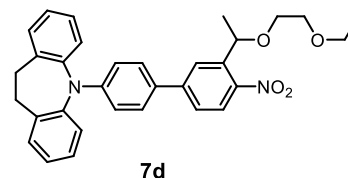
^1H NMR (400MHz, CDCl_3)



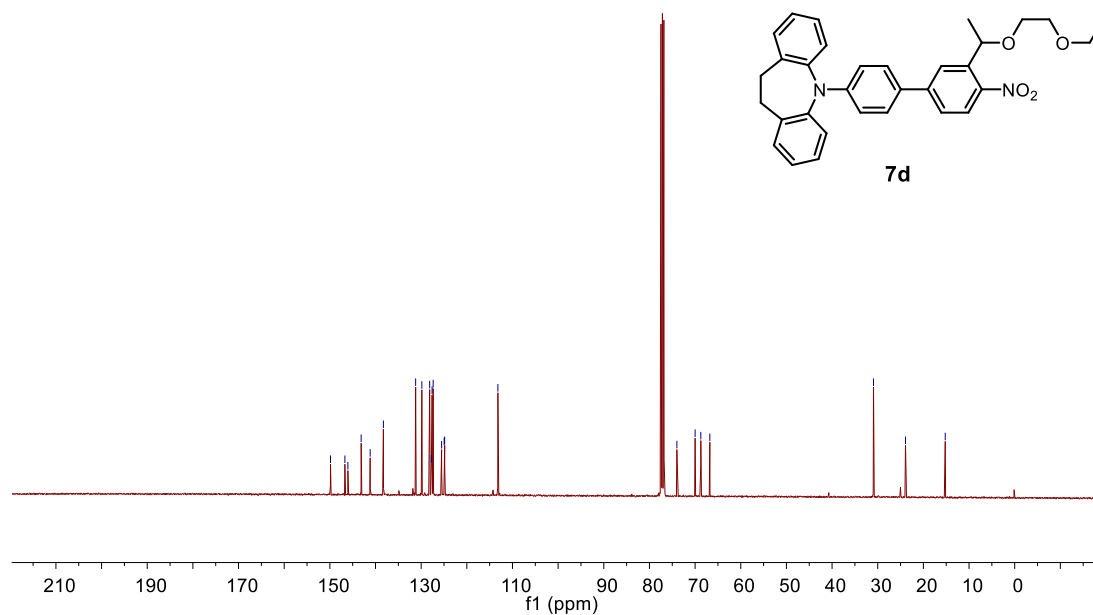
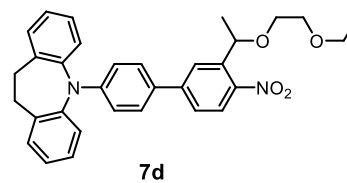
$^{13}\text{C}\{^1\text{H}\}$ NMR (100MHz, CDCl_3)



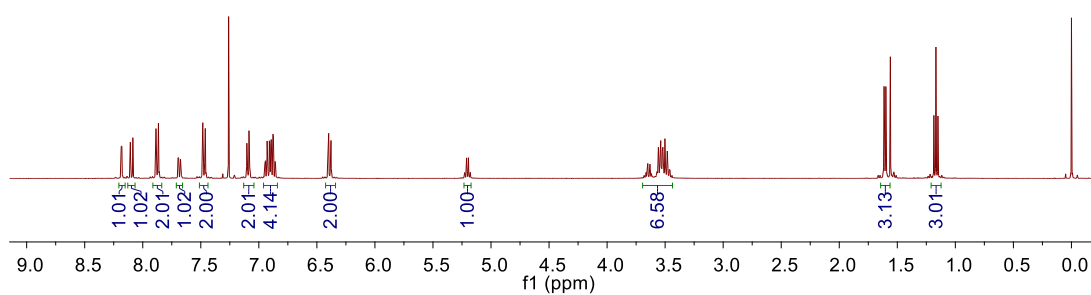
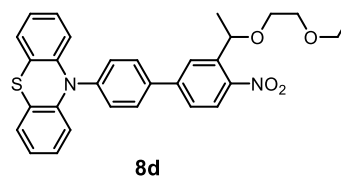
^1H NMR (400MHz, CDCl_3)



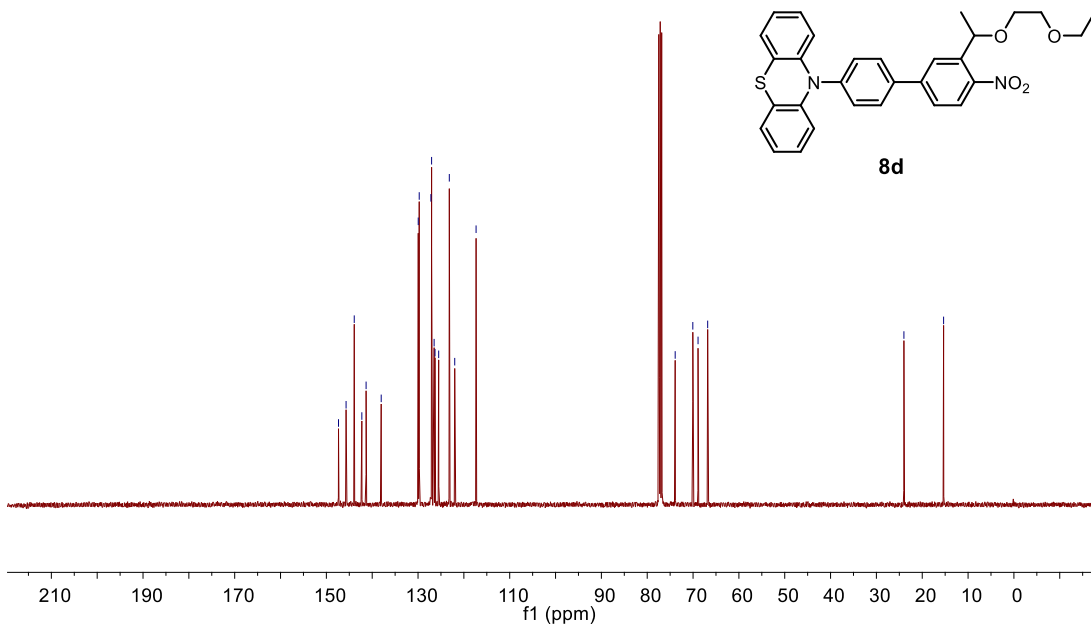
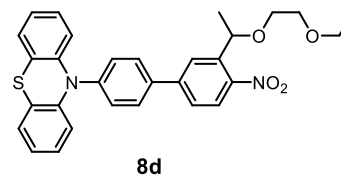
$^{13}\text{C}\{^1\text{H}\}$ NMR (100MHz, CDCl_3)



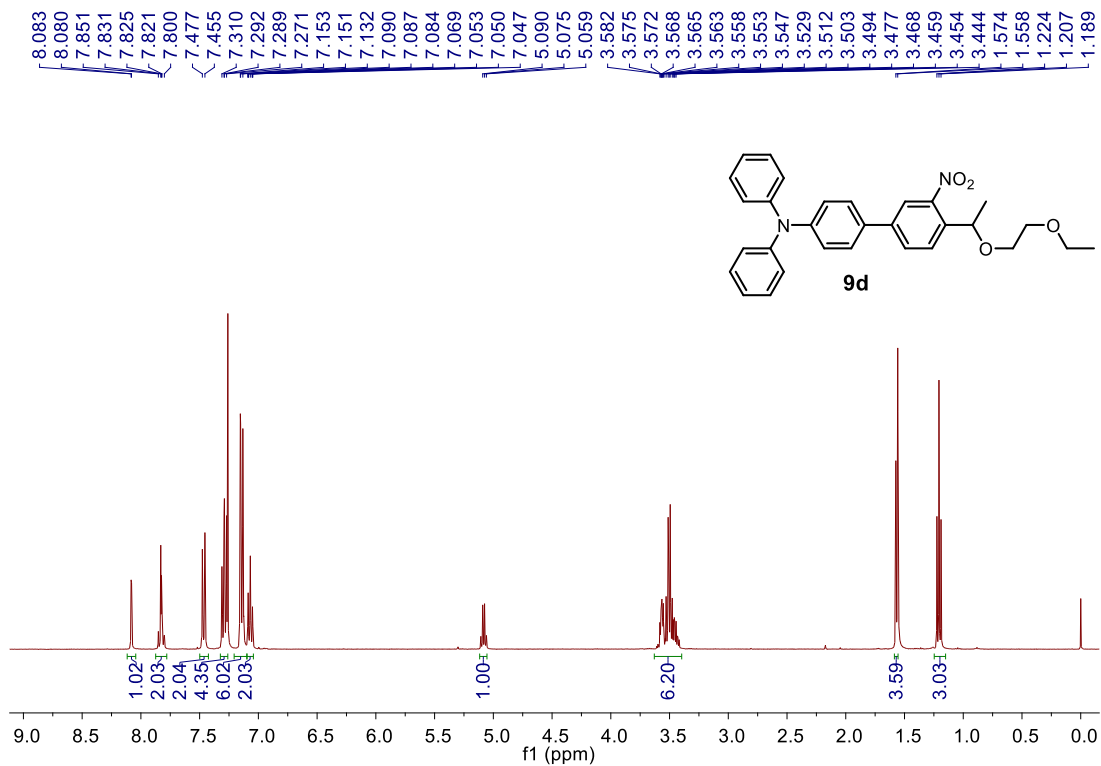
^1H NMR (400MHz, CDCl_3)



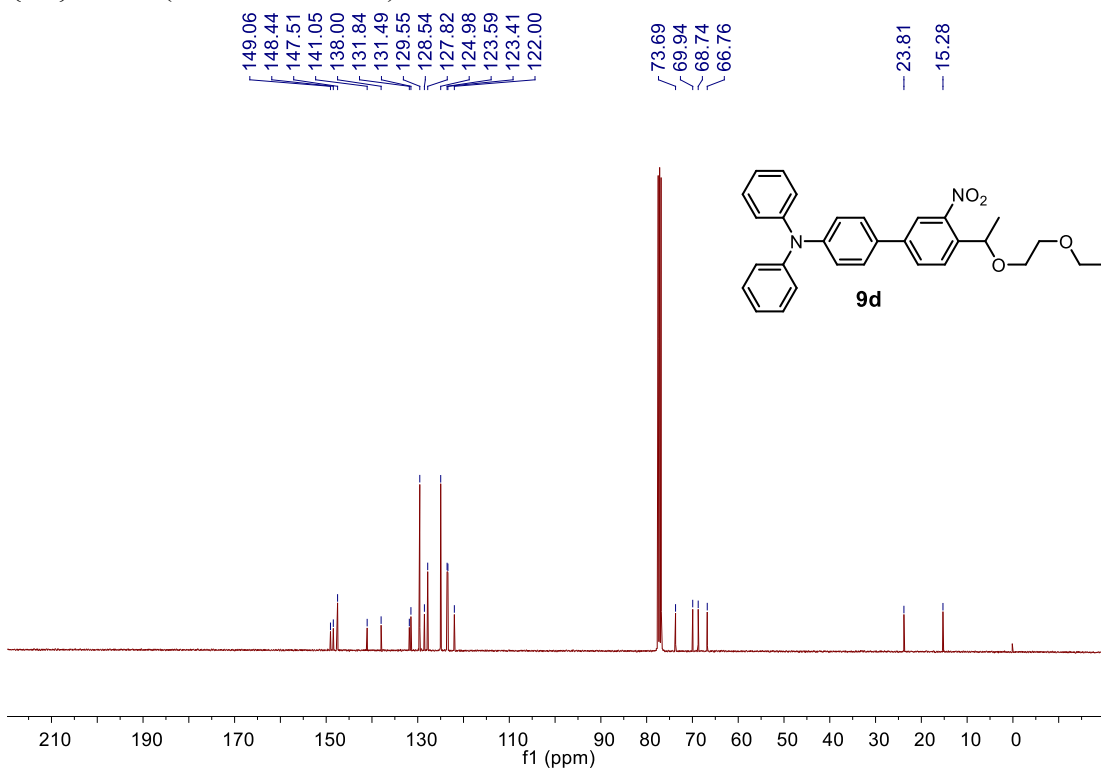
$^{13}\text{C}\{^1\text{H}\}$ NMR (100MHz, CDCl_3)



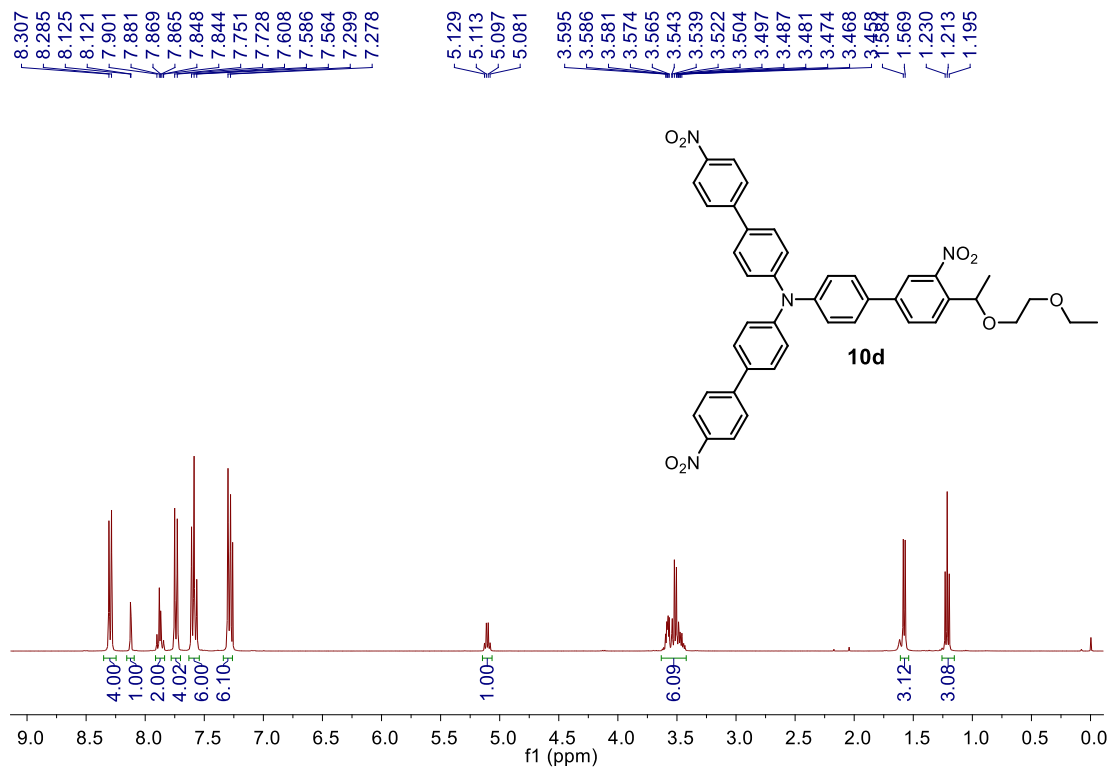
^1H NMR (400MHz, CDCl_3)



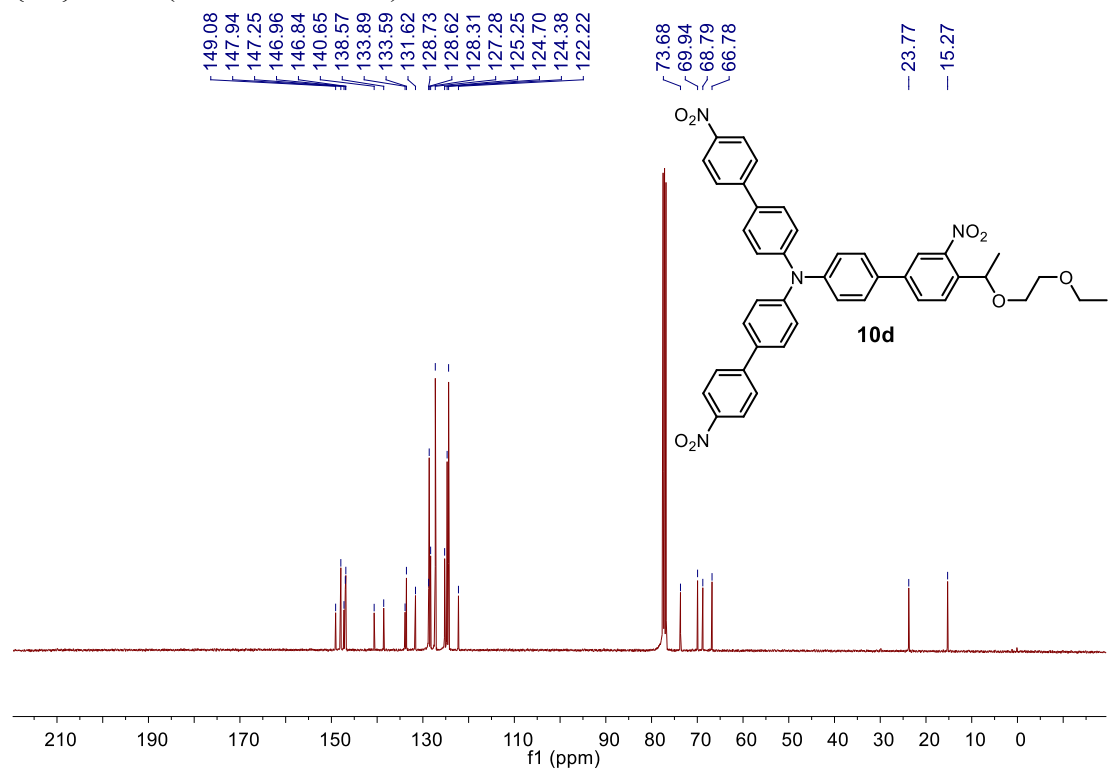
$^{13}\text{C}\{^1\text{H}\}$ NMR (100MHz, CDCl_3)



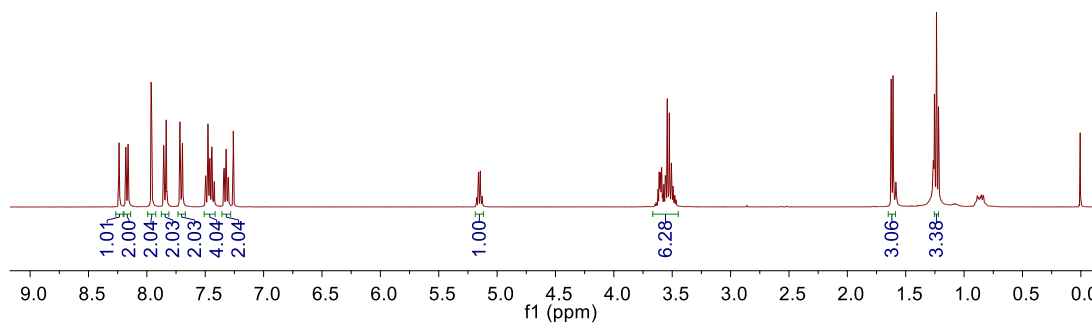
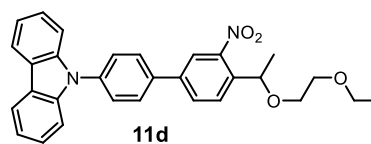
^1H NMR (400MHz, CDCl_3)



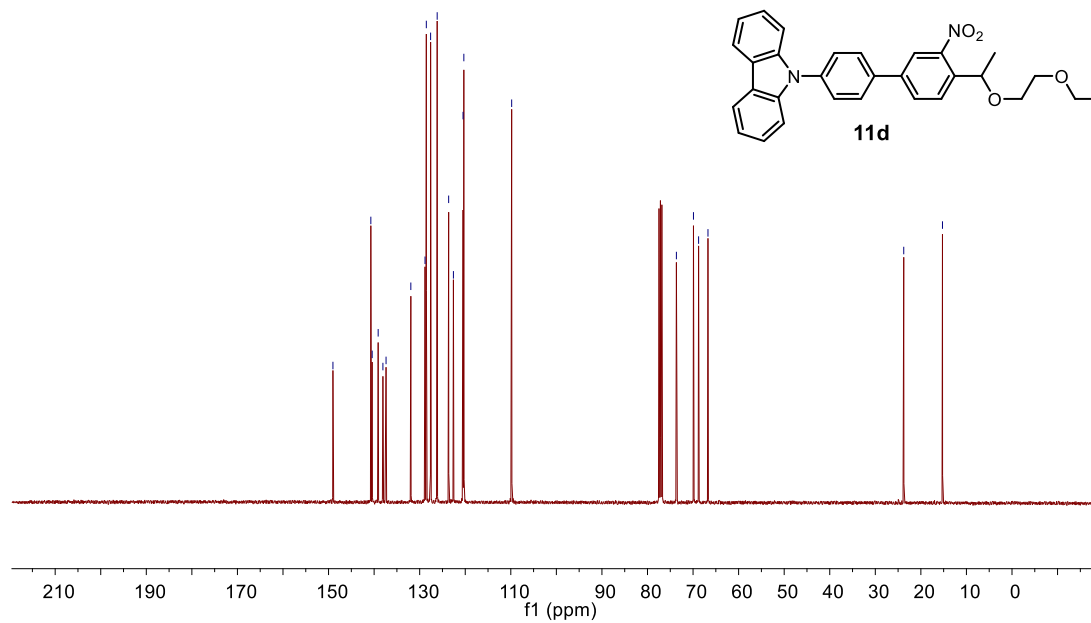
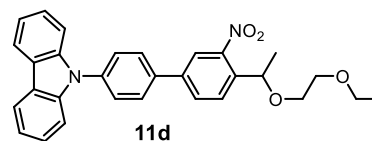
$^{13}\text{C}\{^1\text{H}\}$ NMR (100MHz, CDCl_3)



^1H NMR (400MHz, CDCl_3)



$^{13}\text{C}\{^1\text{H}\}$ NMR (100MHz, CDCl_3)



Chapter 4

Conclusion and outlook

The π -extended systems suffer from the loss of quantum efficiencies, although they may induce the bathochromic shift of absorption spectra and enhance the 2P responses. We also successfully observed the uncaging of Ca^{2+} from the calcium chelator of an octupolar chromophore. On the other hand, the cyclic structures of the diarylamino moiety could increase the photoreaction quantum yield. This was due to the destabilization of CT transition and preservation of local $n-\pi^*$ excitation, which is essential for achieving efficient photo-uncaging. This study can contribute to improving the understanding of factors affecting uncaging quantum yield and the need to balance optical properties and quantum efficiencies to accelerate the evolution of high-quality PPGs for proficient applications in physiological and therapeutic research.

References

- 1 M. Goeldner, R. Givens, *Dynamic studies in biology: phototriggers, photoswitches and caged biomolecules*, John Wiley & Sons, **2006**.
- 2 G. C. R. Ellis-Davies, *Nat. Methods* **2007**, *4*, 619.
- 3 G. C. R. Ellis-Davies, *Angew. Chemie Int. Ed.* **2023**, *62*, e202206083.
- 4 P. Klán, T. Solomek, C. G. Bochet, A. Blanc, R. Givens, M. Rubina, V. Popik, A. Kostikov, J. Wirz, *Chem. Rev.* **2013**, *113*, 119.
- 5 R. Weinstain, T. Slanina, D. Kand, P. Klan, *Chem. Rev.* **2020**, *120*, 13135.
- 6 M. Abe, Y. Chitose, S. Jakkampudi, P. T. T. Thuy, Q. Lin, B. T. Van, A. Yamada, R. Oyama, M. Sasaki, C. Katan, *Synthesis (Stuttg.)*. **2017**, *49*, 3337.
- 7 L. T. B. Nguyen, M. Abe, *Bull. Chem. Soc. Jpn.* **2023**, *96*, 899.
- 8 K. Roy, X. Zhou, R. Otani, P.-C. Yuan, S. Ioka, K. E. Vogt, T. Kondo, N. H. T. Farag, H. Ijiri, Z. Wu, *Nat. Commun.* **2024**, *15*, 3661.
- 9 G. C. Ellis-Davies, J. H. Kaplan, *Proc. Natl. Acad. Sci.* **1994**, *91*, 187.
- 10 S. R. Adams, J. P. Y. Kao, R. Y. Tsien, *J. Am. Chem. Soc.* **1989**, *111*, 7957.
- 11 H. K. Agarwal, R. Janicek, S.-H. Chi, J. W. Perry, E. Niggli, G. C. R. Ellis-Davies, *J. Am. Chem. Soc.* **2016**, *138*, 3687.
- 12 T. T. T. Pham, S. Jakkampudi, K. Furukawa, F.-Y. Cheng, T.-C. Lin, Y. Nakamura, N. Morioka, M. Abe, *J. Photochem. Photobiol. A Chem.* **2021**, *409*, 113154.
- 13 M. T. Richers, J. M. Amatrudo, J. P. Olson, G. C. R. Ellis-Davies, *Angew. Chemie* **2017**, *129*, 199.
- 14 L. Sansalone, J. Zhao, L. T. B. Nguyen, S. Gupta, D. L. Benson, M. Abe, G. C. R. Ellis-Davies, *Angew. Chemie* **2024**, *136*, e202315726.

- 15 Y. Sakamoto, S. Boinapally, C. Katan, M. Abe, *Tetrahedron Lett.* **2013**, *54*, 7171.
- 16 K. Sitkowska, M. F. Hoes, M. M. Lerch, L. N. Lameijer, P. van der Meer, W. Szymański, B. L. Feringa, *Chem. Commun.* **2020**, *56*, 5480.
- 17 Q. Lin, R. Guo, K. Hamao, R. Takagi, M. Abe, *Chem. Lett.* **2022**, *51*, 153.
- 18 J. A. Barltrop, *Chem. Commun* **1966**, 822.
- 19 Y. V Il'ichev, M. A. Schwörer, J. Wirz, *J. Am. Chem. Soc.* **2004**, *126*, 4581.
- 20 J. Engels, E. J. Schlaeger, *J. Med. Chem.* **1977**, *20*, 907.
- 21 J. H. Kaplan, B. Forbush III, J. F. Hoffman, *Biochemistry* **1978**, *17*, 1929.
- 22 B. Schade, V. Hagen, R. Schmidt, R. Herbrich, E. Krause, T. Eckardt, J. Bendig, *J. Org. Chem.* **1999**, *64*, 9109.
- 23 R. S. Givens, C.-H. Park, *Tetrahedron Lett.* **1996**, *37*, 6259.
- 24 O. D. Fedoryak, T. M. Dore, *Org. Lett.* **2002**, *4*, 3419.
- 25 P. P. Goswami, A. Syed, C. L. Beck, T. R. Albright, K. M. Mahoney, R. Unash, E. A. Smith, A. H. Winter, *J. Am. Chem. Soc.* **2015**, *137*, 3783.
- 26 M. Sasaki, L. Tran Bao Nguyen, S. Yabumoto, T. Nakagawa, M. Abe, *ChemPhotoChem* **2020**, *4*, 5392.
- 27 M. Göppert-Mayer, *Ann. Phys.* **1931**, *401*, 273.
- 28 W. Denk, J. H. Strickler, W. W. Webb, *Science (80-.)*. **1990**, *248*, 73.
- 29 F. Helmchen, W. Denk, *Nat. Methods* **2005**, *2*, 932.
- 30 A. R. Sarkar, D. E. Kang, H. M. Kim, B. R. Cho, *Inorg. Chem.* **2014**, *53*, 1794.
- 31 W. G. Fisher, W. P. Partridge Jr, C. Dees, E. A. Wachter, *Photochem. Photobiol.* **1997**, *66*, 141.

- 32 T. Furuta, S. S.-H. Wang, J. L. Dantzker, T. M. Dore, W. J. Bybee, E. M. Callaway, W. Denk, R. Y. Tsien, *Proc. Natl. Acad. Sci.* **1999**, *96*, 1193.
- 33 N. I. Kiskin, R. Chillingworth, J. A. McCray, D. Piston, D. Ogden, *Eur. Biophys. J.* **2002**, *30*, 588.
- 34 R. Pantell, F. Pradere, J. Hanus, M. Schott, H. Puthoff, *J. Chem. Phys.* **1967**, *46*, 3507.
- 35 R. J. M. Anderson, G. R. Holtom, W. M. McClain, *J. Chem. Phys.* **1979**, *70*, 4310.
- 36 F. Terenziani, C. Katan, E. Badaeva, S. Tretiak, M. Blanchard-Desce, *Enhanced two-photon absorption of organic chromophores: Theoretical and experimental assessments*, **2008**.
- 37 M. Albot, D. Beljonne, J.-L. Bredas, J. E. Ehrlich, J.-Y. Fu, A. A. Heikal, S. E. Hess, T. Kogej, M. D. Levin, S. R. Marder, *Science (80-.)*. **1998**, *281*, 1653.
- 38 G. C. R. Ellis-Davies, *Chem. Rev.* **2008**, *108*, 1603.
- 39 A. Momotake, N. Lindegger, E. Niggli, R. J. Barsotti, G. C. R. Ellis-Davies, *Nat. Methods* **2006**, *3*, 35.
- 40 S. Jakkampudi, M. Abe, N. Komori, R. Takagi, K. Furukawa, C. Katan, W. Sawada, N. Takahashi, H. Kasai, *ACS omega* **2016**, *1*, 193.
- 41 L. Porrès, O. Mongin, C. Katan, M. Charlot, T. Pons, J. Mertz, M. Blanchard-Desce, *Org. Lett.* **2004**, *6*, 47.
- 42 D. Cvejn, E. Michail, K. Seintis, M. Klikar, O. Pytela, T. Mikysek, N. Almonasy, M. Ludwig, V. Giannetas, M. Fakis, *RSC Adv.* **2016**, *6*, 12819.
- 43 Y.-P. Tian, L. Li, J.-Z. Zhang, J.-X. Yang, H. Zhou, J. Wu, P. Sun, L. Tao, Y. Guo, C.-K. Wang, *J. Mater. Chem.* **2007**, *17*, 3646.

- 44 V. Parthasarathy, S. Fery-Forgues, E. Campioli, G. Recher, F. Terenziani, M. Blanchard-Desce, *Small* **2011**, *7*, 3219.
- 45 P. Hrobárik, V. Hrobáriková, I. Sigmundová, P. Zahradník, M. Fakis, I. Polyzos, P. Persephonis, *J. Org. Chem.* **2011**, *76*, 8726.
- 46 A. Bhaskar, G. Ramakrishna, Z. Lu, R. Twieg, J. M. Hales, D. J. Hagan, E. Van Stryland, T. Goodson, *J. Am. Chem. Soc.* **2006**, *128*, 11840.
- 47 F. Kournoutas, K. Seintis, N. Karakostas, J. Tydlitat, S. Achelle, G. Pistolis, F. Bureš, M. Fakis, *J. Phys. Chem. A* **2018**, *123*, 417.
- 48 B. Dumat, G. Bordeau, E. Faurel-Paul, F. Mahuteau-Betzer, N. Saettel, G. Metge, C. Fiorini-Debuisschert, F. Charra, M.-P. Teulade-Fichou, *J. Am. Chem. Soc.* **2013**, *135*, 12697.
- 49 R. Lartia, C. Allain, G. Bordeau, F. Schmidt, C. Fiorini-Debuisschert, F. Charra, M.-P. Teulade-Fichou, *J. Org. Chem.* **2008**, *73*, 1732.
- 50 O. Mongin, L. Porrès, M. Charlot, C. Katan, M. Blanchard-Desce, *Chem. Eur. J.* **2007**, *13*, 1481.
- 51 C. Katan, S. Tretiak, M. H. V Werts, A. J. Bain, R. J. Marsh, N. Leonczek, N. Nicolaou, E. Badaeva, O. Mongin, M. Blanchard-Desce, *J. Phys. Chem. B* **2007**, *111*, 9468.
- 52 C. Katan, F. Terenziani, O. Mongin, M. H. V Werts, L. Porres, T. Pons, J. Mertz, S. Tretiak, M. Blanchard-Desce, *J. Phys. Chem. A* **2005**, *109*, 3024.
- 53 R. D. Fonseca, M. G. Vivas, D. L. Silva, G. Eucat, Y. Bretonnière, C. Andraud, C. R. Mendonca, L. De Boni, *J. Phys. Chem. Lett.* **2019**, *10*, 2214.
- 54 W. J. Yang, D. Y. Kim, C. H. Kim, M. Y. Jeong, S. K. Lee, S. J. Jeon, B. R. Cho, *Org.*

- Lett.* **2004**, *6*, 1389.
- 55 G. C. R. Ellis-Davies, R. J. Barsotti, *Cell Calcium* **2006**, *39*, 75.
- 56 I. Aujard, C. Benbrahim, M. Gouget, O. Ruel, J. Baudin, P. Neveu, L. Jullien, *Chem. Eur. J.* **2006**, *12*, 6865.
- 57 N. Komori, S. Jakkampudi, R. Motoishi, M. Abe, K. Kamada, K. Furukawa, C. Katan, W. Sawada, N. Takahashi, H. Kasai, *Chem. Commun.* **2016**, *52*, 331.
- 58 H. Y. Woo, B. Liu, B. Kohler, D. Korystov, A. Mikhailovsky, G. C. Bazan, *J. Am. Chem. Soc.* **2005**, *127*, 14721.
- 59 S. L. Murov, I. Carmichael, G. L. Hug, *Handbook of photochemistry*, Crc Press, **1993**.
- 60 C. Xu, W. W. Webb, *JOSA B* **1996**, *13*, 481.
- 61 N. S. Makarov, M. Drobizhev, A. Rebane, *Opt. Express* **2008**, *16*, 4029.
- 62 A. Ionescu, R. Lento, T. F. Mastropietro, I. Aiello, R. Termine, A. Golemme, M. Ghedini, N. Bellec, E. Pini, I. Rimoldi, *ACS Appl. Mater. Interfaces* **2015**, *7*, 4019.
- 63 O. P. Lee, A. T. Yiu, P. M. Beaujuge, C. H. Woo, T. W. Holcombe, J. E. Millstone, J. D. Douglas, M. S. Chen, J. M. J. Fréchet, *Adv. Mater.* **2011**, *23*, 5359.
- 64 G. Wang, K.-Y. Pu, X. Zhang, K. Li, L. Wang, L. Cai, D. Ding, Y.-H. Lai, B. Liu, *Chem. Mater.* **2011**, *23*, 4428.
- 65 J. Liu, W. Li, M. Liu, Y. Dong, Y. Dai, Q. Song, J. Wang, C. Zhang, *Phys. Chem. Chem. Phys.* **2018**, *20*, 28279.
- 66 A. Patchornik, B. Amit, R. B. Woodward, *J. Am. Chem. Soc.* **1970**, *92*, 6333.
- 67 A. C. Pease, D. Solas, E. J. Sullivan, M. T. Cronin, C. P. Holmes, S. P. Fodor, *Proc. Natl. Acad. Sci.* **1994**, *91*, 5022.

- 68 T. K. Bader, F. Xu, M. H. Hodny, D. A. Blank, M. D. Distefano, *J. Org. Chem.* **2019**, *85*, 1614.
- 69 Y. Becker, E. Unger, M. A. H. Fichte, D. A. Gacek, A. Dreuw, J. Wachtveitl, P. J. Walla, A. Heckel, *Chem. Sci.* **2018**, *9*, 2797.
- 70 S. Bühler, I. Lagoja, H. Giegrich, K. Stengele, W. Pfeleiderer, *Helv. Chim. Acta* **2004**, *87*, 620.
- 71 S. Boinapally, B. Huang, M. Abe, C. Katan, J. Noguchi, S. Watanabe, H. Kasai, B. Xue, T. Kobayashi, *J. Org. Chem.* **2014**, *79*, 7822.
- 72 L. Donato, A. Mourrot, C. M. Davenport, C. Herbivo, D. Warther, J. Léonard, F. Bolze, J.-F. Nicoud, R. H. Kramer, M. Goeldner, *Angew. Chem. Int. Ed. Engl.* **2012**, *51*, 1840.
- 73 A. Specht, F. Bolze, L. Donato, C. Herbivo, S. Charon, D. Warther, S. Gug, J.-F. Nicoud, M. Goeldner, *Photochem. Photobiol. Sci.* **2012**, *11*, 578.
- 74 L. T. B. Nguyen, C.-L. Wu, T.-C. Lin, M. Abe, *J. Org. Chem.* **2022**, *87*, 15888.
- 75 E. Riguet, C. G. Bochet, *Org. Lett.* **2007**, *9*, 5453.
- 76 K. Schaper, M. Etinski, T. Fleig, *Photochem. Photobiol.* **2009**, *85*, 1075.
- 77 F. Terenziani, C. Le Droumaguet, C. Katan, O. Mongin, M. Blanchard-Desce, *ChemPhysChem* **2007**, *8*, 723.
- 78 S. Sumalekshmy, K. R. Gopidas, *New J. Chem.* **2005**, *29*, 325.
- 79 B. Szczepanik, S. Styrz, *J. Mol. Struct.* **2013**, *1046*, 21.
- 80 S. Sasaki, Y. Niko, A. S. Klymchenko, G. Konishi, *Tetrahedron* **2014**, *70*, 7551.
- 81 C. Wang, W. Chi, Q. Qiao, D. Tan, Z. Xu, X. Liu, *Chem. Soc. Rev.* **2021**, *50*, 12656.
- 82 A. M. Wallace, C. Curiac, J. H. Delcamp, R. C. Fortenberry, *J. Quant. Spectrosc.*

- Radiat. Transf.* **2021**, 265, 107544.
- 83 M. Chen, D. Chen, P. Chou, *Chempluschem* **2021**, 86, 11.
- 84 P. Klán, J. Wirz, *Photochemistry of organic compounds: from concepts to practice*, John Wiley & Sons, **2009**.
- 85 J. E. Bloor, B. R. Gilson, R. J. Haas, C. L. Zirkle, *J. Med. Chem.* **1970**, 13, 922.
- 86 M. J. Frisch, G. W. Trucks, H. B. Schlegel, G. E. Scuseria, M. A. Robb, J. R. Cheeseman, *Gaussian Inc, Walling-form CT* **2010**.
- 87 J.-H. Cho, Y.-S. Ryu, S.-H. Oh, J.-K. Kwon, E.-K. Yum, *Bull. Korean Chem. Soc.* **2011**, 32, 2461.
- 88 M. Ince, F. Cardinali, J. Yum, M. V. Martínez-Díaz, M. K. Nazeeruddin, M. Grätzel, T. Torres, *Chem. Eur. J.* **2012**, 18, 6343.
- 89 T. Ramsingh Girase, S. Bhilare, S. Sankar Murthy Bandaru, N. Chrysochos, C. Schulzke, Y. S. Sanghvi, A. R. Kapdi, *Asian J. Org. Chem.* **2020**, 9, 274.
- 90 C. Wang, J. Li, S. Cai, Z. Ning, D. Zhao, Q. Zhang, J.-H. Su, *Dye. Pigment.* **2012**, 94, 40.
- 91 X. Yang, Q. Yu, N. Yang, L. Xue, J. Shao, B. Li, J. Shao, X. Dong, *J. Mater. Chem. B* **2019**, 7, 2454.
- 92 S. Hu, J. Zeng, X. Zhu, J. Guo, S. Chen, Z. Zhao, B. Z. Tang, *ACS Appl. Mater. Interfaces* **2019**, 11, 27134.
- 93 T. T. T. Pham, Y. Chitose, T. T. T. Tam, W.-L. Tseng, T.-C. Lin, M. Abe, *Chem. Lett.* **2021**, 50, 1810.
- 94 Z. Li, H. Ishizuka, Y. Sei, M. Akita, M. Yoshizawa, *Chem. Asian J.* **2012**, 7, 1789.

- 95 J. Xu, H. Zheng, H. Liu, C. Zhou, Y. Zhao, Y. Li, Y. Li, *J. Phys. Chem. C* **2010**, *114*, 2925.
- 96 F. Mo, Y. Jiang, D. Qiu, Y. Zhang, J. Wang, *Angew. Chemie Int. Ed.* **2010**, *49*, 1846.
- 97 Y. Liu, S. Lou, D. Xu, Z. Xu, *Chem. Eur. J.* **2010**, *16*, 13590.

List of Publications

Main articles

1. “Tris(4'-nitrobiphenyl)amine – an octupolar chromophore with high two-photon absorption cross-section and its application for uncaging of calcium ions in the near-infrared region”

Linh Tran Bao Nguyen, Cheng-Lin Wu, Tzu-Chau Lin*, and Manabu Abe*

J. Org. Chem. **2022**, *87*, 15888–15898

2. “Study on factors affecting quantum yield for the design of improved ortho-nitrobenzyl photoremovable protecting groups”

Linh Tran Bao Nguyen and Manabu Abe*

Bull. Chem. Soc. Jpn. **2024**, uoae067

Supplementary articles

1. “Development of photoremovable protecting groups responsive to near-infrared two-photon excitation and their application to drug delivery research”

Linh Tran Bao Nguyen and Manabu Abe*

Bull. Chem. Soc. Jpn. **2023**, *96*, 899–906

2. “Structural Transformation of the 2-(*p*-Aminophenyl)-1-hydroxyinden-3-ylmethyl Chromophore as a Photoremovable Protecting Group”

Miyu Sasaki, Linh Tran Bao Nguyen, Sohshi Yabumoto, Tatsuo Nakagawa, and Manabu Abe*

ChemPhotoChem **2020**, *4*, 5392–5398

3. “Photoexcitation of (diarylmethylene)amino benziodoxolones for alkylamination of styrene derivatives with carboxylic acids”

Daichi Okumatsu, Kensuke Kiyokawa*, Linh Tran Bao Nguyen, Manabu Abe*, and Satoshi Minakata*

Chem. Sci. **2024**, *15*, 1068–1076

4. “Bidirectional Neuronal Actuation by Uncaging with Violet and Green Light”

Lorenzo Sansalone, Jun Zhao, Linh T. B. Nguyen, Swati Gupta, Deanna L. Benson, Manabu Abe, and Graham C. R. Ellis-Davies*

Angew. Chem. Int. Ed. **2024**, *63*, e202315726

Acknowledgments

The research described in this thesis was carried out under the guidance of Professor Manabu Abe at the Department of Chemistry, Graduate School of Advanced Science and Engineering, Hiroshima University.

This study was supported by JST and the establishment of university fellowships for the creation of science and technology innovation (Grant Number JPMJFS2129).

Firstly, I would like to express my appreciation to Professor Manabu Abe for his dedicated advices and encouragement during my PhD course.

I also give a special thanks to Dr. Ryukichi Takagi and Dr. Sayaka Hatano for their technical support and helpful discussions on my reseach.

In addition, I would like to thank Professor Tzu-Chau Lin (National Central University, Taiwan) for his collaboration, and National Science Center for Basic Research and Development (N-BARD, Hiroshima University) for high resolution mass spectroscopy measurement.

Thanks all the members of Reaction Organic Chemistry Laboratory for their kind help and support during the last five years.

Finally, thanks to my family and my friends, I had more encouragement, motivation and excitement to complete this thesis.

July 2024

Nguyen Tran Bao Linh

Reaction Organic Chemistry

Department of Chemistry

Graduate School of Advanced Science and Engineering

Hiroshima University